UNIVERSIDADE DE LISBOA

INSTITUTO SUPERIOR TÉCNICO

Co-Simulation Methods for Multidisciplinary Problems in Railway Dynamics

Pedro Cabaço Antunes

Supervisor: Doctor Jorge Alberto Cadete Ambrósio

Co-Supervisor: Doctor João Carlos Elói de Jesus Pombo

Thesis approved in public session to obtain the PhD Degree in Mechanical Engineering

Jury final classification: Pass with Distinction and Honour

2018

TÉCNICO LISBOA

UNIVERSIDADE DE LISBOA

INSTITUTO SUPERIOR TÉCNICO

Co-Simulation Methods for Multidisciplinary Problems in Railway Dynamics

Pedro Cabaço Antunes

Supervisor: Doctor Jorge Alberto Cadete Ambrósio

Co-Supervisor: Doctor João Carlos Elói de Jesus Pombo

Thesis approved in public session to obtain the PhD Degree in Mechanical Engineering

Jury final classification: Pass with Distinction and Honour

Jury

Chairperson: Doctor Hélder Carriço Rodrigues, Instituto Superior Técnico, Universidade de Lisboa

Members of the Committee:

Doctor Rui Artur Bártolo Calçada, Faculdade de Engenharia, Universidade do Porto;

Doctor Jorge Alberto Cadete Ambrósio, Instituto Superior Técnico, Universidade de Lisboa;

Doctor Alan Facchinetti, Dipartimento di Meccanica, Politecnico di Milano, Italy;

Doctor Virgínia Isabel Monteiro Nabais Infante, Instituto Superior Técnico, Universidade de Lisboa;

Doctor António Ramos Andrade, Instituto Superior Técnico, Universidade de Lisboa;

Lic. Sérgio Pissarra de Abreu dos Santos, Direção da Rede Ferroviária, IP.

Funding Institutions

Fundação para a Ciência e a Tecnologia

2018

Abstract

The railway system is increasingly becoming a key-player in worldwide transport policies where besides the problems of sustainability, the railway also offers a reliable and efficient mode of transport with recognized high levels of safety and comfort. The development of computer resources allowed for computer simulations to be an essential part of the design and research process of railway systems. The quest for novel solutions for the increasing demands for network capacity, either by increasing the traffic speed or the axle loads, put pressure on the existing infrastructures that find the computational analysis of potential solutions a tool for their virtual testing. The dynamic analysis of modern railway systems involves complex multidisciplinary problems for which the most recent computer codes for railway applications, in general, only allow the study of a particular phenomenon at a time, each with its own complex mathematical model. By analysing such phenomena independently, it is not possible to capture all the dynamics of the complete railway system if relevant coupling phenomena exist. Multibody dynamics formulations are the basis for the most efficient computational techniques that deal with large overall motion, being able to handle intricate models which include a large number of mechanical and structural components and exhibit complex interactions. Formulations based on linear or nonlinear finite element methods provide the most powerful and versatile procedures to describe the flexibility of the system components and some of their interactions. Correspondingly, in railway applications, the vehicle dynamics are better analysed by using a multibody dynamics formulation in which the large relative motion between the vehicle components is well described. The surrounding structures composed by the overhead catenary and the track, with which the vehicle interacts, are better described via detailed finite element models, analysed in dedicated finite element based formulations. This work portrays the development and employment of two advanced and innovative numerical dynamic analysis tools for pantograph-catenary and vehicle-track interaction, in which co-simulation plays a

fundamental role on coupling the dynamic behaviour between the finite element models of the catenary and track and the multibody models of pantograph and vehicle. This includes the detailed representation of the vehicle, track, pantograph and catenary to evaluate their dynamics including the interaction between each other as well. Such an application not only presents new solutions with technological relevance but also offers to the industry the most recent computational solutions, thus contributing to improve the competitiveness of the railway transport system. Furthermore, in this work, case studies are presented where the developed methodologies enable the study of pantograph-catenary interaction with realistic catenary models catenaries set in general railway tracks, including curves. With respect to vehicle-track interaction, the proposed methodologies also allowed to account for track flexibility in the dynamic analysis of railway vehicles.

Keywords: Railway Dynamics, Co-Simulation, Pantograph-Catenary Interaction, Vehicle-Track Interaction, Finite Element Method, Multibody Dynamics.

Resumo

O sistema de transporte ferroviário apresenta-se cada vez mais como um elemento chave nas políticas de transporte em todo o mundo. Além dos problemas de sustentabilidade, o transporte ferroviário oferece um modo fiável e eficiente de transporte com elevados níveis de segurança e conforto. O desenvolvimento de ferramentas computacionais especializadas, acompanhado do aumento da disponibilidade de recursos computacionais, permitiu que estas se tenham tornado parte essencial do processo de projeto, investigação e desenvolvimento dos sistemas ferroviários. As crescentes necessidades de uma maior capacidade de rede, seja pelo aumento da velocidade de tráfego ou das cargas por eixo, pressionam os fabricantes e construtores de infraestrutura a procurar novas soluções tecnológicas. Estes reconhecem que a análise computacional e correspondentes aplicações numéricas são uma forma indispensável de desenvolver novas soluções evitando dispendiosos ensaios experimentais. Presentemente, a análise dinâmica de sistemas de transporte ferroviário modernos envolve problemas multidisciplinares complexos, para os quais as ferramentas computacionais mais recentes, em geral, permitem apenas o estudo de um fenômeno específico de cada vez e cada qual com o seu próprio modelo matemático complexo. Ao analisar estes fenómenos independentemente não é possível capturar a dinâmica do sistema ferroviário completo, caso existam fenômenos de acoplamento relevantes. As formulações de dinâmica multicorpo são a base para as técnicas computacionais mais eficientes. Estas lidam com grandes deslocamentos e rotações generalizados, sendo capazes de considerar modelos complexos que incluem um grande número de componentes mecânicos e estruturais e exibem interações complexas. Formulações baseadas no método de elementos finitos lineares ou não-lineares fornecem a base para os procedimentos numéricos mais poderosos e versáteis capazes de descrever a flexibilidade dos componentes de uma estrutura e algumas das suas interações. Correspondentemente, em

aplicações ferroviárias, a dinâmica do veículo é melhor analisada considerando uma formulação de dinâmica multicorpo em que o grande movimento relativo entre os componentes de um veículo é bem descrito. As estruturas circundantes compostas pela catenária e pela via, com as quais o veículo interage, são melhor descritas através de modelos detalhados e analisados em formulações dedicadas baseadas em elementos finitos. No presente trabalho, são desenvolvidas e empregues duas ferramentas computacionais avançadas e inovadoras, para a análise dinâmica da interação pantógrafo-catenária e veículo-via. Em estas, a aplicação de procedimentos de co-simulação faz um papel fundamental no acoplamento do comportamento dinâmico entre os modelos de elementos finitos da catenária e da via ferroviária com os modelos multicorpo do pantógrafo e do veículo. Estas ferramentas computacionais desenvolvidas, não só apresentam novas soluções com relevância tecnológica, mas também oferecem à indústria as mais recentes soluções computacionais, contribuindo para melhorar a competitividade do sistema de transporte ferroviário. Mais ainda, neste trabalho, são apresentados estudos de caso onde os métodos desenvolvidos possibilitam o estudo da interação pantógrafo-catenária com modelos de catenária realistas inseridos em linhas férreas com geometria de via generalizada, incluindo curvas. Em respeito à interação veículo-via, as metodologias propostas permitiram a consideração da flexibilidade da via na análise dinâmica de veículos ferroviários.

Palavras-Chaves: Dinâmica Ferroviária, Co-Simulação, Interação Pantógrafo-Catenária, Interação Veículo-Via, Método dos Elementos Finitos.

Acknowledgments

It is with great pleasure that I express here my sincere gratitude to a group of people which in many ways have contributed for the success of this work.

To Prof. Jorge Ambrósio, my supervisor, I want to state my appreciation for his invaluable support, availability and guidance throughout this thesis. His work discipline and commitment have inspired me. For his close attention to my thesis progression and all the teachings that came along the way I leave my grateful acknowledgment.

To my co-supervisor, Prof. João Pombo, I want to express thanks for the given dedication and help on the work here presented. His encouragement and support, provided along the thesis, was detrimental.

I would also like to relay my gratitude to Prof. Manuel Pereira and Prof. Virgínia Infante. Between both of them their energy and enthusiasm in research have motivated me. For their accessibility, willingness to help and guidance I wish to express my gratitude. Furthermore, Prof. Manuel Pereira was a great Professor, a valued Engineer and a true gentleman with whom I was fortunate to cross paths, learn and interact with.

To Prof. Alan Facchinetti and Prof. Stefano Bruni from Politecnico di Milano, I want to express my appreciation for welcoming me to their research institution. Prof. Alan Facchinetti played a key role in the work here developed with his guidance and attention.

I would also like to express my thanks for the support and friendship of my PhD colleagues. In particular, to Hugo Magalhães and João Costa which also fell in the role of collaborating on the work here presented. For their hard effort and the rejoice we took in accomplishing our objectives I express my gratitude.

On my personal acknowledgments, I leave my thanks to my parents and brother who provided the support only family can give. In particular to my Father, I want to thank him for all is support and effort which was, even for Father standards, outstanding. Also, to my personal friends I thank all for the encouraging support in accomplishing this work.

For last, to the Portuguese Foundation for Science and Technology (FCT) I would like to thank for the financial support provided under its PhD Programme.

Dissertation

This thesis is comprised of two parts: Part I, which presents an overview of the work developed over the course of the PhD and provides a summary of the chapters presented in the second part; Part II consists in a series of chapters, each one addressing in detail a component of the work developed in this thesis. The structure of the chapters in Part II is built such way that each one of them contains the material of either a published paper or a paper being submitted by the author.

It must be noted that the chapters in Part II were planned and prepared in collaboration with co-authors with the objective of being submitted as individual papers. In all chapters, the major writing and compilation effort was assured by the first author, being all the results, analysis and conclusions, except in *Chapter 17*, the responsibility of the author of this thesis. Also, all the implemented numerical procedures, developed methodologies, models and numeric simulations presented in these works have been produced by the author of this thesis, with the following exceptions. The vehicle models used in *Chapter 17* and *Chapter 18* were developed by H. Magalhães. The railway track models were developed in collaboration, firstly with T. Almeida, in *Chapter 17*, and afterwards with J. Costa, *Chapter 18*. In addition, all the work developed was supervised and co-supervised correspondingly by Prof. J. Ambrósio and Prof. J. Pombo.

The final developments of the work portrayed on this thesis are presented in *Chapter 16* and *Chapter 18*.

Contents

PART I

1 Introduction

From the beginnings of the 19th century, along with the Industrial Revolution, railway transportation has played a critical role in socio-economic development across the world breaking down barriers of distance, time and delay. Since their early times railway technologies went through several technical innovations and railway transportation prevailed as a primary form of land transport either for freight or passengers. One of the main premises for the success of this system is the reduced friction between the wheel and rail which enable the transport of heavier loads with less power in an energy efficient manner. Later on, the railway electrification along with the introduction of the electric traction vehicles have reinforced this aspect.

Nowadays, the railway system is increasingly becoming a key player in worldwide transport policies. This results from the predictable limitations on the availability of carbon based fuels and the urgency for reduction of greenhouse gas emissions. Besides the problems of sustainability, the railway also offers a reliable and efficient mode of transport with recognized high levels of safety and comfort. In addition, with the effects of globalization and long-term economic growth it is expected a significant increase on the demand for transportation at a worldwide level. Here the railway system will play a fundamental role involving not only a substantial capital investment but also a considerable research and development compromise [1].

The railway system is cost-effective, nevertheless it remains a capital intensive mode of transport. Besides requiring a considerable investment outlay for infrastructure, vehicle, track and overhead line, among others, it has a significative upkeep and overhead expenditures, such has maintenance and operation costs. Furthermore it still has to compete with other modes of transportation, all of them having their own advantages and drawbacks. For short and medium distances, modern high speed trains are able to compete with air transportation, having the

advantage of presenting better energy efficiency and causing less pollution. For larger distances the railway system is still the most economical mean for land transportation of goods. With the quest to overcome interoperability issues between railway lines from different countries it also starts to have some competitive edge in passengers transport over other means of transportation.

In order to improve the competitiveness and attractiveness of railway networks in respect to other transportation systems, and also to meet the future needs of transportation, trains have to travel faster, within higher levels of safety and comfort, and with lower life cycle and development costs. Correspondingly, railway operators and owners are demanding reductions in the overall operational costs, with particular attention to the railway vehicles maintenance costs and to the aggressiveness of rolling stock on the infrastructures. Also, the quest for interoperability, as in the compatibility between different existing and projected railway networks, puts an extra level of demand on the ability to control their interfaces.

The development of computer resources allowed for computational methods to be an essential part of the design and research process of railway systems. The quest for novel solutions for the increasing demands for network capacity, either by increasing the traffic speed or the axle loads, put pressure on the existing infrastructures that find the computational analysis of potential solutions a tool for their virtual testing. The European Strategic Rail Research Agenda [2] and the European Commission for Transports [3] white papers have identified key scientific and technological priorities for rail transport over the next 20 years. One of the points emphasized is the need to reduce the cost of approval for new vehicles and infrastructure products with the introduction of virtual certification. Moreover, an important issue arising during the design phase of new trains is the improvement of its dynamic performance. The concurrent use of different computational tools allows to carry out several simulations, under various scenarios, in order to reach optimized designs. In this way, studies to evaluate the impact of design changes or failure modes can be performed in a much faster and less costly way than the physical implementation and test of those changes in real prototypes.

Due to their multidisciplinary, all the issues involving railway systems and the study of their dynamic behaviour have a substantial order of complexity. Therefore, the use and development of computational tools that represent the state of the art and are able to characterize modern designs is essential. Additionally, to predict the overall equipments performance within an acceptable order or accuracy and integrity, validated mathematical models are a fundamental requirement. Recent computer programs for railway applications use specific methodologies that, in general, only allow studying each particular phenomenon at a time. By analysing such phenomena independently, it is not possible to capture all the dynamics of the complete railway

system and relevant coupling effects. However, developing innovative and more complex methodologies in a co-simulation environment allow, not only to integrate all physical phenomena, but also to assess the cross influence between them. Furthermore, each part of the system can be analysed with its most suitable numerical procedure without compromising its detailed representation.

The work here presented integrates advanced methodologies in a computational tool able to handle the dynamic analysis of a complete railway system. For this purpose, the detailed modelling and dynamic behaviour evaluation of the vehicle, track, pantograph and catenary are implemented and the methodologies employed for their analysis integrated in a co-simulation environment able to handle the vehicle-track and pantograph-catenary interaction. Besides developing new computational tools and updating existing ones to their state of the art, which by itself is a valuable contribution, the main innovation of this work lies on the integration of this applications in a co-simulation platform where the interaction among each pair of subsystems can be considered. Contrary to a more traditional approach in which these systems are handled independently, here they coexist in a common and reliable tool which can be used accordingly to the extent of the modelling requirements of particular case scenarios. This provides a flexible solution not only to integrate the considered subsystems but also to assess the cross influence between them. Thus, avoiding the development of a unique and complex formulation with a respective numerical solver that often force compromises on the analysis of each phenomenon as also become computationally expensive and time intensive. Moreover, each subsystem in the co-simulation environment can be modelled according to its most suitable formulation and developed individually as a stand-alone application.

1.1 Objectives and Motivation

The main objective of the work presented is to develop two numerical dynamic analysis tools for pantograph-catenary and vehicle-track interaction, in which co-simulation plays a fundamental role on coupling the dynamic behaviour between the finite element models of the catenary and track to correspondingly the multibody models of the pantograph and vehicle.

Multibody dynamics formulations, [4], are the basis for the most efficient computational techniques that deal with large overall motion, being able to handle intricate models which include a large number of mechanical and structural components and exhibit complex interactions. Formulations based on linear or nonlinear finite element methods, [5], provide the most powerful and versatile procedures to describe the flexibility of the system components

and some of their interactions. Correspondingly, in railway applications, the vehicle dynamics are better analysed by using a multibody dynamics formulation in which the large relative motion between the vehicle components is well described [6,7]. The surrounding structures composed by the overhead catenary and the track, with which the vehicle interacts, are better described via detailed finite element models, analysed in dedicated finite element based formulations [8,9].

In this sense the numeric simulation tool developed for pantograph-catenary interaction analysis is built with the aim to perform the dynamic analysis of catenaries mounted in any generalized track trajectory. This includes curved tracks which, until now, have been outside of the scope of any present pantograph-catenary software package [10]. Besides the novel methodologies to model the catenary system in finite elements considering curves, one other challenge presented is to cope with the generalized trajectory of the pantograph. In this work, this issue is dealt by modelling the pantograph with a three dimensional multibody dynamics formulation which in turn is coupled to the catenary model by a co-simulation procedure. This work follows previous developments, where a pantograph-catenary interaction tool was developed and the basis for the co-simulation procedure was implement [11,12]. The success of this first implementation led to the continuation of the work in this thesis. Nevertheless, to fulfil the objectives of this work a new, more robust and consolidated implementation of the co-simulation was required as well as all other aspects regarding the modelling of the systems and the numerical implementation of all procedures.

Regarding the vehicle-track interaction tool, here the main objective is to build a vehicle-track simulation software where the dynamics of advanced multibody vehicle models can be evaluated taking into consideration the flexibility of the track which in many vehicle-track interaction tools is generally disregarded. The motivation for this work relies on the successful implementation of the first pantograph-catenary procedure which opened the possibility to similarly implement the coupling of the multibody vehicle dynamics with a finite element model of the track. This requires not only the implementation of a new customized co-simulation procedure but also of a track modelling methodology and all following numerical implementations. In this case, the numerical vehicle dynamic analysis tool considered here has been previously developed Prof. J. Pombo and Prof. J. Ambrósio [13,14].

The methods and computational tools developed in the course of this work are aimed to be used by the industry. This is ensured as this work has contributed and benefited from recently developed European, EUROPAC and PANTOTRAIN, and National projects, SMARTRACK and WEARWHEEL, in which key rail industries are involved. The foreseen technology

transfer, resulting from the work now proposed, will impact not only in new design paradigms for industry but also in new virtual acceptance methodologies for railway equipment. Furthermore, the work proposed here is a current key-topic of research with high scientific and technological relevance for the railway industry and with significant economic impact on this transport sector. In fact, industrial integrators, like ALSTOM and Bombardier, and operators, such as DB (Germany) and SNCF (France), are interested in studying these problems and are investing large resources on research and development in these activities.

1.2 Thesis Outline

The main body of this thesis, Part I, offers a description of the developed applications and its associated methodologies. Note that, the work here proposed is an interdisciplinary exercise that requires the use and computational implementation of different numerical tools for the dynamic analysis of the involved systems. The finite element method is used to model the catenary and track structures while the pantograph and the vehicles are modelled using multibody dynamics. On the other hand, contact models to couple the systems also need to be addressed where the contact will also serve as the bridge of the developed co-simulation procedures which link the considered subsystems. Furthermore, the contact formulation as also the modelling of the track and catenary systems requires an accurate geometric description of the railway track and its rails centrelines. Here, not only the definition of the centrelines in form of a parametrized curve is required but also a corresponding moving frame of reference is necessary in order to define a spatial orientation. Furthermore, the use of the numerical tools developed is portrayed in Part II.

2 Pantograph-Catenary Interaction

The railway vehicles with electrical traction are, today, the most economical, ecological and safe means of transportation. Its energy collection system is the crucial element for their reliable running. This system is generally composed by a pantograph attached to the roof of the train vehicles and an overhead electrical structure laid along the track, represented in Figure 2.1 (a). As this structural system, commonly denominated by catenary, is in contact with the pantograph the electrical current that carries is drawn into the electrical traction system of the train. This way, the pantograph-catenary interface plays a critical role concerning the ability to supply the proper amount of energy required to run the engines and maintain the trains operational speed [15]. In fact, on present modern high-speed trains, as more electrical current is required, this issue remains one of the major limiting factors on their top operational velocity.

Railway overhead systems are subjected to tight functional requirements to deliver electrical energy to trains engines while still ensuring their reliability and to control their maintenance periods. The quality of the current collection is of fundamental importance as the loss of contact between the contact pantograph contact strip and the contact wire of the catenary with consequent arching, as shown in Figure 2.1 (b), not only limit the top velocity of high-speed trains but also imply the deterioration of the functional conditions of these mechanical equipments. Thus, it is of the outmost concern that not only the supply of energy remains uninterrupted but also that its electro-mechanical wear is as reduced as possible.

The increase of the average contact force, between the pantograph catenary interface, would improve the energy collecting capabilities with less incidents of loss of contact but would also lead to higher wear of the catenary contact wire and pantograph collector strip [16,17]. A balance between contact force characteristics and wear of the energy collection system is the objective of improving contact quality. Even in normal operating conditions, a control on the

catenary-pantograph contact force is required to ensure longer maintenance cycles and a better reliability of the systems. Furthermore, the current need to increase the rail network capacity and the quest for interoperability of different pantographs, in existing and projected catenary systems, puts an extra demand on the ability to control their dynamic behaviour [2,3].

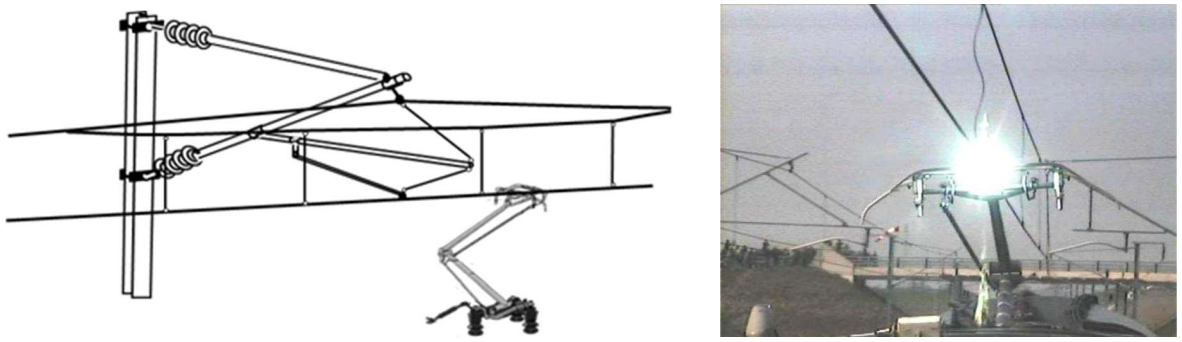

(a) (b)

Figure 2.1 : (a) Representation of the pantograph-cateanry interaction; (b) Pantograph-catenary contact, during a high-speed train operation, with the occurrence of contact loss and arcing.

To address such important aspects for the design and analysis of the pantograph-catenary system, it is necessary to develop reliable, efficient and accurate computational procedures that allow capturing all the relevant features of their dynamic behaviour. This has been object of active research where an extensive amount of publications, on the development and application of computational methods for the dynamic analysis of pantograph-catenary interaction, is found in the literature. This address several aspects such as analysis of multiple pantograph operations [18–20], analysis of critical catenary sections [21–23], and optimisation of pantograph and catenary designs [24–26] among other issues of importance. The perturbation of the quality of contact in the pantograph-catenary interface due to aerodynamics effects, vehicle vibration and catenary irregularities [7,27–30] are also considered in the literature. The hardware-in-the-loop hybrid simulations of pantograph-catenary interaction is also another approach to find improved dynamic performance for the two systems [31,32]. The pantograph-catenary benchmark, [8], and its associated references portrait the state-of-art of current numerical analysis tools, developed by world leading research institutions. It is worth verifying that in all applications, methods or cases considered in the long list of present publications on the topic of pantograph-catenary interaction modelling and analysis, almost all catenary models consider exclusively straight railway tracks.

As already stated, the work presented here purposes an approach for the numerical dynamic analysis of pantograph-catenary interaction in curved tracks or for that matter in any generalized track trajectory. Here, both the catenary model and the trajectory path of the pantograph are set in relation to the spatial description of the track running surface, which is

defined as parametric curve with an associated local reference frame that defines the orientation of the track layout. The track geometry is obtained using the standard information required for railway vehicle dynamics applications, i.e., curvature, cross level and vertical profile as function of the track length. The finite element method is used to model and evaluate the dynamic behaviour of a catenary system following the methodology presented in previous works [12]. To cope with the general geometry of the track and the path of its base, the pantograph model is developed using a spatial multibody dynamics formulation [4]. The pantograph base motion, which is fixed to the railway vehicle roof, is defined by a prescribed kinematic motion constraint [33,34]. As both pantograph and catenary use different formulations, their interaction is established through a co-simulation procedure where a penalty method is used to evaluate the contact force between the pantograph and the catenary [35].

3 Vehicle-Track Interaction

For rolling-stock manufacturers, railway operators and infrastructure owners the dynamics of the railway vehicle is an important aspect required to be taken into consideration with special attention to the safety, such as risk of derailment, and passenger comfort. It is a challenge for railway systems to comply with specifications such as the international standards and technical specifications for interoperability (TSIs). Another very sensitive issue for railway industry is the evaluation of the impact of traffic on the infrastructure and the damage on vehicles due to the track conditions. In fact, there is a growing tendency to define the track access charges, this is the prices billed by the infrastructure managers to the railway operators, according to the predicted damage that the trainsets cause to the infrastructure. Finally, the uncertainties associated with the maintenance intervals and the costs involved in such procedures also raise the urgency of acquiring a better understanding on how the vehicle characteristics, the track features and the service conditions influence the life cycle costs of the railway equipments. The quest for novel solutions to answer the increasing demands for network capacity, either by increasing the traffic speed or the axle loads, also put pressure on the existing infrastructures that find in the computational analysis of potential solutions a tool for their virtual testing. One of the points emphasized is the need to reduce the cost of approval for new vehicles and infrastructure products with the introduction of virtual certification. Certainly, an important issue arising during the design phase of new railway vehicles is the improvement of its dynamic performance. The concurrent use of different computational tools allows carrying several simulations, under various scenarios, to reach optimized designs. Studies to evaluate the impact of design changes or failure modes risks can be performed in a much faster and less costly way than the physical implementation and test of those changes in real prototypes.

Current computer codes for railway applications use specific methodologies that, in general, either handle the vehicle dynamics on a rigid track or deal with moving loads on flexible track. By analysing such phenomena independently, it is not possible to capture all the dynamics of the complete railway system and relevant coupling effects. However, developing innovative and more relevant comprehensive methodologies, in a co-simulation environment, allow not only to integrate all physical phenomena, but also to assess the cross influence between them.

The work presented here purposes a co-simulation procedure for the dynamic analysis of vehicle-track interaction where the main objective is to account for track flexibility in the dynamic behaviour analysis of railway vehicles, which in turn, is reflected on the rolling contact of the rail-wheel interaction, shown in Figure 3.1.

Figure 3.1: Snapshot of the wheel-rail interaction.

Vehicle-Track interaction is a subject where contributions from a wide range of fields are required. Different modelling approaches are used, depending on the objective of the study. Railway dynamics is a subject where contributions from a wide range of fields are required. Different modelling approaches are used, depending on the objective of the study. The importance of the modelling aspects for the vehicle and track, in the context of their interaction, is related with the frequencies of interest associated to the particular phenomena under study in a State-of-Art review by Knothe and Grassie [36]. Although this focus mostly on noise and it does not address the track geometry, it presents fundamental modelling considerations required for flexible tracks in order to achieve meaningful analysis results. Addressing the vehicle-track interaction, from a perspective of evaluating the dynamic behaviour of a railway vehicle, the usual and most popular approach is to model the vehicle using a multibody system formulation model being the track considered a rigid structure [14,37,38]. This methodology provides acceptable results for dynamic analysis on a perspective of vehicle behaviour for ride safety and comfort [39]. These models are adequate to evaluate low frequency dynamic responses such as lateral stability and curving behaviour, as most of the high frequency excitation is

filtered by the vehicles suspension, up to a certain degree. Gialleonardo et al. [40] show that the track flexibility has a significant effect on the evaluation of the vehicle critical speed and in the wheel/rail contact forces. Dynamic effects at mid to high frequency ranges require the introduction of track flexibility [9]. Even in the low frequency domain track flexibility must be considered when its effects on the railway dynamics are significant, such as when the track is considered to be flawed [41,42], or switches and crossings are considered [43]. The work by Martinez-Casas et al. [44] shows the importance of considering the flexibility of the railway track, and also of the wheelset, in the interaction between vehicle and track. Although in their work only a single wheelset and a perfect circular track are considered, it can be accepted that the interaction phenomena identified is expected to be present in more general scenarios. Furthermore, as the wheel-rail contact forces evaluation depends on the geometry of the wheel and the rail, as much as in the relative position between them, track flexibility must be considered when analysing the development of these rolling contact forces along the track. In scenarios with tangent tracks models, in which modal superposition is used to reduce the size of the finite element track model, Dietz, Hippmann and Schupp [45] present the implementation of a coupled vehicle-track dynamics in a commercial multibody code. Due to the use of a modal representation of the flexible track this approach cannot handle to full dynamics of the system without considering an excessive number of modes for the track, which not only leads to computational inefficiency but also prevents the introduction of nonlinear elements, localized deformations and more general geometries. To this end, the work by Zhai, Wang and Cai [46] demonstrates the importance of considering the coupled vehicle-track dynamics with flexible tracks by developing a simulation scenario, validated experimentally, in which the spatial vehicle multibody model operates in a two tracks, one with large radius and another with a small radius. However, in all the works cited here the track geometry is either a tangent track or a curved track with constant radius, never considering a more general, and realistic geometry.

In this work, a multibody formulation is used to model the railway vehicle and a finite element formulation is presented to model the railway track. To establish the interaction between these models a novel co-simulation procedure, able to handle the dynamics between the systems, is proposed. This approach allows to analyse the vehicle dynamics in a flexible track with a general geometry modelled with finite elements, i.e., including curvature, cant, vertical slopes and irregularities, which is another novel contribution that can be used not only to address the running scenarios studied in this work but also to contribute to a number of challenging engineering problems associated to the train-track interaction occurring in tracks with small radius curves such as squeal noise and short pitch corrugation.

4 Railway Geometry

The dynamic analysis of modern railways systems involves complex multidisciplinary problems for which a computational geometric definition of the railway track and rails must be set. In particular, for the applications here presented, both the track and catenary layout are defined in relation to the track travel length, or track arc-length, and its running surface. Also, the trajectory of the pantograph is defined here by the position of the vehicle roof top relative to the track surface. Therefore, to define the absolute position in space of the catenary, the track and corresponding rails, as also the trajectory path of the pantograph, a spatial reference frame is required. When dealing with straight railway tracks this process is straight forward. However, when dealing with a generalized track trajectory a more systematic approach is required to account for the track curvature and cross level, which influence the orientation of the running surface of the track. Moreover, it is required that this geometric description is accurate and promptly available in a compressive and efficient manner for all applications.

By industry standards, the railway track geometry is generally described as a function of its travel length, by the curvature, cross level and elevation [47]. Though this description defines the track geometry along its travel length it does not provide an absolute definition frame with respect to which position other systems. To fulfil this requirement, in this work, the spatial geometry of the track, *c*, and the left and right rails, *Lr* and *Rr*, is established by a reference moving frame parametrized in function of its travel length, s, as represented in Figure 4.1 [48,49]. Here, each reference moving frame is composed by a curve, defined by a collection of points, where for any given point, $\mathbf{r}$, at a specified curve length a local reference frame, (ξ,η,ζ), is defined. In particular, the track moving frame is composed by a curve that represents its centreline and at any given travel length the local reference frame is set such way

that ξ_t is tangent to the track centreline, η_t is transversal to the track and parallel to the running surfaces of the rails while ζ_c is normal to the track running surface. On each rail, the moving frame is defined by a centreline curve that passes through the cross section centre of the rails and the associated local reference frames, $(\xi,\eta,\zeta)_{Lr}$ and $(\xi,\eta,\zeta)_{Rr}$, are set in such way that η is parallel to the running of the rail and ξ is normal to the its cross section surface.

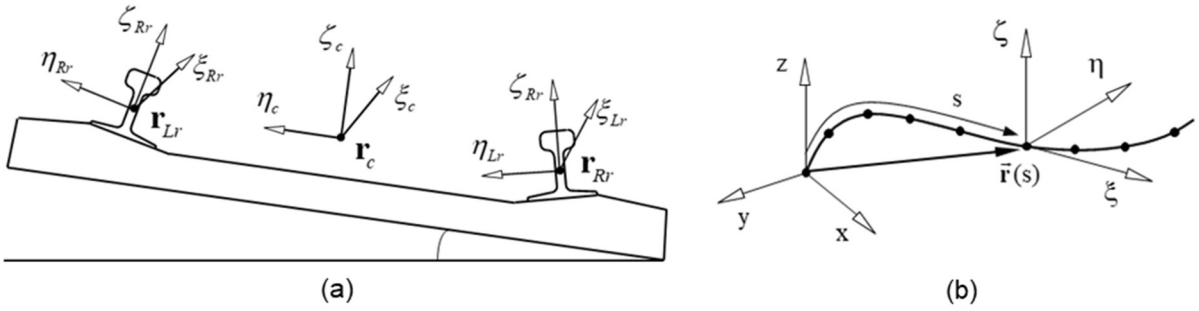

Figure 4.1: (a) Representation of the track and rails local reference frames in relation to the track; (b) Representation of the track and rail centrelines parameterisation.

For the purpose of the computational applications here employed, the reference moving frames of the track and rail are discretized in particular locations and stored as a track and rail geometry database, such way that, by linear interpolation, the complete track geometry is available whenever required.

The procedure to obtain the track and rails reference moving frames is schematized in Figure 4.2.

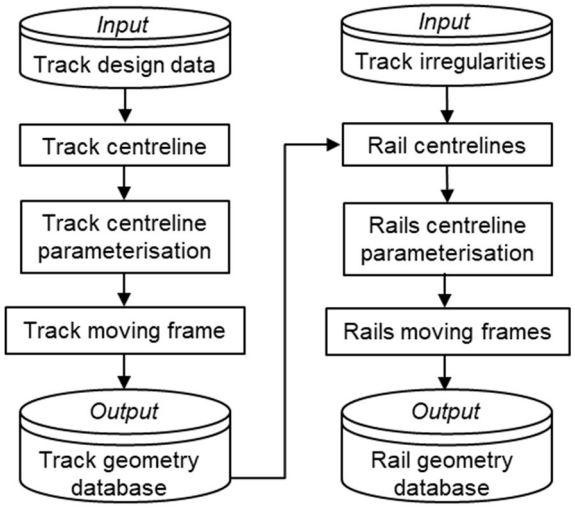

Figure 4.2: Schematic representation of the procedure to build the track and rails moving reference frames.

The track centreline spatial curve is obtained by performing the geometric reconstruction of the track geometry using the curvature and elevation data of the selected track [50]. Afterwards, the track centreline is parametrized using a polynomial interpolation scheme

through which a local moving frame of reference is built along the track using a methodology based on the evaluation and rotation of Frenet-Serret frame, [34]. The reference moving frame of each rail is constructed in similar fashion with the exception of the rails centrelines. These are obtained by superimposing the track moving frame with the geometry of the railway track such as the gauge, the rail inclination, β, and optionally, track irregularities.

4.1 Track and rail centrelines

By industry standards the general geometry of the track is described by the curvature, cross level and elevation in respect to the track length. Following the procedure proposed by Iverson W. C. [50], the track centreline, discretized by a set of coordinate points *(x,y,z)*, is obtained by the numerical solution of a set of differential equations expressed as:

$$\begin{aligned} dx/ds &= \sin(\theta)\cos(\phi) \\ dy/ds &= \sin(\theta)\sin(\phi) \\ dz/ds &= \cos(\theta) \\ d\phi/ds &= k(s)/\sin(\theta) \end{aligned} \tag{4.1}$$

where k corresponds to the track curvature in function of the track travelled length, s, and the derivative dz/ds is provided following the numerical differentiation of the track elevation. Note that the track cross level, or correspondingly the track cant angle, are not used here being this information only required afterwards when establishing the track moving frame.

The left and right rail centrelines are obtained with the aid of the track moving frame, established posteriorly. Here, for each given track length used to discretize the rail centrelines, the vector positions, $\mathbf{r}_{Lr}$ and $\mathbf{r}_{Rr}$, containing the Cartesian coordinate points that define respectively the left and right rails, are obtained by:

$$\begin{aligned} \mathbf{r}_{Lr} &= \mathbf{r}_c + \mathbf{A}_c \mathbf{s}'^{c}_{Lr} \\ \mathbf{r}_{Rr} &= \mathbf{r}_c + \mathbf{A}_c \mathbf{s}'^{c}_{Rr} \end{aligned} \tag{4.2}$$

where $\mathbf{r}_c$ is the global position vector that defines the track centreline and is the origin of the track local reference frame $(\xi,\eta,\zeta)_c$, as represented in Figure 4.3. Matrix $\mathbf{A}_c$ is the rotation matrix associated to the same local reference frame. Vectors $\mathbf{s}'^{c}_{Lr}$ and $\mathbf{s}'^{c}_{Rr}$ are correspondingly the positions of the rail geometric centres relative to the track local frame of reference evaluated as:

$$\mathbf{s}'^{Q}_{Lr} = \begin{Bmatrix} 0 \\ \frac{D}{2} + AL_{Lr} + \frac{\Delta G}{2} \\ LL_{Lr} \end{Bmatrix} \quad ; \quad \mathbf{s}'^{R}_{Rr} = \begin{Bmatrix} 0 \\ -\frac{D}{2} + AL_{Rr} - \frac{\Delta G}{2} \\ LL_{Rr} \end{Bmatrix} \tag{4.3}$$

where D is the distance between the rails cross section centres determined accordingly to the gauge, G, and the rail section profile as represented in Figure 4.4 .

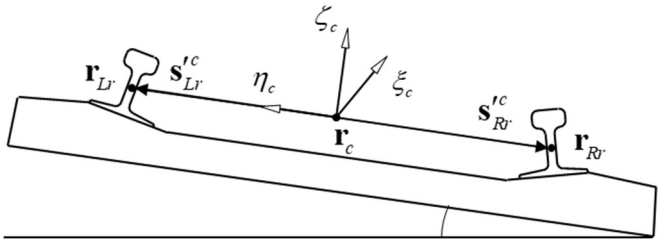

Figure 4.3: Geometric definition of the left and right rail centreline nodal points in relation to the track moving frame.

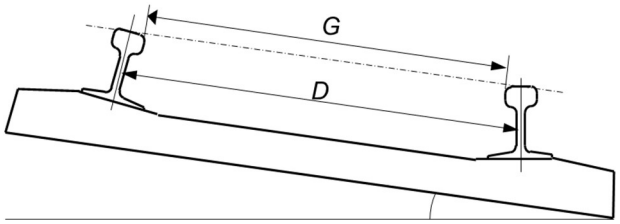

Figure 4.4: Representation of the track gauge, G, and the distance between left and right rail profiles, D.

Optionally, track irregularities can be considered such as the track gauge variation ΔG and the alignment, AL, and longitudinal level, LL, of the left, Lr, and right, Rr, rails. These represent the lateral and vertical displacements of the rails relative to their nominal position as presented in Figure 4.5. If these irregularities are not to be considered they are left null in Equation (4.3) .

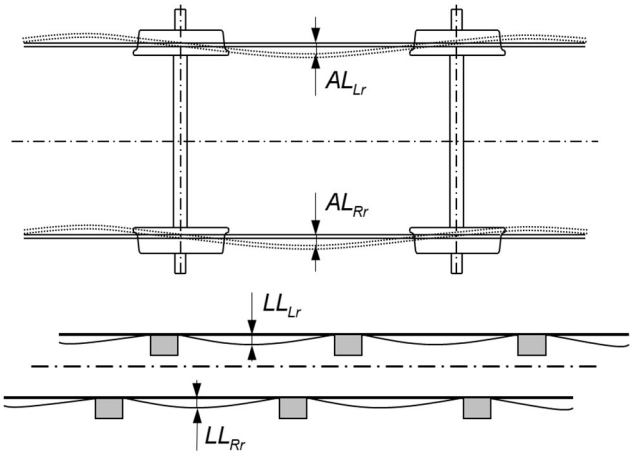

Figure 4.5: Representation of the left and right rails alignment and longitudinal level.

4.2 Centreline curve parameterisation

The parametrisation of complex curve geometries, such as the track and rails centrelines considered in this work, is generally realized by piecewise polynomial schemes [51]. The advantage of these interpolating procedures is that they exhibit local geometrical control, i.e., the variation of the position of a control point only affects the neighbourhood of that point, maintaining unchanged the rest of the curve. In order to establish the parameterization procedure, let us consider a collection of $k+1$ point coordinates, $\mathbf{p}$, that represent either the track or rail centreline curve, where the parametrized curve of the track is defined by k segments, $\mathbf{g}$. Each of these is defined by a n^{th} order interpolating polynomial, as represented in Figure 4.6.

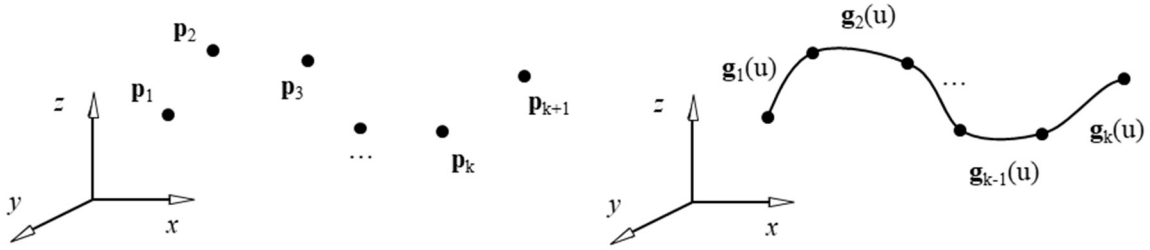

Figure 4.6: Track centreline curve parameterisation.

The interpolating polynomial segments that interpolate a set of control points are defined as:

$$\mathbf{g}(u) = \begin{Bmatrix} x(u) \\ y(u) \\ z(u) \end{Bmatrix} = \mathbf{a}_0 + \mathbf{a}_1\, u + \mathbf{a}_2\, u^2 + \mathbf{a}_3\, u^3 + \cdots + \mathbf{a}_n\, u^n \qquad (4.4)$$
$$\mathrm{u} \in \mathbb{R} : 0 \le \mathrm{u} \le 1$$

where $\mathbf{g}(u)$ is a point on the curve, u is the local parametric variable and $\mathbf{a}_i$ are the unknown algebraic coefficients that must be calculated using the boundary conditions, this is, segment end points [48,52]. Although equation (4.4) is generic for any polynomial interpolation, in this work, the consideration of the most reliable and adequate piecewise interpolation methodology is of critical importance. For this reason a cubic shape preserving spline, proposed by Irvine [53], is used.

In order to associate the spatial geometric characteristics of the track along its length, the local parametric variable u must be expressed as a function of the curve length, s. This association between s and u is defined such that:

$$s(u) = \sum_{n=1}^{k-1} s_n^1 + \mathrm{s}_k^{\mathrm{u}}(u) \qquad (4.5)$$

where k is the number of the interpolating segments from the first through where the point is actually located and s_i^{u} corresponds to the length of the i^{th} segment, from the start to where the local parametric variable u is located, given by:

$$s_k^{\mathrm{u}} = \int_0^u \sqrt{\mathbf{g}_k^{u^T} \mathbf{g}_k^u}\, du \tag{4.6}$$

where $\mathbf{g}^u$ is the derivative of $\mathbf{g}$ with respect to u. Note that, following this parameterization, the relationship between the local parametric variable $u \in [0,1]$ and the curve arc length, s, is not linear. Therefore, for a curve length, s, the corresponding local parametric variable, u, is found from equation (4.5) and (4.6) by solving:

$$\int_0^u \sqrt{\mathbf{g}_k^{u^T} \mathbf{g}_k^u}\, du - L_k^{\mathrm{u}} = 0 \tag{4.7}$$

Being a non-linear equation, it is solved numerically using the Newton-Raphson method [4,54].

4.2.1 Track and rail centreline curves moving frame

Although there are different available frames definitions for the purpose, the Frenet frame [55] is the basis to establish the track and rail moving reference frames as it provides an appropriate curve referential at every point. For a given track length, s, in correspondence to its local parametric variable, u, the unit vectors that characterize the Frenet frame are the unit tangent vector $\mathbf{t}$, the principal unit normal vector $\mathbf{n}$ and the binormal vector $\mathbf{b}$. These vectors, defined in the intersection of the normal, rectifying and osculating planes shown in Figure 4.7, are evaluated as [48,51],

$$\mathbf{t} = \frac{\mathbf{g}^u}{\left\| \mathbf{g}^u \right\|} \quad ; \quad \mathbf{n} = \frac{\mathbf{k}}{\left\| \mathbf{k} \right\|} \quad ; \quad \mathbf{b} = \tilde{\mathbf{t}}\,\mathbf{n} \tag{4.8}$$

where $\tilde{\mathbf{t}}\,\mathbf{n}$ means a cross product and the auxiliary vector $\mathbf{k}$ given by

$$\mathbf{k} = \mathbf{g}^{uu} - \frac{\mathbf{g}^{uuT}\mathbf{g}^u}{\left\| \mathbf{g}^u \right\|^2} \mathbf{g}^u \tag{4.9}$$

where $\mathbf{g}^u$ and $\mathbf{g}^{uu}$ denote, respectively, the first and second derivatives of the parametric curve $\mathbf{g}(u)$ with respect to the parametric variable u.

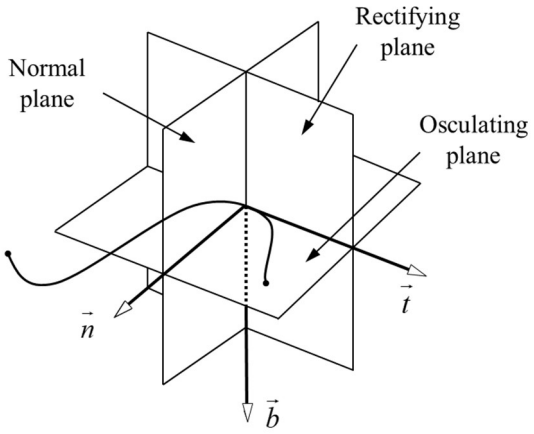

Figure 4.7: Representation of the Frenet frame (**t**,**n**,**b**).

Note that, at this point, the obtained Frenet frame does not consider the track cross level, *h*, or the corresponding cant angle, φ ,represented in Figure 4.8. For tracks with a full spatial geometry it is not clear what reference plane relative to which the cant angle should be defined, as in the horizontal plane represented on Figure 4.8. It is proposed here that the osculating plane [49], associated to the Frenet frame, plays the role of the horizontal plane in flat tracks, when measuring the cant angle.

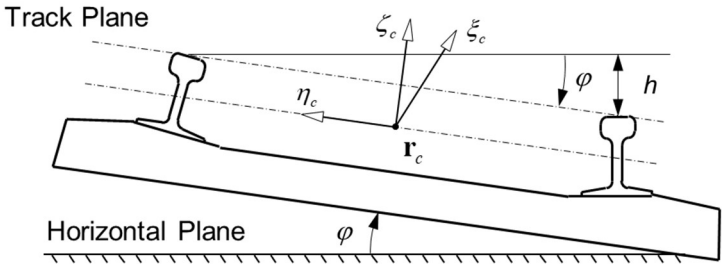

Figure 4.8: Representation of the track cross level, *h*, and corresponding cant angle, φ.

Therefore, the cant angle φ sets the angle between the principal unit normal vector **n**, which lies in the osculating plane as represented in Figure 4.8, and the track unit normal vector η_c, which is associated to the defined track moving frame $(\xi,\eta,\zeta)_c$. Hence the track moving frame is obtained after the rotation of the Frenet frame, (**t**,**n**,**b**) , about the **t** axis by the cant angle, φ, as depicted in Figure 4.9.

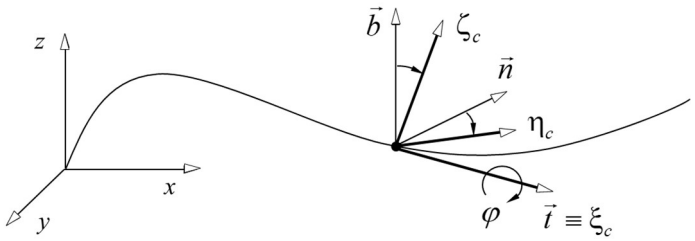

Figure 4.9: Cant angle contribution to the track model.

This way, at a given track length, the principal unit vectors, $(\xi,\eta,\zeta)_c$ that define the track moving frame are obtained as:

$$\xi_c = \mathbf{A}^T\mathbf{t} \quad ; \quad \eta_c = \mathbf{A}^T\mathbf{n} \quad ; \quad \zeta_c = \mathbf{A}^T\mathbf{b} \tag{4.10}$$

where **A** is the rotation matrix expressed, in the compact form, as:

$$\mathbf{A} = (2e_0^{\,2} - 1)\mathbf{I} + 2(\mathbf{e}\mathbf{e}^T + e_0\tilde{\mathbf{e}}) \tag{4.11}$$

such that e_0 and the components of vector **e** are the Euler parameters associated with the finite, φ, rotation about **t** axis, defined as:

$$\begin{aligned} e_0 &= \cos(\varphi) \\ \mathbf{e} &= \begin{bmatrix} e_1 \\ e_2 \\ e_3 \end{bmatrix} = \mathbf{t}\sin\left(\frac{\varphi}{2}\right) \end{aligned} \tag{4.12}$$

Note that, in this procedure the track cant irregularity, $\Delta\varphi$, may also be considered such that at a given track, *s*, that the rotation angle, φ, is defined as:

$$\varphi(s) = \varphi_n(s) + \Delta\varphi(s) \tag{4.13}$$

where φ_n is the nominal track cant angle and $\Delta\varphi$ is the corresponding irregularity. Furthermore, the rail centrelines are obtained following the same procedure considering the addition of the rail inclination on the track.

5 Finite Element Methodology for the Railway Catenary and Track

The motion of both the catenary and track systems is characterized by small rotations and small deformations, therefore a finite element formulation to tackle the modelling of these systems is the most appropriate computational procedure to be used. Each of these systems has their own modelling requirements that the established finite element formulation must be able to handle. Nevertheless, the overall modelling needs can be arranged into one unique formulation. Since the use of a nonlinear finite element formulation can significantly impact the numerical computation effort, in this work steps are taken to solve well identified nonlinearities using a linear finite element formulation. Furthermore, the selection of a time integration numerical procedure to solve the governing dynamic equilibrium equations of a system is usually decided by engineering judgement. Such decision must consider not only the stability and accuracy of the selected algorithm but also its computer processing effort. In the case of the systems here studied, an integration algorithm based on the implicit Newmark trapezoidal rule is proposed.

5.1 Catenary Modelling

Railway catenaries are periodic structures that ensure the availability of electrical energy for the train vehicles running under them. A typical catenary structure, of the simple type, is composed by two main suspended cable wires, the contact wire and the messenger wire, which are set in tension along the track by mechanical tensioning devices mounted at the end poles of each catenary section. Both the contact and messenger wires are periodically supported by cantilevered consoles, known as cantilevers, mounted in poles, as represented in Figure 5.1. To provide clearance for the pantograph passage and to allow vertical movement of the contact

wire its supporting connection to the cantilever is achieved by a steady arm, which is fixed on the cantilever by a pin joint. In between each pole, the contact wire is promptly supported by dropper cables that hang from de messenger wire to reduce its sag and keep its vertical elasticity as uniform as possible along its span.

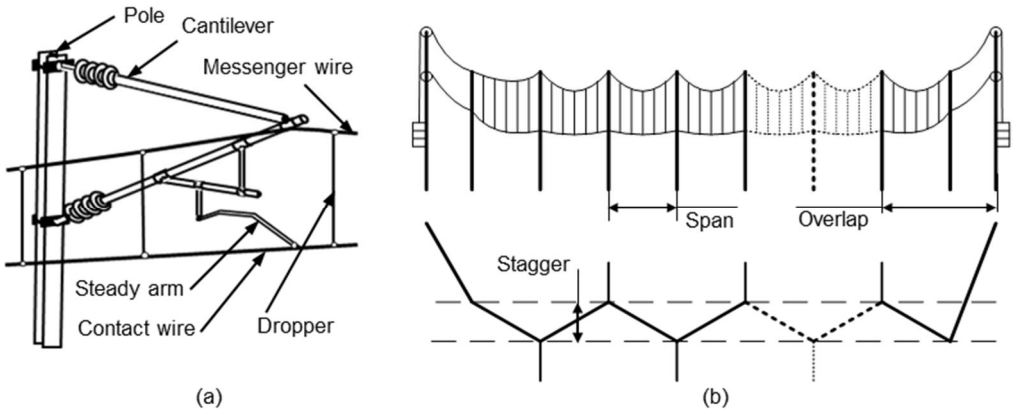

Figure 5.1: Catenary structure and its main components: (a) Cantilever; (b) Longitudinal and top view.

Due to physical limitations each section as a limited length, hence the continuity of the contact wire, as seen by the pantograph contact strip, is assured by overlapping catenary sections at its ends.

Note that different catenary designs exist [12,56], with slightly different or more accentuated topological arrangements such as the stich-wire and compound catenaries. However, simple alternatives are more extensively used due to being more cost-effective and easier to maintain. Nevertheless, in all cases both messenger and contact wires are tensioned with high axial forces not only to ensure the correct geometry, i.e., to limit the contact wire sag between poles, but also to allow the correct wave travelling speed to develop. One of the critical parameters that limits the operational velocity of the trains is the wave propagation velocity on the contact wire [57]. When the train speeds approach the wave propagation velocity of the contact wire, called critical velocity, the contact between the pantograph and the catenary is harder to maintain due to increase in the amplitude of the catenary oscillations and bending effects. In order to avoid this deterioration of the contact quality the train speed should not exceed 70-80% of the contact wire wave propagation speed [15].

To avoid grooving and ensure, as much as possible, a uniform wear of the pantograph contact strip an alternating lateral offset of the contact wire, commonly known as stagger, is imposed by the steady arm at each cantilever. The positioning of these offsets along each cantilever must take into consideration the catenary design, the track geometry and specified operational requirements set by the infrastructure owners/managers and standards [58,59].

Generally, the offsets are determined in order to keep the span lengths as long as possible, to reduce construction costs, while still ensuring that the contact wire deflection, under wind conditions, never exceeds a permissible lateral displacement, e_{perm}, such that the contact wire is always within the usable length of the contact strip [60]. In straight lines and very large radius curves this results in an alternating offset pattern *(±b)*, or *zig-zag*, as represented in Figure 5.2 (a). Note that the lateral forces, $\mathbf{f}_{sp}$, at the contact wire supports, which result from the imposed change of direction of the tensioned contact wire, have defined maximum and minimum tolerances. Also, a minimum lateral sweep of the contact wire must be ensured to avoid grooving [56]. As a result of these constraints with the track curvature increase a reduction of the offset at the inner side of the curve is required, thus forcing $b_1 \neq b_2$.

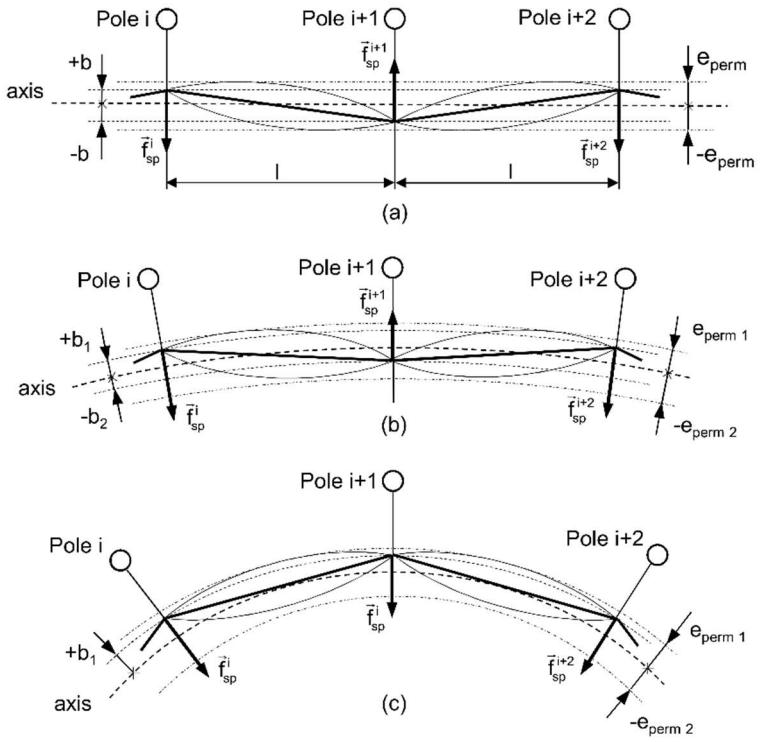

Figure 5.2: Contact wire lateral position on: (a) Straight track, (b) Large radius curves; (c) Small radius curves.

For small radius curves the offset is placed always on the outside side of the curve, i.e., *(+b1,+b1).* Eventually, for even smaller radius it is not possible to use suitable offsets while maintaining the span length and shorter spans need to be used.

5.1.1 Catenary geometry along the track

Given that the catenary models considered in this work are set in any generalized trajectory of the track, the geometric description of the catenary, defined by the catenary layout geometry in relation to the track running surface, is the basis of the construction of the models. In this work

the spatial geometry of the catenary starts being defined by establishing the geometric positions of the contact and messenger wire at the cantilever. With reference to Figure 5.3, at each cantilever, the positions of the contact wire at the steady arm, $\mathbf{r}_{cw}$, and the messenger wire at its cantilever support, $\mathbf{r}_{mw}$, are determined as:

$$\begin{aligned} \mathbf{r}_{cw} &= \mathbf{r}_t + \mathbf{A}_t \mathbf{s}'^t_{cw} \\ \mathbf{r}_{mw} &= \mathbf{r}_{cw} + \mathbf{s}^{cw}_{mw} \end{aligned} \tag{5.1}$$

where $\mathbf{r}_t$ is the position vector of the track centreline and $\mathbf{A}_t$ is the rotation matrix associated to the local reference frame, $(\xi,\eta,\zeta)_t$, which defines the track running surface orientation. These quantities are obtained by the evaluation of the track moving frame, described in Section 4, at the track length in which the pole is mounted. Vectors $\mathbf{s}'^t_{cw}$ and $\mathbf{s}^{cw}_{mw}$ are, respectively, the position of the contact wire with respect to the local reference frame $(\xi,\eta,\zeta)_t$ and the position of the messenger wire relation to the contact wire position, $\mathbf{r}_{cw}$, evaluated as:

$$\begin{aligned} \mathbf{s}'^t_{cw} &= \begin{bmatrix} 0 & \pm b & h_{cw} \end{bmatrix}^T \\ \mathbf{s}^{cw}_{mw} &= \begin{bmatrix} 0 & 0 & h_e \end{bmatrix}^T \end{aligned} \tag{5.2}$$

where the parameters b, h_{cw} and h_e are respectively, the contact wire lateral offset relative to the track centreline, the nominal contact wire height relative to the running surface and the encumbrance of the cantilever which sets the distance between the contact and messenger wire.

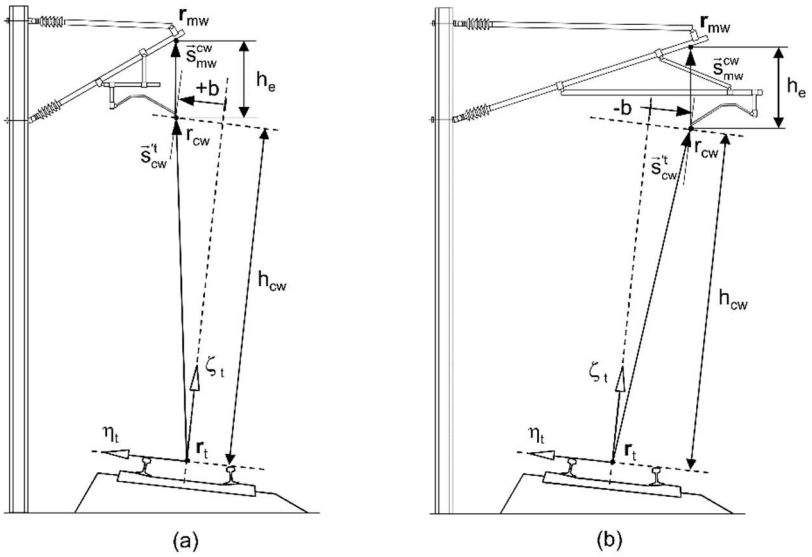

Figure 5.3: Representation of the contact and messenger wire position on the cantilever, in a curved track: (a) pull-off configuration; (b) push-off configuration.

To complete the spatial definition of the catenary geometry it is also required to define

the geometric positions of the contact and messenger wires at their dropper connections, $\mathbf{d}_{cw}$ and $\mathbf{d}_{mw}$, as presented in Figure 5.4. At each span, these positions are found by superimposing the already determined contact and messenger wire position at the cantilevers, $\mathbf{r}_{cw}$ and $\mathbf{r}_{mw}$, with the catenary span layout geometry defined by the dropper spacings, a_d, the dropper lengths, l_d, and the appointed contact wire pre-sag set at each dropper, s_d. In practice these parameters are set in pre-calculated span tables for a collection of normalised span lengths, l_{span}, of a particular catenary design.

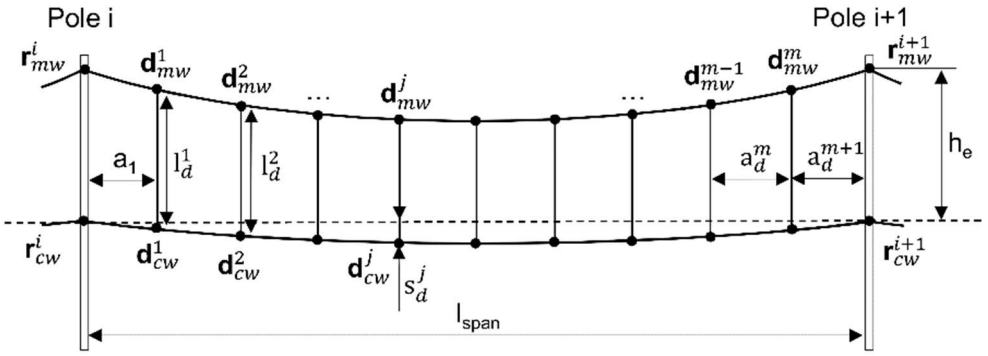

Figure 5.4: Catenary span geometric parameters.

5.1.2 Finite element catenary model

When modelling catenary systems, two main concerns need to be addressed, the line tensioning and the dropper slacking.

The line tensioning on a catenary, refers to the constant mechanical tension imposed on the catenary wires, respectively the contact wire, $\mathbf{f}_{cw}$, and the messenger wire, $\mathbf{f}_{mw}$, as depicted in Figure 5.5 (a). This effect is achieved by a set of pulley system with weights mounted on both ends of a catenary section, as shown in Figure 5.5 (b). Less often hydraulic tensioners are also employed but in either cases these systems ensure a constant tension imposed on the wires considering temperature changes. By tension the wires their oscillations resulting from the pantograph-catenary contact have a wave propagation speed faster than the train. This avoids the increase in the amplitude of the catenary oscillations and bending effects that would otherwise not only introduce more disturbances on the contact but also cause excessive wear and possible wire breakage. Also, the line tensioning has a direct effect on the contact wire sag which should be as reduced as possible. Evidently the more sag is present in a contact wire the less constant the contact force will be as more perturbation is introduced on the contact.

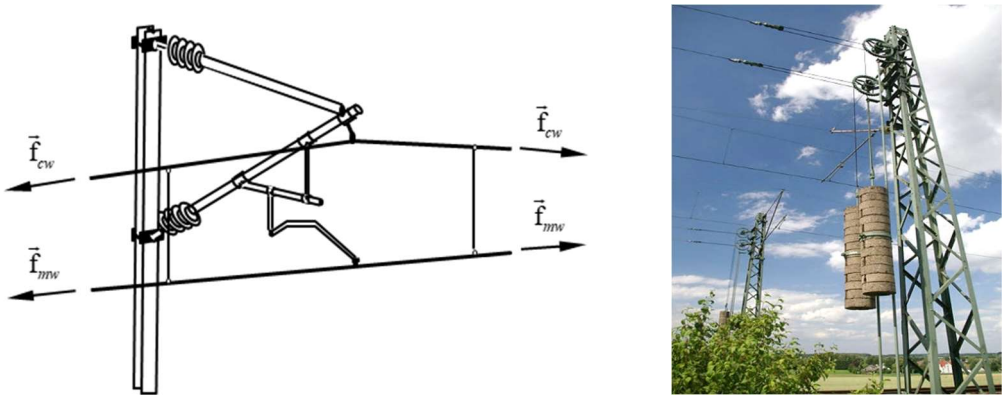

(a) (b)

Figure 5.5: (a) Representation of the line tensioning forces on the catenary wires; (b) Pulley system for line tensioning (Photo by Rainer Knäpper / CC BY-SA 2.0 DE)

The dropper slacking is also an important nonlinear behaviour that is necessary to consider in any catenary dynamic analysis tool. When supporting the contact wire, the dropper is in a tension stress state. However, when the pantograph passes under the dropper, it is compressed and its tension vanishes. As the dropper is a braided cable, which does not offer any compressive resistance, it slacks transmitting no reaction forces to the rest of the catenary system, as depicted in Figure 5.6.

(a) (b)

Figure 5.6: Dropper slacking: (a) Pantograph-catenary contact is maintained, (b) Loss of contact with arcing.

The dropper slacking represents a nonlinearity when modelling the dynamic behaviour of the catenary. Nonlinear problems usually require more complex numerical methodologies that lead to a larger computational cost. However, this nonlinearity is well localized and its implied behaviour is known. Thus, by adding corrective measures on the numerical solution of the problem a linear methodology can still be used, avoiding the use of more complex methodologies and saving valued computational time.

As motion of the catenary is characterized by small rotations and small deformations the catenary is here modelled with linear finite elements, [5], where compensating forces are

added whenever dropper slacking occurs. Also, to account for the high-tension forces on the contact and messenger wires, pre-stress forces are added to the finite elements representing them as well as their stress stiffening is considered. The finite element formulation and the solution of the resulting dynamic equilibrium equations is presented in Section 5.3. All catenary structural components are modelled with a 2 node, 6 degree of freedom beam elements based on Euler Bernoulli beam theory [61], with the following two exceptions. The claws and clamps that hold the structure together on the dropper/contact-wire/messenger-wire and steady-arm/contact-wire junctions are modelled as lumped masses. The messenger wire cantilever support is modelled after an equivalent three dimensional spring-damper element with equivalent vertical, transverse and longitudinal stiffness and damping, as represented in Figure 5.7. Moreover, the model is constrained by pinned points at the ends of the contact and messenger wires as also at the steady arm on the cantilever side and at the end of each cantilever messenger wire support.

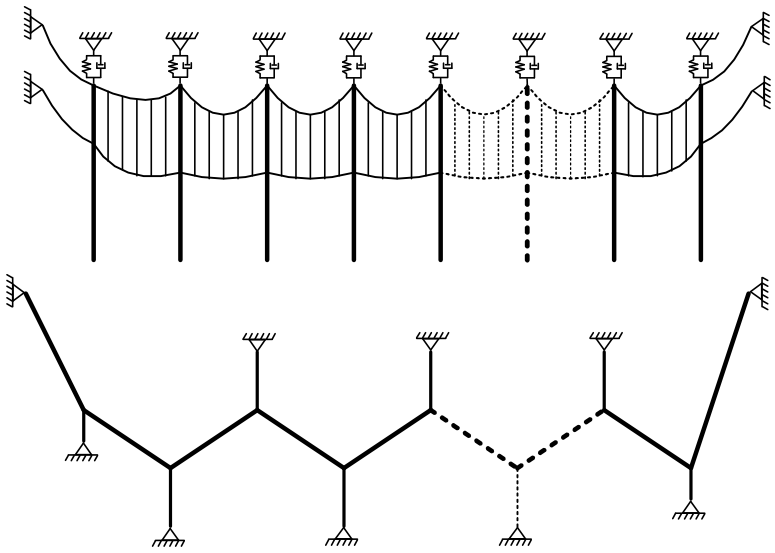

Figure 5.7: Representation of the finite element catenary model.

To ensure the correct representation of the wave propagation, resulting from pantograph-catenary contact, at least 6 elements must be used in between droppers to appropriately model the contact and messenger wires [62]. There is no special requirement on the number of elements required to model each dropper, and steady-arm. The finite element catenary mesh is built according to the catenary geometry data established which is built following provided track design and catenary layout data. As an example of this procedure, for the track geometry followed in Figure 5.8 the resulting finite element mesh is presented in Figure 5.9. Note that the catenary system considered is composed of two sections and includes the representation of the overlapping spans. One other aspect taken into consideration when

constructing the finite element mesh is its resulting statically deformed shape which must present a rigorous representation of the catenary geometry considered. For this propose an initialisation procedure is employed to find the undeformed catenary mesh configuration that upon being statically loaded provides an accurate representation of the catenary.

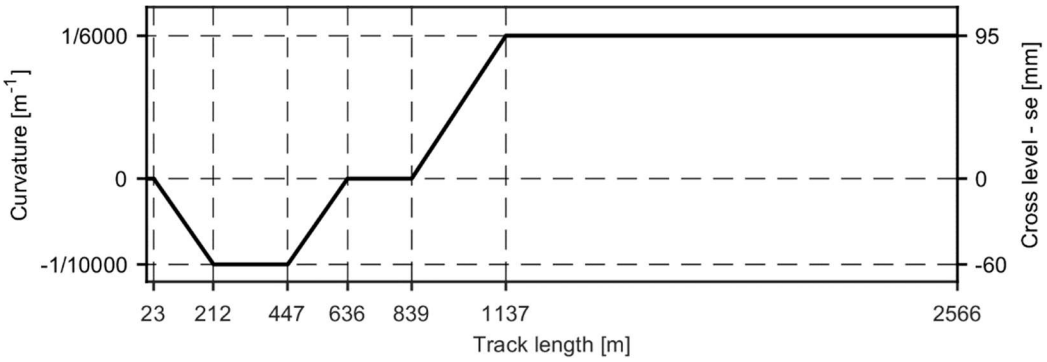

Figure 5.8: Track curvature and cross level set along the track length.

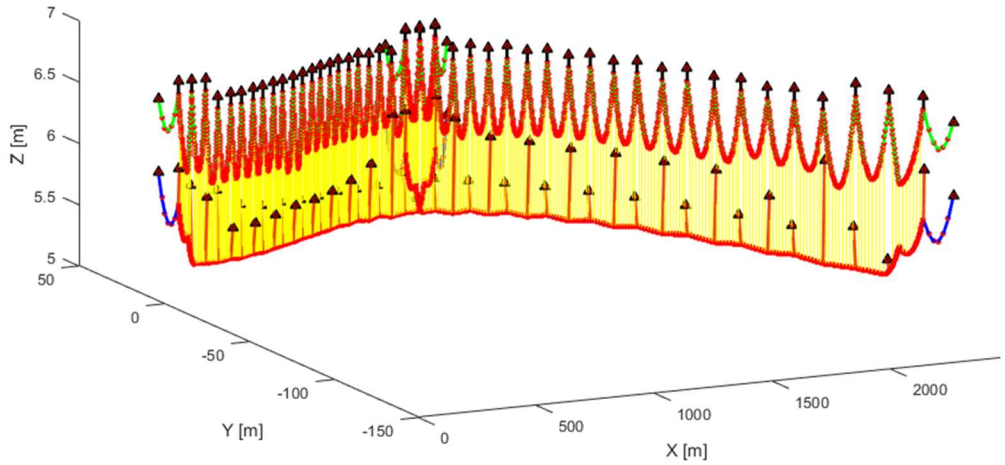

Figure 5.9: Representation of the deformed finite element catenary mesh.

5.1.3 Catenary Initialisation

The catenary initialization corresponds to the procedure set to determine the undeformed mesh of the model that upon being statically loaded by the gravitational and axial tension loads exhibit a correct static deformed shape, with special attention to the contact wire position along the track and its sag. In reality, a similar problem exists when mounting a catenary system on track where, after the first mounting stage, the catenary must be adjusted to fit all geometric specifications. These adjustments are generally comprised on regulating the dropper lengths and the steady arm position at the cantilever in order that the contact wire stays at its defined positions. In analogy to this procedure the catenary initialization is formulated here as a minimisation problem, to be solved using a classical gradient based optimisation procedure [63]. Here the minimization problem is defined as:

$$\min\left(\sum_{1}^{m}\left\|\mathbf{d}_{cw}^{S\,\mathrm{m}}(\mathbf{x})-\mathbf{d}_{cw}^{\mathrm{m}}\right\|\right)$$
$$\text{subject to: } \mathbf{x}=\left[l_0^1, l_0^2, \ \ldots\ , l_0^m\right] \tag{5.3}$$

where the initial dropper lengths, l_0, are set as design variables used to construct the catenary model. The evaluation of the fitness function implies the static analysis of the generated finite element mesh. Afterwards, the deviations between the deformed contact wire positions at the droppers, $\mathbf{d}_{cw}^{S}$, and their nominal positions, $\mathbf{d}_{cw}$, are evaluated. The minimisation problem is solved iteratively for each span where also pinned point constraints are added on the contact and messenger wire cantilever supports, as represented in Figure 5.10 (a). After the minimisation problem being solved, these constraints are released and substituted by pre-stress forces imposed on the messenger wire support element and the steady arm element. At the contact wire support, the solicitation on each constraint is decomposed on a lateral offset force, $\mathbf{f}_{lat}$, which results from the imposed stagger and a vertical force, $\mathbf{f}_z$, resulting from a residual support of the contact wire weight. These forces are not only used to calculate the pre-stress force to be applied on the equivalent steady arm beam element, $\mathbf{f}_{ps}$, but are also used to set its orientation, as represented on Figure 5.10 (b).

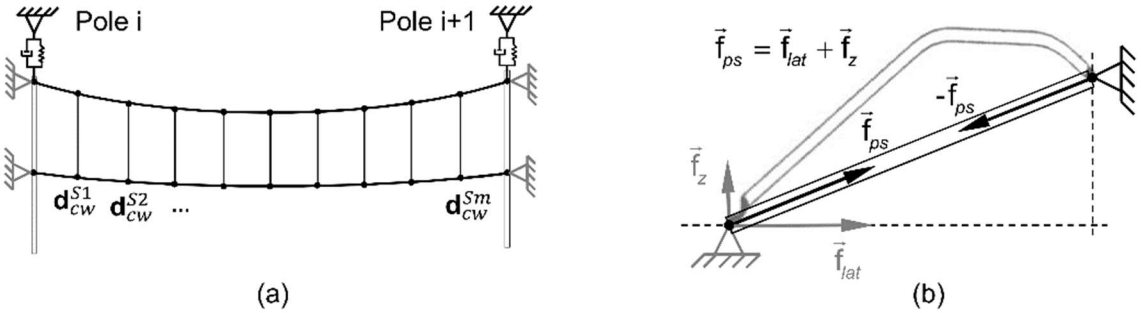

Figure 5.10: (a) Representation of the deformed catenary span resulting from the solution of the minimisation problem; (b) Representation of the steady-arm pre-stress forces and their orientation.

5.2 Track Modelling

The railway track is composed by a set of rails, responsible to guide the vehicles, followed by a series of elements with distinct elasticity. These ensure the correct settlement of the rails in their correct position and provide a gradual transmission of the dynamic loads, solicited by the passage of the trains, to the subsoil. In general, the common railway track is formed by the steel rails which are supported by sleepers positioned transversally to the track, as detailed in Figure 5.11. The connection of these elements is ensured by a fastening system which includes a pad element set in between. The pad provides an extra layer of elasticity and damping which reduces

the impact between the rail and the sleeper and reduces vibration on the railway system. The sleepers are usually made of wood or pre-stressed concrete and rest on a layer of ballast or in other cases, not here considered, are fixed to a specially constructed concrete slab. The track ballast is customarily composed of crushed stone with the purpose to support the sleepers and give way for their adjustment and also allow drainage. Below the ballast stays the substructure comprised of a set of layers, the sub-ballast made of smaller crushed stones, the form layer set to restrict clay and silt to move upwards, and the subsoil.

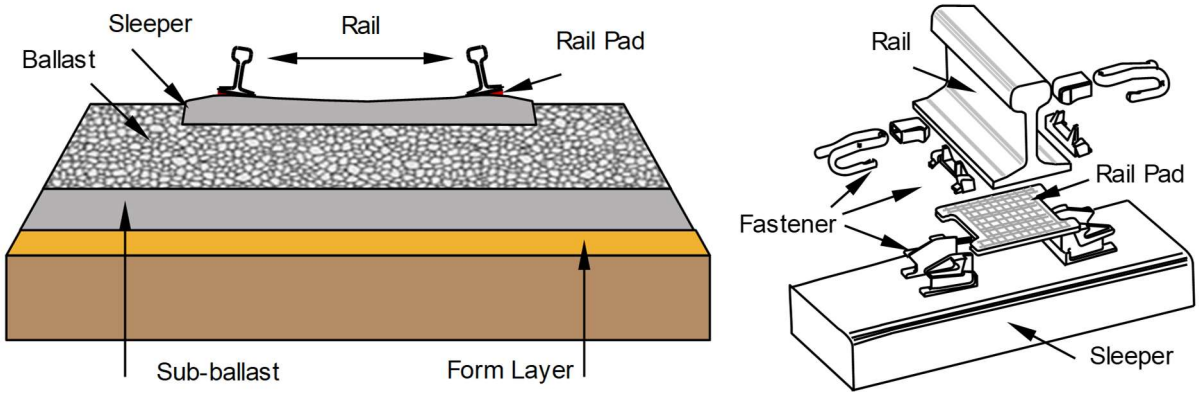

Figure 5.11: Typical construction of a railway track with its structural components: a) Track including the ballast and substructure b) Exploded view of the fixation of the rail to the sleeper

The railway track is modelled using the finite element method being its dynamics analysed with suitable numerical methods. The track model finite element discretisation is first described here being the systematic generation of the finite element model according to the track geometry described afterwards.

5.2.1 Finite element track model discretisation

The railway track is composed by several structural elements: rails, fasteners, rail pads, sleepers, ballast or slab and the substructure. In this work, the track model is assumed to have only linear deformations being its model built with linear finite elements. As represented in Figure 5.12 and Figure 5.13, the rails and sleepers are modelled by three-dimensional beam elements, based on Euler-Bernoulli theory [5], the rail pads and fasteners and track supporting layers are modelled with 6 degrees of freedom spring-damper elements. Lumped mass description of the inertia of the finite elements is used in the finite element mass matrix formulation for the model.

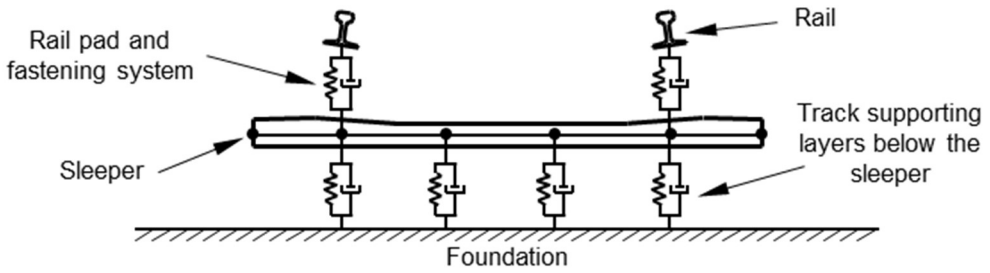

Figure 5.12: Cross section view of the track model.

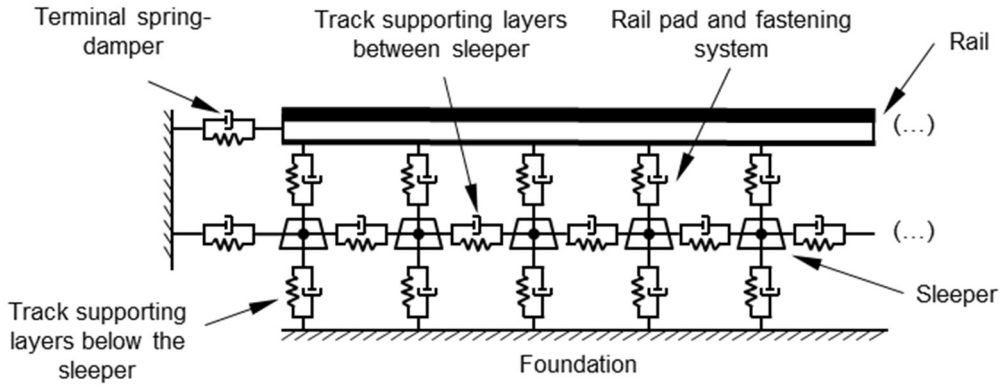

Figure 5.13: Longitudinal view of the track model.

The rails are modelled with beam elements being 6 elements used between sleepers to ensure a proper geometry in curves. The sleepers are symmetric being the model of each one made of 5 beam elements to accommodate transitions of cross-section and/or material properties characteristic of these structural elements. The connection between the sleeper and the rail is modelled using a single spring-damper element with translational stiffness and damping along three perpendicular directions, which represents the sleeper pad, and rotational stiffness along the tangent direction of the rail, which is representative of the rail fastening system that prevents the rail from rotating. The track supporting layers are modelled considering two types of spring-damper elements: those connecting the sleepers to the foundation and those connecting two consecutive sleepers. The sleeper to foundation connection is represented by the vertical elements below the sleepers, depicted in Figure 5.12, and accounts for the flexibility of the supporting layers directly below the sleeper. The sleeper to sleeper connection represented by the in track-plane elements connecting the sleepers, as depicted in Figure 5.13, accounts for the interlocking action of the supporting structure, i.e., the ballast or the slab.

The track supporting layers consider translational stiffness and damping along three perpendicular directions. The foundation is modelled as a fixed “rigid” ground constraining the lower nodes of the track supporting layers finite element mesh. Finally, to avoid the elastic wave reflection characteristic of finite length models intended to represent infinite or very long tracks, massless spring-damper elements are added to the beginning and to the end of the

railway track and constrained. By selecting proper damping characteristics for the terminal spring-damper elements the elastic wave reflection is prevented.

5.2.2 Systematic generation of the track finite element model

The track geometrical description, based on the track and rail reference moving frames, described in Section 4, is the basis of the finite element model construction [33,64]. Here, the finite element mesh of the track is obtained by superimposing the track geometrical description, with the track finite element model discretisation, as represented in Figure 5.14.

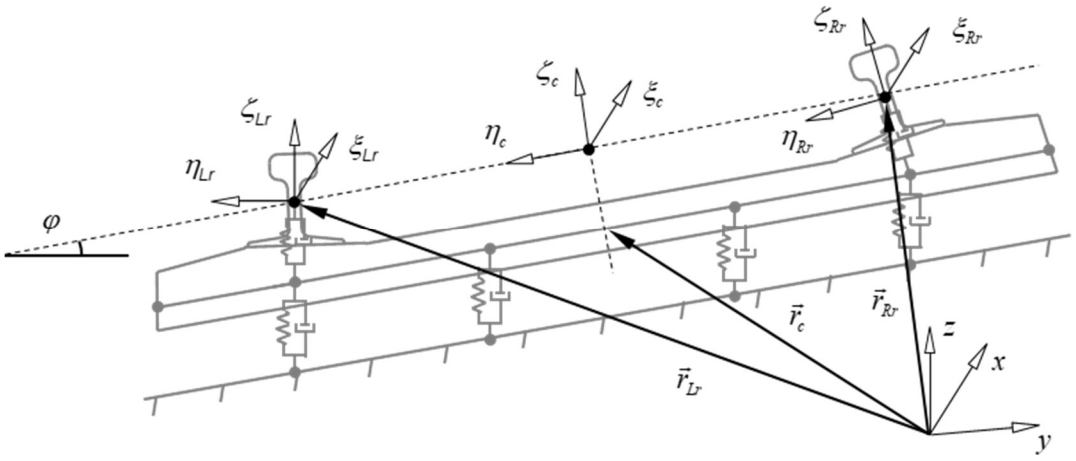

Figure 5.14: Elements of the finite element mesh of the track: (a) Position coordinates and local reference frame of the track and rails; (b) Mesh for the railway track.

Using the geometric description of the left and right rails, as a function of their arc length, the position of the nodes of the rails, $\mathbf{r}_{Lr}$, $\mathbf{r}_{Rr}$, are defined as well as the local nodal coordinate frames ($\xi_{Lr},\eta_{Lr},\zeta_{Lr}$) and ($\xi_{Rr},\eta_{Rr},\zeta_{Rr}$), for the left and right rails respectively. The finite element mesh of the track includes nodes placed in planes for which the tangent vector to the track centreline is normal spaced such a way, along the centreline arc-length, that they include the sleepers, pads and fasteners. In this case, there are two nodes associated with the rail cross-section centre, six nodes along the sleepers to enable modelling mono-block, twin-block and timber sleepers, and four nodes for the track foundations. In-between sleepers, there are five rail nodes equally spaced along the rail curves. The beam finite elements used for the rails have their cross-section oriented according to the local reference frame of each rail. The beam elements used to model the sleepers depend on their geometry while the spring-damper elements used to represent the ballast resistance in the tangent-to-track plane and in its vertical direction are set in between the sleeper nodes and either the foundation or other sleeper nodes. In Figure 5.15 a representation of the finite element mesh, for a track composed by a straight section followed by a 500m radius curve, is presented.

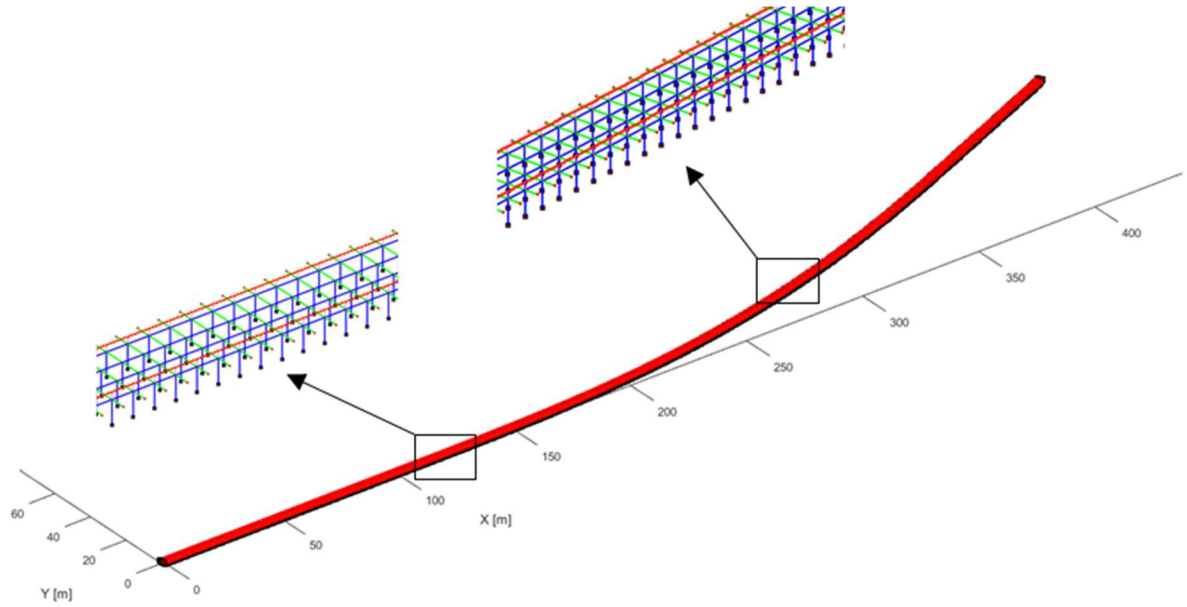

Figure 5.15: Representation of a finite element mesh of a track model.

5.3 Dynamic analysis of the catenary and track finite element models

Using the finite element method, the dynamic equilibrium equations for the catenary and track structural system, at time $t+\Delta t$, are assembled as [5,65],

$$\mathbf{M}\,\mathbf{a}_{t+\Delta t} + \mathbf{C}\,\mathbf{v}_{t+\Delta t} + \mathbf{K}\,\mathbf{d}_{t+\Delta t} = \mathbf{f}_{t+\Delta t} \tag{5.4}$$

where **M**, **C** and **K** are the finite element global mass, damping and stiffness matrices of the considered finite element models. The accelerations, velocities and displacements vector are represented respectively as **a**, **v** and **d** while the sum of all external applied forces is depicted by vector **f**. In order to represent accurately the stress stiffening of the catenary contact and messenger wire, due to their tension stress state caused by the wire tensioning with high axial forces, the beam finite element used for these wires, designated as element *i*, is written as:

$$\mathbf{K}_i^e = \mathbf{K}_L^e + F\,\mathbf{K}_G^e \tag{5.5}$$

in which $\mathbf{K}^e{}_L$ is the linear Euler-Bernoulli beam element stiffness matrix, F is the axial tension and $\mathbf{K}^e{}_G$ is the element geometric matrix. The global stiffness and mass matrices, **K** and **M**, are built by assemblage of the matrices of the elements according to the mesh and type of element. To model the damping behaviour of the system, proportional damping is used, also known as Rayleigh damping [65], such that the global damping matrix **C** is evaluated as

$$\mathbf{C} = \alpha\mathbf{K} + \beta\mathbf{M} \tag{5.6}$$

where parameters α and β are defined to represent an adequate damping response of the system within the reasoning of the overall stiffness and mass characteristics of the system. It is also

possible to implement a more particular approach of this method by evaluating a proper damping matrix $\mathbf{C}^e$ for each element as

$$\mathbf{C}^e = \alpha^e \mathbf{K}^e + \beta^e \mathbf{M}^e \tag{5.7}$$

where α^e and β^e are proportionality factors associated with each type of catenary element *e*. In this case the global **C** matrix is also obtained by assemblage of the elements damping matrices. The force vector, **f,** containing the sum of all external applied loads, is evaluated at every time step of the time integration. For a time $t+\Delta t$, the force vector is calculated as:

$$\mathbf{f}_{t+\Delta t} = \mathbf{f}^g + \mathbf{f}^t + \mathbf{f}^c_{t+\Delta t} + \mathbf{f}^d_{t+\Delta t} \tag{5.8}$$

where the vector $\mathbf{f}^g$ contains the gravitational forces of all elements. Exclusively for the catenary model and otherwise null, vector $\mathbf{f}^t$ is made of the forces responsible for tensioning the catenary wires, individually applied at each tensioned element as pre-stress. Both $\mathbf{f}^g$ and $\mathbf{f}^t$ remain constant along time. The force vector $\mathbf{f}^c$ represents either the pantograph-catenary or wheel-rail contact forces being evaluated as,

$$\mathbf{f}^c_{t+\Delta t} = \sum_i \left(\mathbf{B}_c \mathbf{f}_c\right)_i \tag{5.9}$$

where $\mathbf{f}_c$ contains the equivalent contact forces and transport moments to be applied at the appropriate nodes of the element where a resulting contact force *i*, at time $t+\Delta t$, is to be applied. Matrix $\mathbf{B}_c$ means the Boolean operation of assembling each contact force $\mathbf{f}_{c\ \mathrm{i}}$ in the global force vector. The point of application of the contact forces and its evaluation is done at each integration time step by geometric interference using the respective contact model. Also, exclusively for the catenary model, the force vector $\mathbf{f}^d_{t+\Delta t}$ contains dropper slacking compensating terms which need to be evaluated at each time step whenever a dropper is slack. Otherwise this vector is null. Although the droppers perform as bar elements during extension, which is most of the time, their stiffness during compression is either null or about $1/100^{\text{th}}$ of the extension stiffness. This extent occurs when contact forces are applied in the vicinity of the dropper. As the droppers stiffness is included in the global stiffness matrix $\mathbf{K}$, anytime one of the droppers is compressed its contribution to the catenary stiffness needs to be removed or modified to include the dropper slacking. In order to keep the dynamic analysis linear, the strategy pursued here is to add dropper compensating forces that cancel the stiffness contribution of any compressed dropper *i*, in the stiffness matrix. This is done by adding the vector force $\mathbf{f}^d_{t+\Delta t}$, to the global vector $\mathbf{f}$, equal the dropper compression force such that:

$$\mathbf{f}_{t+\Delta t}^{d} = \sum_{i} \left(\mathbf{B}_{d} \mathbf{K}_{d}^{e} \tilde{\mathbf{d}}_{t+\Delta t} \right)_{i} \tag{5.10}$$

where $\mathbf{K}_{d}^{e}$ is the dropper *i* element stiffness matrix and $\tilde{\mathbf{d}}_{t+\Delta t}$ is a close prediction of the dropper node displacements. The Boolean matrix $\mathbf{B}_{d}$ simply maps the global nodal coordinates into the coordinates of the dropper element, having the same meaning as for the contact forces.

In other to solve the equations of motion established in (5.4) a time integration numerical procedure is developed based on an implicit Newmark family integration algorithm [65,66] with trapezoidal rule (γ =1/4, ζ=1/2) and fixed time step. This particular method was chosen due to its unconditional stability nature when used implicitly and its proven robustness in finite element applications of the type demonstrated in this work. Furthermore, this methodology, is compatible with a **LU** factorization which significantly improves the efficiency of the numerical evaluation, as represented in Figure 5.16.

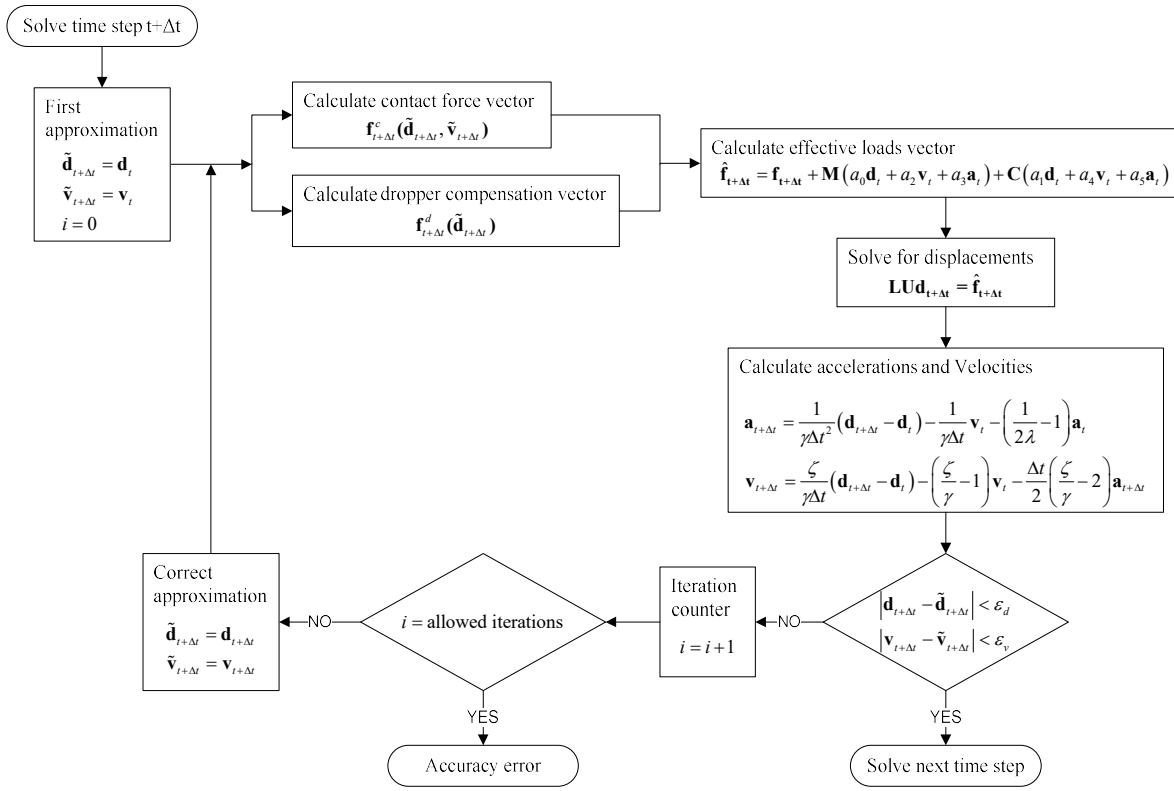

Figure 5.16: Flowchart of the integration algorithm steps as each time step.

The integration algorithm established involves the calculation of the effective loads vector iteratively. As the external loads vector, is not constant in time the effective loads vector must be calculated at every integration time step. Moreover the evaluation of the contact forces and dropper compensation forces, as expressed in equations (5.9) and (5.10), depend on a close prediction of the node displacements and velocities that would belong to the solution of the

dynamic equilibrium equations at the same time step. In order to be accurately close to this prediction, the approximation of the displacements and velocities is evaluated iteratively within each time step of the integration algorithm until a good convergence is reached. Thus, this correction procedure is done iteratively until, $\left|\mathbf{d}_{t+\Delta t} - \tilde{\mathbf{d}}_{t+\Delta t}\right| < \varepsilon_d$ and $\left|\mathbf{v}_{t+\Delta t} - \tilde{\mathbf{v}}_{t+\Delta t}\right| < \varepsilon_v$, being ε_d and ε_v user defined tolerances.

6 Multibody Dynamics Methodology for Railway Pantograph and Vehicle

Since the vehicle and pantograph mechanical systems present a dynamic behaviour with large displacements and rotations a multibody dynamics formulation is well suited to model these systems. The development of realistic and accurate multibody computational models for these systems is by itself a complex task that, not being the main focus of this work. For this reason, the models considered here were already or are currently being developed alongside this work by other collaborating researchers [37,67–69]. Nevertheless, in order to develop a co-simulation procedure for the coupled systems addressed here, the computational implementation of the multibody dynamics methodology must be carefully considered with special attention to numerical integration procedure and to the contact formulations that ultimately couple the sub-systems.

6.1 Pantograph Modelling

The railway roof pantographs, represented in Figure 6.1 (a), are the systems responsible for collecting the energy from the overhead line. Mechanically, they are characterized as a mechanism with three loops that ensures that the movement of the head is constrained to a straight line, perpendicular to the plane of the base, while always maintained levelled with the pantograph base. The pantographs are always mounted in the train in a perfect vertical alignment with the centre of the bogies of the vehicle in order to ensure that during curving the centre of the bow does not deviate from the centre of the railroad, more than what is expected from the normal railway operations. To guarantee a smooth operation, without contact loss with the contact wire or requiring an excessive contact force, which lead not only to high wear but

also large uplifts of the steady arms, the pantographs must be dynamically responsive to the different range of frequencies with which they are excited. Furthermore, the pantograph and catenary must have characteristics that allow for multiple pantograph operation without the degradation of the contact quality of any of the pantograph collector strips [70]. The use of active control strategies for the pantograph may lead to an improvement of the pantograph contact, especially for the trailing pantographs. However many of the prototypes of active pantographs are still experimental and are not considered here [24,71].

Two different types of models are generally used to represent pantographs, lumped mass and multibody models. Each of them has advantages and shortcomings in their use, however both can be formulated with a multibody dynamics methodology.

A pantograph multibody model consists of a collection of bodies and mechanical elements, as depicted in Figure 6.1 (b).

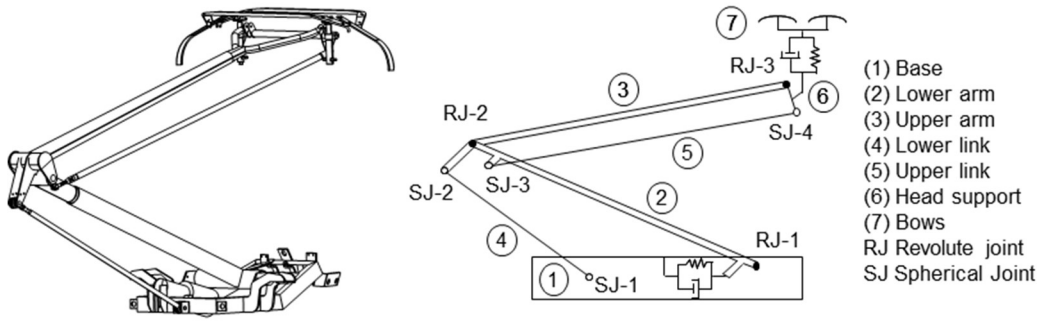

(a) (b)

Figure 6.1: (a) Roof pantograph; (b) Representation of a pantograph multibody model.

The data required to build a multibody model of the pantograph concerns the mass, inertia, initial positions and initial orientations of all bodies in the system, plus the type and location of all kinematic joints that connect the different bodies of the system and the force elements characteristics, i.e., springs, dampers and actuators. One of the criticisms to this modelling procedure is that the pantograph multibody models developed until now are modelled after rigid bodies connected by perfect kinematic joints. Consequentially, these models only have 2 degrees-of-freedom, i.e., the raising of the pantograph and the head suspension. Laboratory dynamic analysis of real pantographs leads to frequency response measurements that exhibit the presence of three resonances, implying that a basic requirement for the pantograph models is to have three degrees of freedom, at least. The third degree-of-freedom of the multibody pantograph may be associated with the clearance or with bushings existing in the joints [72,73] or even with the flexibility of one or more of the bodies considered

in this model [74,75]. In any case, the minimal requirements for modelling multibody pantographs that can have a realistic behaviour in the complete frequency range of their operation, this is, in the 0-20 Hz range, are still to be identified. For this reason, despite that in the procedures here developed either a multibody pantograph or a lumped mass pantograph can be used, the latter is adopted for the work here presented.

Alternatively, to a full multi-body pantograph model a more commonly used modelling approach is to model the pantograph as a lumped mass system. The lumped mass pantograph model, depicted on Figure 6.2 (a), is composed of a simple series of lumped masses linked consequently to a base by spring/damper elements. Although in the literature pantograph models are presented with two, three of more mass stages, for high-speed train applications, there is a minimal requirement of three stages to well represent the system [62]. While the multi-body pantograph models can be built with design data alone, for example with data obtained from technical drawings complemented with measured physical characteristics from selected components, the lumped mass pantograph model parameters, such as the mass of the bodies and the spring/damper properties, must be identified experimentally. In this sense, the lumped mass pantograph model can be thought as a transfer function in which an experimental procedure, represented on Figure 6.2 (b) is used. While exciting the contact strips of the desired pantograph to model with prescribed motions, Z(t), of known frequencies and amplitudes the response of the pantograph is measured, namely the contact forces on the collector strip and positions, velocities and accelerations at prescribed points of the mechanical pantograph. This acquired data is then used to build the frequency response function of the pantograph where it has to match that of the lumped mass model by identifying its parameters [76,77]. Thus, while the lumped mass pantograph reproduces with recognised fidelity the dynamic behaviour of a pantograph its identified parameters have no physical realism.

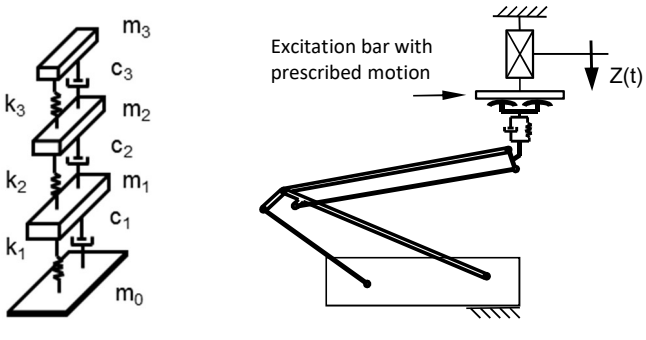

Figure 6.2: Lumped mass pantograph model: (a) Three stage lumped mass model; (b) Laboratory parameter identification procedure.

Regardless of this matter due to the simplicity of their construction and fidelity of their dynamic response, the lumped mass models are commonly used by operators, manufacturers and homologation bodies instead of more complex models. Furthermore when using a lumped mass pantograph model for the dynamic analysis of pantograph-catenary interaction it is possible to use the same finite element code to solve the equations of motion of both pantograph and catenary [78]. This however inhibits the use of more complex pantograph models such as a full multibody pantograph modelling approach as it also limits the spatial representation of the lumped mass pantograph. Therefore, in the work here presented for the dynamic analysis of pantograph-catenary interaction on catenaries set on curved track, a lumped mass multibody model is used. This way, using a spatial multibody dynamics formulation, the pantograph model is able to cope with the general trajectory path of the pantograph as also the absolute spatial position of its bodies is readily available.

6.1.1 Multibody lumped mass pantograph model

The detailed representation of the multibody lumped mass model considered for this work is depicted in Figure 6.3. The model is composed by four aligned bodies, $b_{0\text{-}3}$, representing the three staged lumped masses and the pantograph base. Each lumped mass body as a mass, $m_{1\text{-}3}$, corresponded to the lumped mass model identified parameters. The spatial position and orientation of each body are defined through a set of Cartesian coordinates with the position of its centre of mass and a set of Euler parameters that define its orientation via a local reference frame, $(\xi,\eta,\zeta)_{0-3}$. These are obtained by the time integration of the body accelerations resultant from the solution of the multibody equations of motion. Both the multibody formulation and time integration scheme used are presented ahead in Section 6.3. The linear spring and damper elements placed in between the masses are formulated as force elements, using their respective spring and damping coefficients, $k_{1\text{-}3}$, and $c_{1\text{-}3}$. The externally applied forces consist of the resultant pantograph-catenary contact force and transport moment, $\mathbf{f}_3^c$ and $\mathbf{n}_3^c$, applied on the lumped mass pantograph top body centre, b_3, and the pantograph static uplift force, $\mathbf{f}_{up}$, applied on the bottom lumped mass body, b_1, which is set to raise the pantograph lumped masses and adjust the resulting average contact force. To maintain the pantograph model unidimensional actuation, three prismatic joints, $pris_{1\text{-}3}$, are set between each lumped mass body and the pantograph base such that the motion of the lumped masses is constrained to be along an axis perpendicular to the plane of the pantograph base as also preventing their relative rotation.

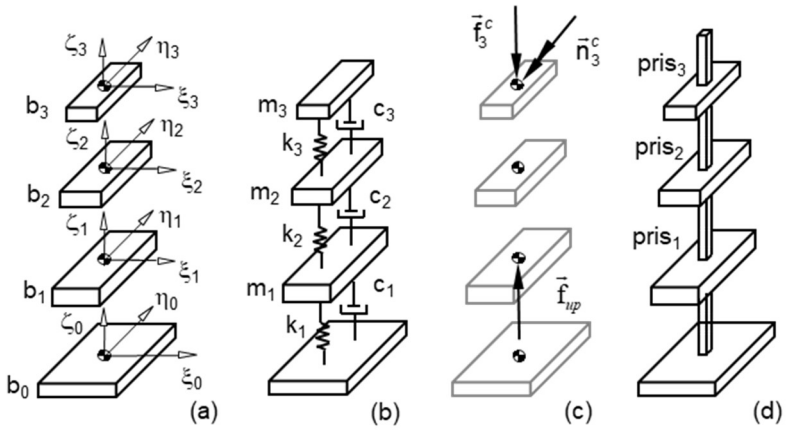

Figure 6.3: Representation of the multibody lumped mass model: (a) Lumped mass bodies; (b) Spring and damper elements; (c) External applied forces; (d) Prismatic constraints.

To set the trajectory of the pantograph along the track path a prescribed kinematic motion constraint is set to the pantograph base body, b_0, where its position, $\mathbf{r}_0$, and orientation, $(\xi,\eta,\zeta)_0$, is set to follow a moving frame correspondent to the trajectory of the pantograph, as represented in Figure 6.4. At a given track length , the position, $\mathbf{r}_p$, and local reference frame, $(\xi,\eta,\zeta)_p$, that define the pantograph trajectory are built in relation to the track moving frame, such that:

$$\begin{gathered}\mathbf{r}_p = \mathbf{r}_t + \mathbf{A}_t \mathbf{s}_0'^t \\ \xi_p \equiv \xi_t \;\; ; \;\; \zeta_p \equiv \zeta_t \;\; ; \;\; \boldsymbol{\eta}_p \equiv \boldsymbol{\eta}_t\end{gathered} \tag{6.1}$$

where $\mathbf{s}_0'^t$ is the coordinate position of the pantograph base relative to the track local reference frame, $(\xi,\eta,\zeta)_t$, which is defined by the position of the vehicle rooftop, in relation to the track running surface. Vector $\mathbf{r}_t$ is the track centreline position evaluated for the respective track travelled length and matrix $\mathbf{A}_t$ is the rotation matrix associated to the corresponding track centreline local reference frame $(\xi,\eta,\zeta)_t$.

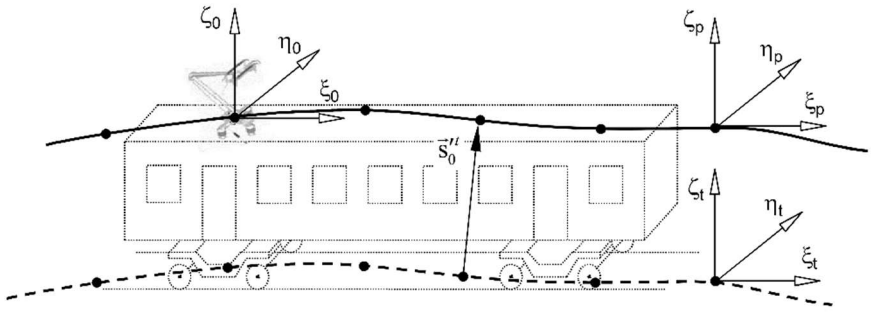

Figure 6.4: Representation of the prescribed kinematic motion constraint set to the pantograph base.

6.2 Vehicle Modelling

The development of advanced railway vehicle multibody models that accurately represent realistic railway compositions requires not only the access to each model technical specifications and drawings but also a significant effort in generating their correspondent computational models to a degree where they are accurate enough to perform realist dynamic behaviour analysis. As this effort is beyond the main scope of this work the models used here are either already developed or in current development outside of the scope of this work. Among these models there are a light railway vehicle, the LRV2000 [37], where a general overview of the model is shown in Figure 6.5, a underground metro vehicle ML95 [68] and an elevated speed railway vehicle tilting train Alfa Pendular [67] .

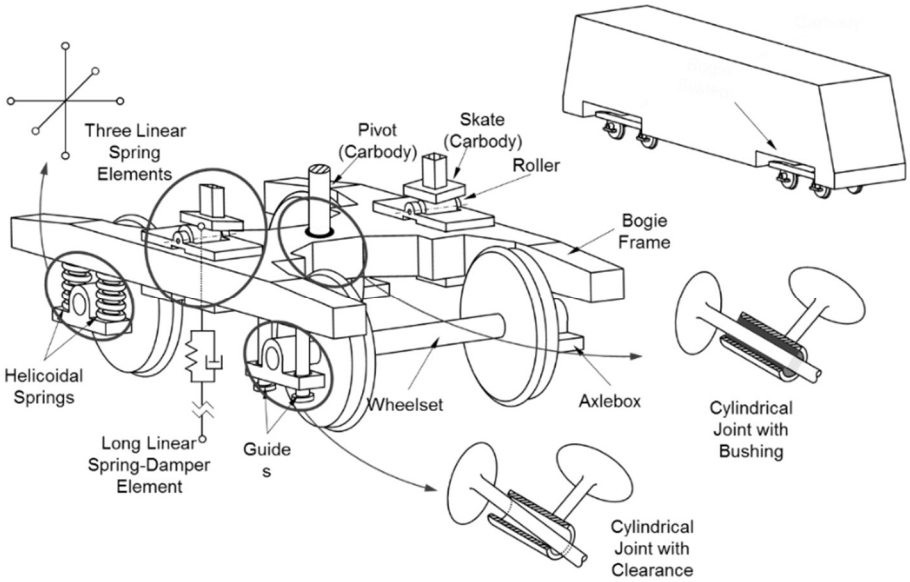

Figure 6.5: General overview of the LRV200 vehicle multibody model.

In general, the vehicle multibody model is characterized by a set of rigid and/or flexible bodies that are interconnected by force elements and joints. In turn, the representation of the mechanical elements that constrain the relative motion between structural elements allows the modelling of the relative mobility of the system components.

As represented in Figure 6.6, the multibody models considered in this work comprise a carbody, bogie frames, wheelsets and axleboxes which are modelled as rigid bodies with specified mass and inertial properties.

The mechanical joints, in general, are modelled as kinematic constraints, being their modelling parameters associated to their geometric properties. The primary and secondary suspension elements, depicted in Figure 6.7, are represented as springs and dampers with appropriate constitutive relations, being included in the multibody formulation as force

elements.

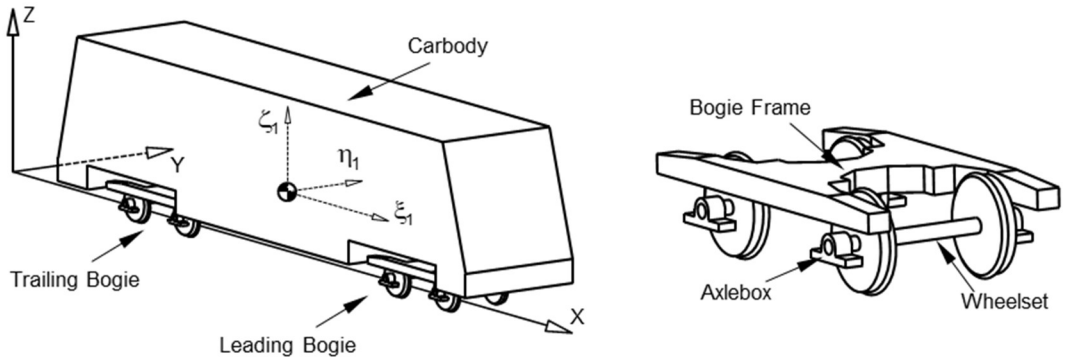

Figure 6.6: General multibody model of a railway vehicle.

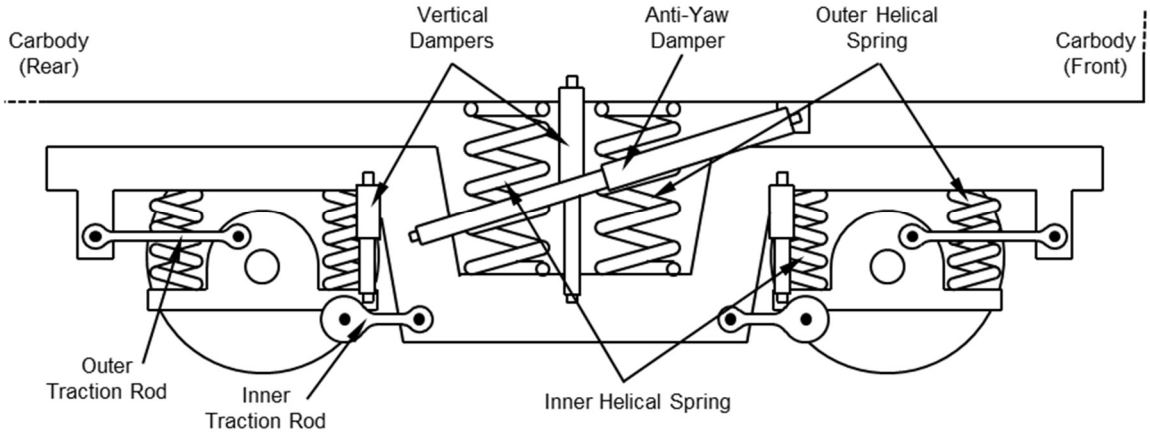

Figure 6.7: Suspension system of the railway vehicle.

6.3 Dynamic analysis of the pantograph and vehicle multibody models

A typical multibody model is defined as a collection of rigid or flexible bodies that have their relative motion constrained by kinematic joints and is acted upon by external forces. The forces applied over the system components may be the result of springs, dampers, actuators or external applied forces describing gravitational, contact/impact or other forces. A wide variety of mechanical systems can be modelled as the schematic system represented in Figure 6.8.

Let the configuration of the multibody system be described by *n* Cartesian coordinates **q**, and a set of *m* algebraic kinematic independent holonomic constraints **Φ** be written in a compact form as [43].

$$\mathbf{\Phi}(\mathbf{q}, t) = \mathbf{0} \tag{6.2}$$

Differentiating equation (6.2) with respect to time yields the velocity constraint equation. After a second differentiation with respect to time the acceleration constraint equation is obtained

$$\mathbf{\Phi}_{\mathbf{q}}\dot{\mathbf{q}} = \boldsymbol{\upsilon} \tag{6.3}$$

$$\boldsymbol{\Phi}_{\mathbf{q}}\ddot{\mathbf{q}} = \boldsymbol{\gamma} \tag{6.4}$$

where $\boldsymbol{\Phi}_{\mathbf{q}}$ is the Jacobian matrix of the constraint equations, $\boldsymbol{\upsilon}$ is the right side of velocity equations, and $\boldsymbol{\gamma}$ is the right side of acceleration equations, which contains the terms that are exclusively function of velocity, position and time.

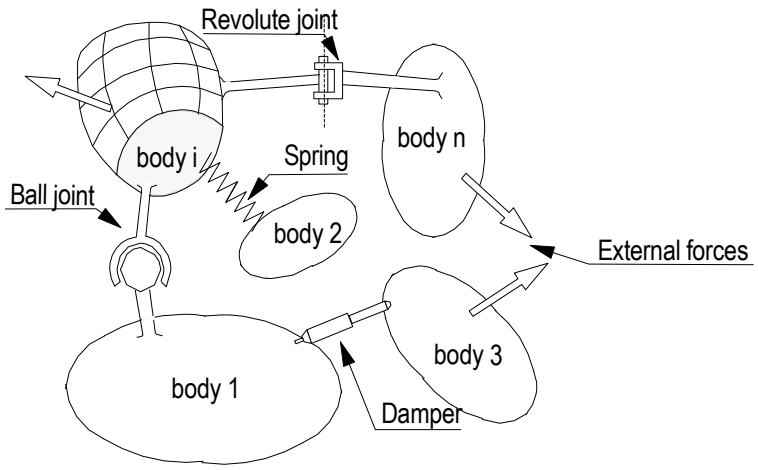

Figure 6.8: Generic multibody system.

The equations of motion for a constrained multibody system (MBS) of rigid bodies are written as

$$\mathbf{M}\ddot{\mathbf{q}} = \mathbf{g} + \mathbf{g}^{(\mathbf{c})} \tag{6.5}$$

where $\mathbf{M}$ is the system mass matrix, $\ddot{\mathbf{q}}$ is the vector that contains the state accelerations, $\mathbf{g}$ is the generalized force vector, which contains all external forces and moments, and $\mathbf{g}^{(c)}$ is the vector of constraint reaction equations. The joint reaction forces can be expressed in terms of the Jacobian matrix of the constraint equations and the vector of Lagrange multipliers

$$\mathbf{g}^{(c)} = -\boldsymbol{\Phi}_{\mathbf{q}}^{T}\boldsymbol{\lambda} \tag{6.6}$$

where $\boldsymbol{\lambda}$ is the vector that contains m unknown Lagrange multipliers associated with m holonomic constraints. Substitution of Equation (6.6) in Equation (6.5) yields

$$\mathbf{M}\ddot{\mathbf{q}} + \boldsymbol{\Phi}_{\mathbf{q}}^{T}\boldsymbol{\lambda} = \mathbf{g} \tag{6.7}$$

In dynamic analysis, a unique solution is obtained when the constraint equations are considered simultaneously with the differential equations of motion with proper set of initial conditions. Therefore, equation (6.4) is appended to equation (6.7), yielding a system of differential algebraic equations that are solved for $\ddot{\mathbf{q}}$ and $\boldsymbol{\lambda}$. This system is given by

$$\begin{bmatrix} \mathbf{M} & \boldsymbol{\Phi}_q^T \\ \boldsymbol{\Phi}_q & \mathbf{0} \end{bmatrix} \begin{bmatrix} \ddot{\mathbf{q}}_r \\ \boldsymbol{\lambda} \end{bmatrix} = \begin{bmatrix} \mathbf{g} \\ \boldsymbol{\gamma} \end{bmatrix} \tag{6.8}$$

In each integration time step, the accelerations vector, $\ddot{\mathbf{q}}$, together with velocities vector, $\dot{\mathbf{q}}$, are integrated in order to obtain the system velocities and positions at the next time step. This procedure is repeated up to final time will be reached. The solution of the multibody equations of motion and their integration in time is depicted in Figure 6.9. The set of differential algebraic equations of motion, Equation (6.8) does not use explicitly the position and velocity equations associated to the kinematic constraints, Equations (6.2) and (6.3), respectively. Consequently, for moderate or long time simulations, the original constraint equations are rapidly violated due to the integration process. Thus, the kinematic constraint violations are stabilized using the Baumgarte stabilization method, while kept under prescribed thresholds, or eliminated by using a coordinate partition when they exceed a pre-established value [79]. Also, the solution of the forward dynamics problem, for the multibody model, is obtained by using a variable time step and variable order numerical integrator [80].

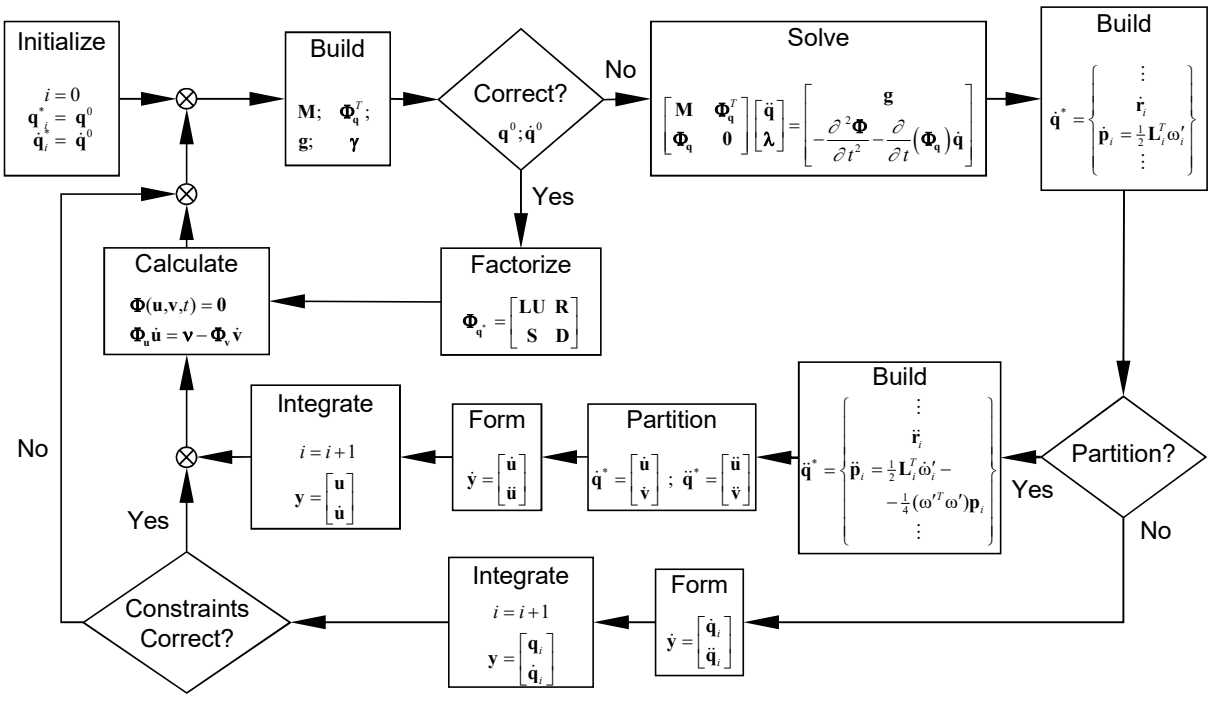

Figure 6.9: Flowchart with the forward dynamic analysis of a multibody system.

Note that the numerical approach described implies the use of Cartesian coordinates. If other types of coordinates are used, such as joint coordinates, the flowchart shown in Figure 6.9 must suffer the appropriate adaptations.

7 Contact Modelling of Finite Elements with Rigid Bodies

On the course of the work proposed here two contact problems are addressed. These are the contact between the pantograph contact strips and the catenary contact wire, and the contact between the railway vehicle wheels and the track rail. The contact evaluation between the systems considered here is a critical aspect of the work here developed as not only represent the effective pantograph-catenary and vehicle-tack interaction but are part of the coupling approach used in the co-simulation procedures.

Generally, contact problems can be treated either by a kinematic constraint or by a penalty formulation of the contact force. In the first procedure the contact force is simply the joint reaction force of the kinematic constraint [81,82]. With the second procedure the contact force defined in function of the relative penetration between the two surfaces [72,83]. The use of the kinematic constraint forces its elements to be in permanent contact, being this approach valid only if no contact loss exists. The penalty formulation allows for the loss of contact and it is the method of choice to tackle both contact problems considered here. The nature and complexity of the pantograph-catenary and wheel-rail contact problems is different, being their implementation and modelling requirements distinct. Nevertheless, the correct evaluation of the contact forces developed in both cases requires that flexibility of both the catenary contact wire and the track rail be considered.

7.1 Pantograph-Catenary contact model

From the contact mechanics point of view, the contact between the pantograph contact strip and the catenary contact wire is physically a contact between a flat surface, made of carbon, and a cylinder surface, made of a copper alloy, as represented in Figure 7.1. In this work the contact

problem is dealt with a penalty force based formulation, [83], where the contact force is defined as function of the relative pseudo penetration between the two surfaces. Due to the nature of the contact between both types of materials and contact surfaces the sliding friction forces are neglected, being only the normal contact force, perpendicular to the flat surface of the contact strip considered here.

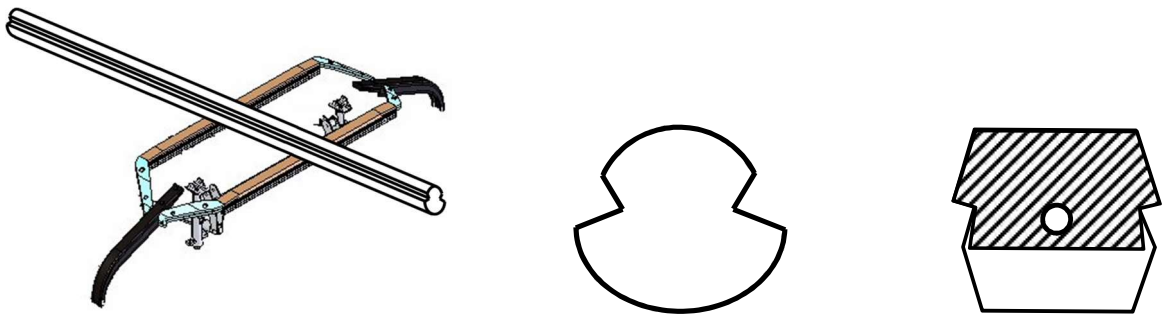

a) b) c)

Figure 7.1: Pantograph-catenary contact: (a) Pantograph bow and catenary contact wire; (b) Cross-section of the contact wire; (c) Cross-section of the collector strip

As a penalty force formulation is used, the contact force evaluation is dependent on the contact geometry between both surfaces. In this sense, consider the contact geometry presented in Figure 7.2 where points *a* and *b* represent the extremities of the top surface of the pantograph contact strip. The point positions, $\mathbf{r}_a$ and $\mathbf{r}_b$, are evaluated as:

$$\begin{aligned} \mathbf{r}_a &= \mathbf{r}_3 + \mathbf{A}_3\mathbf{s}'^3_a \quad ; \quad \mathbf{s}'^3_a = \begin{bmatrix} 0 & -l_{cs}/2 & 0 \end{bmatrix}^T \\ \mathbf{r}_b &= \mathbf{r}_3 + \mathbf{A}_3\mathbf{s}'^3_b \quad ; \quad \mathbf{s}'^3_b = \begin{bmatrix} 0 & l_{cs}/2 & 0 \end{bmatrix}^T \end{aligned} \tag{7.1}$$

where $\mathbf{r}_3$ is the global coordinate position of the lumped mass pantograph top body and $\mathbf{A}_3$ is the rotation matrix associated to its local reference frame $(\xi,\eta,\zeta)_3$. Vector $\mathbf{s}'^3_a$ and $\mathbf{s}'^3_b$ are correspondingly the positions of points *a* and *b* relative to the body local reference frame, evaluated as:

$$\begin{aligned} \mathbf{s}'^3_a &= \begin{bmatrix} 0 & -l_{cs}/2 & 0 \end{bmatrix}^T \\ \mathbf{s}'^3_b &= \begin{bmatrix} 0 & l_{cs}/2 & 0 \end{bmatrix}^T \end{aligned} \tag{7.2}$$

being l_{cs} the length of the pantograph contact strip.

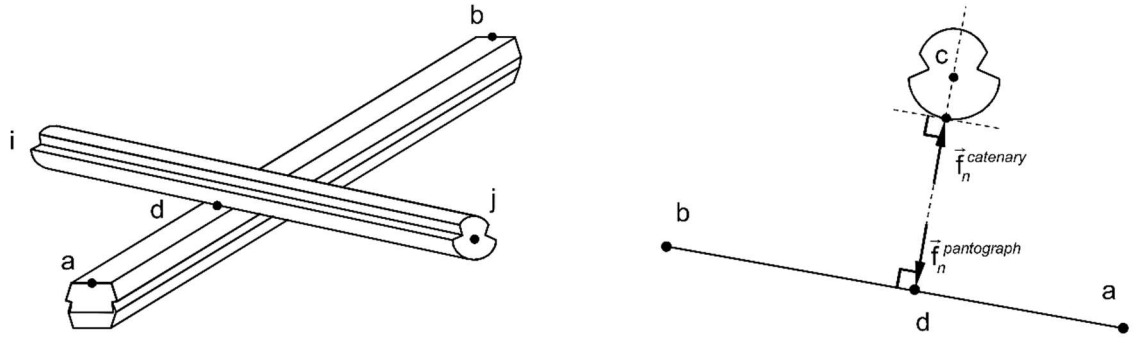

Figure 7.2: Representation of the pantograph-catenary contact geometry.

Point *c* is the position of the centre of the contact wire cross section, which includes the candidate contact point on the catenary. As the catenary geometry is described in a finite element formulation point *c* belongs to one of the catenary finite elements that is connected to nodes *i* and *j*, as represented in Figure 7.3 (a). Therefore, the coordinate position of *c*, $\mathbf{r}_c$, is evaluated as:

$$\begin{aligned} \mathbf{r}_c &= \mathbf{r}_c^0 + \mathbf{N}(\xi)[\mathbf{d}_i \quad \mathbf{d}_j] \\ \mathbf{r}_c^0 &= \mathbf{r}_i^0 + \xi(\mathbf{r}_j^0 - \mathbf{r}_i^0) \end{aligned} \tag{7.3}$$

where $\mathbf{d}_i$ and $\mathbf{d}_j$ are the node displacements of the contact wire finite element and $\mathbf{r}_c^0$ refers to the corresponding position of *c*, c^0, in the undeformed finite element mesh of the catenary, such that:

$$\mathbf{r}_c^0 = \mathbf{r}_i^0 + \xi(\mathbf{r}_j^0 - \mathbf{r}_i^0) \tag{7.4}$$

Matrix $\mathbf{N}(\xi)$ contains the beam element shape functions, [84], evaluated at the parametric length coordinate of the finite element, ξ, in which the contact takes place with correspondence to point *c*. The parametric coordinate, ξ, is obtained by finding the intersection between the lines defined by points *a* and b and points i and j, when projected on the same plane. For convenience, as represented in Figure 7.3 (b), the *xy* plane is used here. The interception between both lines of the contact strip and the contact wire is expressed as:

$$\mathbf{r}_i^{xy} + \hat{\mathbf{u}}_{ij}^{xy}\lambda_{ic}^{xy} = \mathbf{r}_a^{xy} + \hat{\mathbf{u}}_{ab}^{xy}\lambda_{ac}^{xy} \tag{7.5}$$

where the superscript *xy* denotes here the projection on the *xy* plane and $\hat{\mathbf{u}}_{mn}$ is the versor of a generic vector that goes from node *m* to node *n*. The scalar values λ_{ic}^{xy} and λ_{ac}^{xy} are the distance between points *i* and *c* and points *a* and *c* in the *xy* plane. These can be obtained by solving equation (7.5) from which the parametric coordinate ξ can be evaluated as:

$$\xi = \frac{\lambda_{ic}^{xy}}{\left\| \mathbf{r}_j^{xy} - \mathbf{r}_i^{xy} \right\|} \tag{7.6}$$

where $\xi \in [0,1]$. If $\xi \notin [0,1]$ the catenary finite element considered does not fit the contact geometry and another element along the contact wire must be tested for contact.

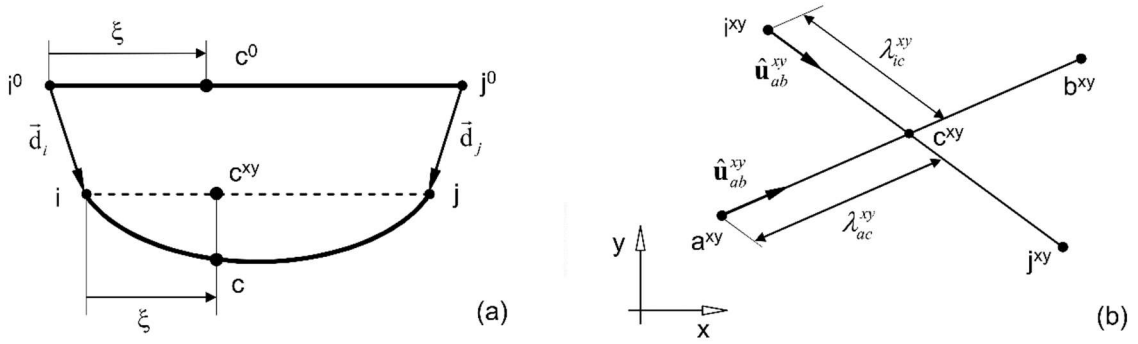

Figure 7.3: (a) Representation of the contact wire finite element in which contact occurs; (b) Contact geometry on *xy* plane.

In Figure 7.2, point *d* represents the contact point on the contact strip surface which is geometrically determined by assuming that the normal contact force, $\mathbf{f}_n$, and its corresponding pseudo penetration are perpendicular to both the flat surface of the contact strip and the contact wire cylindrical contact surface. As point *c* is collinear with *a* and *b*, its coordinate position is obtained as:

$$\begin{aligned} \mathbf{r}_d &= \mathbf{r}_a + \lambda_{ad}\hat{\mathbf{u}}_{ab} \\ \lambda_{ad} &= \hat{\mathbf{u}}_{ab} \cdot \mathbf{r}_{ac} = \hat{\mathbf{u}}_{ab} \cdot (\mathbf{r}_c - \mathbf{r}_a) \end{aligned} \tag{7.7}$$

such that λ_{ad} is the length between point *a* and *d* which can be retrieved as the scalar projection between the versor $\hat{\mathbf{u}}_{ab}$ and vector $\mathbf{r}_{ac}$ that goes from point *a* to *c*:

$$\lambda_{ad} = \hat{\mathbf{u}}_{ab}^T \mathbf{r}_{ac} = \hat{\mathbf{u}}_{ab}^T (\mathbf{r}_c - \mathbf{r}_a) \tag{7.8}$$

With the contact geometry established, in this work the normal contact force, f_n, is obtained by using a purely elastic Hertzian normal contact force model, written as:

$$f_n = \begin{cases} K\delta & , \ \delta > 0 \\ 0 & , \ \delta \le 0 \end{cases} \tag{7.9}$$

where K is the contact stiffness, $\delta = \left\| \mathbf{r}_c - \mathbf{r}_d \right\| - r_{cw}$ is the pseudo normal penetration and r_{cw} is the contact wire radius.

As the contact surface of the contact wire is concentric with its cross section centre, the normal contact force is directly applied in point *c*, being the equivalent contact forces and

moments, $\mathbf{f}_i^c$ and $\mathbf{f}_j^c$, applied at nodes *i* and *j* of the contact wire finite element, evaluated as:

$$\begin{bmatrix} \mathbf{f}_i^c \\ \mathbf{f}_j^c \end{bmatrix} = \mathbf{N}(\xi)^T f_n \hat{\mathbf{u}}_{dc} \tag{7.10}$$

On the contact strip the normal force is applied on point *d* such that the resultant force and transport moment, $\mathbf{f}_3^c$ and $\mathbf{n}_3^c$, to be applied on the lumped mass pantograph top body mass centre are evaluated as:

$$\begin{aligned} \mathbf{f}_3^c &= f_n \hat{\mathbf{u}}_{cd} \\ \mathbf{n}_3^c &= \tilde{\mathbf{s}}_d'^3 \, \mathbf{A}_3^T \mathbf{f}_3^c \end{aligned} \tag{7.11}$$

where $\mathbf{s}_d'^3$ is the position of point *d* relative to the top body local reference frame $(\xi,\eta,\zeta)_3$.

7.2 Wheel-Rail contact model

The rolling contact problem that characterizes the wheel-rail interaction is solved in two steps: the contact detection in which the contact points, or areas, are identified, and; the contact force modelling in which the interaction forces involved are evaluated. The online wheel-rail contact detection method proposed by Pombo et al [13,64] is the starting point for the approach proposed here, in which the track flexibility is included.

The wheel-rail contact detection problem is similar to the contact detection between two parametric surfaces, as those depicted in Figure 7.4, described by parameters u_i, w_i, u_j and w_j. The location of the potential contact points in the surfaces must be such that the tangent planes to the surfaces, in those points, are parallel to each other. The surface parallelism condition is described by the nonlinear system of equations:

$$\begin{cases} \mathbf{d}_j^T \mathbf{t}_i^u = 0 \\ \mathbf{d}_j^T \mathbf{t}_i^w = 0 \\ \mathbf{n}_i^T \mathbf{t}_j^u = 0 \\ \mathbf{n}_i^T \mathbf{t}_j^w = 0 \end{cases} \tag{7.12}$$

where $\mathbf{d}_j$ is the distance vector between the potential points of contact, $\mathbf{n}_i$ and $\mathbf{n}_j$ are the normal vector of surfaces *i* and *j*, $\mathbf{t}_i^u$ and $\mathbf{t}_i^w$ are tangential vectors of surface *i* and $\mathbf{t}_j^u$ and $\mathbf{t}_j^w$ are tangential vectors of surface *j*, shown in Figure 7.4, all defined as function of the surfaces parameters.

For each potential contact pair in the wheel-rail contact, i.e. the tread-rail and flange-rail

contact pairs, contact exists if:

$$\mathbf{d}_j^T \mathbf{n}_i > 0 \tag{7.13}$$

If contact exists in a particular contact pair, normal and tangential forces are calculated and applied to the bodies in contact on the contact points identified.

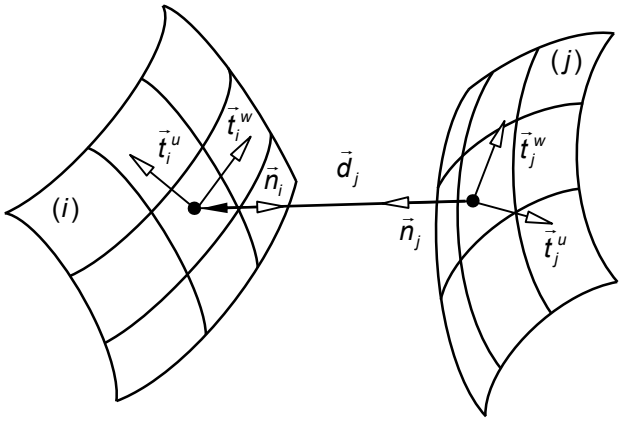

Figure 7.4: Contact detection between two surfaces.

The interaction between the wheel and the rail is represented by the contact model proposed by Pombo *et al* [13,64]. This model considers that the wheel surface is described by two parametric surfaces, for the tread and for the flange, while the rail is described by a single parametric surface. Therefore, two potential contact points may develop between wheel and rail, the tread-rail and the flange-rail contact points shown in Figure 7.5.

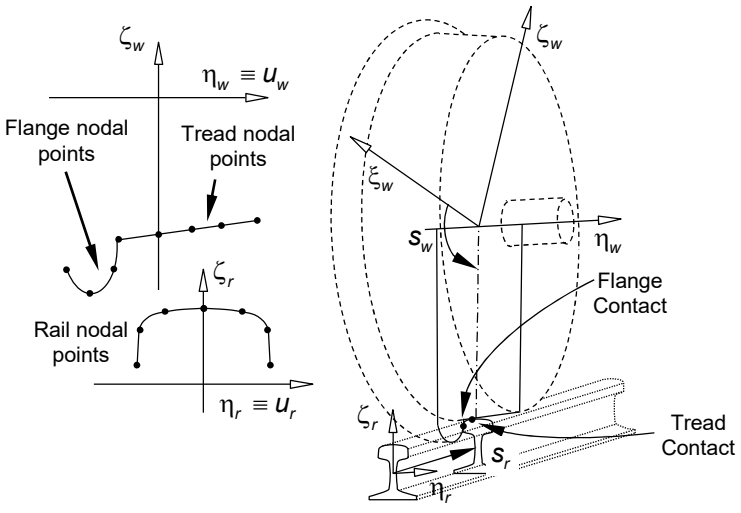

Figure 7.5: Identification of the parameters used in the wheel and rail parametric surfaces including the wheel tread and flange and rail profiles and surface parameters for the wheel (s_w,u_w) and for the rail (s_r,u_r).

The wheel profile is defined by two sets of nodal points, one for the tread and the other for the flange profile. These nodal points are interpolated to define the cross section of the wheel profile, as a function of parameter u_w, which in turn is rotated about the wheel axis η_w, with the

angle s_w starting from ξ_w, to form the parametric surface of revolution that defines the geometric shape of the wheel. The rail profile is also obtained by the interpolation of another set of nodal points, which are interpolated to define the rail cross-section, as a function of parameter u_r, which, in turn, is swept along the rail arc with the length of the sweep being defined by the arc-length s_r, starting from the origin of the rail. Consequently, the parametric surfaces of the wheel tread and flange and of the rail, depicted in Figure 7.5, are fully described by parameters s_w, u_w, s_r and u_r that play the role of parameters u_i, w_i, u_j and w_j in Eq. (7.12).

The effect of the flexibility of the track on the rail position and orientation is graphically shown in Figure 7.6(a), where a rail finite element is displaced with respect to its initial position, in grey, and for which the cross-sections are rotated relatively to their initial orientations. Let the finite element in which wheel-rail contact occurs connect node i to node j, as shown in Figure 7.6(a). The position and orientation of the centre of the rail cross-sections in the beam finite element is related to the initial geometry, finite element nodal displacements and shape functions by:

$$\begin{Bmatrix} \mathbf{r}_r \\ \boldsymbol{\theta}_r \end{Bmatrix} = \begin{Bmatrix} \mathbf{r}(s_r) \\ \mathbf{0} \end{Bmatrix} + \begin{bmatrix} \mathbf{N}_i^{dd}(\xi) & \mathbf{N}_i^{d\theta}(\xi) & \mathbf{N}_j^{dd}(\xi) & \mathbf{N}_j^{d\theta}(\xi) \\ \mathbf{N}_i^{\theta d}(\xi) & \mathbf{N}_i^{\theta\theta}(\xi) & \mathbf{N}_j^{\theta d}(\xi) & \mathbf{N}_j^{\theta\theta}(\xi) \end{bmatrix} \begin{Bmatrix} \boldsymbol{\delta}_i \\ \boldsymbol{\theta}_i \\ \boldsymbol{\delta}_j \\ \boldsymbol{\theta}_j \end{Bmatrix} \tag{7.14}$$

where $\mathbf{r}(s_r)$ is the position of the centre of the rail cross-section that includes the contact point for the rigid track, as described in the work by Pombo *et al* [13,64], $\boldsymbol{\delta}_i$ and $\boldsymbol{\delta}_j$ the nodal displacements , $\boldsymbol{\theta}_i$ and $\boldsymbol{\theta}_j$ the nodal rotations and $\mathbf{N}^{dd}$, $\mathbf{N}^{d\theta}$, $\mathbf{N}^{\theta d}$ and $\mathbf{N}^{\theta\theta}$ are submatrices with the shape functions of the beam element [5]. Eq. (7.14) is written as function of $\xi = (s_r - s_i)/(s_j - s_i)$, which is the parametric length coordinate of the finite element in which the contact takes place, being s_r the arc-length of the rail up to the contact point and s_i and s_j the rail arc-lengths up to nodes i and j, respectively.

Due to the rail deformation the rail cross-sections rotate with respect to their orientation on the rigid track, such a way that they remain perpendicular to the tangent of the arc line of their centres. The linear beam bending theory is used in the formulation of the linear beam finite elements being the infinitesimal rotations of a cross-section of the element, given, in Eq. (7.14), by $\boldsymbol{\theta}_r$. The transformation matrix from the rigid rail cross-section frame $(\xi,\eta,\zeta)_r^{rigid}$ to the deformed rail cross-section frame $(\xi,\eta,\zeta)_r$, both shown in Figure 7.6(b), is given by

$$\mathbf{A}_\theta = \begin{bmatrix} 1 & -\theta_\zeta & \theta_\eta \\ \theta_\zeta & 1 & -\theta_\xi \\ -\theta_\eta & \theta_\xi & 1 \end{bmatrix} \tag{7.15}$$

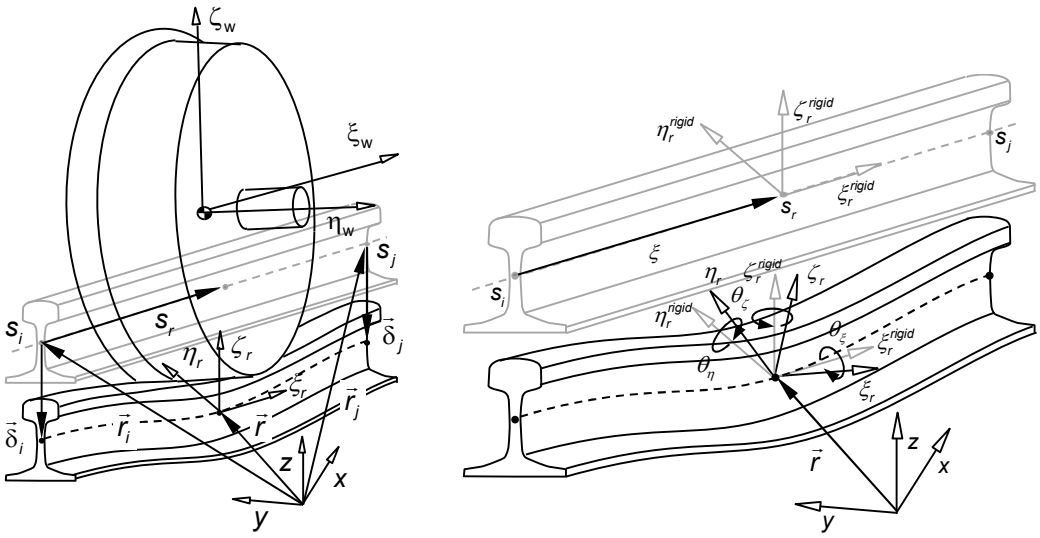

Figure 7.6: Deformation of the rail due to the wheel contact: (a) displacement of the rail cross-section that includes the contact point; (b) rotation of the rail cross-section.

The consequence of the displacement and rotation of the rail cross-section on the wheel tread and flange to rail contact searches is that not only the evaluation of vector $\mathbf{d}_j$ in Eq.(7.12) must take into account the new location of the centre of the cross-section $\mathbf{r}_r$ as given by Eq.(7.14) but also the rail surface vectors $\mathbf{n}_j$, $\mathbf{t}^u_j$ and $\mathbf{t}^w_j$ need to be rotated. Therefore, for a flexible rail, the searches for the wheel tread and flange contact with the rail are done by solving a system of nonlinear equations given by:

$$\begin{cases} \mathbf{d}_j^T \mathbf{t}_i^u = 0 \\ \mathbf{d}_j^T \mathbf{t}_i^w = 0 \\ \mathbf{n}_i^T \mathbf{A}_\theta \mathbf{t}_j^u = 0 \\ \mathbf{n}_i^T \mathbf{A}_\theta \mathbf{t}_j^w = 0 \end{cases} \tag{7.16}$$

Note that in the wheel-rail contact formulation with a rigid track, by Pombo *et al* [13,64], the normal, bi-normal and tangent vectors of the left and right rails are pre-calculated and included in a database that is accessed online during the contact search. The computational procedure proposed here, for the flexible track, is efficiently implemented by rotating the original vectors from the rigid track database by matrix $\mathbf{A}_\theta$ and adding $\mathbf{r}_r$ to the rigid rail position before being used in the contact search algorithm.

If Eq.(7.13) is fulfilled for a particular contact pair, normal and tangential contact forces

need to be evaluated. These forces depend on the contact geometry and on the material properties of the wheel and rail. Assuming that the contact between the wheel tread or flange and the rail is non-conformal, the normal contact forces are calculated using an Hertzian contact force model with hysteresis damping is given by [85]

$$f_n = K\left(1+\frac{3\left(1-e^2\right)}{4}\frac{\dot{\delta}}{\dot{\delta}^{(-)}}\right)\delta^n \tag{7.17}$$

where K is the stiffness coefficient, e is the restitution coefficient, n is a constant equal to 1.5 for metals, δ is the amount of indentation between the surfaces, $\dot{\delta}$ is the indentation velocity and $\dot{\delta}^{(-)}$ is the relative indentation velocity as impact starts.

The tangential forces are evaluated using the formulation proposed by Polach in which the longitudinal creep, or tangential, force is [86]

$$f_\xi = f\frac{\upsilon_\xi}{\upsilon_C} \tag{7.18}$$

while the lateral creep force is written as

$$f_\eta = f\frac{\upsilon_\eta}{\upsilon_C} + f_{\eta S}\frac{\phi}{\upsilon_C} \tag{7.19}$$

being f the tangential contact force caused by longitudinal and lateral relative velocities between the contacting surfaces, generally designated as creepages in rolling contact, υ_ξ, υ_η and ϕ are the longitudinal, lateral and spin creepages, respectively, in the point of contact, υ_C is the modified translational creepage, which accounts the effect of spin creepage and $f_{\eta S}$ is the lateral tangential force, or creep, caused by spin creepage. The Polach algorithm requires as input the normal contact force, the semi-axes of the contact ellipse, the combined modulus of rigidity of wheel and rail materials, the friction coefficient and the Kalker creepage and spin coefficients c_{ij} [87].

The contact forces on the wheel tread and flange, shown in Figure 7.7 as vectors $\mathbf{f}_{tr,w}$ and $\mathbf{f}_{fl,w}$, respectively, are generically written as

$$\mathbf{f}_{k,w} = f_{k,n}\,\mathbf{n}_k + f_{k,\xi}\,\mathbf{t}_{k,w} + f_{k,\eta}\,\mathbf{t}_{k,u} \qquad k = tr, fl \tag{7.20}$$

where $\mathbf{n}_k$ is the vector normal to the wheel surface, $\mathbf{t}_{k,w}$ is the tangent vector to the surface in the longitudinal direction of the wheel motion and $\mathbf{t}_{k,u}$ is the tangent vector in the lateral direction. In turn, the forces $\mathbf{f}_{tr,r}$ and $\mathbf{f}_{fl,r}$ represent the forces applied on the rails, which are opposite to those calculated for the wheels, i.e., $\mathbf{f}_{fl,w}$ and $\mathbf{f}_{fl,r}$.

7.2.1 Wheel-rail contact model on vehicle

In the multibody model, the information related to the wheel-rail contact forces is added to the force vector **g** in Equation (6.5), in which all forces are supposed to be applied in the rigid bodies mass centres, i.e., the origin of the body fixed coordinate systems. The forces due to the wheel-rail contact are applied in the contact points of the wheelset, shown Figure 7.7 for the tread and flange contacts. Therefore, the contact forces are first transferred to the centre of the wheelset by adding all the contact forces to a force resultant and a transport moment due to the transference of the points of application to the wheel centre, as

$$\begin{aligned} \mathbf{f}_{wheel} &= \mathbf{f}_{tr,w} + \mathbf{f}_{fl,w} \\ \mathbf{n}'_{wheel} &= \tilde{\mathbf{s}}'_{tr,w}\,\mathbf{A}_{ws}^{T}\mathbf{f}_{tr,w} + \tilde{\mathbf{s}}'_{fl,w}\,\mathbf{A}_{ws}^{T}\mathbf{f}_{fl,w} \end{aligned} \tag{7.21}$$

where $\mathbf{s}'_{tr,w}$ and $\mathbf{s}'_{fl,w}$ are the position vectors of the tread and flange contact points with respect to the wheel centre and expressed in the wheelset body coordinate frame, and $\mathbf{A}_{ws}$ is the transformation matrix from the wheelset body frame to the inertia frame.

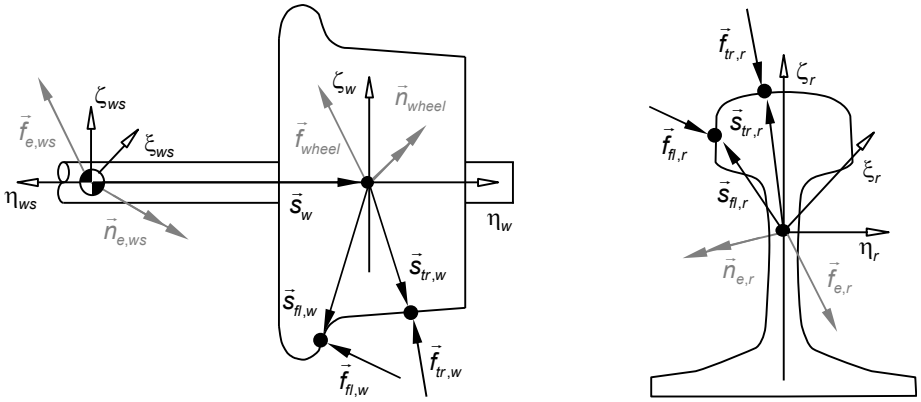

Figure 7.7: Wheel and rail contact forces, points of contact and equivalent forces and moments in the wheel centre and in the rail cross-section centre.

In the most common applications the wheels on the same wheelset are not independent, and consequently they are part of a single rigid body designated by wheelset. Therefore, the resultant force applied in the wheel mass centre is transferred to the wheelset mass centre, being the resultant force and transport moment on the wheelset due to the wheel-rail contact given by

$$\begin{aligned} \mathbf{f}_{e,ws} &= \mathbf{f}_{wheel} \\ \mathbf{n}'_{e,ws} &= \tilde{\mathbf{s}}'_{w}\,\mathbf{A}_{ws}^{T}\mathbf{f}_{wheel} + \mathbf{n}'_{wheel} \end{aligned} \tag{7.22}$$

where $\mathbf{s}'_w$ is the position of the wheel centre with respect to the wheelset mass centre, expressed in the wheelset body fixed coordinate system. Thus, the contribution of the wheel-rail contact forces to the force vector **g** is simply $\mathbf{g}_{e,ws} = [\mathbf{f}^{T}_{e,ws}, \mathbf{n}'^{T}_{e,ws}]^{T}$.

7.2.2 Wheel-rail contact model on track

In a finite element model lumped forces, such as the wheel-rail contact forces, can be applied on the nodes of the mesh but not in the middle of the element. As observed in Figure 7.7, the wheel-rail contact forces applied on the rail surface whereas the beam element used in the model for the rail considers only its geometric centre. Therefore, the resultant of the contact forces, $\mathbf{f}_{e,r}$, is applied on the rail cross-section centre and a transport moment, $\mathbf{n}_{e,r}$, is added to obtain the equivalent force system, depicted in Figure 7.7, expressed as

$$\begin{aligned} \mathbf{f}_{e,r} &= \mathbf{f}_{tr,r} + \mathbf{f}_{fl,r} \\ \mathbf{n}_{e,r} &= \tilde{\mathbf{s}}_{tr,r}\,\mathbf{f}_{tr,w} + \tilde{\mathbf{s}}_{fl,r}\mathbf{f}_{fl,w} \end{aligned} \tag{7.23}$$

Where $\mathbf{s}_{tr,r}$ and $\mathbf{s}_{fl,r}$ are the contact position vectors defined in the inertia reference frame. Note that the transformation of coordinates of the contact position points from rail cross-section coordinates to global coordinates is done by $\mathbf{s}_{tr,r} = \mathbf{A}_r\,\mathbf{s}'_{tr,r}$ and $\mathbf{s}_{fl,r} = \mathbf{A}_r\,\mathbf{s}'_{fl,r}$ with the transformation matrix $\mathbf{A}_r = \begin{bmatrix} \mathbf{u}_\xi & \mathbf{u}_\eta & \mathbf{u}_\zeta \end{bmatrix}_r$.

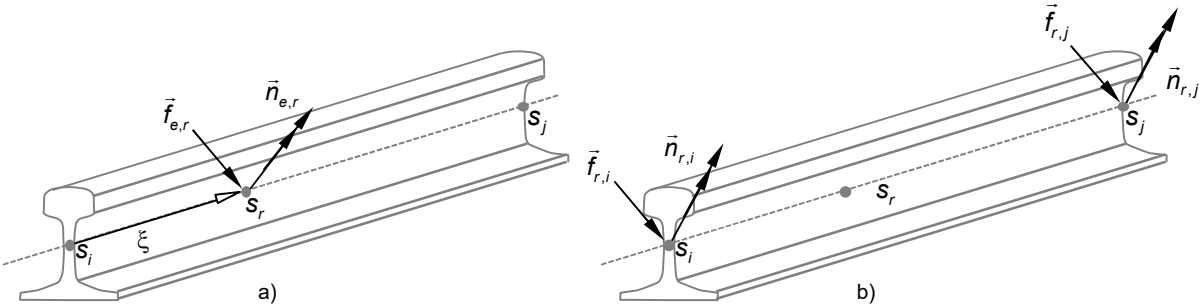

Figure 7.8: Wheel-rail contact force: (a) real and (b) equivalent.

An equivalent system of forces and moments applied in the beam finite element nodes, shown in Figure 7.8, that represents contact forces and transport moment applied to the rail-cross-section centre needs to be evaluated. The equivalent nodal forces are related to the concentrated forces and moments via the shape functions matrix as

$$\begin{Bmatrix} \mathbf{f}_{r,i} \\ \mathbf{n}_{r,i} \\ \mathbf{f}_{r,j} \\ \mathbf{n}_{r,j} \end{Bmatrix} = \begin{bmatrix} \mathbf{N}_i^{dd}(\xi) & \mathbf{N}_i^{d\theta}(\xi) & \mathbf{N}_j^{dd}(\xi) & \mathbf{N}_j^{d\theta}(\xi) \\ \mathbf{N}_i^{\theta d}(\xi) & \mathbf{N}_i^{\theta\theta}(\xi) & \mathbf{N}_j^{\theta d}(\xi) & \mathbf{N}_j^{\theta\theta}(\xi) \end{bmatrix}^T \begin{Bmatrix} \mathbf{f}_{e,r} \\ \mathbf{n}_{e,r} \end{Bmatrix} \tag{7.24}$$

and applied on the finite element nodes, i.e., $\mathbf{f}_{r,i}$ and $\mathbf{n}_{r,i}$ are applied on node i while $\mathbf{f}_{r,j}$ and $\mathbf{n}_{r,j}$ are applied on node j, as shown in Figure 7.8.

8 Pantograph-Catenary and Vehicle-Track Co-Simulation

Co-simulation procedures form a generalist approach of simulating coupled systems on a time depended basis [88–90]. As the dynamic analysis of multi-disciplinary models is most often composed by sub-systems, co-simulation exploits this modular structure by addressing to each sub-system its own distinct formulation and time integration method as an individual system. Thus, avoiding the use of a unique and complex formulation with a respective time integration method that often forces compromises on the dynamic analysis of each subsystem and consequently become computationally expensive and time intensive. There can be found several cases where co-simulation methodologies have been advantageously applied. A wide range of these applications use the methodology in order to couple systems with different formulations [45,91–97]. There are also applications where co-simulation is employed to improve computational performance using parallel computation [98,99], establish active control on mechatronic systems [100,101], and enable the use of third party applications [102].

In respect to the work here presented, co-simulation is used to establish the interaction between the dynamic analyses of both the pantograph and the catenary, as well as the vehicle and the track models. In each interaction considered here, each sub-system has its own distinct formulation and integration methodology. The catenary and track systems are modelled with a finite element formulation being a dynamic linear system integrated with a Newmark family numerical integrator set implicitly with fixed time step [65]. On the other hand, the nonlinear dynamics of the multibody pantograph and vehicle model is evaluated as a forward dynamics problem being its solution obtained with a variable time step and variable order numerical

integrator of the Gear type [80]. Therefore, to establish the interaction between each pair of the two sub-systems, where the overall sum of the two dynamic analyses and their cross effects will represent the solution of a coupled problem, careful consideration must be taken to achieve a numerically stable and accurate dynamic analysis of the coupled system [103].

The construction of the co-simulation procedure implemented is this work is structured on upon three main key steps, addressed hereafter. The first step is to establish an interface between the sub-systems where a set of state variables within each sub-system are defined and set to be shared between each other. The second step is to establish a fast and reliable data exchange procedure for the state variables. The third, and final, step is to establish a communication protocol that manages the use of the state variables through the integration scheme of both sub-systems during their dynamics analysis.

8.1 Interface

One aspect that is detrimental in defining the interface between the subsystems involved is the coupling approach used. Generally, in co-simulation the coupling between two sub-systems is set either by imposing a kinematic constraint between the models or by defining a set of constitutive interaction laws [104]. Such constitutive laws result on a set of solicitations that are applied on each sub-system. In this work, due to the obvious nature of the coupled problems here dealt with, where their interaction is defined by either the pantograph-catenary contact or the wheel-rail contact, the coupling of the sub-systems is established through the contact evaluation between the sub-systems and the application of the resulting contact forces/torques on each model. This requires careful consideration in selecting the needed state variables to be shared between the sub-systems so that the contact evaluation implemented on one of the sub-systems is efficient and the volume of data shared between applications is as reduced as possible.

8.1.1 Pantograph-Catenary interface

In respect to the pantograph-catenary co-simulation, since the contact evaluation needs to access the deformed finite element mesh of the catenary to search for contact along the catenary wire, the contact is evaluated on the finite element dynamic solver, on the catenary side. To this effect, as depicted in Figure 8.1, the state variables supplied by the multibody code in which the pantograph is defined, are the position of the contact strip extremities, $\mathbf{r}_a$ and $\mathbf{r}_b$. With these the catenary subsystem evaluates the contact and returns, as its state variables, the resulting

contact force vector, $\mathbf{f}_c$, and its point of application $\mathbf{r}_c$ on the collector strip.

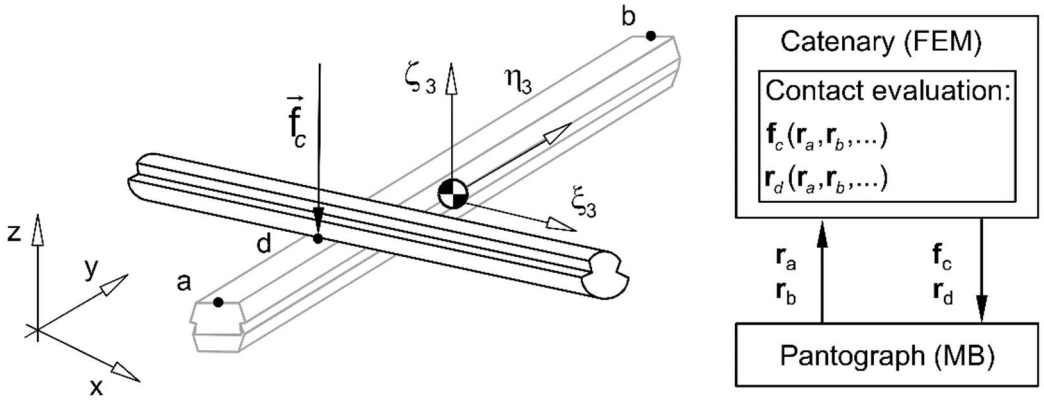

Figure 8.1: State variable exchange between catenary and pantograph sub-systems.

8.1.2 Vehicle-Track interface

As the wheel-rail contact forces provide the link between the two sub-systems, the evaluation of the contact is done in one of the sub-systems while the other provides the parameters required to make such evaluation possible, in this case the state variables that allow for the solution of the contact problem. Evaluating the wheel-rail contact on the track sub-system, as shown in Figure 8.2, avoids a computationally expensive communication scheme. The contact model requires the deformed centre position of the rails, in the neighbourhood of the arc length of the track in which contact occurs, s_r, to allow for the solution of the nonlinear Equation **(7.12)** for contact detection, which in turn requires all information associated to the finite element mesh of the rails already available in the track sub-system. The vehicle sub-system is set to provide the spatial position, $\mathbf{q}_w$, and velocity, $\dot{\mathbf{q}}_w$, of each wheel centre of the vehicle model. The wheel-rail contact problem is solved in the track sub-system and, in return, the vehicle sub-system receives from the track sub-system an equivalent wheel-rail contact force, $\mathbf{f}_{e,w}$, and transport moment, $\mathbf{n}'_{e,w}$, to be applied at the corresponding wheel centres.

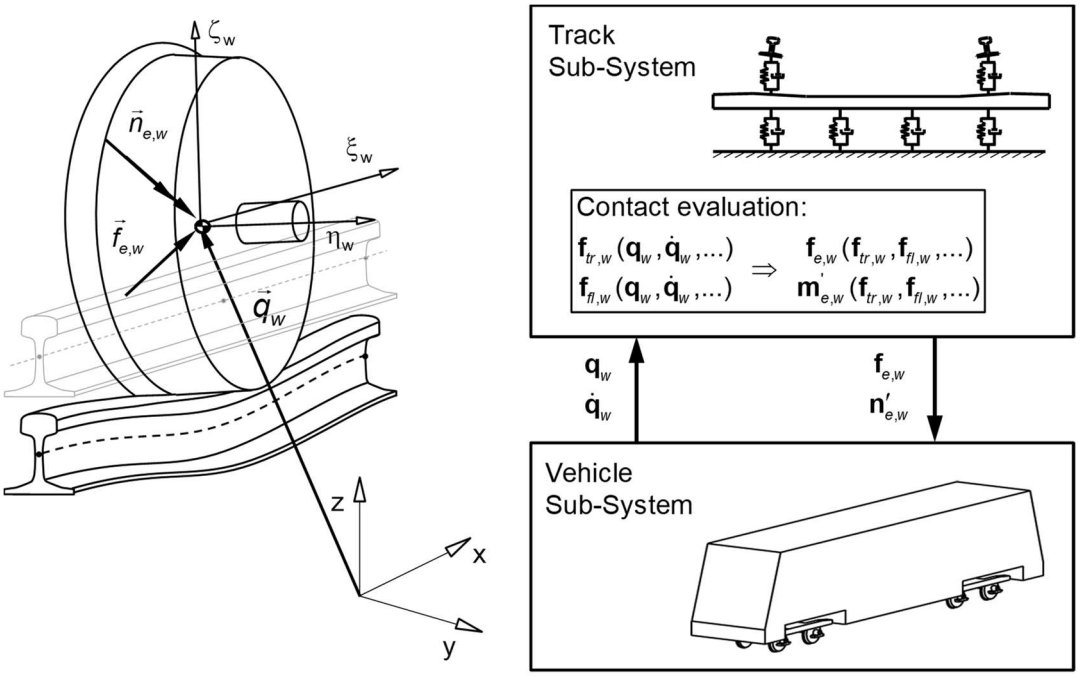

Figure 8.2: State variable exchange between vehicle and track sub-systems.

8.2 Data exchange methodology

As the interface between two sub-systems is defined and correspondingly the collection of state variables that each sub-system is required to share with the other, an efficient and robust data exchange method needs to be established. As the state variables are a common resource shared between two concurrent processes this procedure plays a critical role in the co-simulation where it is not only responsible for exchanging the state variable data between sub-systems but also to control their access. This leads to two important requirements that the data exchange method needs to fulfil. First, given the frequency at which data needs to be exchanged, it must be sufficiently fast so that it does not become a bottleneck of the co-simulation procedure. Second, it must provide a mechanism where both sub-systems stay synchronized without forming a race condition, [105,106], i.e., guarantee that the two sub-subsystems do not overstep themselves by performing their respective state variable reads and writes out of turn.

Given the above requirements the data exchange method here developed method is built upon two communication files, as depicted in Figure 8.3. One file, denoted as *A2B*, includes the stated variables evaluated in sub-system A that are to be shared to sub-system B, while the other file, denoted as *B2A,* passes the stated variables evaluated in sub-system B to sub-system A. This way, each file carries the state variables data that are meant to be written by one subsystem and red by the other always ensuring the correct flow of data. Each file also carries the time at which the states variables were evaluated, t_A and t_B. In order to keep both sub-systems

synchronised and to avoid data do be overwritten without being read first, a binary semaphore based implementation is used [107]. Hence, each communication file also includes a binary flag as a state variable which according to its value either gives permission of one subsystem to read the data or the other to overwrite. This method not only controls the reading/writing access of the state variables but also provides means to control the progress of the integration algorithms of each one of the individual analysis codes so that they stay synchronized.

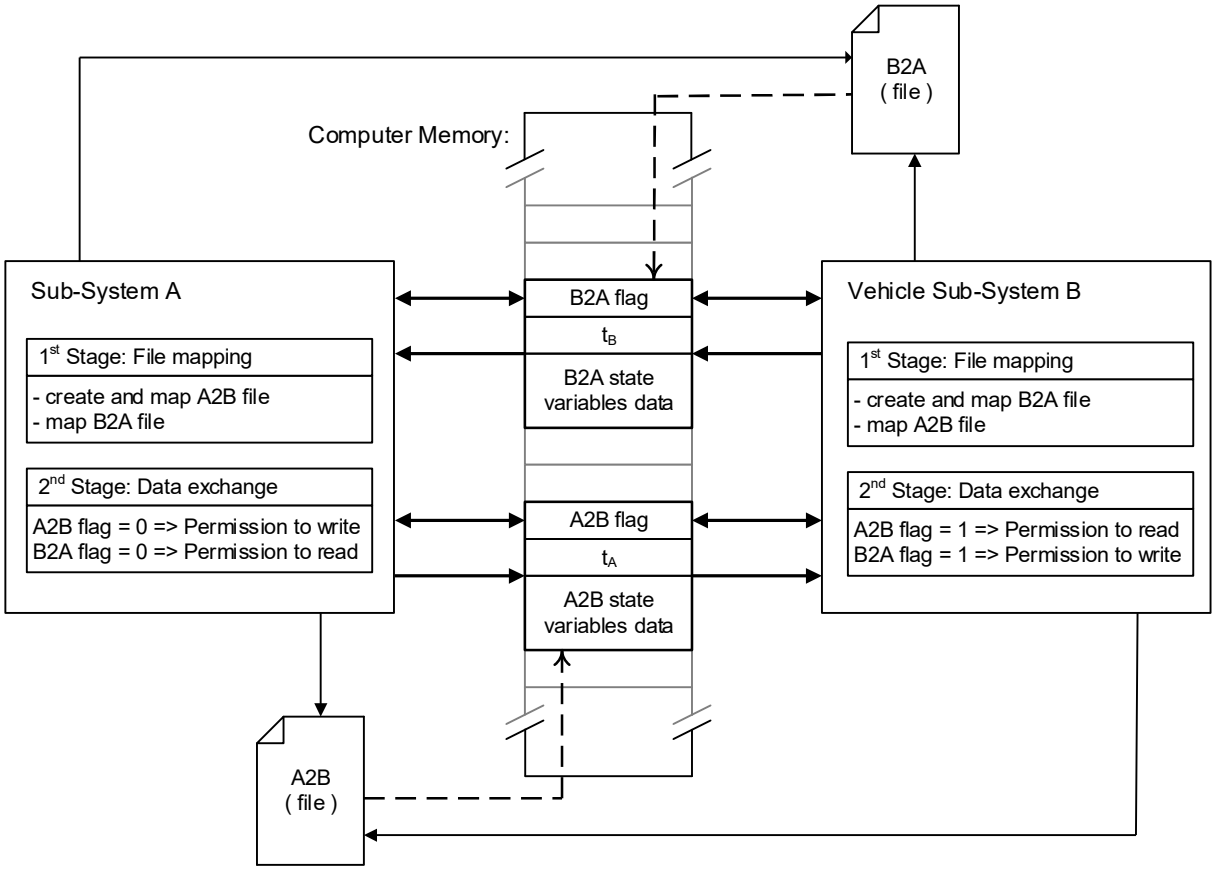

Figure 8.3: Data exchange procedure.

The data exchange methodology implemented here also takes into consideration the time spent on data exchange between sub-systems, which must be negligible when compared to the computation time costs of the independent analyses. This is critical when dealing with large data or, as in this case, it is accessed frequently. The use of physical data files for information exchange, also known as file input/output, is a robust, well known and very popular methodology. However, for either a recursive use or for large data sets it leads to a slow data exchange. Therefore, the data exchange procedure exchanges the file data by memory sharing via memory mapped files. A memory mapped file is a segment of computer memory which is mapped in order to have a direct byte-for-byte assignment to a hard disk file or other resource that the operating system can reference with. Once this correlation is established, or using a

proper term “mapped”, the memory mapped file can be accessed by multiple processes directly from computer memory becoming a much faster data exchange process. This memory sharing implementation is also depicted in Figure 8.3. At the start of the analysis, one of the applications creates a file and maps it to memory while the other waits for the file to be created. Whenever this file is found by the waiting application the file is also mapped to the same corresponding memory address. Having both applications mapped the same file in memory they can communicate using a common memory address whereas the created file only serves has a point of reference for both applications to map the same dataset in memory.

8.3 Communication protocol

The communication protocol is responsible for managing the use and update of the state variables along the integration scheme of each sub-system. In this work, the heterogeneity of the integration schemes, used between each sub-subsystem, and the premise to keep them independent and fundamentally unchanged requires careful consideration. Thus, the compatibility between the two integration algorithms imposes that the state variables of the two sub-systems, or a reliable prediction, are readily available at every time step. This is guaranteed by a state variable time interpolation/extrapolation scheme presented in Figure 8.4. Note that this scheme is used for both the pantograph-catenary and vehicle-track interactions, being one the sub-systems correspondent to the finite element model, *FEM*, of either the catenary or the track, while the other correspondent to the multibody model, *MB*, of either the pantograph or the vehicle. Following the interpolation/extrapolation scheme presented, the finite element model is evaluated with a fixed time step where at a given time, t_n, it requires state variable data of the multibody model of to evaluate, either the pantograph-catenary or wheel-rail contact forces at time, t_{n+1}, and proceed with its dynamics analysis. Meanwhile, the multibody model, evaluated with a predictor-corrector, variable time step integration algorithm scheme, requires the resulting contact forces to be applied on its respective bodies and proceed with its own integration. Therefore, there is the need of one of the sub-systems to make a prediction to a forthcoming time to proceed. Given the multibody model integration algorithm requires to make predictor steps at unknown times before committing to a corrector step, it is selected as the leading sub-system. Hence, it predicts the state variable data from the finite element sub-system using a linear extrapolation scheme, based on posterior provided data, until its time step is higher than t_{n+1}. At this point the multibody subsystem interpolates the results from its neighbouring time steps and builds its states variables for time t_{n+1}, *(1)*, to be shared with the

finite-element sub-system, (2). Thus, the finite element sub-system is then able to solve its following time step t_{n+1}, (3), and built its state variables to be passed to the multibody subsystem (4). Hereafter the multibody subsystem is able to lead again and extrapolate the latest finite element state variable data, (5), and solve its next time steps until it passes time t_{n+2}. It is important to note that the accuracy and stability of this methodology relies on ensuring that the multibody sub-system variable time step size is never larger than the fixed time step of the finite element model. Furthermore, the multibody integrator time step size is also required to be small enough so it does not critically overextend the state variable extrapolation. This is guaranteed by limiting its maximum step size to be smaller than the track time step size.

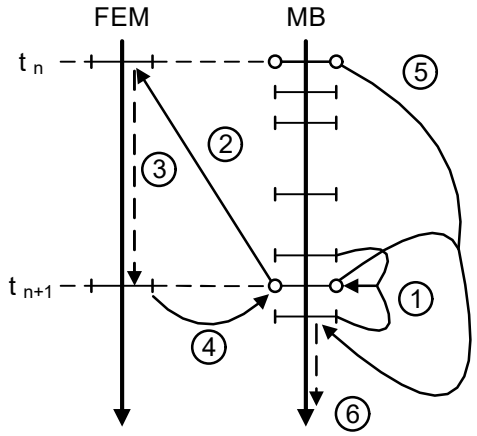

Figure 8.4: Sate variable time interpolation/extrapolation scheme.

With the interpolation/extrapolation scheme defined, a communication protocol is established between both sub-systems, where the use and update of the state variables are scheduled along the integration scheme of each sub-system are set. Note that this procedure implies that, at times, one of the sub-systems must wait on the other until state variable data is available to continue. This process is guaranteed by the flag system established on the data exchange procedure presented earlier. The communication protocol implemented for the vehicle-track interaction is presented in Figure 8.5, being the one for pantograph-catenary analogous such that the only change are the state variables used.

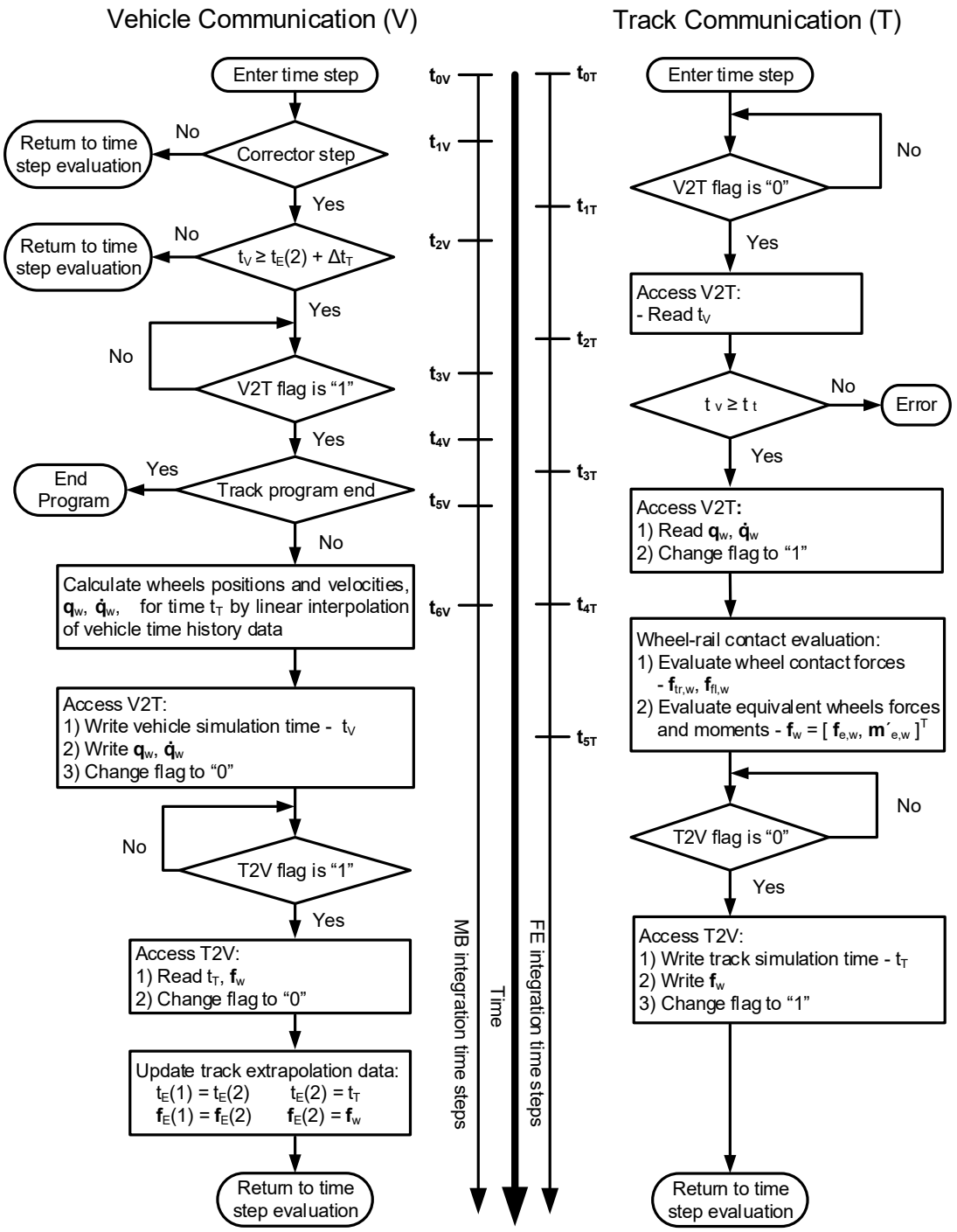

Figure 8.5: Vehicle-Track communication protocol

.

9 Summary of the Chapters Presented in Part II

The chapters presented in Part II of this thesis aim to present the development and use of the numerical analysis tools developed in this work. *Chapter 11* to *Chapter 16* are related to pantograph-catenary interaction while *Chapter 17* and *Chapter 18* to vehicle-track interaction. Furthermore, *Chapter 16* and *Chapter 18* present the final stage of the developed numeric analyses tools proposed on this work.

9.1 PantoCat statement of method

Chapter 11 is a statement of method produced as part of the pantograph–catenary interaction benchmarks initiative [108]. This initiative was proposed by Politecnico di Milano in order to benchmark software packages for the simulation of pantograph–catenary interaction developed by the leading companies, research institutes and universities. The aim of the benchmark was to compare modelling approaches across the existing software and to quantitatively analyse the results produced, thereby assessing their dispersion allow the identification of open issues. Each participant on the initiative was assigned to provide a statemented of method describing the methodologies employed and the software package capabilities so a comprehensive overview of the present state-of-the-art could be obtained. *Chapter 11* is one of these statement of methods, describing, *PantoCat*, a pantograph-catenary interaction numeric analysis tool developed by the author of this thesis, prior to the start of the PhD, and by Prof. J. Ambrósio and Prof. J. Pombo, following European projects EUROPAC and PantoTRAIN. Hence, the work developed to produce this statement of method conveniently started in synch with the initial work developed on this PhD work where the thesis author was responsible for all model implementations, numeric simulations and analyses. It was required to update and consolidate the developed numerical analysis tool, including the addiction of a catenary initialization

procedure, presented in Chapter 14. It was also required to ensure that the developed numerical tool provides reliable results. This was achieved by comparing the numerical results obtained against experimental results, made available from PantoTRAIN project, and by successfully reviewing and fulfilling all the requirements set on European standard EN50318. The benchmark initiative also required for each participant to provide the results of a set of static and dynamic simulation cases on which their input data was previously agreed on by all participants. The compilation and comparison of these results was presented on a single article, [10], where due to the extensive number of collaborators the list of authors was limited only one representative member of each participation, excluding the author of this thesis. Nevertheless, the *PantoCat* results were part of the work developed on this thesis, by its author, and can be found in [10].

9.2 A Comparative Study between Two Pantographs in Multiple Pantograph High-Speed Operations

Chapter 12 portraits the use of the developed pantograph-catenary numerical analysis tool to study the dynamic behaviour of pantograph-catenary interaction under a multiple pantograph operation scenario. As large majority of the pantographs in operation have been developed with particular catenary systems in mind, forming national pantograph-catenary pairs such as the CX-LN2 (France), DSA380-Re330 (Germany) and ATR95-C270 (Italy), this study also considers pantograph-catenary interaction in an interoperability scenario. For this purpose, the interaction of different pantographs, CX and ATR95, between the same catenary, LN2, was evaluated considering single and multiple pantograph operation scenarios.

The comparison between the obtained results showed that in multiple pantograph operations the passage of the front pantograph affects the performance of the rear one. Depending on the distance between pantographs, this influence can be positive or negative when compared with a single pantograph operation. On the other hand, it is observed that the presence of the rear pantograph has a negligible influence on the contact quality on the leading one, at least for the pantograph interval distances considered. The results also show that the French pantograph-catenary pair, CX-LN2, provided acceptable contact quality results in the framework of the regulation set by European standard EN50367. However, with the interoperable pair considered, ATR95-LN2, a noticeable contact quality degradation is observed where the standard deviation of the developed contact forces exceeds the regulated limit. This suggests that there is an inherited compatibility between the pantograph-catenary pairs used on each railway network and indicate that questions of compatibility in several

operational conditions, including interoperability scenarios, can be addressed by numerical tools such as the one here presented, reducing the costs and time required for vehicle homologation.

9.3 Dynamic Analysis of the Pantograph-Catenary Interaction on Overlap Sections for High-Speed Railway Operations

As stated, one of the objectives of the PhD work is to build a pantograph-catenary interaction numerical analysis tool with a detailed representation of a catenary system set along the general trajectory of the track. This includes the consideration of catenary overlap sections which in respect to the contact quality represent a critical zone having the responsibility to provide a smooth transition between subsequent catenaries. These irregularities in the system can lead to increased contact force variation and thereby contact loss possibility with consequent contact quality degradation. In Chapter 13, the developed numerical tool is employed to study the dynamic behaviour of pantograph-catenary interaction on overlap sections in a realistic case scenario. Single and multi pantograph operations are also considered in this work. The comparison between the results obtained allowed to relate the contact quality degradation between a normal and an overlap section of the same catenary as also identify that the uplift imposed on the contact wire at the section overlap contact has a significant influence on the quality of the contact. Moreover, the contact quality degradation is particularly noticeable for the leading pantograph in multi pantograph operations when close separations between pantographs are used.

9.4 Catenary Finite Element Model Initialization using Optimization

In Chapter 14, an implementation of a catenary initialization procedure is presented, i.e., a methodology that allows to determine the undeformed mesh of the catenary model that upon being statically loaded by the gravitational and axial tension loads exhibit a correct static deformed shape, with special attention to the contact wire position along the track and its prescribed sag. The methodology here presented is based on obtaining the solution of a minimization problem by means of a classical gradient based optimization.

The results reveal that this methodology is effective and provides accurate finite element catenary models for further dynamic behaviour analysis studies. The proposed methodology also opens the possibility to model catenary systems that have defects such as irregularities on

its sag caused by damaged, poorly maintained or ill mounted overhead lines. Nevertheless, this last option is left for future research not being the main aim of the work in this thesis.

Note also, that the methodology considered is only applied to catenary models set on straight tracks. Further research revealed the need to consider an alternative approach when dealing with catenaries in curved track. Nevertheless, this alternative approach, presented in Chapter 16, is based on the same methodology principles explored here.

9.5 On the Requirements of Interpolating Polynomials for Path Motion Constraints

In the work developed on this thesis, an accurate spatial definition of the track and its rails is required. This is established through the parametrization of the track and rails centreline curves using a polynomial interpolation scheme and the definition of a local reference frame which defines the orientation of the track running surface and the rails cross section. In fact, this procedure is used for two distinct functions, one is to establish a geometry database to build the track and catenary finite element models. The other is to define the path of the pantograph which is set by path motion constraint using a multibody dynamics formulation. The formulation of this kinematic constraint requires the evaluation of the fourth derivative of the curve with respect to its arc length where strictly from a geometric point of view C^2 polynomials would suffice. Moreover, higher order polynomials lead to unwanted curve oscillations on its interpolated geometry such that the use of lower order polynomials provide a better local geometric control.

In Chapter 15 it is shown that for multibody dynamic formulations with dependent coordinates the use of cubic polynomials is possible, being the dynamic response similar to that obtained with higher order polynomials. The stabilization of the equations of motion, always required to control the constraint violations during long analysis periods due to the inherent numerical errors of the integration process, is enough to correct the errors introduced by using a lower order polynomial interpolation and thus forfeiting the analytical requirement for higher order polynomials.

This research permitted the use a cubic shape preserving spline, [53], for the parametrization of the track and rail centrelines, which avoids unwanted oscillations and overshooting on curve transitions, providing a more accurate representation of the geometries considered.

9.6 A New Methodology to Study the Pantograph-Catenary Dynamics in Curved Railway Tracks

Chapter 16 portraits the final development of the pantograph-catenary numerical analysis tool proposed in this work, where an approach for the fully three-dimensional dynamic analysis of pantograph-catenary interaction in general railway tracks, including curves, is presented. This approach advances the state-of-the-art on pantograph-catenary interaction modelling and analysis as currently only catenaries in straight track are considered. In this work, Both the catenary model and the trajectory of the pantograph are defined with respect to the track geometry considering the conventional definition used by the rail industry, i.e., curvature, cross level and vertical position of the track. The finite element method is used to model and evaluate the dynamic behaviour of a catenary system following the methodology presented in previous works. To cope with the general geometry of the track and its resulting path, the pantograph model is developed using a spatial multibody dynamics formulation where the pantograph base motion, which is fixed to the railway vehicle roof, is defined by a prescribed kinematic motion constraint. As both pantograph and catenary use different formulations, their interaction is established through a co-simulation procedure where a penalty method is used to evaluate the contact force between the pantograph and the catenary.

Two demonstration cases are presented, one represents an existing scenario where both the catenary layout and track geometry are obtained from the technical designs of a railway network in current operation. The other case study presents a variation on the benchmark study of pantograph–catenary interaction in which the tracks are set with a different curve radius and an alternative contact wire staggering approach is used. It is shown that for large curve radius tracks the contact quality is marginally affected by the curvature. For smaller radius curves, the staggering design and the resulting support forces at the cantilever support play a fundamental role in maintaining the contact quality.

9.7 Finite Element Methodology for Flexible Track Models in Railway Dynamics Applications

Chapter 17 reports the first steps in the development of the finite element methodology to build a flexible model of the track. This includes the track finite element model discretization and a description of all the required geometric and property data of all the structural elements considered. Also in this work, to validate the finite element numeric procedure that evaluates the track model, developed by the author of the thesis, a realistic flexible track model is built

and subjected to static loads representing the wheel set of a railway vehicle. The obtained results are compared against the ones provided by ANSYS.

Later on, the methodology to build a discretized finite element model of the track was further developed by J. Costa in collaboration with the author of this thesis. The main improvement being the automatic generation of the finite element model with respect to provided track and rail geometry data such that the model could consider generalized track trajectories. This methodology is presented in *Chapter 16* and [109].

9.8 A co-simulation approach to the wheel-rail contact with flexible railway track

Chapter 18 presents the final development of the vehicle-track numerical analysis tool proposed in this thesis. The standard approach to railway vehicle dynamic analysis is performed by running vehicle multibody models in rigid railway tracks. This traditional approach disregards the coupling effects between the railway vehicle dynamics and the railway track flexibility. In the work here presented the assumption of rigidity of the railway track is released and a finite element model of the complete track, i.e., rails, pads, sleepers, ballast and infrastructure, is used to represent the track geometry and flexibility. A rail-wheel contact model that evaluates the contact conditions and forces is used online. The dynamics of the railway vehicle is described using a multibody methodology while the track structure is described using a finite element approach. Due to the fact that not only the multibody and the finite element dynamic analysis use different integration algorithms but also because the vehicle and track models are simulated in different codes a co-simulation procedure is proposed and demonstrated to address the coupled dynamics of the system.

The methodology proposed here is demonstrated in an application in which the railway vehicle-track interaction shows the influence of the vehicle dynamics on the track dynamics and vice-versa. Not only significative differences on the vehicle kinematics exist when considering the track flexibility, namely during curve negotiations, but also the contact forces are modified, being the lateral, or creep, forces higher for a flexible track. The track deformations are clearly identified, and closely related to the train wheelset kinematics. However, the results obtained do not allow to understand up to what extend the track flexibility influences the vehicle dynamics being this object of further research.

10 Concluding Remarks

In this work, two numerical analysis tools are developed and employed to study the dynamic behaviour of railway systems. One of these applications is a state-of-the-art numerical implementation to analyse the dynamics of pantograph-catenary interaction. Besides being able to employ multibody pantograph model its main novelty is the capability to consider catenaries mounted in any generalised track trajectory, including curves. The second application is able to analyse the dynamic behaviour of vehicle-track interaction with detailed models of the vehicle and the track considering track flexibility. On both these tools the implementation of a co-simulation procedure, developed on this work, plays a fundamental role on coupling the dynamic behaviour between the finite element models of the catenary and track finite element models and the multibody models of pantograph and vehicle. Thus, bringing the advantage to employ a specific formulation and time integration scheme for each sub-system that better suit its modelling requirements.

Furthermore, in this work, both the finite element models of the catenary and the track are built according to track design geometry data. Here a common railway geometry database provides a spatial definition of the track and rails centrelines which includes, for a given track length, its position and orientation. This database is assembled by a railway geometry processing tool which reconstructs standard information required for railway vehicle dynamics applications, i.e., curvature, cross level and vertical profile as function of the track arc-length.

As represented in Figure 10.1, the modularity and integration of all the numerical tools and procedures developed provides the ability to diligently update any methodology as needed. Thus, it stays open for additional implementations that may be required for particular research topics with specific modelling requirements, where a basis computational framework is already established.

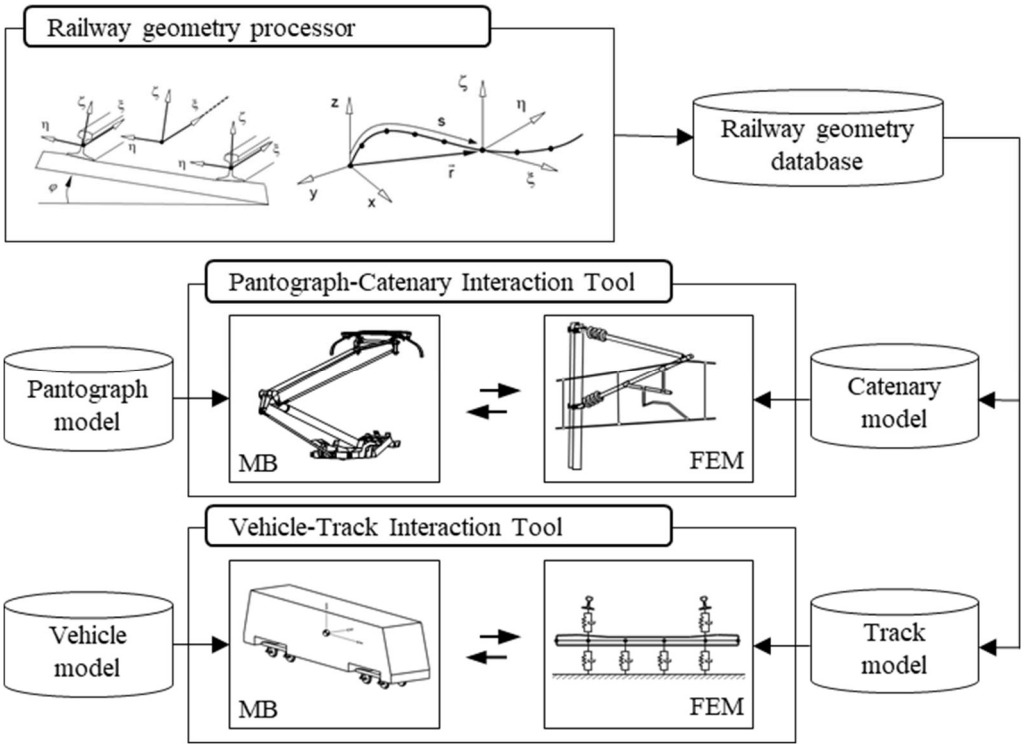

Figure 10.1: Diagram of the workflow between the numerical applications.

10.1 Overview of novel developments

Enclosed in the work of this thesis several novel developments are captured. These are a current topic of research and present innovative methodologies that give rise to advancements in the computational analysis of railway systems. Listed below in an overview of the main novelties development on the course of this work which represent a significant contribution to the state-of-the-art on both the academic research stratum and the railway industry:

- A new methodology to analyse the dynamic behaviour of pantograph-catenary interaction in generalised railway track trajectories including curved tracks.
- Generation of realistic catenary models based on industry standard catenary layout and track geometry data including overlap sections.
- Initialization of the pre-deformed shape of static loaded catenaries using optimisation techniques.
- A new methodology to include track flexibility in the dynamic analysis of vehicle-track interaction.
- Methodology for the loading of long beam discretised structures for traveling contact loads due to rigid bodies of a multibody system.

- A systematic and robust interpolation methodology based on cubic or quintinc polynomials for the representation of railways and roller coaster tracks.
- Unified and consistent geometry generation of rigid and flexible railway tracks and catenary geometries.
- Development of co-simulation procedures for the coupling of the dynamic behaviour between finite element and multibody models.

Furthermore, the numeric simulation tools developed for the dynamic analysis of pantograph-catenary and vehicle-track interaction offer solutions, with technological relevance, which provide answers to the industry most recent needs in better understanding the dynamic behaviour of railway systems. Besides being able to perform dynamic behaviour evaluations for analysis and project design, the numeric tools developed are capable of performing virtual certification and homologation analyses, accordingly, to specified railway standards, which minimize the need for very costly and time consuming line tests. Thus, contributing on the research and development effort to improve the competitiveness of railways.

10.2 Future research directions

With the two numerical analysis tools presented here, for the dynamics analysis of pantograph-catenary and vehicle-track interaction, two general research directions can be followed. One relates to the use of the numerical tools developed to study particular problems in the railway industry. The other follows the further development of the numeric tools and methodologies used.

In the realm of pantograph-catenary dynamics the developed tool opens the possibility to analyse novel case studies of interest to the rail industry. One is the influence of wind loads on the pantograph-catenary contact quality in curved tracks, where the wind solicitations imply a change on the lateral forces imposed by the contact wire at its cantilever support. There are also cases where optimisation procedures in conjunction with pantograph-catenary dynamic analysis applications can be used to reach optimised designs of pantograph or catenary systems. In such cases, considering the optimisation only in straight tracks might be limitative when contemplating a generalised track path. One other aspect of interest is the analysis of pantograph-catenary interaction over tracks with small radius curves, particularly on railway tracks that are to be upgraded for higher operational speeds, which often require a change on the contact and messenger wire axial tension, as well as the catenary layout geometry.

Furthermore, one aspect that was left out on the work of this thesis was the further development of full multibody pantograph models. Although these models have its advantages and are able to be used on the software here developed further research is required in order to understand the minimal requirements for modelling multibody pantographs with a realistic behaviour in the complete frequency range of their operation.

Regarding vehicle-track interaction considering flexible tracks and generalised track trajectories. Although the presented results show that the flexibility of the track is being reflected in the vehicle movement, and therefore the implemented co-simulation procedure is presenting itself as an acceptable methodology to account for track flexibility in the analyses, the validity of the track model is still uncertain. This is mainly due to its characterization being made by several parameters that must be tuned, where also some of which, such as the track lateral stiffness, are still a current topic of research. In any case, it is predictable to obtain very precise models with respect to experimental results and further investigation. Furthermore, it is still unknown to what extend the track flexibility influences the vehicle dynamics as also what implications this phenomenon can have in aspects such as wheel-rail contact and resulting wear. Further studies on these aspects of vehicle-track coupled dynamics are currently being carried in collaboration with other researchers. This includes the implementation of new non-Hertzian wheel-rail contact models and the development of 3D general curved beam finite elements to better discretize the rails. There is also interest on further developing the modelling methodologies employed in order to reach other topics in current research such as unsupported sleepers and other track flaws, as also vehicle-track interaction in switches and crossings where the flexibility of the rails is required to be considered.

In addition, it is possible for the co-simulation procedure developed in this work to be further developed. One of the most critical aspects of this procedure is ensuring its accuracy and stability which is guaranteed by ensuring that a close prediction of the state variables, on one side of the sub-systems, can be relied upon. In this work, this is ensured by controlling the integration time step sizes between both algorithms which in turn, depending of the problem, may have implications on the efficiency of the procedure. By changing the steeping scheme and/or applying a more robust prediction method of the state variables it may be possible to overcome this issue. Moreover, the application of this co-simulation procedure in other areas of research may be of interest such as co-simulation with active control modules on tilting trains or active pantographs, or in other applications outside the realm of railways.

References

[1] OECD. Strategic Transport Infrastructure Needs to 2030. Paris, France: OECD Publishing; 2012.

[2] ERRAC - European Rail Research Advisory Council. Strategic Rail Research Agenda 2020. Brussels, Belgium, Belgium; 2007.

[3] EC - European Commission. Roadmap to a Single European Transport Area - Towards a Competitive and Resource Efficient Transport System. Brussels, Belgium, Belgium; 2011.

[4] Nikravesh PE. Computer-Aided Analysis of Mechanical Systems. Englewood Cliffs, New Jersey: Prentice-Hall; 1988.

[5] Przemieniecki JS. Theory of Matrix Structural Analysis. New York: McGraw-Hill; 1968.

[6] Iwnicki S. The Manchester Benchmarks for rail simulators - An introduction. Veh. Syst. Dyn. 1998;30:717–722.

[7] Pombo J, Ambrósio J, Pereira M, et al. Influence of Pantograph Characteristics on the Overhead Contact Quality for High Speed Trains. Veh. Syst. Dyn. 2009;47:1327–1347.

[8] Bruni S, Ambrosio J, Carnicero A, et al. The results of the pantograph–catenary interaction benchmark. Veh. Syst. Dyn. 2014;53:412–435.

[9] Escalona JL, Sugiyama H, Shabana A a. Modelling of structural flexiblity in multibody railroad vehicle systems. Veh. Syst. Dyn. 2013;51:1027–1058.

[10] Bruni S, Ambrosio J, Carnicero A, et al. The results of the pantograph-catenary interaction benchmark. Veh. Syst. Dyn. 2015;53:412–435.

[11] Ambrósio J, Pombo J, Pereira M, et al. A Computational Procedure for the Dynamic Analysis of the Catenary-Pantograph Interaction in High-Speed Trains. J. Theor. Appl. Mech. 2012;50:681–699.

[12] Ambrósio J, Pombo J, Pereira M, et al. Recent Developments in Pantograph-Catenary Interaction Modelling and Analysis. Int. J. Railw. Technol. 2012;1:249–278.

[13] Pombo J, Ambrósio J, Silva M. A New Wheel-Rail Contact Model for Railway Dynamics. Bruni Ed. S, editor. Veh. Syst. Dyn. 2007;45:165–189.

[14] Pombo J, Ambrósio J. Application of a Wheel-Rail Contact Model to Railway Dynamics in Small Radius Curved Tracks. Multibody Syst. Dyn. 2008;19:91–114.

[15] Collina A, Bruni S. Numerical Simulation of Pantograph-Overhead Equipment Interaction. Veh. Syst. Dyn. 2002;38:261–291.

[16] Shing AWC, Wong PPL. Wear of pantograph collector strips. J. Rail Mass Transit. 2008;222:169–176.

[17] Bucca G, Collina A. A Procedure for the Wear Prediction of Collector Strip and Contact Wire in Pantograph-Catenary System. Wear. 2009;266:46–59.

[18] Pombo J, Antunes P. A Comparative Study Between Two Pantographs In Multiple Pantograph High-Speed Operations. Internatinal J. Railw. Technol. 2013;2:83–108.

[19] Liu Z, Jönsson PA, Stichel S, et al. Implications of the operation of multiple pantographs on the soft catenary systems in Sweden. Proc. Inst. Mech. Eng. Part F J. Rail Rapid Transit. 2016;230:971–983.

[20] Bucca G, Carnevale M, Collina A, et al. Adoption of different pantographs preloads to improve multiple collection and speed up existing lines. Veh. Syst. Dyn. 2012;50:403–418.

[21] Antunes P, Ambrósio J, Pombo J, et al. Dynamic Analysis of the Pantograph-Catenary Interaction on Overlap Sections for High-Speed Railway Operations. Proc. Second Int. Conf. Railw. Technol. Res. Dev. Maint. Stirlingshire, UK: Civil-Comp Press; 2014.

[22] Harèll P, Drugge L, Reijm M. Study of Critical Sections in Catenary Systems During Multiple Pantograph Operation. Proc. Inst. Mech. Eng. Part F J. Rail Rapid Transit. 2005;219:203–211.

[23] Mei G, Zhang W, Zhao H, et al. A hybrid method to simulate the interaction of pantograph and catenary on overlap span. Veh. Syst. Dyn. 2006;44:571–580.

[24] Ambrósio J, Pombo J, Pereira M, et al. Optimization of high-speed railway pantographs for improving pantograph-catenary contact. Theor. Appl. Mech. Lett. 2013;3.

[25] Gregori S, Tur M, Nadal E, et al. An approach to geometric optimisation of railway catenaries. Veh. Syst. Dyn. 2017;3114:1–25.

[26] Bruni S, Bucca G, Collina A, et al. Numerical and Hardware-In-the-Loop Tools for the Design of Very High Speed Pantograph-Catenary Systems. J. Comput. Nonlinear Dyn. 2012;7:041013.

[27] Van OV, Massat JP, Laurent C, et al. Introduction of variability into pantograph-catenary dynamic simulations. Veh. Syst. Dyn. 2014;52:1254–1269.

[28] Carnicero A, Jimenez-Octavio JR, Sanchez-Rebollo C, et al. Influence of Track Irregularities in the Catenary-Pantograph Dynamic Interaction. J. Comput. Nonlinear Dyn. 2012;7:041015.

[29] Kulkarni S, Pappalardo CM, Shabana AA. Pantograph/Catenary Contact Formulations. J. Vib. Acoust. 2016;139:011010.

[30] Song Y, Liu Z, Wang H, et al. Nonlinear analysis of wind-induced vibration of high-speed railway catenary and its influence on pantograph–catenary interaction. Veh. Syst. Dyn. 2016;54:723–747.

[31] Facchinetti A, Bruni S. Hardware-in-the-loop hybrid simulation of pantograph–catenary interaction. J. Sound Vib. 2012;331:2783–2797.

[32] Schirrer A, Aschauer G, Talic E, et al. Catenary emulation for hardware-in-the-loop pantograph testing with a model predictive energy-conserving control algorithm. Mechatronics. 2017;41:17–28.

[33] Ambrósio J, Antunes P, Pombo J. On the Requirements of Interpolating Polynomials for Path Motion Constraints. In: Kecskeméthy A, Geu Flores F, editors. Mech. Mach. Sci. Springer International Publishing; 2015. p. 179–197.

[34] Pombo J, Ambrósio J. General Spatial Curve Joint for Rail Guided Vehicles: Kinematics and Dynamics. Multibody Syst. Dyn. 2003;9:237–264.

[35] Ambrósio J, Pombo J, Rauter F, et al. A Memory Based Communication in the Co-

Simulation of Multibody and Finite Element Codes for Pantograph-Catenary Interaction Simulation. In: Bottasso C.L. E, editor. Multibody Dyn. Dordrecht, The Netherlands: Springer; 2008. p. 211–231.

[36] Knothe K, Grassie SL. Modelling of Railway Track and Vehicle/Track Interaction at High Frequencies. Veh. Syst. Dyn. 1993.

[37] Magalhaes H, Ambrosio J, Pombo J. Railway vehicle modelling for the vehicle-track interaction compatibility analysis. Proc. Inst. Mech. Eng. Part K J. Multi-body Dyn. 2016;230:251–267.

[38] Mazzola L, Bruni S. Effect of suspension parameter uncertainty on the dynamic behaviour of railway vehicles. Appl. Mech. Mater. Trans Tech Publ; 2012. p. 177–185.

[39] Polach O, Evans J. Simulations of Running Dynamics for Vehicle Acceptance: Application and Validation. Int. J. Railw. Technol. 2013;2.

[40] Di Gialleonardo E, Braghin F, Bruni S. The influence of track modelling options on the simulation of rail vehicle dynamics. J. Sound Vib. 2012;331:4246–4258.

[41] Lundqvist A, Dahlberg T. Load impact on railway track due to unsupported sleepers. Proc. Inst. Mech. Eng. Part F J. Rail Rapid Transit. 2005;219:67–77.

[42] Recuero AM, Escalona JL, Shabana AA. Finite-element analysis of unsupported sleepers using three-dimensional wheel–rail contact formulation. Proc. Inst. Mech. Eng. Part K J. Multi-body Dyn. 2011;225:153–165.

[43] Johansson A, Pålsson B, Ekh M, et al. Simulation of wheel–rail contact and damage in switches and crossings. Wear. 2011;271:472–481.

[44] Martínez-Casas J, Di Gialleonardo E, Bruni S, et al. A comprehensive model of the railway wheelset–track interaction in curves. J. Sound Vib. 2014;333:4152–4169.

[45] Dietz S, Hippmann G, Schupp G. Interaction of Vehicles and Flexible Tracks by Co-Simulation of Multibody Vehicle Systems and Finite Element Track Models. Dyn. Veh. Roads Tracks. 2002;37:372–384.

[46] Zhai W, Wang K, Cai C. Fundamentals of vehicle–track coupled dynamics. Veh. Syst. Dyn. 2009;47:1349–1376.

[47] Esveld C. Modern Railway Track. Duisburg, Germany: MRT-Productions; 1989.

[48] Yamaguchi F. Curves and Surfaces in Computer Aided Geometric Design. Springer-Verlag; 1988.

[49] Mortenson ME. Geometric Modeling. New York, New York: Wiley; 1985.

[50] Iverson W. Analysis of the Reconstruction of Rail Geometry from Curvature Data. IEEE Trans. Ind. Appl. 1974. p. 368–379.

[51] Farin GE. Curves and Surfaces for Computer Aided Geometric Design: A Practical Guide. 2nd Editio. Comput. Sci. Sci. Comput. Boston, Massachussetts: Academic Press; 1990.

[52] De Boor C. A Practical Guide to Splines. Appl. Math. Sci. ; 27. New York, New York: Springer-Verlag; 1978.

[53] Irvine LD, Marin SP, Smith PW. Constrained interpolation and smoothing. Constr. Approx. 1986;2:129–151.

[54] Pina HLG. Métodos Numéricos (Numerical Methods). Lisbon, Portugal: McGraw-Hill; 1995.

[55] Tandl M. Dynamic Simulation and Design of Roller Coaster Motion. [Duisburg, Germany]: Universitat Duisburg-Essen; 2008.

[56] Friedrich K, Puschmann R, Schmieder A, et al. Contact Lines for Electric Railways: Planning, Design, Implementation, Maintenance. 3rd ed. Publicis; 2018.

[57] Dahlberg T. Moving force on an axially loaded beam - with applications to a railway overhead contact wire. Veh. Syst. Dyn. 2006;44:631–644.

[58] TSI ENE. Technical specifications for interoperability relating to the 'energy' subsystem of the rail system in the Union. Official Journal of the European Union. 1301/2014/EU; 2014.

[59] ERA - European Rail Agency. Study on Interface EURO/1950 pantographs and OCL design - ERA/2013/INTEROP/OP/01. European Union; 2013.

[60] UIC 606-1 OR standart. Consequences of the application of the kinematic gauges defined by UIC leaflets in the 500 series on the design of the contact lines. UIC; 1987.

[61] Poetsch G, Evans J, Maisinger R, et al. Pantograph/Catenary Interaction and Control. Veh. Syst. Dyn. 1997;28:159–195.

[62] Ambrósio J, Pombo J, Facchinetti A, et al. Key Parameters for Pantograph/Catenary Numerical Models - PantoTRAIN Technical Report D1.1. Brussels, Belgium: UNIFE; 2010.

[63] Arora JS. Introduction to Optimum Design. 3ed. Boston: Academic Press; 2012.

[64] Pombo J, Ambrósio J. An Alternative Method to Include Track Irregularities in Railway Vehicle Dynamic Analyses. Nonlinear Dyn. 2012;68:161–176.

[65] Bathe K-J. Finite element procedures in engineering analysis. Prentice-Hall Civ. Eng. Eng. Mech. Ser. Englewood Cliffs, N.J.: Prentice-Hall; 1982.

[66] Newmark N. A Method of Computation for Structural Dynamics. ASCE J. Eng. Mech. Div. 1959;85:67–94.

[67] Pombo J, Almeida T, Magalhães H, et al. Finite Element Methodology for Flexible Track Models in Railway Dynamics Applications. Int. J. Veh. Struct. Syst. 2013;5:43.

[68] Pombo J, Ambrósio J. Dynamic Analysis of the Railway Vehicle ML95. Lisbon, Portugal: IDMEC - Institute of Mechanical Engineering, Instituto Superior Técnico; 2004.

[69] Vieira R. High Speed Train Pantograph Models Identification (MSc Thesis). Instituto Superior Técnico; 2016.

[70] Ambrósio J, Pombo J, Rauter F, et al. Multiple Pantograph Interaction with Catenaries in High-Speed Trains. Proc. 8th World Congr. Railw. Res. Seoul, Korea; 2008.

[71] Carnevale M. Innovative Solutions for Improving Pantograph Dynamics and Current Collection. [Milan, Italy]: Politecnico di Milano; 2011.

[72] Flores P. Kinematics and dynamics of multibody systems with imperfect joints : models and case studies. Lect. notes Appl. Comput. Mech. Berlin: Springer; 2008.

[73] Ambrósio J, Verissimo P. Improved Bushing Models for Vehicle Dynamics", Multibody System Dynamics. Multibody Syst. Dyn. 2009;22:341–365.

[74] Ambrósio J, Rauter F, Pombo J, et al. A Flexible Multibody Pantograph Model for the Analysis of the Catenary-Pantograph Contact. In: Arczewski et al. (Ed.), editor. Multibody Dyn. Comput. Methods Appl. Dordrecht, The Netherlands: Springer; 2010. p. 1–27.

[75] Zhou N, Zhang W. Investigation of the Influence of the Pan-Head Elasticity on Pantograph-Catenary Dynamic Performance. Proc. 21st Symp. Dyn. Veh. Roads Tracks. Stockholm, Sweden; 2009.

[76] Vyasarayani CP, Uchida T, Carvalho A, et al. Parameter identification in dynamic systems using the homotopy optimization approach. Multibody Syst. Dyn. 2011;26:411–424.

[77] Ambrósio J, Pombo J, Massat J-P, et al. Pantograph Design Optimisation Methodology. Brussels, Belgium: UNIFE; 2012.

[78] Ambrósio J, Pombo J, Antunes P, et al. PantoCat statement of method. Veh. Syst. Dyn. 2015;53:314–328.

[79] Ambrósio J, Neto A. Stabilization Methods for the Integration of DAE in the Presence of Redundant Constraints. Multibody Syst. Dyn. 2003;10:81–105.

[80] Gear CW. Simultaneous Numerical Solution of Differential-Algebraic Equations. IEEE Trans. Circuit Theory. 1971;18:89–95.

[81] Seo J-H, Sugiyama H, Shabana A a. Three-Dimensional Large Deformation Analysis of the Multibody Pantograph/Catenary Systems. Nonlinear Dyn. 2005;42:199–215.

[82] Seo J-H, Kim S-W, Jung I-H, et al. Dynamic Analysis of a Pantograph-Catenary System Using Absolute Nodal Coordinates. Veh. Syst. Dyn. 2006;44:615–630.

[83] Pereira C, Ramalho A, Ambrósio J. A Critical Overview of Internal and External Cylinder Contact Force Models. Nonlinear Dyn. 2011;63:681–697.

[84] Toridis TG, Khozeimeh K. Computer analysis of rigid frames. Comput. Struct. 1971;1:193–221.

[85] Lankarani HM, Nikravesh PE. A Contact Force Model with Hysteresis Damping for Impact Analysis of Multibody Systems. AMSE J. Mech. Des. 1990;112:369–376.

[86] Polach O. A Fast Wheel-Rail Forces Calculation Computer Code. Veh. Syst. Dyn. 1999;33:728–739.

[87] Wen Z, Wu L, Li W, et al. Three-dimensional elastic–plastic stress analysis of wheel–rail rolling contact. Wear. 2011;271:426–436.

[88] Felippa CA, Park KCC, Farhat C. Partitioned analysis of coupled mechanical systems. Comput. Methods Appl. Mech. Eng. 2001;190:3247–3270.

[89] Hulbert G, Ma Z-D, Wang J, et al. Gluing for Dynamic Simulation of Distributed Mechanical Systems. In: Ambrósio (Ed.) J, editor. Adv. Comput. Multibody Syst. Dordrecht, The Netherlands: Springer; 2005. p. 69–94.

[90] Kubler R, Schiehlen W. Modular Simulation in Multibody System Dynamics. Multibody Syst. Dyn. 2000;4:107–127.

[91] Heckmann A, Arnold M, Vaculín O. A modal multifield approach for an extended flexible body description in multibody dynamics. Multibody Syst. Dyn. 2005;13:299–322.

[92] Liu F, Cai J, Zhu Y, et al. Calculation of Wing Flutter by a Coupled Fluid-Structure Method. J. Aircr. 2001;38:334–342.

[93] Bathe KJ, Zhang H. Finite element developments for general fluid flows with structural interactions. Int. J. Numer. Methods Eng. 2004;60:213–232.

[94] Naya M, Cuadrado J, Dopico D, et al. An Efficient Unified Method for the Combined Simulation of Multibody and Hydraulic Dynamics: Comparison with Simplified and Co-Integration Approaches. Arch. Mech. Eng. 2011;LVIII:223–243.

[95] Busch M, Schweizer B. Coupled simulation of multibody and finite element systems: an efficient and robust semi-implicit coupling approach. Arch. Appl. Mech. 2012;82:723–741.

[96] Carstens V, Kemme R, Schmitt S. Coupled simulation of flow-structure interaction in turbomachinery. Aerosp. Sci. Technol. 2003;7:298–306.

[97] Spreng F, Eberhard P, Fleissner F. An approach for the coupled simulation of machining processes using multibody system and smoothed particle hydrodynamics algorithms. Theor. Appl. Mech. Lett. 2013;3:013005.

[98] Anderson KS, Duan S. A hybrid parallelizable low-order algorithm for dynamics of multi-rigid-body systems: Part I, chain systems. Math. Comput. Model. 1999;30:193–215.

[99] Wang J, Ma Z, Hulbert GM. A Gluing Algorithm for Distributed Simulation of Multibody Systems. Nonlinear Dyn. 2003;34:159–188.

[100] Verhoef M, Visser P, Hooman J, et al. Co-simulation of Distributed Embedded Real-Time Control Systems. In: Davies J, Gibbons J, editors. Integr. Form. Methods 6th Int. Conf. IFM 2007, Oxford, UK, July 2-5, 2007. Proc. Berlin, Heidelberg: Springer Berlin Heidelberg; 2007. p. 639–658.

[101] Spiryagin M, Simson S, Cole C, et al. Co-simulation of a mechatronic system using Gensys and Simulink. Veh. Syst. Dyn. 2012;50:495–507.

[102] Gu B, Asada HH. Co-Simulation of Algebraically Coupled Dynamic Subsystems Without Disclosure of Proprietary Subsystem Models. J. Dyn. Syst. Meas. Control. 2004;126:1.

[103] Schweizer B, Li P, Lu D, et al. Stabilized implicit co-simulation methods: solver coupling based on constitutive laws. Arch. Appl. Mech. 2015.

[104] Schweizer B, Li P, Lu D. Explicit and Implicit Cosimulation Methods: Stability and Convergence Analysis for Different Solver Coupling Approaches. J. Comput. Nonlinear Dyn. 2015;10:051007.

[105] Quinn MJ. Parallel Programming in C with MPI and OpenMP. McGraw-Hill Higher Education; 2004.

[106] Wilkinson B, Allen CM. Parallel Programming: Techniques and Applications Using Networked Workstations and Parallel Computers. Pearson/Prentice Hall; 2005.

[107] Downey AB. The Little Book of Semaphores. Science (80-.). 2009;211:1–291.

[108] Facchinetti A, Bruni S. Special issue on the pantograph–catenary interaction benchmark. Veh. Syst. Dyn. 2015;53:303–304.

[109] Costa J, Antunes P, Magalhães H, et al. Development of Flexible Track Models for Railway Vehicle Dynamics Applications. In: Pombo J, editor. Proc. Third Int. Conf. Railw. Technol. Res. Dev. Maint. Stirlingshire, UK: Civil-Comp Press; 2016.

[110] Collina A, Melzi S, Facchinetti A. On the Prediction of Wear of Contact Wire in OHE Lines: a Proposed Model. Veh. Syst. Dyn. 2002;37:579–592.

[111] European Commission EC. White Paper: Roadmap to a Single European Transport Area - Towards a Competitive and Resource Efficient Transport System. Brussels, Belgium; 2011.

[112] Arora JS. Introduction to Design Optimization. Introd. to Optim. Des. Elsevier; 2012.

[113] Bazaraa MS, Sherali HD, Shetty CM. Nonlinear Programming: Theory and Algorithms. 3rd ed. Wiley-Interscience; 2006.

[114] Ambrósio J, Antunes P, Pombo J, et al. A Computational Procedure for the Dynamic Analysis of the Catenary-Pantograph Interaction in High-Speed Trains. J. Theor. Appl. Mech. 2012;50:681–699.

[115] Reddy JN. An Introduction to the Finite Element Method. 3rd Editio. McGraw-Hill; 2005.

[116] MathWorks. MATLAB R2015a Documentation. The MathWorks, Inc.; 2015.

PART II

11 PantoCat statement of method

[1] The Pantograph-Catenary Dynamic Interaction Analysis Program (`PantoCat`) addresses the need for a dynamic analysis code able to analyse models of the complete overhead energy collecting systems that include all mechanical details of the pantographs and the complete topology and structural details of the catenary. `PantoCat` is a code based on finite elements method, for the catenary, and on multibody dynamics methods, for the pantograph, integrated via a co-simulation procedure. A contact model based on a penalty formulation is selected to represent the pantograph-catenary interaction. `PantoCat` enables models of catenaries with multiple sections, including their overlap, the operation of multiple pantographs and the use of any complex loading of the catenary or pantograph mechanical elements including aerodynamic effects. The models of the pantograph and catenary are fully spatial being simulated in tangential or curved tracks, with or without irregularities and perturbations. User-friendly interfaces facilitate the construction of the models while the post-processing facilities provide all quantities of interest of the system response according to the norms and industrial requirements.

11.1 Introduction

`PantoCat` is a software that allows modelling and performing the dynamic simulation of the pantograph-catenary interaction. The program includes 3 modules that, being able to operate independently, are interfaced in the same user environment: `PantoCatFEM`, which is a Finite

[1] The work presented in this chapter has been published, as it is, in: J. Ambrósio, J. Pombo, P. Antunes, M. Pereira, *PantoCat statement of method*, Vehicle System Dynamics, 53:3, 314-328, (2014).

Element dynamic analysis code responsible for handling the catenary dynamics, PantoCatMB that is a Multibody Dynamics analysis code responsible to handle the dynamic simulation of the pantograph, and PantoCatPro that handles the models initialization and the results post-processing. The dynamic analysis code use methods defined in the time domain that handle all nonlinear effects present in the pantograph and catenary dynamics, such as the dropper slacking, friction, large rotations and nonlinearities of the pantograph system or the contact developing between components of the pantograph or between the pantograph registration strips and the catenary contact wires.

The pantograph dynamic analysis code was first developed as a tool for the fully detailed modelling and analysis of realistic pantographs, including general motion trajectories and control models [1][2]. This module, PantoCatMB, is featured to be interfaced with catenary modelling and analysis software via co-simulation approaches [3]. In the scope of the European project EUROPAC the software, with the name Europacas-MB that is the basic version of the current module, was fully tested and advanced modelling features specific to pantograph mechanical systems were made available. However, the use of Europacas-MB in the framework of system optimization or other specific task soon showed limitations, due to the interactive features of the companion software [4][5]. These limitations were overcome by the development of the catenary dynamic analysis module, PantoCatFEM, whose implementation addresses not only the common dynamic analysis in a co-simulation environment with PantoCatMB but also design optimization, active control or any other environment in which it is necessary to run batches of simulations [6]. The advanced features of the software allow for the simulation of sophisticated and detailed models of the pantograph and catenary that have large sets of data, which are cumbersome, if not impossible, to manipulate by hand. The set of output data includes not only the contact forces but also all the kinematics of each mechanical element of the pantograph and catenary and the internal forces on both systems. In order to provide user friendly interfaces, the PantoCatPro module was released. The complete set of modules is simply designated by PantoCat. Within the European project PantoTRAIN the software was fully tested and used for a wide range of scenarios, being its results compared with those of other software or with inline experimental data, when available, building not only the confidence on its quality but also identifying the required features for its use in practical applications [7]. Models for many of the European catenaries have been developed and analysed with PantoCat, being it able to handle stitch wire, composite or simple catenary types with one or more contact wires.

The models for the catenaries are developed using the finite element method for tangent and curved tracks being the analysis fully 3-dimensional. The pantograph models may be lumped mass or fully 3-dimensional multibody and their base motion is defined as if the pantograph is roof-mounted in a vehicle that follows the track for which the catenary is developed. With this approach it is possible to include pantograph motion perturbations originated either from the general vehicle railway dynamics or from any other source [8]. Due to the detailed pantograph modelling, wind forces acting on the pantograph elements can be included in the analysis [9]. Basically, any mechanical element existing in current pantograph construction technology can be included in the `PantoCatMB` models [10]. The catenary and pantograph dynamic analysis codes run in a co-simulation environment. It is possible to simulate single or multiple pantograph operations in catenaries that may include overlap sections [11][12]. All outputs considered in current regulations are standard in the `PantoCatPro` code. The current output of `PantoCat` include:

- Kinematics of the overhead system, i.e., displacement, velocity and acceleration of all nodes of the model
- Kinematics of all components of the pantograph, i.e., displacement, velocity and acceleration of the center of mass of all components or of any particular point
- Contact forces between the pantographs registration strips and the catenary contact wires, raw and filtered
- Position of the contact points in the contact wires and registration strips
- Joint reaction forces between the pantograph mechanical elements.
- Forces in the catenary droppers
- Uplifts of the catenary steady arms.
- Statistical parameters of the contact forces including average, standard deviation, maximum, minimum, number of contact losses, etc.
- Histograms of the contact forces
- PSD of the contact forces.
- RMS of the contact forces.
- Animation of the catenary and pantograph kinematics

The software `PantoCatFEM` is written in Matlab as well as the `PantoCatPro` pre and post processing, including its graphical user interface. The multibody code `PantoCatMB` is programmed in Fortran95 while the post-processed results are displayed in Microsoft Excel.

11.2 Methods applied in the benchmark

The `PantoCat` code is structured into two independent modules that handle the catenary dynamics, `PantoCatFEM` which is a finite element module programmed in Matlab, and the pantograph, `PantoCatMB` which is a multibody dynamics module programmed in Fortran. These modules run in a co-simulation computational environment being their interaction achieved via the contact force between the contact strips of the pantographs and the contact wire of the catenary for which a penalty contact force formulation is used.

11.2.1 Catenary Analysis Module and Models

The finite element method is used to describe the catenary dynamics. The equilibrium equations for the catenary structural system are assembled as [12]

$$\mathbf{M}\,\mathbf{a} + \mathbf{C}\,\mathbf{v} + \mathbf{K}\,\mathbf{x} = \mathbf{f} \tag{11.1}$$

where **M**, **C** and **K** are the finite element global mass, damping and stiffness matrices of the finite element model of the catenary. All catenary elements, contact and messenger wires are modelled by using Euler-Bernoulli beam elements. Due to the need to represent the high axial tension forces the beam finite element used for the messenger, stitch and contact wire, designated as element *i*, is written as

$$\mathbf{K}_i^e = \mathbf{K}_L^e + F\,\mathbf{K}_G^e \tag{11.2}$$

in which $\mathbf{K}^e{}_L$ is the linear Euler-Bernoulli beam element, F is the axial tension and $\mathbf{K}^e{}_G$ is the element geometric matrix. The droppers and the registration and steady arms are also modelled with the same beam element but disregarding the geometric stiffening. The mass of the gramps, attaching droppers to wires, are modelled here as lumped masses.

Proportional damping is used to evaluate the damping matrix of each finite element, i.e., $\mathbf{C}^e = \alpha^e\,\mathbf{K}^e + \beta^e\,\mathbf{M}^e$ with α^e and β^e being proportionality factors associated with each type of catenary element, such as dropper, messenger wire, stitch wire, etc. Alternatively, the global damping matrix is evaluated with the same proportionality factors associated to all structural elements, i.e., $\mathbf{C} = \alpha\,\mathbf{K} + \beta\,\mathbf{M}$.

The nodal displacements vector is **x** while **v** is the vector of nodal velocities, **a** is the vector of nodal accelerations and **f** is the force vector, written as

$$\mathbf{f} = \mathbf{f}_{(c)} + \mathbf{f}_{(a)} + \mathbf{f}_{(d)} \tag{11.3}$$

which contains the pantograph contact forces, $\mathbf{f}_{(c)}$, the aerodynamic forces, $\mathbf{f}_{(a)}$, and the dropper slacking compensating terms, $\mathbf{f}_{(d)}$. Equation (11.1) is solved for **x** or for **a** depending on the integration method used.

The integration of the nodal accelerations uses a Newmark family integration algorithm. The contact forces are evaluated for $t+\Delta t$ based on the position and velocity predictions for the FE mesh and on the pantograph predicted position and velocity. The finite element mesh accelerations are calculated by

$$\left(\mathbf{M}+\gamma\,\Delta t\,\mathbf{C}+\beta\,\Delta t^2\mathbf{K}\right)\mathbf{a}_{t+\Delta t}=\mathbf{f}_{t+\Delta t}-\mathbf{C}\tilde{\mathbf{v}}_{t+\Delta t}-\mathbf{K}\tilde{\mathbf{d}}_{t+\Delta t} \tag{11.4}$$

Predictions for new positions and velocities of the nodal coordinates of the linear finite element model of the catenary are found as

$$\tilde{\mathbf{d}}_{t+\Delta t}=\mathbf{d}_t+\Delta t\,\mathbf{v}_t+\frac{\Delta t^2}{2}\left(1-2\beta\right)\mathbf{a}_t \tag{11.5}$$

$$\tilde{\mathbf{v}}_{t+\Delta t}=\mathbf{v}_t+\Delta t\left(1-\gamma\right)\mathbf{a}_t. \tag{11.6}$$

Then, with the acceleration $\mathbf{a}_{t+\Delta t}$ the positions and velocities of the finite elements at time $t+\Delta t$ are corrected by

$$\mathbf{d}_{t+\Delta t}=\tilde{\mathbf{d}}_{t+\Delta t}+\beta\,\Delta t^2\mathbf{a}_{t+\Delta t} \tag{11.7}$$

$$\mathbf{v}_{t+\Delta t}=\tilde{\mathbf{v}}_{t+\Delta t}+\gamma\,\Delta t\,\mathbf{a}_{t+\Delta t}. \tag{11.8}$$

In the current applications, to highspeed catenary dynamics, the coefficients used in the integration scheme depicted by Equations (11.4) through (11.8) are $\beta = ¼$ and $\gamma = ½$.

The droppers slacking is also corrected in each time step. Although the droppers perform as a bar during extension their stiffness during compression is either null or about $1/100^{\text{th}}$ of the extension stiffness. As the droppers stiffness is included in the stiffness matrix **K** as a bar element, anytime one of them is compressed such contribution for the catenary stiffness has to be removed or modified. In order to keep the dynamic analysis linear the strategy pursued here is to compensate the contribution to the stiffness matrix by adding a force to vector **f** equal to the bar compression force

$$\mathbf{f}_{(d)t+\Delta t}=\mathbf{K}^e_{dropper}\mathbf{B}\tilde{\mathbf{d}}_{t+\Delta t} \tag{11.9}$$

where the Boolean matrix **B** simply maps the global nodal coordinates into the coordinates of the dropper element.

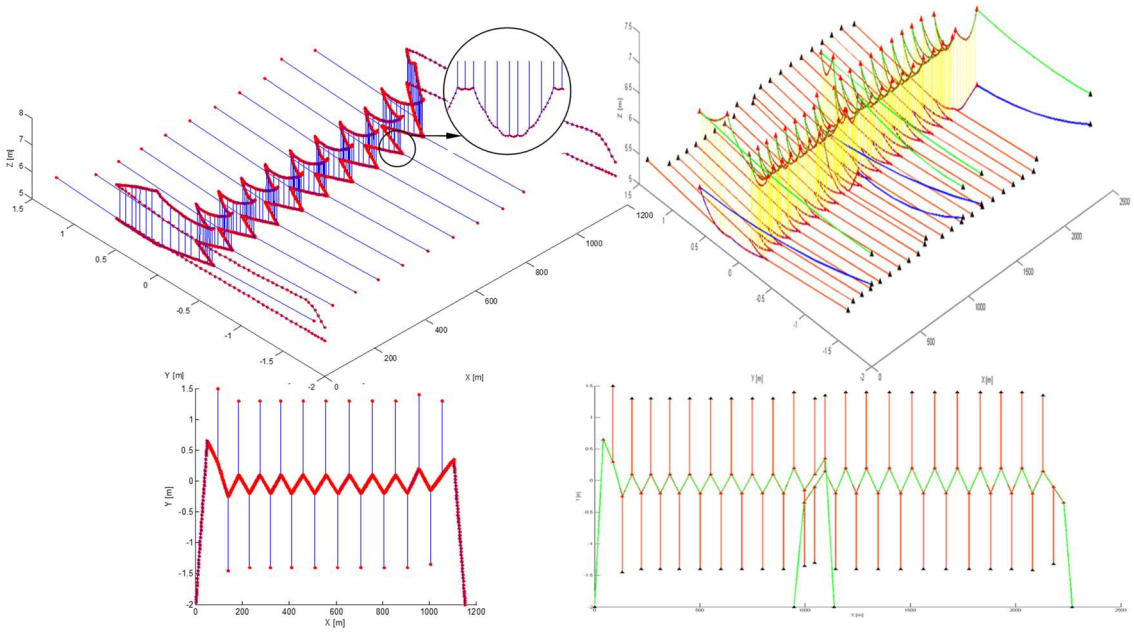

Figure 11.1: Finite element models of a catenary: single section with the sag highlighted and a plant view displaying the stagger; multiple sections and a plant view showing the overlap.

The correction procedure expressed by using Equations (11.5) through (11.9) and solving Equation (11.4) is repeated until convergence is reached for a given time step, i.e., until $\left|\mathbf{d}_{t+\Delta t}-\tilde{\mathbf{d}}_{t+\Delta t}\right|<\varepsilon_d$ and $\left|\mathbf{v}_{t+\Delta t}-\tilde{\mathbf{v}}_{t+\Delta t}\right|<\varepsilon_d$ being ε_d and ε_v user defined tolerances. At least 6 iterations must be allowed for the convergence process, although it is recommended that a maximum of 10 iterations is defined in order to prevent that residual compressive forces appear in the dropper elements.

The European project Pantotrain presented recommendations on the minimum number of elements to be used for the discretization of each structural component of the catenary finite element models [5]. The models studied here use 6 beam elements, between droppers, to represent the contact, messenger and stitch wires. For the droppers, steady arms and registration arms, if needed, a single beam element is used. In order to preserve the bar behaviour of the droppers under traction, steady arms and registration arms the moments of inertia of the beam elements used for their representation are keep to a minimum, lower than 10^{-11}. In this form not only the numerical stability of the methods used in the solution of the equations of motion is ensured but also the use of these residual values do not represent any rotational stiffness of the bar components of the model.

The wave travelling velocity and the dissipative effects of the damping on the catenary are of crucial importance for its dynamic response. Therefore, the catenary model allows differential damping coefficients for its different structural components. The two entering and

two exiting spans on each catenary section, where no contact with the pantograph exists, account for about 100 m of wire length in each end. Furthermore, the boundary conditions for the contact and messenger wire correspond to a spring-damper element. Besides increasing the realism of the catenary models, these two modelling features ensure that the reflection of the elastic wave does not influence the pantograph contact during the dynamic analysis, due to the lengths of the entering and exiting spans and that the elastic wave is attenuated, due to the boundary conditions.

11.2.2 Pantograph Analysis Methods and Models

A typical multibody model is defined as a collection of rigid or flexible bodies that have their relative motion constrained by kinematic joints and that are acted upon by external forces. The forces applied on the system components may be the result of springs, dampers, actuators or external applied forces describing gravitational, contact/impact or other forces. The pantograph models, being lumped mass or detailed 3-dimensional, may use any of the features available in multibody methodologies [14].

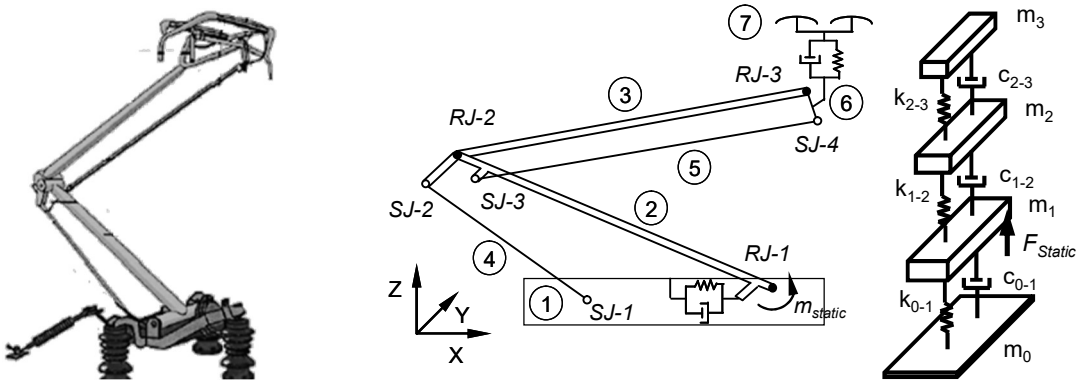

Figure 11.2: Typical pantograph and its multibody and lumped mass models.

The equations of motion for a constrained multibody system of rigid bodies are written as a system of differential algebraic equations, solved for $\ddot{\mathbf{q}}$ and $\boldsymbol{\lambda}$ as [14]

$$\begin{bmatrix} \mathbf{M} & \boldsymbol{\Phi}_q^T \\ \boldsymbol{\Phi}_q & \mathbf{0} \end{bmatrix} \begin{bmatrix} \ddot{\mathbf{q}}_r \\ \boldsymbol{\lambda} \end{bmatrix} = \begin{bmatrix} \mathbf{g} \\ \boldsymbol{\gamma} \end{bmatrix} \tag{11.10}$$

where $\mathbf{M}$ is the system mass matrix, $\ddot{\mathbf{q}}$ is the vector that contains the state accelerations, $\boldsymbol{\lambda}$ is the vector that contains m unknown Lagrange multipliers associated with m holonomic constraints, $\mathbf{g}$ is the generalized force vector, which contains all external forces and moments, and $\boldsymbol{\Phi}_q^T \boldsymbol{\lambda} = \mathbf{f}^{(c)}$ is the vector of constraint reaction forces.

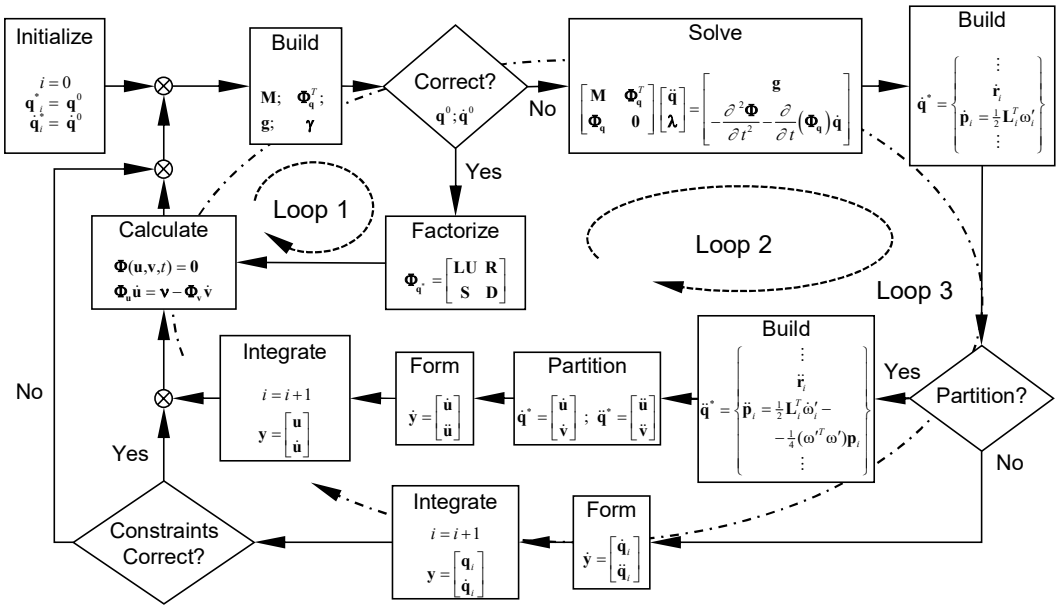

Figure 11.3: Flowchart with the forward dynamic analysis of a multibody system.

In dynamic analysis, a unique solution is obtained when the constraint equations are considered simultaneously with the differential equations of motion and a proper set of initial conditions is specified. In each integration time step, the accelerations vector, $\ddot{\mathbf{q}}$, together with velocities vector, $\dot{\mathbf{q}}$, are integrated in order to obtain the system velocities and positions at the next time step. This procedure is repeated until the final time is reached, as depicted in Figure 6.9. An integration algorithm with variable time-step and integration order is used to solve the multibody equations of motion [15].

To initialize the solution process the positions and velocities of the mechanical elements must be compatible with the kinematic constraint equations. Such constraint fulfilment is ensured by loop1 of the solution scheme described in Figure 6.9. The set of differential algebraic equations of motion, Equation (11.10) does not use explicitly the position and velocity equations associated to the kinematic constraints. Consequently, when using the route labelled as loop 3 in Figure 6.9, the original constraint equations are rapidly violated due to the integration process. Thus, in order to stabilize or keep under control the constraints violation, Equation (11.10) is solved by using the Baumgarte stabilization method or the augmented Lagrangean formulation [16]. Due to the long simulations time typically required for pantograph-catenary interaction analysis, it is also necessary to use of a coordinate partition method, as implied in loop 2 of Figure 6.9, whenever the stabilization of the constraints is not possible otherwise.

11.2.3 Pantograph-Catenary Contact Force Model

The contact problem is treated with a penalty formulation in which the contact force is a function of the relative penetration between the two cylinders. The contact model used here includes hysteresis damping in the impact between bodies in the systems

$$F_N = K\delta^n \left[1 + \frac{3(1-e^2)}{4} \frac{\dot{\delta}}{\dot{\delta}^{(-)}} \right] \tag{11.11}$$

where K is the generalized stiffness contact, e is the restitution coefficient, $\dot{\delta}$ is the relative penetration velocity and $\dot{\delta}^{(-)}$ is the relative impact velocity. K can be obtained from the Hertz contact theory as the external contact between two cylinders with perpendicular axis [17]. Although standard EN50318 specifies a value of K=50 10^3 N/m, the findings of the European Project PantoTRAIN [7] suggest that a more realistic value is K=200 10^3 N/m for current highspeed catenaries. Although all parameters used in the `PantoCat` code are user inputs, the parameters used in the contact model for the purpose of this benchmark are K=200 10^3 N/m, e=1 and n=1.

11.2.4 Numerical Integration Procedures

Linear finite elements provide all modelling features for the development of the catenary dynamic analysis while (nonlinear) multibody mechanisms include all modelling features required for any type of pantograph model. In order to take the best advantage of the two different types of dynamic analysis a co-simulation environment between `PantoCatFEM` and `PantoCatMB` codes is implemented in the `PantoCat` program. The multibody code provides the finite element code with the positions and velocities of the pantographs registration strips. The finite element code calculates the contact force, using the contact model represented by Equation (11.11), and the location of the application points in the pantographs and catenary, using geometric interference functions. The contact forces are applied to the catenary, in the finite element code, and to the pantograph model, in the multibody code, as implied in Figure 11.4. Each code handles separately the equations of motion of each sub-system based on the shared force information.

The key of the synchronization procedure between the multibody and finite element codes is the time integration step, ensuring the correct dynamic analysis of the pantograph-catenary system, including intermittent contact. The finite element integration code is of the Newmark family and has a constant time step that is small enough not only to assure the stability of the

integration of the catenary but also to capture the initiation of the contact between the pantograph registration strip and the contact wire of the catenary.

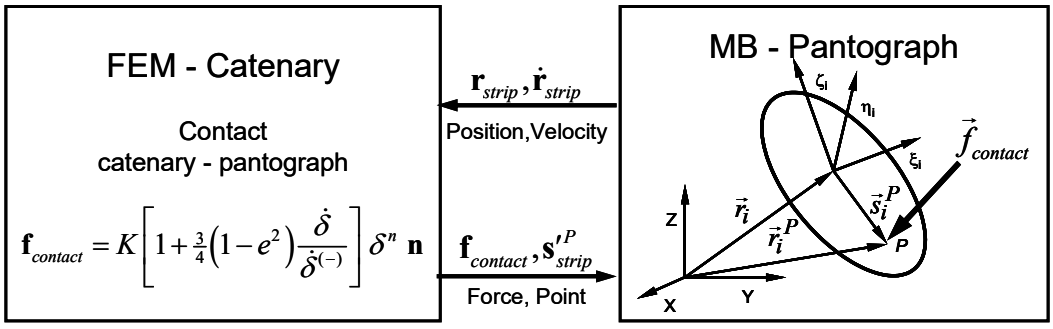

Figure 11.4: Co-simulation between a finite element and a multibody code

The multibody code uses a predictor-corrector integrator that can be an Adams-Bashforth or the Gear algorithm, with variable order and time-step [14]. The only restriction that is imposed in the integration algorithm of the multibody module is that its time step cannot exceed the time step of the finite element code. Both modules can start independently from each other, i.e., the catenary finite element model and the pantograph multibody model include the initial conditions for the start of the analysis expressed in terms of the initial positions and velocities of all components of the systems.

In order to ensure that the initiation and loss of contact is captured a maximum time step of 10^{-3} s is allowed. Note that in some particular applications, such as those focusing analysis of irregularities and singularities in the contact wire, the maximum allowable time step may have to be reduced.

The co-simulation procedure was validated for a very wide number of scenarios of tangent tracks that included models of different catenary types and various lumped mass pantograph models at different operating velocities. All results obtained using the co-simulation approach are indistinguishable from the results obtained when the pantograph lumped mass models are analysed with the finite element code without co-simulation.

11.2.5 Models and Analysis Initialization

The initialization of the catenary and pantograph models, i.e., the initial positions and velocities of the catenary finite element nodes and of the pantograph body components have different requirements due to the different methods used in the solution of their dynamics. The definition of the initial conditions for the catenary finite element model poses a different set of challenges. Recognizing that the geometric specification of the catenary geometry is defined for its static deformed state due to gravitational loading, the definition of the finite element nodal positions

of the catenary model in its undeformed configuration are found before the dynamic analysis starts. For this purpose an optimization problem is defined to minimize the function that quantifies the distance between the static deformed geometry of the contact wire and its specified position, as

$$\begin{aligned} &\min \mathcal{F}(\mathbf{b}) = \sum_{i=1}^{n} \left(z_i^r - z_i \right)^2 \\ &s.t. \quad \mathbf{l} \le \Psi(\mathbf{b}) \le \mathbf{u} \end{aligned} \tag{11.12}$$

in which the vector of design variables is $\mathbf{b}=[z_1, z_2, \ldots, z_n]^T$, being z_i the position of node i of the messenger wire along the height direction, assuming the position of the dropper node in the contact wire as unchanged. The design variables are equivalent to the dropper length. Only the nodes of the messenger wire located at the droppers and steady arm are considered in vector **b**. The reference height of each node i, i.e., the height of each node of the messenger wire at the steady arm, specified as input for the catenary geometry is defined as z_i^r. The constraints of the optimization problem include the orientations of steady arms and lengths of the droppers. Note that the catenary axial tensioning of the wires and the gravitational loading lead to catenary deformations require a nonlinear static analysis due to the large displacements and rotations of the finite element mesh. During the optimization problem a solution for a static analysis is required, every iteration, as if the deformation of the catenary model is linear. Although good solutions for the initial catenary positions have been obtained with the approach used here there is no guarantee that a good solution for the initial catenary configuration is always obtained.

In the case of the multibody pantograph model the initial velocities of all mechanical elements must be not only compatible with the forward velocity of the system along the track but also consistent with the kinematic constraints used [16]. In case of small errors the `PantoCatMB` module initialization, the code ensures their correction via loop 1 in Figure 6.9 so that the state variables ensure the kinematic consistency of the model.

Having the pantograph and catenary properly initialized, with the position of the pantograph contact strips located under the contact wire, in its close vicinity but without contact, the dynamic analysis starts. Some trial runs may be necessary before the pantograph lifting force/moment is fine tuned to ensure that the average contact force in the catenary-pantograph interface meets the required average force [18]. In any dynamic analysis of the system the dynamic response is not collected, or processed, during the first 2-3 spans after contact between the pantograph and catenary starts. Such transient response is discarded from any further analysis.

11.3 Additional methods available and not used in the benchmark

The `PantoCat` program has a number of analysis features that allows the study of pantograph and catenary models with characteristics that go well beyond the requirements of the benchmark. In terms of dynamics analysis `PantoCat` allows for:

- The application to the pantograph base of the kinematics of the train roof, including all disturbances resulting from track/wheel interaction, vehicle suspensions and operating conditions of the train.
- Generation of catenary geometries consistent with general track geometries including horizontal and vertical curves.
- Dynamics of the pantograph models that represent all of its constructive details including imperfections of the mechanical joints, dynamics of the pneumatic actuators, flexibility of the system components, fully spatial kinematics of all system components and any nonlinearity of the suspension mechanical elements.
- The simulation of catenary models with multiple sections, including realistic representations of the overlapping in the transition between sections.
- The introduction of active control by providing for the effect all necessary interfaces to test active control algorithms in realistic pantograph models.

Although without direct influence on the analysis features implemented in the `PantoCat` code, the ability to input catenary data in a neutral format widens the applicability of the program. By using the data format agreed in the PantoTrain project, implemented in an Excel database file, all geometric and material characteristics of the catenary are specified. This allows also the inclusion of any particular element and singularity in the catenary construction such as defects or dampers, as those being tested in some Japanese catenaries [19].

The implementation of other advanced features in `PantoCat`, such as the ability to include the flexibility of the pantograph mechanical elements in the dynamic analysis, is underway. Some of the initial results are available showing that in particular conditions there is an influence of the system flexibility in the quality of the contact [20].

11.4 Validation of the software

The norm EN50318 [21] provides two validation steps, defined as steps 1 and 2, for the assessment of a simulation method, one by comparison with other validated simulation methods and other by comparison with line tests. On step 1 simple reference models are provided for

catenary and pantograph. For a successful validation it is necessary to obtain a given number of simulation output parameters within given ranges. Following step 1, which gives assurance on the precision and accuracy of the simulation tool, step 2 states a required accuracy of the method used concerning key parameters extracted from line tests. The `PantoCat` code has been validated according to both steps of the EN50318 norm.

In the first step of EN50318 reference models of the catenary and pantograph are defined being the simulation outputs deemed to fall within pre-defined ranges, for two different pantograph speeds. The pantograph is represented by a two stage lumped mass model while the catenary model is obtained by the basic geometry and material norm definitions, for a length of ten spans. These minimal modelling data requirements are short of the detailed definition of the catenary characteristics used in the benchmark, particularly with respect to the mechanical characteristics of the supports and structures. Another critical aspect concerns the norm specification of no damping on the catenary model, which ultimately leads to the reflection of the wave propagation if neither energy absorbing boundary conditions nor entrance and exiting spans are used for the contact wire. The pantograph-catenary interaction is evaluated for pantograph speeds of 250 km/h and 300 km/h, being the results processed only for the 5th and 6th spans. The forces are filtered with a cut-off frequency of 20 Hz, fulfilling the norm specifications.

The statistical characteristics of the contact forces defined by the norm as requirement for the 1st step of the validation as well as the range of acceptance are shown in Table 11.1. All quantities required for the software acceptance fall, successfully, inside the ranges specified by EN50318.

The 2nd step of the validation procedure consists on modelling existing catenary and pantograph and verifying the correlation of the model response with inline acquired data. The simulation results and acquired data are filtered similarly. The successful validation of the simulation tool, and implicitly of the models developed, requires a maximum deviation of 20% for the standard deviation of the contact force, maximum uplift at the supports and the vertical displacements of the contact point. For this type of validation, it is necessary to access not only experimental inline measured data but also the modelling data for the catenary and pantograph of the existing system. The data concerning the LN2 catenary of the TGV Atlantique line and the Faiveley CX pantograph running at an operational speed of 300 km/h, was made available by SNCF for the PANTOTRAIN European project and used here. Two numerical simulations were produced for a pantograph to catenary contact force model, considering elastic contact only or including hysteresis damping.

speed	[km/h]	250		300	
		Norm	Model	Norm	Model
Mean contact force	[N]	110 - 120	114.6	110 - 120	115.5
Standard deviation	[N]	26 - 31	28.6	32 - 40	34.3
Statistical maximum	[N]	190 - 210	200.4	210 - 230	218.5
Statistical minimum	[N]	20 - 40	28.9	-5 - 20	12.5
Actual maximum	[N]	175 - 210	196.7	190 - 225	195.7
Actual minimum	[N]	50 - 75	52.6	30 - 55	34.7
Maximum uplift at support	[mm]	48 - 55	54	55 - 65	60
Percentage of loss of contact	[%]	0	0	0	0

Table 11.1: Statistical quantities required by EN50318, and range of acceptance, for the pantograph-catenary simulation software.

	Experimental	Elastic	Damped
Maximum [N]	319.3	283.5	298.5
Minimum [N]	73.7	100.6	97.0
Amplitude [N]	245.5	182.9	201.5
Mean [N]	179.8	179.4	179.5
Standard Deviation [N]	44.3	44.4	46.9
Standard Deviation Accuracy [%]	-	0.08	5.92
Statistical Maximum [N]	312.8	312.5	320.3
Statistical Minimum [N]	46.9	46.3	38.6
Contact Loss [%]	0	0	0

Table 11.2: Statistical parameters for the experimental and simulated contact forces.

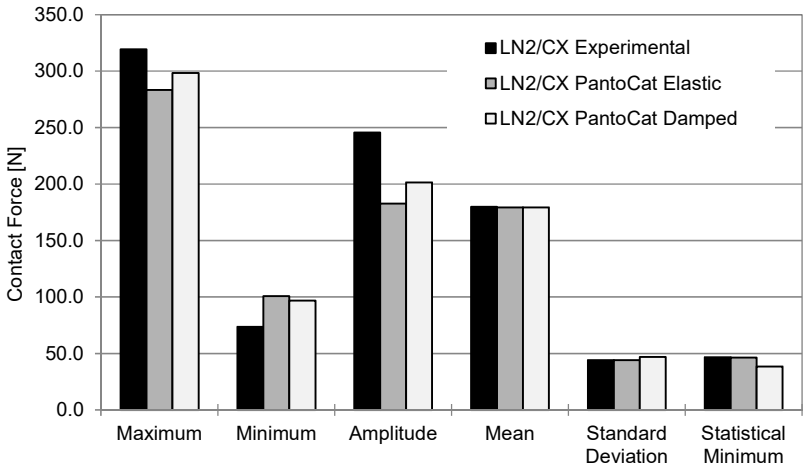

Figure 11.5: Statistics of the contact force for the experimental and simulated data.

The statistical analysis of the experimental and simulated contact forces are presented on Table 11.2 and Figure 11.5. The standard deviation accuracy also presented shows that its values, either for the elastic or damped contact models, are well inside the 20% required accuracy required by the norm for validation. For the elastic contact results the standard deviation is very close to the experimental results, however the deviation from the maximum and minimum contact force is more significant than the ones presented by damped contact result.

11.5 Considerations about the benchmark results

In general, for all important quantities in the study of the pantograph-catenary interaction problem, the dynamic response obtained with all software tested is similar. The few particular differences can be justified by modelling assumptions, sometimes forced by the software capabilities of analysis. The dynamic response obtained for the benchmark, with `PantoCat`, is analysed here with reference to both modelling assumptions and software analysis capabilities.

11.5.1 Static analysis and initialization

The relevant results of the static analysis of the catenary concerns the position of the contact wire and the elasticity of the catenary, depicted respectively in Figures 4 and 5 of the benchmark general paper [22]. The position of contact wire at the regulation arms obtained by `PantoCat` is basically 5mm lower than what most of the remaining codes obtain, for the planar catenary, as seen in right side of Figure 11.6 . This may be due to either the initialization procedure for the catenary geometry, to the finite element model used or to the model for the regulator arm. For the three-dimensional catenary model the height of the contact wire at the regulation arm, depicted in the left side of Figure 11.6 is coincident with that of most of the other codes. Note that the optimization procedure depicted by equation (11.12) is used to fine tune to position the steady arm. All rotations of the steady arms during the analysis are considered small, and consequently no large deviations on the steady arm positions are considered. The steady arms are pined to a fixed element in one end and pinned to the contact wire in the other end in the models considered here.

The catenary elasticity can be evaluated with a pure static analysis or with a dynamic analysis in which the pantograph moves with a velocity low enough to disregard any dynamic effects on the response. For the load F=200N the two methods of identifying the catenary elasticity, with `PantoCat`, lead to slightly different results, as shown in Figure 11.7. For a load F=100N there is no difference between the two methods of identifying the catenary flexibility, which suggests that the compression of the droppers, inexistent for the lower force, plays a role in the dynamical system due to the inertia forces.

The catenary geometric initialization is a critical step in the process of setting any catenary in general, and in this benchmark in particular. The gravitational forces tend to force the contact wire downwards while the axial tension in the wires tends to raise the messenger and contact wires. In most of the catenaries these two opposite trends almost cancel each other and the equilibrium position of the loaded catenary is not too far from the reference position.

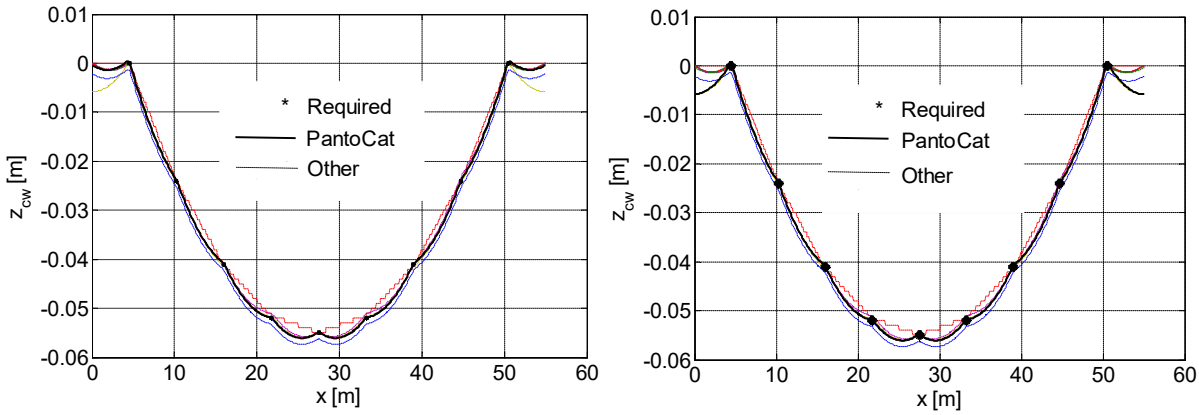

Figure 11.6: Position of the contact wire across the 6th span with 0.1 m reporting step for the 3D model (left) and 2D model (right).

From the mechanical point of view this situation means that small variations on the unloaded geometry of the catenary allow for the complete system, upon loading, to reach a predefined geometry while assumptions for linearity of the system behaviour remain valid. However, for some particular catenary geometries, topologies and loadings the assumption of linearity of the catenary during loading may not be valid, due in particular to large rotation of the elements. In these cases, the identification of a preloaded geometry, which after loading is the specified configuration, may be difficult to find without using a nonlinear analysis.

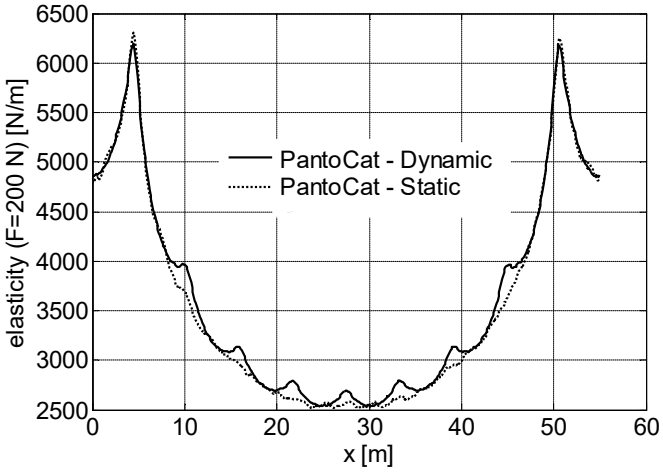

Figure 11.7: Elasticity of the catenary in the central span for a contact fore F=200N, evaluated with `PantoCat` with a static analysis and with a dynamic analysis using a very slow moving pantograph.

11.5.2 Dynamic analysis

In the catenary models used here the starting and exiting spans are not specified, neither is the type of boundary conditions used to fix the messenger and contact wires. This is a particularly sensitive issue for dynamic analysis at speeds for which the reflection of the catenary elastic deformation wave plays a role in the pantograph-catenary interaction. In order

to avoid problems associated to the elastic wave reflection the catenary models used in PantoCat have two initial and two terminal spans similar to those of current highspeed lines in which no contact exists, i.e., the two spans account for a total length in the order of 100 m. Furthermore, the boundary conditions for the messenger and contact wires are defined with energy absorption. This is achieved by considering the elements that connect each of the wires to each attachment point as a spring and damper element in which the damper is used to fine tune the energy absorption.

A critical characteristic of the system that affects the pantograph-catenary interaction is the catenary damping. While in the benchmark the damper is completely characterized, in an existing catenary it has to be identified. Ambrosio et al. [6] actually shows that in a multiple pantograph operation scenario, depending on the catenary damping, the contact of the leading pantograph can be heavily affected by the rear, in the case of very lightly damped catenaries, or the inverse, in the case of more damped catenaries.

The contact law used for the pantograph-catenary interaction in this benchmark is not fixed. PantoCat allows the user to choose the parameters. According to the findings of the PantoTRAIN project [5] the recommended stiffness for the contact is F=50-200 kN and the damping null for the higher stiffness. It is found that variations on the stiffness and damping of the contact law lead to variations in the results that may not be negligible.

The emphasis on the pantograph catenary interaction modelling issues is generally put on the catenary side and not the pantograph because the lumped mass pantograph models result from a system identification being their dynamic response, for the type of displacements observed, basically obtainable with a linear pantograph model. For larger head displacements, or when used in lines with curves, the lumped mass pantograph model cannot be used anymore, being a multibody approach to pantograph modelling unavoidable. However, clear specifications on how to model and use multibody pantographs do not exist yet. Preliminary studies show how the existing laboratory tests used for the identification of the lumped pantograph models can still be used to identify the selected unknown modelling parameters of multibody pantographs [23].

It must be referred that PantoCat presents good computational efficiency allied to the accuracy demonstrated in the benchmark. In order to measure such efficiency, for the cases simulated in this benchmark and other cases simulated throughout the life of PantoCat, each 1s of real time takes about 11s of computer time for the single pantograph case and 16 s for the two pantograph scenarios in a computer equipped with the Intel i7 2600K, or using another

measure, a simulation of a pantograph running at 300 km/h in 1 km of track takes about 132s of computer time.

Finally, it must be referred that the benchmark now developed does not allow to understand the importance, or lack of it, of using spatial catenary models in place of the planar models. That is mainly because the pantograph model used in the benchmark is one dimensional, i.e., its mobility is only in the vertical direction and consequently, even if excited in any other direction, its dynamic response is only in the direction it is modelled. Physically realistic pantographs models use a fully three-dimensional representation of all mechanical components being them allowed to develop a spatial motion. The understanding of the differences between planar and spatial catenary models is clarified when interacting with fully three-dimensional pantograph models.

11.6 Conclusions

The `PantoCat` code is a dynamic analysis software that accepts fully three dimensional finite element models of catenaries and spatial nonlinear multibody models of pantographs. A co-simulation procedure, via the contact force model is used to couple the simulation of both models. By using the finite element method for the dynamic analysis of the catenary and a multibody methodology for the dynamics of the pantograph `PantoCat` can take advantage of the best features of each method and handle detailed models with complex topologies and geometries. Although many of the features of the software are not used in this benchmark, such as the curved track with curved catenaries, the multibody pantographs or the perturbations of the pantograph trajectory, all features required exist by nature in the original `PantoCat`. The interaction force between the pantograph and catenary very sensitive to the catenary geometry, effort to develop a more advanced initialization procedure for the geometry of the catenary and for the initial conditions of the pantograph is underway. The benchmark in which the code `PantoCat` is used considers models for the catenary and pantograph not only more detailed than those used in EN50318 but much closer to the current highspeed railway lines and to the modelling capabilities of modern pantograph-catenary dynamic analysis codes. Among the catenary characteristics not specified in this benchmark that have influence in some of the results it must be emphasized the characteristics of the boundaries of the contact and messenger wires and/or the geometry of the first and last spans on the catenary. Another aspect of the benchmark that must be taken into account is the impossibility to use the dynamic response in the first 2-3 spans after the effective contact between the pantograph head and the catenary

contact wire takes place, due to the need to raise the pantograph head until line contact is achieved at a correct contact force.

References

[1] J. Pombo, J. Ambrósio, *EUROPACAS Software – Pantograph Module Users' Manual*. Deliverable D1.7: Technical Report EUROPAC_D17_IST_R4.0, Instituto Superior Técnico, Lisboa, Technical University of Lisbon, Portugal, 2006.

[2] F. Rauter, J. Pombo, J. Ambrósio, J. Chalansonnet, A. Bobillot and M. Seabra Pereira, Contact Model for the Pantograph-Catenary Interaction, *JSME International Journal of System Design and Dynamics*, **1**(3), 447-457, 2007.

[3] J. Ambrósio, J. Pombo, F. Rauter and M. Pereira, A Memory Based Communication in the Co-Simulation of Multibody and Finite Element Codes for Pantograph-Catenary Interaction Simulation. In: *Multibody Dynamics* (C.L. Bottasso, ed.). Springer, Dordrecht, the Netherlands, 231-252, 2008.

[4] J. Ambrosio, J. Pombo, P. Antunes, M. Pereira, Optimization of highspeed railway pantographs for improved pantograph-catenary interaction, *Theoretical & Applied Mechanics Letters*, DOI: 10.1063/2.1301306, **3**, 013006, 2013.

[5] J. Ambrosio, J.Pombo, A. Facchinetti, S. Bruni, J.-P. Massat, H. Dupuis, *D1.1 – Key parameters for pantograph/catenary numerical models*. PANTOTRAIN Technical Report, Instituto Superior Tecnico, Technical University of Lisbon, Portugal, 2010.

[6] J. Ambrósio, J. Pombo, M. Pereira, P. Antunes and A. Mósca, A Computational Procedure for the Dynamic Analysis of the Catenary-Pantograph Interaction in High-Speed Trains, *Journal of Theoretical and Applied Mechanics/Poland*, **50**(3), 681-699, 2012.

[7] J. Ambrosio, J.Pombo, M. Leouatri, A. Facchinetti, S. Bruni, *D1.3 – Criteria to validate pantograph / catenary simulation tools* PANTOTRAIN Technical Report, Instituto Superior Tecnico, Technical University of Lisbon, Portugal, 2010.

[8] J. Pombo, J. Ambrosio, Environmental and Track Perturbations on Multiple Pantograph Interaction With Catenaries in High-Speed Trains, *Computers and Structures*, **124**, 088-101, 2013.

[9] J. Pombo, J. Ambrósio, M. Pereira, F. Rauter, A. Collina, A. Facchinetti, Influence of the Aerodynamic Forces on the Pantograph-Catenary System for High Speed Trains, *Vehicle Systems Dynamics*, **47**(11), 1327-1347, 2009.

[10] J. Pombo, J. Ambrósio, Influence of pantograph suspension characteristics on the contact quality with the catenary for high speed trains, *Computers and Structures*, DOI:10.1016/j.compstruc.2012.06.005, **110–111**, 32–42, 2012.

[11] J. Ambrósio, J. Pombo, F. Rauter and M. Pereira, Multiple Pantograph Interaction with Catenaries in High-Speed Trains, In: *Proceedings of the 8th World Congress on Railway Research*, Seoul, Korea, May 18-22, 2008.

[12] J. Pombo, J. Ambrósio, Multiple Pantograph Interaction With Catenaries in High-Speed Trains, *Journal of Computational and Nonlinear Dynamics*, DOI:10.1115/1.4006734, **7**, 041008-1/7, 2012.

[13] T. Hughes, *The finite element method: linear static and dynamic finite element analysis*, Prentice-Hall, Englewood-Cliffs, New Jersey, 1987

[14] P. Nikravesh, *Computer-Aided Analysis of Mechanical Systems*, Prentice-Hall, Englewood Cliffs, New Jersey, 1988

[15] C. W. Gear, Simultaneous Numerical Solution of Differential-Algebraic Equations, *IEEE Transactions on Circuit Theory*, **18**(1), 89-95, 1971.

[16] M. A. Neto and J. Ambrósio, Stabilization methods for the integration of differential-algebraic equations in the presence of redundant constraints, *Multibody Systems Dynamics*, **10**(1), 81-105, 2003.

[17] H. Lankarani and P. Nikravesh, Continuous Contact Force Models for Impact Analysis in Multibody Systems, *Nonlinear Dynamics*, **5**, 193-207, 1994

[18] J.Ambrósio, J. Pombo, M. Pereira, P. Antunes and A. Mósca, Recent Developments in Pantograph-Catenary Interaction Modelling and Analysis, *International Journal of Railway Technologies*, DOI:10.4203/ijrt.1.1.12, 1(1), 249-278, 2012.

[19] K. Ikeda, Optimization of Overhead Contact Lines for Sinkansen Speed Increases, *JR East Technical Review*, **12**, 6469, 2008

[20] J. Ambrosio, F. Rauter, J. Pombo, M. Pereira, A flexible multibody pantograph model for the analysis of the catenary-pantograph contact. In: *Multibody Dynamics: Computational Methods and Applications*. W. Blajer, J. Fraczek, K. Krzysztof (Eds.), Springer, Dordrecht, The Netherlands, 1-27, 2011.

[21] EN50318 standard, Railway applications - Current collection systems - Validation of simulation of the dynamic interaction between pantograph and overhead contact line, CENELEC European Committee for Electrotechnical Standardization, Brussels, Belgium, 2002.

[22] S. Bruni, J. Ambrosio, A. Carnicero López, Y. H. Cho, L. Finner, M. Ikeda, S. Y. Kwon, J.-P. Massat, S. Stichel, M. Tur, W. Zhang, THE pantograph-catenary interaction benchmark, *Vehicle System Dynamics*, (to be published), 2014.

[23] J. Ambrósio and J. Pombo, Minimal requirements of multibody pantograph models for high-speed railway applications, In: WCRR2013 – 10th World Congress on Railway Research, Sydney, Australia, November 25-28, 2013

12 A Comparative Study between Two Pantographs in Multiple Pantograph High-Speed Operations

[2] The pantograph-catenary system represents one of the major barriers to rolling stock interoperability. Traditionally, each country has developed its own overhead equipment, which is reflected in different catenary and pantograph designs. Hence, a unified approval method, able to consider the diversity of existing solutions, is a key subject that must be addressed to provide a competitive railway system. Furthermore, the limitation on the top velocity of high-speed trains is associated to the ability to provide, through the pantograph-catenary interface, the proper amount of energy required to run the trainset motors. If loss of contact exists, not only the energy supply is interrupted but also arching between the collector bow of the pantograph and the contact wire of the catenary occurs, leading to the deterioration of the functional conditions of the two systems. All these situations require that the dynamics of the pantograph-catenary are properly modelled and that the software used for analysis and design, or to support maintenance and homologation decisions, is not only accurate and efficient but also allows for modelling all details relevant to the train overhead energy collector operation. In this work a multibody dynamics approach and a finite element method are implemented in a validated computational tool to handle the pantograph and the catenary dynamics, respectively. The performance of two different pantographs, when running on the same catenary, is studied. Multiple pantograph operation scenarios, with different distances between them, are also

[2] The work presented in this chapter has been published, as it is, in: J. Pombo, P. Antunes, *A Comparative Study between Two Pantographs in Multiple Pantograph High-Speed Operations*, International Journal of Railway Technology, 2, 83-108, (2013).

analysed here. The purpose is to understand the consequences on the contact force characteristics and on the catenary uplift. The results are assessed according to the European standards and provide indications on how the pantograph parameters can be modified, in a design environment, or tuned, in high-speed train operations, to improve the performance of the overhead contact system.

12.1 Introduction

The development of computer resources led simulations to be an essential part of the design process of railway systems. Moreover, the increasing demands for network capacity, either by increasing the traffic speed or the axle loads, put pressure on the existing infrastructures and the effects of these changes have to be carefully considered. The European Strategic Rail Research Agenda [1] has identified key scientific and technological priorities for rail transport over the next 20 years. One of the points emphasized is the need to reduce the cost of approval for new vehicles and infrastructure products with the introduction of virtual homologation.

Introducing virtual testing would reduce the costs of certification since models would be available and the need for additional and expensive tests would be minimized. In a first step, the physical test would be replaced by a corresponding virtual test. When a proven virtual methodology has been established, it is possible to have better controlled environmental testing conditions and introduce new scenarios. In order to use virtual testing for certification, the methodology needs to be defined and validated. With the continuous development of computer capacity and numerical tools, virtual testing represents an opportunity for homologation.

When certifying a rail vehicle according to regulations, two elements constitute a significant challenge: vehicle cost and time to market. A large part of vehicle certification requires in line testing for safety, performance and infrastructure compatibility in each individual network. Thus, the certification process can take up to 30 months and cost several millions of euros, imposing a huge competitive disadvantage on the development of rail products, and thus jeopardizing the development of reliable and sustainable transport networks.

Within this panorama, the pantograph-catenary system represents one of the major obstacles for rolling stock interoperability. In general, each country has developed its overhead equipment, with variations in components and mechanical properties, so that national networks are now largely incompatible. A major source of incompatibility is the different equipment that is operated for AC power and for DC power, which is then reflected as different catenary designs.

Furthermore, pantographs have been optimized for use on a single national network so that a major challenge for interoperability is now to design and homologate pantographs which are capable of operating satisfactorily on a range of different overhead equipments [2]. To this end, a unified performance based on approval method that establish very clear and objective relationships with the pantograph design process is a key subject that can and must be addressed in order to provide a competitive railway system within Europe.

A large number of works dedicated to the study of the pantograph-catenary interaction are being presented to different communities emphasizing not only the mechanical aspects of construction, operation and maintenance but also the challenges for simulation due to the multi-physics characteristic of the problem. Gardou [3] presents a rather simple model for the catenary, using 2D finite elements, where all nonlinear effects are neglected. Jensen [4] presents a detailed study on the wave propagation problem on the catenary and a 2D model for the pantograph-catenary dynamics. In a similar line of work Dahlberg [5] describes the contact wire as an axially loaded beam and uses modal analysis to represent its deflection when subjected to transversal and axial loads, showing in the process its relation to the critical velocity of the pantograph. In both references [3] and [4] not only the representation of the contact forces is not discussed but also no reference is made on how the integration algorithms are able to handle the contact loss and impact between contact strip and contact wire. Labergri [6] presents a very thorough description of the pantograph-catenary system that includes a 2D model for the catenary based on the finite element method, and a pantograph model based on a multibody approach, being the contact treated by unilateral constraints. In all works mentioned it is claimed that the catenary structural deformations are basically linear and, consequently, the catenaries are modelled using linear finite elements, except for the droppers' slacking which is handled as a nonlinear effect but not by nonlinear finite elements. Seo, et al. [7] state the need to treat the catenaries as being nonlinear due to their large deformations. They treat the catenary contact wire with finite elements based on the absolute nodal coordinate formulation while the pantograph is a full 3D multibody model. The contact is represented by a kinematic constraint between contact wire and contact strip and no loss of contact is represented. None of the models used has been validated and no comparative studies are provided to support the claims regarding the need to handle nonlinear catenary deformations or the suitability of using linear deformations only.

Most of the works focusing the pantograph-catenary interaction elect the finite element method to develop and analyse linear models catenaries and use lumped mass pantograph models due to the need to maintain the linearity of the analysis. However, it is recognized by a

large number of researchers that the nonlinearities of the pantograph system play a very important role in the energy collection and, therefore, either nonlinear finite element or multibody models can deliver superior analysis capabilities [7-20]. Due to the multiphysics problem involved in modelling the catenary-pantograph system and the need for its simulation Arnold and Simeon [11] suggest the co-simulation between the finite difference discretization of the catenary and the multibody representation of the pantograph. Mei, Zhang et al. [13,20] suggest a coupling procedure between a finite element discretization of the catenary and a physical prototype of a pantograph. This work shows the possibility of coupling numerical and experimental techniques. Ambrósio, Pombo, Rauter et al. [8-10,14-16] show how the coupling between finite element software, to solve the dynamics of the catenary, and multibody software, to obtain the dynamic response of the pantograph, can be efficiently achieved. In these references it is observed that the finite element code ANSYS [21] is the most popular choice of software for the catenary while no major preferences for a particular multibody code are stated.

There are, currently, no accepted general numerical tools designed to simulate the pantograph-catenary system in nominal, operational, and deteriorated conditions. Here it is understood that operating conditions must take into account the wear effects and the deteriorated conditions that include extreme climatic conditions, material defects or mechanical problems. Several important efforts have been reported to understand the mechanisms of wear in catenaries [22,23] and collector strip [24,25], to describe the aerodynamic effects [26-28] and extreme temperatures [29] on the quality of the pantograph-catenary contact, to analyse the running dynamics of the railway vehicle [30], to study the deformability of the pantograph mechanical system [31-33] and to assess how the structural components of the pantograph, and the respective linking elements, affect the quality of the pantograph-catenary contact [34]. The dynamic analysis procedures and the models developed for catenaries and pantographs are also used for designing pantograph control systems [35-38] or even wire-actuator control and contact force observers [39].

The different computational procedures and methods developed for representing the pantograph-catenary interaction led to the development of several computer programs used by designers and analysts. The code CATMOS [40], developed in the early 1990s, allows for the vibration analysis of the system. The pantograph is represented by a lumped-mass model and the catenary by Euler-Bernoulli and Timoshenko beam elements. No nonlinearities are considered in the system. Using finite element models in the framework of the nonlinear finite element code ABAQUS, the program FAMOS [41] enables the development of linear finite

element models for the catenary and nonlinear finite element models for the pantograph. This program enables the analysis of fully three dimensional pantograph models. Veitl and Arnold [42] proposed a co-simulation strategy between the code PROSA, where a catenary is described by the finite difference method and the SIMPACK commercial multibody code used to simulate the pantograph. All models involved in this work are 3D but the catenaries are hard coded, and therefore, the models and programs can hardly be used for different catenary systems. The program DINACAT/WINCAT [43] uses the finite element method to represent both catenary and pantograph. This is a two-dimensional program in which the lumped-mass pantograph models are used.

In this work, a validated computational tool is used to study the pantograph-catenary interaction. The software is composed by two modules, the finite element [44,45] one is used to describe the catenary and the multibody [46-48] module is applied to represent the pantograph. The contact between the two subsystems is described using a penalty contact formulation [16,49-51]. The finite element and multibody codes run independently and use different time integration algorithms. For this reason, a co-simulation procedure that allows the communication between the modules using shared computer memory and suitable contact force models, is implemented [15,16,52]. In order to enable industrial application, an extra concern of this tool was the development of very efficient algorithms in what computational time is concerned.

This methodology is applied to study the performance of the high speed French CX and Italian ATR95 pantographs when running on the French 25 kV LN2 catenary. Studies involving multiple pantograph operations are also performed here in the framework of the application of the regulation EN50367 [53]. This application addresses one of the limiting factors in high-speed railway operation that is the need to use more than a single pantograph for current collection and the disturbance that the pantographs cause on each other dynamics that worsens the quality of the pantograph-catenary contact. All studies are carried out for high speed trains running at 300 km/h.

This paper is an updated and revised version of the conference paper [54]. In this new version, detailed description of the implemented methodologies is included, together with further analysis of the results presented. Problems such as track flexibility, wear and the influence of the track irregularities on the pantograph-catenary interaction are not addressed in this text. The interested readers are referred to the works [55-64].

12.2 Computational Model of the Pantographs

Multibody [28,30,31] and lumped mass [37,65] models, both requiring a multibody dynamics methodology [46] to be simulated, are generally used to represent the pantograph. While the multibody model can be built solely based on manufacturer information, such as the design drawings and the mechanical element characteristics, the lumped mass model is identified by performing laboratory tests, as shown in Figure 12.1 for the POLIMI (Politecnico di Milano) test bench. The mass, stiffness and damping properties of the lumped mass model are obtained in such a way that its frequency response matches the experimentally acquired response of the real pantograph [65]. In this work, the lumped mass models of the French CX and Italian ATR95 pantographs are considered.

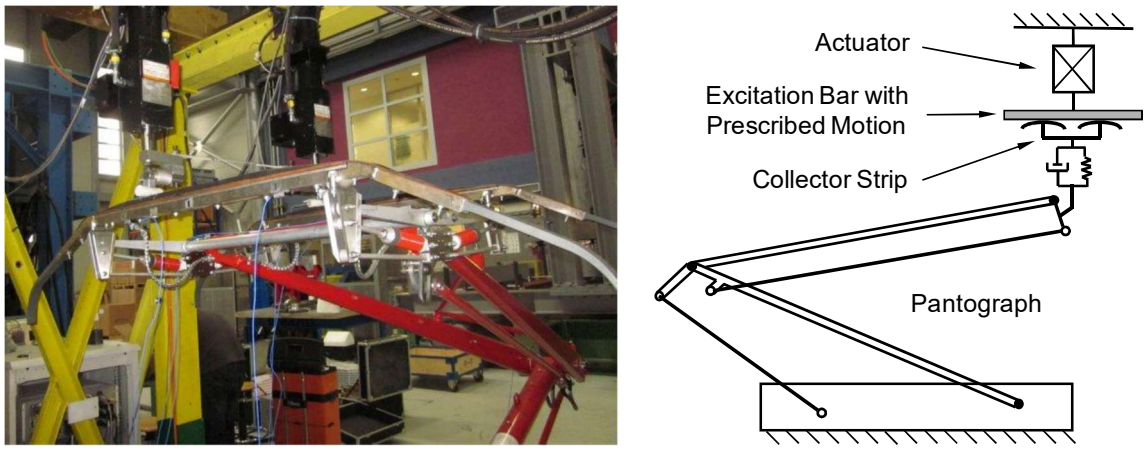

Figure 12.1: Laboratory tests for pantograph model identification (POLIMI test bench)

Regardless of the multibody or the lumped mass models being used, the configuration of the system is described by *n* Cartesian coordinates $\mathbf{q}$, and a set of *m* algebraic constraints written as [46]:

$$\mathbf{\Phi}(\mathbf{q},t)=\mathbf{0} \tag{12.1}$$

Differentiating equation (12.1) with respect to time yields the velocity constraint equation. After a second differentiation with respect to time the acceleration constraint equation is obtained as:

$$\mathbf{\Phi}_{\mathbf{q}}\ddot{\mathbf{q}}=\boldsymbol{\gamma} \tag{12.2}$$

where $\mathbf{\Phi}_{\mathbf{q}}$ is the Jacobian matrix of the constraint equations and $\boldsymbol{\gamma}$ is the right side of acceleration equations, which contains terms that are exclusively function of velocity, position and time.

The equations of motion for a constrained multibody system (MBS) of rigid bodies, such as a pantograph, are written as [46]:

$$\mathbf{M}\ddot{\mathbf{q}} + \boldsymbol{\Phi}_{\mathbf{q}}^{T}\boldsymbol{\lambda} = \mathbf{g} \tag{12.3}$$

where **M** is the system mass matrix, $\ddot{\mathbf{q}}$ is the vector that contains the state accelerations, **g** is the generalized force vector, which contains all external forces and moments, and $\boldsymbol{\lambda}$ is the vector that contains *m* unknown Lagrange multipliers associated with *m* holonomic constraints. In dynamic analysis, a unique solution is obtained when the constraint equations are considered simultaneously with the differential equations of motion with proper set of initial conditions. Therefore, equation (12.2) is appended to equation (12.3), yielding a system of differential algebraic equations written as:

$$\begin{bmatrix} \mathbf{M} & \boldsymbol{\Phi}_{q}^{T} \\ \boldsymbol{\Phi}_{q} & \mathbf{0} \end{bmatrix} \begin{bmatrix} \ddot{\mathbf{q}}_{r} \\ \boldsymbol{\lambda} \end{bmatrix} = \begin{bmatrix} \mathbf{g} \\ \boldsymbol{\gamma} \end{bmatrix} \tag{12.4}$$

that are solved for $\ddot{\mathbf{q}}$ and $\boldsymbol{\lambda}$. In each integration time step, the accelerations vector, $\ddot{\mathbf{q}}$, together with velocities vector, $\dot{\mathbf{q}}$, are integrated in order to obtain the system velocities and positions at the next time step. This procedure is repeated up to final time will be reached. The Gear integration method [66,67] is used here for the numerical integration of the velocities and accelerations. In order to allow for long integration times keeping the process stable, the Baumgarte stabilization method [68] or the augmented Lagrangean formulation [69] are used eventually complemented by the coordinate partition method [46,48]. The detailed description of the multibody formulation and of the numerical methods used to perform the dynamic analyses is outside the scope of this work. The interested readers are referred to references [46-48] for further details on the numerical procedures used.

12.2.1 The French CX Pantograph

The first pantograph considered in this work, used in the French high speed trains, is the Faiveley CX pantograph shown in Figure 12.2. By performing laboratory tests, it is possible to represent the dynamic behaviour of the CX pantograph by the lumped mass model, represented in Figure 12.3. The mass, stiffness and damping properties of the lumped mass model are obtained experimentally, as previously described. The data required to define the CX lumped mass pantograph, shown in Figure 12.3, is presented in Table 12.1. The vertical static contact force F_{Static} represents the vertical force exerted upwards by the pantograph on the overhead contact line, and caused by the pantograph lifting device, whilst the pantograph is raised. According to the European standards [53,70], good dynamic interaction performance with minimum wear and good current collection quality is achieved by controlling the mean contact force F_m, which, for the velocity of 300 km/h considered in this work, should be 157.3 N.

Therefore, the static contact force F_{Static} is defined so that the mean contact force aligns with the regulation requirements for this speed.

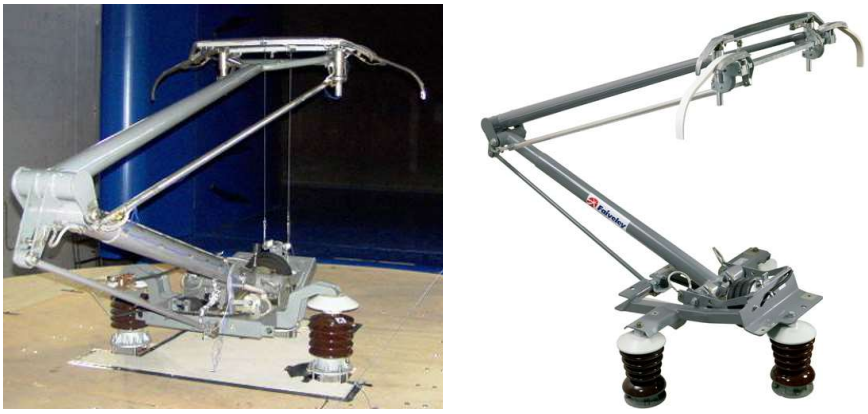

Figure 12.2: French CX pantograph

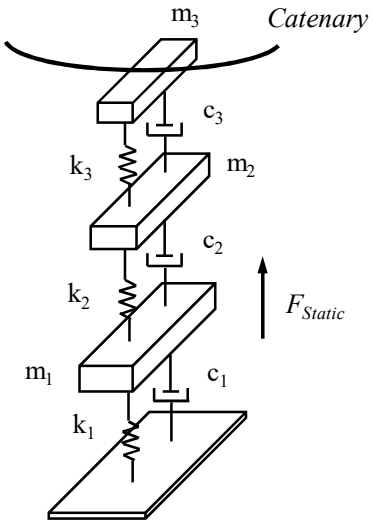

Figure 12.3: Pantograph lumped mass model

Body Mass (kg)			Spring Stiffness (N/m)			Damping Coef. (N.s/m)			F_{Static}
m_1	m_2	m_3	k_1	k_2	k_3	c_1	c_2	c_3	(N)
4.80	4.63	8.50	1.0	5400.0	6045.0	32.00	5.00	10.00	152

Table 12.1: Lumped mass data for the CX pantograph

12.2.2 Italian ATR95 Pantograph

The second pantograph considered here is the Contact ATR95 pantograph, shown in Figure 12.4. By performing laboratory tests, it is possible to represent the dynamic behaviour of the Italian ATR95 pantograph by the lumped mass model, depicted in Figure 12.3. As for the CX pantograph, the mechanical properties of the ATR95 lumped mass model are identified by

performing laboratory tests in such a way that its frequency response matches the one of the real pantograph.

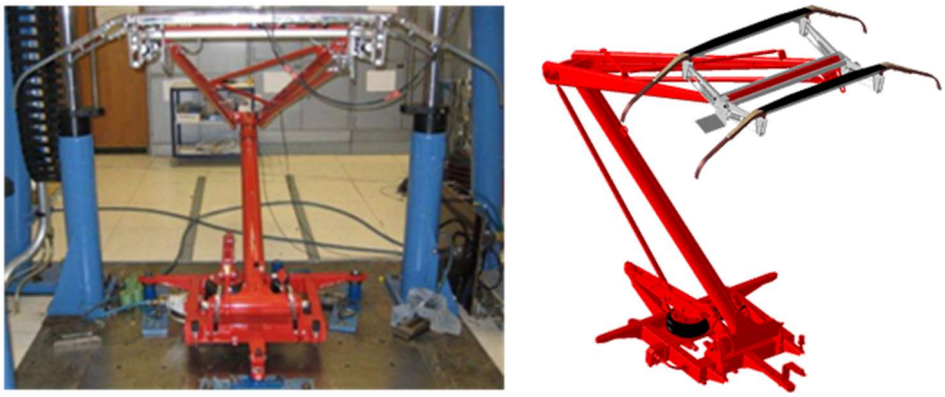

Figure 12.4: Italian ATR95 pantograph

The data required to define the ATR95 lumped mass pantograph, shown in Figure 12.3, is presented in Table 12.2. The vertical static contact force F_{Static} is defined such that it originates a mean contact force F_m, of 157.3 N, as defined by regulations.

Body Mass (kg)			Spring Stiffness (N/m)			Damping Coef. (N.s/m)			F_{Static}
m_1	m_2	m_3	k_1	k_2	k_3	c_1	c_2	c_3	(N)
5.87	11.32	9.30	165.6	22735.6	5156.6	50.27	0.03	28.92	165

Table 12.2: Lumped mass data for the ATR95 pantograph

12.3 Computational Model of the Catenary

High-speed railway catenaries are periodic structures that ensure the availability of electrical energy for the train vehicles. Typical constructions, such as those presented in Figure 12.5, include the masts, serving as support for the registration arms and messenger wire, the steady arms, which not only support the contact wire but also ensure the correct stagger, the messenger wire, the droppers, the contact wire and, eventually, the stitch wire. Both messenger and contact wires are tensioned with high axial forces to limit the sag, to guarantee the appropriate smoothness of the pantograph contact by controlling the wave traveling speed and to ensure the stagger of the contact and messenger wires.

The motion of the catenary is characterized by small rotations and small deformations, in which the only nonlinear effect is the slacking of the droppers. The axial tension on the contact, stitch and messenger wires is constant and cannot be neglected in the analysis. All catenary elements, contact and messenger wires are modelled by using Euler-Bernoulli beam elements [9,10,37,71]. Due to the need to represent the high axial tension forces, the beam finite element used for the messenger, stitch and contact wires, designated as element *i*, is written as:

$$\mathbf{K}_i^e = \mathbf{K}_L^e + F\,\mathbf{K}_G^e \tag{12.5}$$

in which $\mathbf{K}^e{}_L$ is the linear Euler-Bernoulli beam element, F is the axial tension and $\mathbf{K}^e{}_G$ is the element geometric matrix. The droppers and the registration and steady arms are also modelled with the same beam element but disregarding the geometric stiffening. The mass of the gramps that attach the droppers to the wires are modelled as lumped masses. To ensure the correct representation of the wave propagation 4 to 6 elements are used in between droppers of the finite element models.

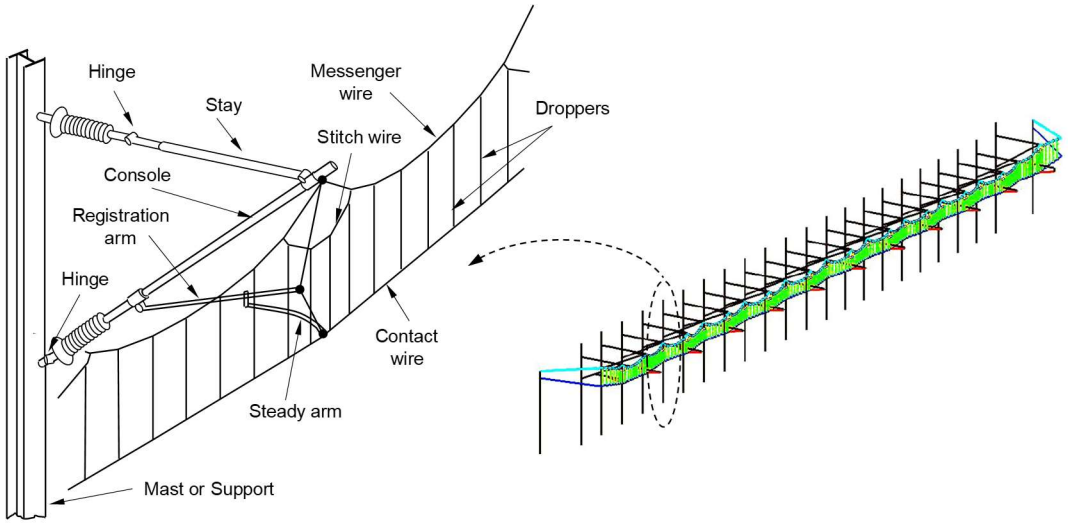

Figure 12.5: Representation of a general catenary

Using the finite element method [44,45], the equilibrium equations for the catenary structural system are assembled as:

$$\mathbf{M}\,\mathbf{a} + \mathbf{C}\,\mathbf{v} + \mathbf{K}\,\mathbf{x} = \mathbf{f} \tag{12.6}$$

where **M**, **C** and **K** are the finite element global mass, damping and stiffness matrices. Proportional damping is used to evaluate the global damping matrix, i.e., $\mathbf{C} = \alpha\,\mathbf{K} + \beta\,\mathbf{M}$, with α and β being suitable proportionality factors [44], or by assembling the individual damping matrices of each finite element, i.e., $\mathbf{C}^e = \alpha^e\,\mathbf{K}^e + \beta^e\,\mathbf{M}^e$ with α^e and β^e being proportionality factors associated with each type of catenary element, such as dropper, messenger wire, stitch wire, etc. The nodal displacements vector is **x** while **v** is the vector of nodal velocities, **a** is the vector of nodal accelerations and **f** is the force vector given by:

$$\mathbf{f} = \mathbf{f}_{(c)} + \mathbf{f}_{(a)} + \mathbf{f}_{(d)} \tag{12.7}$$

being $\mathbf{f}_{(c)}$ the pantograph contact forces, $\mathbf{f}_{(a)}$ the aerodynamic forces, and $\mathbf{f}_{(d)}$ the dropper slacking compensating terms.

For typical catenary finite element models the Newmark family of integration algorithm provide suitable methods for the integration of the equations of motion [72]. The contact forces are evaluated for $t+\Delta t$ based on the position and velocity predictions. The finite element mesh accelerations are calculated by:

$$\left(\mathbf{M}+\gamma\,\Delta t\,\mathbf{C}+\beta\,\Delta t^2\mathbf{K}\right)\mathbf{a}_{t+\Delta t}=\mathbf{f}_{t+\Delta t}-\mathbf{C}\tilde{\mathbf{v}}_{t+\Delta t}-\mathbf{K}\tilde{\mathbf{d}}_{t+\Delta t} \tag{12.8}$$

Predictions for new positions and velocities of the nodal coordinates of the linear finite element model of the catenary are found as:

$$\tilde{\mathbf{d}}_{t+\Delta t}=\mathbf{d}_t+\Delta t\,\mathbf{v}_t+\frac{\Delta t^2}{2}\left(1-2\beta\right)\mathbf{a}_t \tag{12.9}$$

$$\tilde{\mathbf{v}}_{t+\Delta t}=\mathbf{v}_t+\Delta t\left(1-\gamma\right)\mathbf{a}_t. \tag{12.10}$$

Then, with the acceleration $\mathbf{a}_{t+\Delta t}$ the positions and velocities of the finite elements at time $t+\Delta t$ are corrected by:

$$\mathbf{d}_{t+\Delta t}=\tilde{\mathbf{d}}_{t+\Delta t}+\beta\Delta t^2\mathbf{a}_{t+\Delta t} \tag{12.11}$$

$$\mathbf{v}_{t+\Delta t}=\tilde{\mathbf{v}}_{t+\Delta t}+\gamma\Delta t\,\mathbf{a}_{t+\Delta t}. \tag{12.12}$$

The droppers slacking are also corrected in each time step, if necessary. Although the droppers perform as bars during extension, their stiffness during compression is either null or about 1/100$^{\text{th}}$ of the extension stiffness, to represent a residual resistance in buckling at high speed. As the droppers stiffness is included in the stiffness matrix **K** as a bar element, anytime one of them is compressed such contribution for the catenary stiffness has to be removed or modified. In order to keep the dynamic analysis linear the strategy is to compensate the contribution to the stiffness matrix by adding a force to vector **f** equal to the bar compression force as:

$$\mathbf{f}_{(d)t+\Delta t}=\mathbf{K}^e_{dropper}\mathbf{B}\tilde{\mathbf{d}}_{t+\Delta t} \tag{12.13}$$

where the Boolean matrix **B** simply maps the dropper element coordinates into the global nodal coordinates.

The correction procedure expressed by using equations (11.5) through (11.9), followed by the solution of equation (11.4), is repeated until convergence is reached for a given time step, i.e., until $\left|\mathbf{d}_{t+\Delta t}-\tilde{\mathbf{d}}_{t+\Delta t}\right|<\varepsilon_d$ and $\left|\mathbf{v}_{t+\Delta t}-\tilde{\mathbf{v}}_{t+\Delta t}\right|<\varepsilon_d$. ε_d and ε_v are user defined tolerances. Note that the criteria of convergence of the nodal displacements must imply convergence of the force vector also, i.e., the balance of the equilibrium equation right-hand side contribution of

the dropper slacking compensation force with the left-hand-side product of the dropper stiffness by the nodal displacements in equation (11.2). In practice 6 or more iterations must be allowed in the correction process outlined.

In this work, the French LN2 catenary is considered. The description of all details of this catenary and of its finite element model is outside the scope of this text. The interested readers are referred to the work [9].

12.4 Pantograph-Catenary Interaction

The quality of the pantograph-catenary contact required for high-speed train operations is quantified in current regulations [53,70]. The norm EN50367 specifies the thresholds for pantograph acceptance defined in Table 12.3 [53]:

Parameter	Definition	Criterion
F_m	Mean contact force	$F_m = 0.00097\ v^2 + 70$ N
σ	Standard deviation	$\sigma < 0.3\ F_m$
F_{max}	Maximum contact force	$F_{max} < 350$ N
d_{up}	Maximum contact wire uplift at steady arm	$d_{up} \leq 120$ mm
Δ_z	Maximum pantograph vertical amplitude	$\Delta_z \leq 80$ mm
NQ	Percentage of real arcing	$NQ \leq 0.2\%$

Table 12.3: Criteria for pantograph acceptance

The first three parameters in Table 12.3 are obtained from the contact force filtered at 20 Hz. A limitation of the operational speed of the trains is the wave propagation velocity on the contact wire, C, which is given by [5]:

$$C = \sqrt{\frac{\pi^2 EI}{\rho L^2} + \frac{F}{\rho}} \tag{12.14}$$

where F is the tension of the contact wire, ρ is the contact wire mass per length unit, EI is the beam bending stiffness and L is beam length. For high-speed catenaries, the second term of equation (12.14) dominates the critical speed, being the first term negligible. For instance, for a generic catenary, the term $\pi^2 EI/\left(\rho L^2\right) \approx 1.3$ while $F/\rho = 15038$, for which the critical speed is 441 km/h [9,10]. When the train speeds approach the wave propagation velocity of the contact wire, the contact between the pantograph and the catenary is harder to maintain due to increase in the amplitude of the catenary oscillations and bending effects. In order to avoid the deterioration of the contact quality, current regulation imposes a limit to the train speed of $v < 0.7C$.

In the following the performance of the French CX and Italian ATR95 pantographs is analysed when running in a tangent track at 300 km/h on the French LN2 catenary. Afterwards, multiple pantograph operation scenarios, with different distances between them, are studied. The simulations are carried out for one section of the catenary, corresponding to a track length of 1.2 km. In the initial part of the analysis, the pantographs are raised until their bows touch the contact wire. In order to disregard this transient part of the dynamic response, only the contact forces that develop in the pantograph between 400 and 800 m, and the droppers and steady arms that exist in this range are used in the analysis of results. The contact forces are filtered with a cut-off frequency of 20 Hz before being post-processed, as specified by the appropriate regulations [53,70]. The purpose of these studies is to understand the consequences, on the contact force characteristics and on the catenary uplift, of having interoperable railway operations between European countries.

12.4.1 Single Pantograph Operations

Here, the complete overhead electric power system is modelled for the 25 kV LN2 catenary and for the CX and ATR95 lumped mass pantographs, with the characteristics described in the previous sections. The simulation conditions are pictured in Figure 12.6.

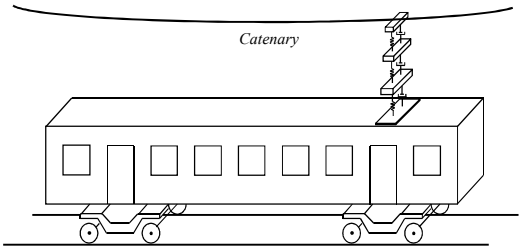

Figure 12.6: Single pantograph operation

The comparative contact force results between seven consecutive masts of the catenary, obtained with both pantographs and filtered at 20 Hz, are presented in Figure 12.7. It is observed that the contact force values increase when the pantograph passes under the steady-arms. Furthermore, the contact force history presents a lower frequency component, corresponding to the passage on the masts and a high frequency component related to the droppers' passage. When comparing the results obtained with both pantographs, it is noticeable that the ATR95 pantograph produces slightly higher amplitude of the contact forces. The pantograph-catenary interaction forces, as shown in Figure 12.7, must be treated statistically in order to emphasize important quantities used in the design of the overhead contact system and for pantograph homologation.

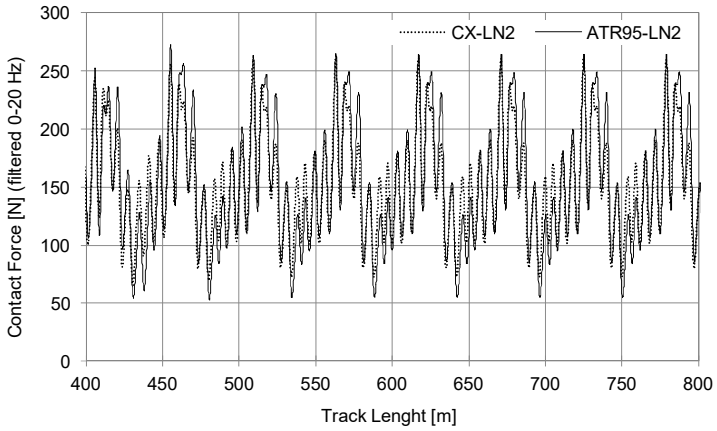

Figure 12.7: Contact force results

In general, the statistical parameters associated to the contact forces that are considered are the maximum and minimum values, the average (mean) value F_m, the standard deviation σ and the statistical minimum of contact force, defined as [53,70]:

$$St_{\min} = F_m - 3\,\sigma \tag{12.15}$$

The contact force statistical parameters, for the CX and ATR95 lumped mass pantographs, are presented in Figure 12.8. The results show that, in both pantographs, the vertical static forces F_{Static}, represented in Figure 12.3, originate mean contact forces of 157 N, as required by the regulations when running at 300 km/h. One important observation of statistical quantities depicted in Figure 12.8 is that the standard deviation of the contact force for CX and ATR95 pantographs are 44 N and 53 N, respectively. This means that the ATR95 pantograph fails to fulfil the second criterion for pantograph acceptance defined in Table 12.3, i.e., $\sigma < 0.3\ F_m$. These values imply that the trainsets using ATR95 pantographs would not be allowed to run at a speed of 300 km/h on the LN2 catenary.

From Figure 12.8 it is also noticeable that the ATR95 pantograph produces higher maximum values and lower minimum values, which implies higher contact force amplitudes. Furthermore, the values obtained for the statistical minimum of the contact forces with CX and ATR95 pantographs are 21 N and -5 N, respectively. This denotes that contact losses and electric arcing are more likely to occur for the ATR95-LN2 pair.

Another characteristic of the contact force that is worth being analysed is its histogram. It represents the distribution of the contact force values among different ranges of forces. The histogram for the CX-LN2 and ATR95-LN2 pairs is presented in Figure 12.9. It is observed that the ATR95 pantograph has a higher number of occurrences of contact forces away from the mean contact value, i.e., the existence of higher and lower contact forces is not sporadic. For the CX pantograph the contact force values are

closer to the mean contact force. In both cases, the mean contact force is 157 N, which satisfies the regulations.

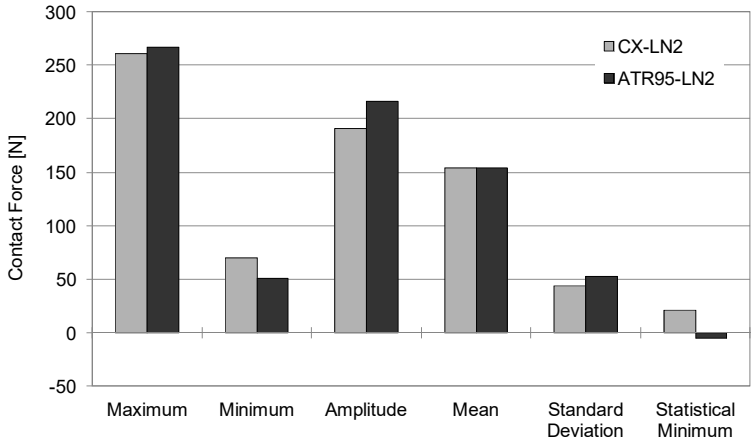

Figure 12.8: Contact force statistical parameters

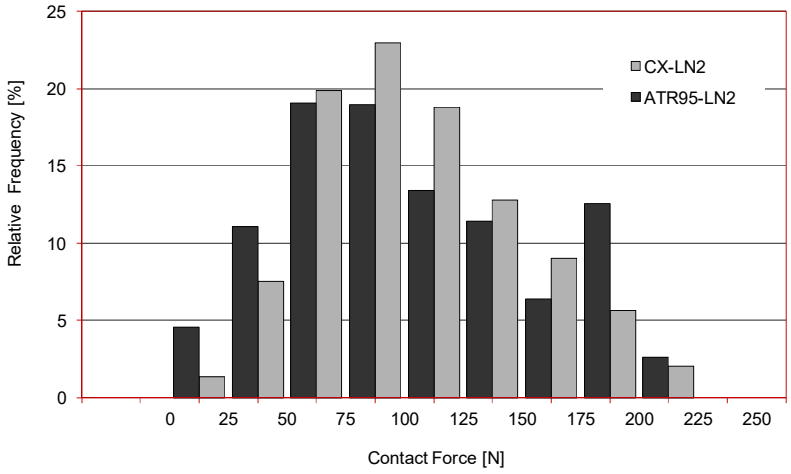

Figure 12.9: Contact force distribution

12.4.2 Multiple Pantograph Operations

In the great majority of cases, high speed trains are operated with two pantographs in constant contact with the catenary. The purpose is to provide the necessary energy required by the electrical motors in order to keep the trainset running at top operational speeds. Notice that in single train configuration, double pantograph can only be operated on DC lines, as on AC lines it would imply problems with the phase change along the line under neutral sections. With double train configuration, this problem does not occur as each train collects the energy to run its own motors.

Another advantage of using double pantograph operations is that it works as a redundant system, i.e., if any incident occurs with one of the pantographs, the other one will keep the trainset running without need to stop the transportation service. Nevertheless, the multiple

pantograph operation raises problems that do not occur when using a single pantograph. In fact, the contact quality of the pantograph-catenary interaction is perturbed due to the mutual influence of the leading and trailing pantographs on each other.

In this work, the operation of two CX and two ATR95 pantographs are compared when running at 300 km/h on the LN2 catenary. The objective is to study the overhead power system performance when the trainset is equipped with two pantographs, assessing how the passage of the front pantograph affects the performance of the rear one and if the presence of the rear pantograph influences the contact quality on the leading one.

The separation between the pantographs depends not only on the trainsets but also on the way the train units are assembled in service. Here, three typical trainset configurations are considered, as shown in Figure 12.10. These configurations correspond to the following scenarios:

- 31 m: Coupling of 2 trainsets (back to front configuration);
- 100 m: One trainset with two active pantographs;
- 200 m: Coupling of 2 trainsets (front to front configuration).

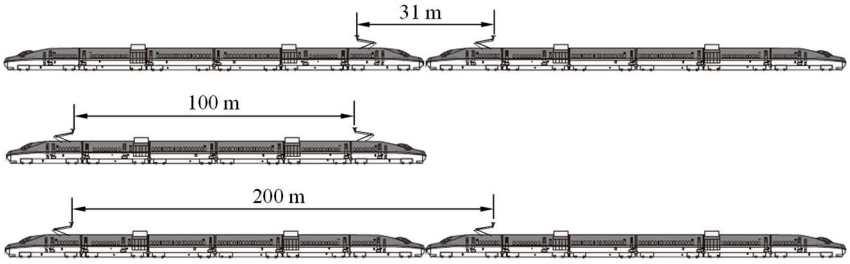

Figure 12.10: Multiple pantograph operation scenarios

The comparison of the contact force statistic values, obtained on front and rear CX paragraphs, is presented in Figure 12.11 for all distances considered here. The results obtained with a single pantograph are also presented as reference. In Figure 12.11a) no noticeable differences are observed among the front pantographs for the multiple pantograph operations considered here. Furthermore, no relevant differences are detected on the front pantograph when comparing multiple and single pantograph operations. Therefore, these results show that the presence of the rear CX pantograph has a negligible influence on the contact quality on the leading one.

When analysing the results from Figure 12.11b) for the rear pantographs, relevant differences are observed. This implies that the passage of the front CX pantograph affects the performance of the rear one. When comparing with a single pantograph operation, this influence can be positive or negative, depending on the distance between pantographs. The better performance of the rear pantograph is for a distance of 31 m, where a smaller standard deviation

and a larger statistical minimum are registered. On the other hand, the worst contact force characteristics are for a distance of 200 m where the rear pantograph exhibits a larger standard deviation and a smaller statistical minimum, implying a higher probability of contact loss.

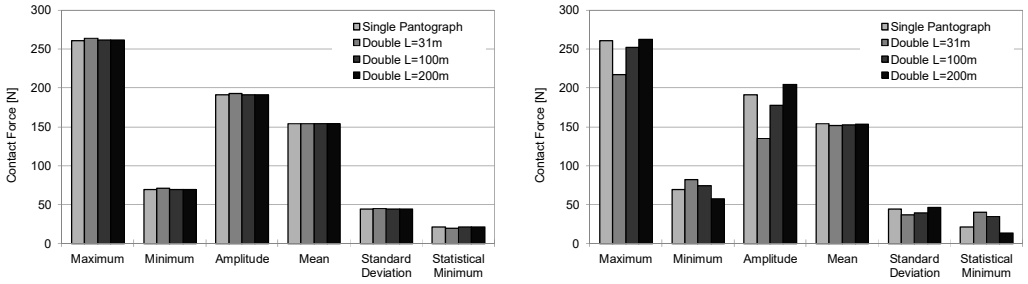

Figure 12.11: Force statistical parameters for 2 CX pantographs: a) Front; b) Rear

Another important observation of statistical quantities depicted in Figure 12.11 is that the standard deviation of the contact force for all pantograph distances and for both front and rear pantographs, are always smaller than 30% of the mean contact force. These results imply that the trains using these pantographs for such distances would be allowed to run at a speed of 300 km/h in the LN2 catenary.

Figure 12.12 shows the comparison of the contact force statistical parameters, obtained on front and rear ATR95 paragraphs, for all distances considered here. From Figure 12.12a) it is evident that there are no relevant differences among the front pantographs for the distances analysed. Moreover, no relevant differences are detected on the front pantograph when comparing multiple and single pantograph operations. Therefore, these results show that the presence of the rear ATR95 pantograph has a negligible influence on the contact quality on the leading one.

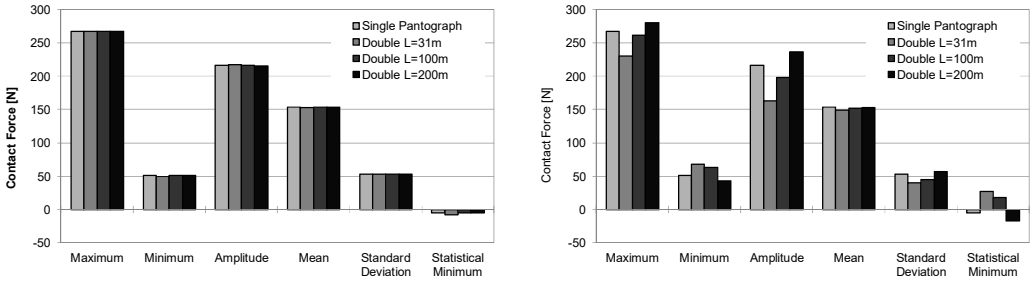

Figure 12.12: Force statistical parameters for 2 ATR95 pantographs: a) Front; b) Rear

The results from Figure 12.12b) reveal significant differences of the contact force statistic values for the rear pantographs. This means that the passage of the front ATR95 pantograph affects the contact quality of the rear one in a positive or negative way, depending on the

distance between pantographs. The better behaviour of the rear pantograph is for a distance of 31 m, where a smaller standard deviation and a larger statistical minimum are registered. The worst performance is obtained for a distance of 200 m, where the rear pantograph exhibits a larger standard deviation and a smaller statistical minimum.

The statistical quantities depicted in Figure 12.12 also show that the standard deviation of the contact force is larger than 30% of the mean contact force for all front pantographs and for the rear pantograph at a distance of 200 m. Such results mean that the ATR95 pantograph, acting single or double, fails to fulfil the second criterion for pantograph acceptance defined in Table 12.3, i.e., $\sigma < 0.3\ F_m$. Consequently, the trainsets using ATR95 pantographs would not be allowed to run at a speed of 300 km/h in the LN2 catenary. In all cases analysed here, none of the pantographs exhibits any contact loss.

At this point it should be referred that, in another work by the same authors [10], it is demonstrated that the contact quality in multiple pantograph operations is strongly dependent on the catenary damping since the tension on the contact wire affects its wave travelling speed and its capacity to dissipate energy. In fact, lightly damped catenaries lead to higher amplitudes of contact forces, higher standard deviations and, eventually, to contact losses. In such a case, higher wave travelling speeds of the contact wire are obtained, implying that the trailing pantograph can affect the contact quality of the leading one, especially for smaller pantograph separations. For larger pantograph distances, it is the leading pantograph that affects adversely the contact quality of the trailing pantograph. In this work, all results show that the critical separation between the leading and trailing pantographs is 200m, i.e., at this separation, the leading pantograph has a greater influence on the contact quality of the trailing pantograph.

One of the reasons why the contact force characteristics has to stay inside a limited range concerns the potential interference between the pantograph head and the catenary mechanical components. The steady arm uplift is a measure of the catenary performance and of its compatibility with the running pantographs, representing an important criterion for pantograph acceptance, as defined in Table 12.3.

The maximum uplift obtained at the steady arms of the catenary for all multiple pantograph scenarios considered here are shown in Figure 12.13 and compared with the single pantograph operations. The results show that, for the pantograph distances of 31 and 100 m, the passage of the front pantograph originates higher vertical displacements of the catenary. For a pantograph separation of 200 m the opposite happens. These results are observed for both CX and ATR95 pantographs. It is also noticeable that, in all single and double pantograph studies

considered here, the ATR95 pantograph exhibits smaller steady arm uplifts than the CX pantograph. Another important observation of the results from Figure 12.13 is that, for all pantograph-catenary interaction scenarios analysed in this work, the maximum steady arm uplift of the catenary is always lower than the 12 cm limit allowed for the type of catenary used. This means that this criterion for pantograph acceptance is fulfilled in all cases studied here.

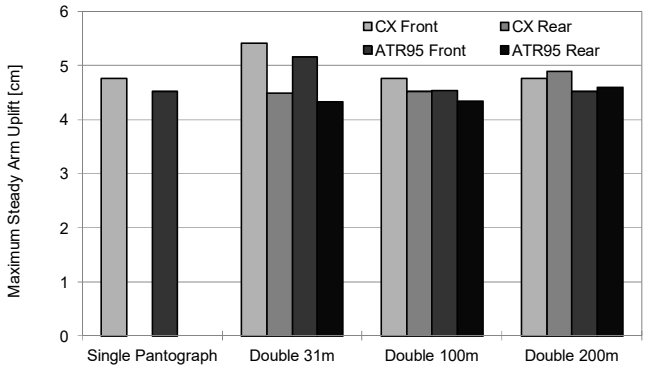

Figure 12.13: Maximum catenary uplift at steady arms

12.5 Conclusions

From the mechanical point of view, the most important feature of the pantograph-catenary system consists in the quality of the contact between the contact wire(s) of the catenary and the contact strips of the pantograph. Therefore, the study of this system requires not only the correct modelling of the catenary and of the pantograph, but also a suitable contact model to describe the interaction between them. The work presented here uses a computational tool based on a co-simulation procedure between a multibody methodology, used to describe the pantograph, and a finite element code, used to model the catenary. A minimal requirement for the software is the ability to collect all data required for the pantograph acceptance.

Single and multiple pantograph operation studies were carried out here for the CX-LN2 and ATR95-LN2 couples. The results show that the passage of the front pantograph affects the performance of the rear one. In fact, as the leading pantograph passes, it originates an excitation of the overhead contact line. Then, when the rear pantograph passes on that location, it will face a perturbed catenary. It was observed that, depending on the distance between pantographs, this influence can be positive or negative when compared with a single pantograph operation. On the other hand, it is observed that the presence of the rear pantograph has a negligible influence on the contact quality on the leading one.

In the case of the ATR95-LN2 pair, the dynamic analyses results also show that, in general, both front and rear pantographs exhibit a standard deviation of contact forces that

exceeds the maximum value of 47.2 N (0.3 F_m) allowed by the regulations. The only exception is observed for the rear pantograph when pantograph separations of 31 and 100 m are considered. When analysing the maximum steady arm uplift obtained in all single and multiple pantograph scenarios, it is evident that the values registered are quite below the limit value of 12 cm set for this catenary. These results show that no problems are anticipated for the uplift criterion. However, as the dynamic analyses results predict an inadequate performance for the standard deviation of the contact forces for the ATR95-LN2 couple, in line tests are recommended for this pair in order to assess the standard deviation criterion.

This work demonstrates that the numerical simulation tools provide the means that allow the enhancement of the regulation criteria and consider other operational aspects besides the single pantograph operation. The results shown here indicate that the questions of compatibility between pantograph and catenary in several operational conditions can be addressed by numerical tools, reducing the costs and time required for vehicle homologation.

References

[1] ERRAC, European Rail Research Advisory Council, "Strategic Rail Research Agenda 2020", Brussels, Belgium, 2007.

[2] Massat, J.-P., Laurent, C., Nguyen-Tajan, T., Facchinetti, A. and Bruni, S., "Simulation Tools for Virtual Homologation of Pantographs", *Proceedings of the First International Conference on Railway Technology: Research, Development and Maintenance*, (J. Pombo, Ed.), Civil-Comp Press, Stirlingshire, UK, Paper 70 (doi:10.4203/ccp.98.70), 2012.

[3] Gardou, M., "Etude du Comportement Dynamique de l'Ensemble Pantographe-Caténaire (Study of the Dynamic Behavior of the Pantograph-Catenary) (in French)", Diploma Thesis, Conservatoire National des Arts et Metiers, Paris, France, 1984.

[4] Jensen, C., "Nonlinear Systems with Discrete and Discontinuous Elements", PhD Thesis, Technical University of Denmark, Lyngby, Denmark, 1997.

[5] Dahlberg, T., "Moving force on an axially loaded beam - with applications to a railway overhead contact wire", *Vehicle System Dynamics*, **44**, No. 8, pp. 631-644, 2006.

[6] Labergri, F., "Modélisation du Comportement Dynamique du Système Pantographe-Caténaire (Model for the Dynamic Behavior of the System Pantograph-Catenary) (in French)", PhD Thesis, Ecole Central de Lyon, Lyon, France, 2000.

[7] Seo, J-H., Kim, S-W., Jung, I-H., Park, T-W., Mok, J-Y., Kim, Y-G. and Chai, J-B., "Dynamic Analysis of a Pantograph-Catenary System Using Absolute Nodal Coordinates", *Vehicle System Dynamics*, **44**, No. 8, pp. 615-630, 2006.

[8] Ambrósio, J., Pombo, J. and Pereira, M., "Optimization of High-Speed Railway Pantographs for Improving Pantograph-Catenary Contact", *International Journal of Theoretical & Applied Mechanics Letters*, **3**, 013006, 2013.

[9] Ambrósio, J., Pombo, J., Pereira, M., Antunes, P. and Mósca, A., "Recent Developments in Pantograph-Catenary Interaction Modelling and Analysis", *International Journal of Railway Technology*, **1**, No. 1, pp. 249-278 (DOI:10.4203/ijrt.1.1.12), 2012.

[10] Ambrósio, J., Pombo, J., Pereira, M., Antunes, P. and Mósca, A., "A Computational Procedure for the Dynamic Analysis of the Catenary-Pantograph Interaction in High-Speed Trains", *Journal of Theoretical and Applied Mechanics*, **50**, No. 3, pp. 681-699, 2012.

[11] Arnold, M. and Simeon, B., "Pantograph and catenary dynamics: A benchmark problem and its numerical solution", *Applied Numerical Mathematics*, **34**, No. 4, pp. 345-362, 2000.

[12] Jerrelind, J. and Stensson, A., "Nonlinear dynamic behaviour of coupled suspension systems", *Meccanica*, **38**, pp. 43-59, 2003.

[13] Mei, G., Zhang, W., Zhao, H. and Zhang, L., "A hybrid method to simulate the interaction of pantograph and catenary on overlap span", *Vehicle System Dynamics*, **44**, S1, pp. 571-580, 2006.

[14] Pombo, J. and Ambrósio, J., "Multiple Pantograph Interaction with Catenaries in High-Speed Trains", *Journal of Computational and Nonlinear Dynamics*, **7**, 041008, 2012.

[15] Rauter, F., Pombo, J., Ambrósio, J. and Pereira, M., "Multibody Modeling of Pantographs for Catenary-Pantograph Interaction", *IUTAM Symposium on Multiscale Problems in Multibody System Contacts*, (P. Eberhard, (Ed.)), Springer, Dordrecht, The Netherlands, pp. 205-226, 2007.

[16] Rauter, F., Pombo, J., Ambrósio, J., Pereira, M., Bobillot, A. and Chalansonnet, J., "Contact Model for the Pantograph-Catenary Interaction", *JSME International Journal of System Design and Dynamics*, **1**, No. 3, pp. 447-457, 2007.

[17] Schaub, M. and Simeon, B., "Pantograph-Catenary Dynamics: An Analysis of Models and Techniques", *Mathematical and Computer Modelling of Dynamic Systems: Methods, Tools and Applications in Engineering and Related Sciences*, **7**, No. 2, pp. 225-238, 2001.

[18] Simeon, B. and Arnold, M., "Coupling DAE's and PDE's for Simulating the Interaction of Pantograph and Catenary", *Mathematical and Computer Modelling of Dynamical Systems*, **6**, pp. 129-144, 2000.

[19] Vera, C., Suarez, B., Paulin, J. and Rodríguez, P., "Simulation model for the study of overhead rail current collector systems dynamics, focused on the design of a new conductor rail", *Vehicle System Dynamics*, **44**, No. 8, pp. 595-614, 2006.

[20] Zhang, W., Mei, G., Wu, X. and Z., Shen., "Hybrid simulation of dynamics for the pantograph-catenary system", *Vehicle System Dynamics*, **38**, No. 6, pp. 393-414, 2002.

[21] Moaveni, S., "Finite Element Analysis Theory and Application with ANSYS", Prentice-Hall, Englewood-Cliffs, New Jersey, 2007.

[22] Collina, A. and Bruni, S., "Numerical Simulation of Pantograph-Overhead Equipment Interaction", *Vehicle System Dynamics*, **38**, No. 4, pp. 261-291, 2002.

[23] Collina, A., Melzi, S. and Facchinetti, A., "On the Prediction of Wear of Contact Wire in OHE Lines: a Proposed Model", *Vehicle System Dynamics*, **37**, S1, pp. 579-592, 2002.

[24] Bucca, G. and Collina, A., "A Procedure for the Wear Prediction of Collector Strip and Contact Wire in Pantograph-Catenary System", *Wear*, **266**, (1-2), pp. 46-59, 2009.

[25] Shing, A. W. C. and Wong, P. L., "Wear of Pantograph Collector Strips", *Institution of Mechanical Engineers, Part F: Journal of Rail and Rapid Transit*, **222**, pp. 169-176, 2008.

[26] Bocciolone, M., Resta, F., Rocchi, D., Tosi, A. and Collina, A., "Pantograph Aerodynamic Effects on the Pantograph-Catenary Interaction", *Vehicle System Dynamics*, **44**, S1, pp. 560-570, 2006.

[27] Pombo, J. and Ambrósio, J., "Environmental and Track Perturbations on Multiple Pantograph Interaction with Catenaries in High-Speed Trains", *Computers and Structures*, **124**, pp. 88-101 (DOI: 10.1016/j.compstruc.2013.01.015), 2013.

[28] Pombo, J., Ambrósio, J., Pereira, M., Rauter, F., Collina, A. and Facchinetti, A., "Influence of the Aerodynamic Forces on the Pantograph-Catenary System for High Speed Trains", *Vehicle System Dynamics*, **47**, No. 11, pp. 1327-1347, 2009.

[29] EUROPAC Project no, 012440, "Modelling of Degraded Conditions Affecting Pantograph-Catenary Interaction", Technical Report EUROPAC-D22-POLI-040-R1.0, Politecnico di Milano, Milan, Italy, 2007.

[30] Pombo, J. and Ambrósio, J., "Environmental and Track Perturbations on Multiple Pantograph Interactions with Catenaries in High-Speed Trains", *Proceedings of the Thirteenth International Conference on Civil, Structural and Environmental Engineering Computing*, (Topping B. and Tsompanakis Y., Eds.), Civil-Comp Press, Stirlingshire, United Kingdom, paper 11, doi:10.4203/ccp.96.11, 2011.

[31] Ambrósio, J., Rauter, F., Pombo, J. and Pereira, M., "A Flexible Multibody Pantograph Model for the Analysis of the Catenary-Pantograph Contact", *Multibody Dynamics: Computational Methods and Applications, Computational Methods in Applied Sciences*, (Arczewski et al., (Ed.)), **23**, Springer, Dordrecht, The Netherlands, pp. 1-27, 2010.

[32] Collina, A., Conte, A. L. and Carnevale, M., "Effect of Collector Deformable Modes in Pantograph-Catenary Dynamic Interaction", *Institution of Mechanical Engineers, Part F: Journal of Rail and Rapid Transit*, **223**, No. 1, pp. 1-14, 2009.

[33] Seo, J-H., Sugiyama, H. and Shabana, A. A., "Three-Dimensional Deformation Analysis of the Multibody Pantograph/Catenary Systems", *Nonlinear Dynamics*, **42**, pp. 199-215, 2005.

[34] Pombo, J. and Ambrósio, J., "Influence of Pantograph Suspension Characteristics on the Contact Quality with the Catenary for High Speed Trains", *Computers and Structures*, **110-111**, pp. 32-42 (DOI: 10.1016/j.compstruc.2012.06.005), 2012.

[35] Goodall, R.M., Bruni, S. and Facchinetti, A., "Active Control in Railway Vehicles", *International Journal of Railway Technology*, **1**, No. 1, pp. 57-85 (DOI:10.4203/ijrt.1.1.3), 2012.

[36] Huang, Y., "Discrete fuzzy variable structure control for pantograph position control", *Electrical Engineering*, **86**, pp. 171-177, 2004.

[37] Poetsch, G., Evans, J., Maisinger, R., Kortum, W., Baldauf, W., Veitl, A. and Wallaschek, J., "Pantograph/Catenary Interaction and Control", *Vehicle System Dynamics*, **28**, pp. 159-195, 1997.

[38] Resta, F., Collina, A. and Fossati, F., "Actively Controlled Pantograph: an Application", *Proceedings of the IEEE/ASME International Conference on Advanced Intelligent Mechatronics*, Como, Italy, July 8-12, pp. 243-248, 2001.

[39] Balestrino, A., Bruno, O., Landi, A. and Sani, L., "Innovative solutions for overhead catenary-pantograph system: wire actuated control and observed contact force", *Vehicle System Dynamics*, **33**, No. 2, pp. 69-89, 2000.

[40] Becker, K., Konig, A., Resch, U. and Zweig, B-W, "Hochgeschwindigkeitsfahrleitung - ein thema fur die forschung (The high-speed catenary - a subject for research)", *ETR - Eisen-bahantechnische Rundschau*, **44**, No. 1-2, pp. 64-72, 1995.

[41] Reinbold, M. and Deckart, U., "FAMOS - Ein programm zur simulation von oberleitungen und stromabnehmer (FAMOS - A program for the simulation of catenaries and pantographs)", *ZEV+DET Glases Annalen*, **120**, No. 6, pp. 239-243, 1996.

[42] Veitl, A. and Arnold, M., "Coupled Simulations of Multibody Systems and Elastic Structures", *Proceedings of EUROMECH Colloquium 404 Advances in Computational Multibody Dynamics*, (J. Ambrósio, et al Eds.), Lisbon, Portugal, September 20-23, pp. 635-644, 1999.

[43] Fernandez, J-A. and Pastor, M., "Analisis mediante elementos finites del acoplamiento di-namico catenaria-pantógrafo (Finite element analysis of the dynamic coupling catenary-pantograph)", Ministério de Fomento, Centro de Estudos y Experimentacion de Obras Públicas, Madrid, Spain, 1998.

[44] Hughes, T., "The Finite Element Method: Linear Static and Dynamic Finite Element Analysis", Prentice-Hall, Englewood Cliffs, New Jersey, 1987.

[45] Zienkiewicz, O. and Taylor, R., "The Finite Element Method", Butterwort-Heinemann, Woburn, Massachussetts, 2000.

[46] Nikravesh, P. E., "Computer-Aided Analysis of Mechanical Systems", Prentice-Hall, Englewood Cliffs, New Jersey, 1988.

[47] Schiehlen, W., "Multibody Systems Handbook", Springer-Verlag, Berlin, Germany, 1990.

[48] Shabana, A. A., "Dynamics of Multibody Systems", 2nd Edition, Cambridge University Press, Cambridge, United Kingdom, 1998.

[49] Flores, P., Machado, M., Silva, M. T. and Martins, J. M., "On the Continuous Contact Force Models for Soft Materials in Multibody Dynamics", *Multibody Systems Dynamics*, **25**, No. 3, pp. 357-375, 2011.

[50] Lankarani, H. M. and Nikravesh, P. E., "Continuous Contact Force Models for Impact Analysis in Multibody Systems", *Nonlinear Dynamics*, **5**, pp. 193-207, 1994.

[51] Pereira, C., Ramalho, A. and Ambrósio, J., "A Critical Overview of Internal and External Cylinder Contact Force Models", *Nonlinear Dynamics*, **63**, No. 4, pp. 681-697, 2011.

[52] Ambrósio, J., Pombo, J., Rauter, F. and Pereira, M., "A Memory Based Communication in the Co-Simulation of Multibody and Finite Element Codes for Pantograph-Catenary Interaction Simulation", *Multibody Dynamics*, (Bottasso C.L., Ed.), Springer, Dordrecht, The Netherlands, pp. 211-231, 2008.

[53] EN 50367, "Railway applications - Current collection systems - Technical criteria for the interaction between pantograph and overhead line", CENELEC European Committee for Electrotechnical Standardization, Brussels, Belgium, 2006.

[54] Pombo, J., Antunes, P. and Ambrósio, J., "A Study on Multiple Pantograph Operations for High-Speed Catenary Contact", *Proceedings of the Eleventh International Conference on Computational Structures Technology*, (Topping B., Ed.), Civil-Comp Press, Stirlingshire, United Kingdom, paper 139, doi:10.4203/ccp.99.139, 2012.

[55] Chamorro, R., Escalona, J. and González, M., "An Approach for Modeling Long Flexible Bodies with Application to Railroad Dynamics", *Multibody Systems Dynamics*, **26**, No. 2, pp. 135-152, 2011.

[56] Hölscher, P., "The Dynamics of Foundations for High Speed Lines on Soft Soils", International *Journal of Railway Technology*, **1**, No. 1, pp. 147-166 (DOI:10.4203/ijrt.1.1.7), 2012.

[57] Lewis, R., Dwyer-Joyce, R., Olofsson, U., Pombo, J., Ambrósio, J., Pereira, M., Ariaudo, C. and Kuka, N., "Mapping Railway Wheel Material Wear Mechanisms and Transitions", *Institution of Mechanical Engineers, Part F: Journal of Rail and Rapid Transit*, **224**, No. 3, pp. 125-137, 2010.

[58] Pombo, J. and Ambrósio, J., "An Alternative Method to Include Track Irregularities in Railway Vehicle Dynamic Analyses", *Nonlinear Dynamics*, **68**, pp. 161-176, 2012.

[59] Pombo, J., Ambrósio, J., Pereira, M., Lewis, R., Dwyer-Joyce, R., Ariaudo, C. and Kuka, N., "A Study on Wear Evaluation of Railway Wheels based on Multibody Dynamics and Wear Computation", *Multibody Systems Dynamics*, **24**, No. 3, pp. 347-366, 2010.

[60] Pombo, J., Ambrósio, J., Pereira, M., Lewis, R., Dwyer-Joyce, R., Ariaudo, C. and Kuka, N., "Development of a Wear Prediction Tool for Steel Railway Wheels Using Three Alternative Wear Functions", *Wear*, **271**, No. 1-2, pp. 238-245, 2011.

[61] Pombo, J., Ambrósio, J., Pereira, M., Verardi, R., Ariaudo, C. and Kuka, N., "Influence of Track Conditions and Wheel Wear State on the Loads Imposed on the Infrastructure by Railway Vehicles", *Computers and Structures*, **89**, No. 21-22, pp. 1882-1894, 2011.

[62] Shabana, A. A., "Absolute Nodal Coordinate Formulation Geometry to Railroad Vehicle System Dynamics", *International Journal of Railway Technology*, **1**, No. 1, pp. 221-230 (DOI:10.4203/ijrt.1.1.10), 2012.

[63] Varandas, J., Hölscher, P. and Silva, M., "Dynamic Behaviour of Railway Tracks on Transitions Zones", *Computers and Structures*, **89**, pp. 1468-1479, 2011.

[64] Varandas, J., Hölscher, P. and Silva, M., "Settlement of Ballasted Track Under Traffic Loading: Application to Transition Zones", *Proceedings of the Institution of Mechanical Engineers, Part F: Journal of Rail and Rapid Transit*, DOI: 10.1177/0954409712471610, 2013.

[65] Facchinetti, A. and Bruni, B., "Hardware-in-the-Loop Hybrid Simulation of Pantograph-Catenary Interaction", *Journal of Sound and Vibration*, **331**, No. 12, pp. 2783-2797 (DOI: 10.1016/j.jsv.2012.01.033), 2012.

[66] Gear, C. W., "Simultaneous Numerical Solution of Differential-Algebraic Equations", *IEEE Transactions on Circuit Theory*, **18**, No. 1, pp. 89-95, 1971.

[67] Gear, C. W. and Petzold, L., "ODE Methods for the Solutions of Differential/Algebraic Equations", *SIAM Journal Numerical Analysis*, **21**, 4, pp. 716-728, 1984.

[68] Baumgarte, J., "Stabilization of Constraints and Integrals of Motion in Dynamical Systems", *Computer Methods in Apllied Mechanics and Engineering*, **1**, pp. 1-16, 1972.

[69] Pereira, M. and Ambrósio, J., "Computational Dynamics in Multibody Systems", Kluwer Academic Publishers, Dordrecht, The Netherlands, 1995.

[70] EN 50318, "Railway applications - Current collection systems - Validation of simulation of the dynamic interaction between pantograph and overhead contact line", CENELEC European Committee for Electrotechnical Standardization, Brussels, Belgium, 2002.

[71] Antunes, P., Mósca, A., Ambrósio, J., Pombo, J. and Pereira, M., "Development of a Computational Tool for the Dynamic Analysis of the Pantograph-Catenary Interaction for High-Speed Trains", *Proceedings of the Eleventh International Conference on Computational Structures Technology*, (Topping B., Ed.), Civil-Comp Press, Stirlingshire, United Kingdom, paper 129, doi:10.4203/ccp.99.129 2012.

[72] Newmark, N., "A Method of Computation for Structural Dynamics", *ASCE Journal of the Engineering Mechanics Division*, **85**, EM 3, pp. 67-94, 1959.

13 Dynamic Analysis of the Pantograph-Catenary Interaction on Overlap Sections for High-Speed Railway Operations

[3] Railway vehicles with electrical traction are, today, the most economical, ecological and safe means of transportation. However, they rely on the supply of the proper amount of energy to run its engines. The pantograph and catenary are the mechanical systems responsible to ensure the trains energy collection representing a crucial element for their reliability. The quality of the current collection is of fundamental importance as the loss of contact and consequent arching, not only limit the top velocity of high-speed trains but also imply the deterioration of the functional conditions of these mechanical equipments. Through a catenary system the overlap section represents a critical zone on the contact quality, having the responsibility to provide a smooth transition between subsequent catenaries. The work here presented purposes a study of the dynamic behaviour of the pantograph-catenary system over these types of catenary sections. In order to do so, a computational methodology able to handle the dynamic analysis of pantograph-catenary interaction over overlap sections is presented. Afterwards it is demonstrated in a case study representing single and multiple pantograph operations in high-speed trains between a realistic catenary and pantograph models. The application of the

[3] The work presented in this chapter has been published, as it is, in: P. Antunes, J. Ambrósio, J. Pombo, M. Pereira, *Dynamic Analysis of the Pantograph-Catenary Interaction on Overlap Sections for High-Speed Railway Operations*, Proceedings of the Second International Conference on Railway Technology, Civil-Comp Press, 142, (2014).

procedures allowed the identification of important quantities of the pantograph-catenary dynamic response necessary to evaluate its behaviour when passing through an overlap section.

13.1 Introduction

The high speed railway systems are becoming key-players in worldwide transport policies. This results from the rising oil prices and from the urgency for reduction of CO2 emissions, among others. To improve the competitiveness and attractiveness of railway networks, the trains have to travel faster, with improved safety and comfort conditions and with lower life cycle costs. Furthermore, the railway operators are demanding reductions in the overall operational costs. They put particular emphasis on the railway vehicles maintenance costs and on the aggressiveness of rolling stock on the infrastructures. The quest for interoperability has in the compatibility of different pantographs with existing and projected catenary systems puts an extra level of demand on the ability to control their interface.

As railway vehicles with electrical traction are, today, the most economical, ecological and safe means of transportation the energy collection of the pantograph on the catenary is a crucial element for their reliable running. A limitation on the velocity of high-speed trains concerns the ability to supply the proper amount of energy required to run the engines, through the catenary-pantograph interface [1]. Due to the loss of contact not only the energy supply is interrupted but also arcing between the collector bow of the pantograph and the contact wire of the catenary occurs leading to the deterioration of the functional conditions of the two systems.

The increase of the average contact force would improve the energy collecting capabilities with less incidents of loss of contact but would also lead to higher wear of the catenary contact wire and pantograph collector strip [2, 3]. A balance between contact force characteristics and wear of the energy collection system is the objective of improving contact quality. Even in normal operating conditions, a control on the catenary-pantograph contact force is required to ensure longer maintenance cycles and a better reliability of the systems.

The development of computer resources led simulations to be an essential part of the design process of railway systems. Moreover, the increasing demands for network capacity, either by increasing the traffic speed or the axle loads, put pressure on the existing infrastructures and the effects of these changes have to be carefully considered. The European Strategic Rail Research Agenda [4] and the European Commission White Paper for Transports [5] have identified key scientific and technological priorities for rail transport over the next 20 years. One of the points emphasized is the need to reduce the cost of approval for new vehicles

and infrastructure products with the introduction of virtual certification. Also, an important issue arising during the design phase of new trains is the improvement of its dynamic performance. The concurrent use of different computational tools allows carrying out several simulations, under various scenarios, in order to reach an optimized design. In this way, studies to evaluate the impact of design changes or failure modes risks can be performed in a much faster and less costly way than the physical implementation and test of those changes in real prototypes. Due to their multidisciplinary, all the issues involving railway systems are complex. Therefore, the use of computational tools that represent the state of the art and that are able to characterize the modern designs and predict their dynamic behaviour by using validated mathematical models is essential.

The complete study of design and operational alternatives for the mechanics of the overhead electrical system require that the dynamics of the pantograph-catenary are properly modelled and that software, used for analysis, design or maintenance support, is not only accurate and efficient but also allows for the modelling of all relevant details to the train overhead energy collector system. Most of the software tools used for the simulation of the pantograph-catenary interaction is based in the finite element method and on multibody dynamic procedures [6-9]. The modelling of contact between the pantograph collector strip and the catenary contact wire can be done using unilateral kinematic constraints [8, 10], which does not require the estimation of any contact law parameter but prevents any loss of contact to be detected. Alternatively, penalty formulations can be used [6, 11] with no limitations on how contact may develop but requiring that the penalty terms of the contact law are estimated. In any case, the use of different methods to handle the dynamics of the catenary and pantograph requires that either a single code in which both methods are implemented is developed or that a co-simulation strategy between the two codes is implemented [9, 12] . The contact modelling plays a central role in the establishment of the co-simulation strategies [12].

The catenary system dynamics exhibits small displacements about the static equilibrium position. The only source of nonlinearity results from the slacking of the droppers. Therefore, the linear finite element method has all features necessary to the modelling of this type of systems, provided that the nonlinear effects are suitably modelled as nonlinear forces, in this case, the dropper slacking can be handled by adding corrective terms to the system force vector. The overhead catenary system is a very lightly damped structure in which the damping characterization is important, in particular when the trains are equipped with multiple pantographs [13]. The introduction of damping devices in the droppers of the catenary has been attempted to better control the contact wire vibrations [14]. Different studies show that the

evaluation of the pantograph-catenary contact quality is highly dependent on the amount of structural damping considered for the catenary structural elements [15]. However, it is also recognized that the estimation of the structural damping of the catenary is still a technological challenge.

Through a catenary system the overlap section represents a critical zone on the contact quality, having the responsibility to provide a smooth transition between subsequent catenaries. These irregularities in the system can lead to increased contact force variation and thereby contact loss possibility with consequent contact quality degradation. The work here presented focuses on the study of the dynamic behaviour of the pantograph-catenary system over overlap sections. The purpose is to understand how much these critical regions affect the overall contact quality on the catenary system and identify what factors come at play. In order to do so, a computational methodology is proposed enabling the dynamic analysis of pantograph-catenary interaction. The finite element method is used to model the catenary system while a lumped mass formulation is applied for the dynamic analysis of the pantograph. A contact model, based on a penalty formulation, is selected to represent the interaction between the two systems. The presented methodology is demonstrated in a case study representing single and multiple pantograph operations in high-speed trains between a realistic catenary and pantograph models. This case addresses one of the limiting factors in high-speed railway operation that is the need to use more than a single pantograph for current collection. The application of the procedures allowed the identification of the important quantities of the pantograph-catenary dynamic response necessary to evaluate its behaviour when passing through an overlap section. It was possible to relate the contact quality degradation between a normal and an overlap section of the catenary as also identity that the uplift on the contact wire imposed by the pantograph-catenary contact has a significant influence on the quality of the contact. The contact degradation is particularly noticeable for the leading pantograph in multi pantograph operations when close separations between pantographs are used.

13.2 Catenary dynamic analysis and modelling

High-speed railway catenaries are periodic structures that ensure the availability of electrical energy for the train vehicles running under them. A typical construction, such as the one presented in Figure 13.1, includes the masts (support, stay and console), serving as support for the registration arms and messenger wire, the steady arms, which not only support the contact wire but also ensure the correct stagger, the messenger wire, the droppers, the contact

wire and, eventually, the stitch wire. Furthermore the functionality of the catenaries impose that spans have limited length, to allow for curve insertion and that the contact and messenger wires are not longer than 1.5 Km, depending each particular network. As shown on Figure 13.2 the catenary geometry requires overlaps between the starting and ending spans of different sections.

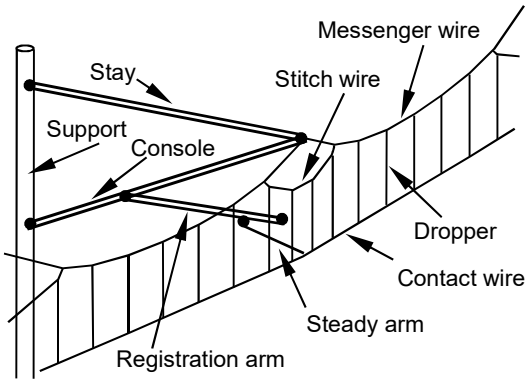

Figure 13.1: General structural and functional elements in a high speed catenary.

Depending on the catenary system installed in a particular high-speed railway all the elements or only some of them may be implemented. However, in all cases both messenger and contact wires are tensioned with high axial forces not only to ensure the correct geometry, i.e., to limit the sag, guarantee the appropriate smoothness of the pantograph contact and ensure the stagger of the contact and messenger wires, but also to allow for the correct wave travelling speed to develop.

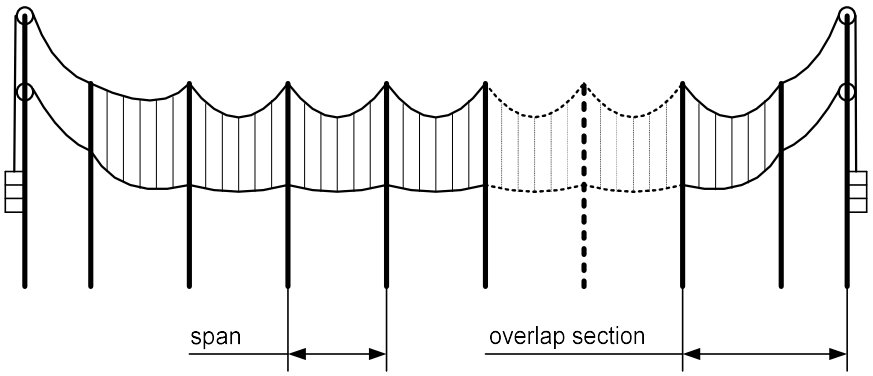

Figure 13.2: Representation of the functional sections of the catenary geometry

13.2.1 Finite element dynamic analysis of the catenary system

The motion of the catenary is characterized by small rotations and small deformations, in which the only nonlinear effect is the slacking of the droppers. The axial tension on the contact, stitch and messenger wire is constant and cannot be neglected in the analysis. Therefore, the catenary system is modelled with linear finite elements in which the dropper nonlinear slacking is

modelled with compensating forces added to the force vector along with the pantograph contact forces and the constant line tensioning forces.

All catenary elements, contact and messenger wires are modelled by using Euler-Bernoulli beam elements [13]. Due to the need to represent the high axial tension forces the beam finite element used for the messenger, stitch and contact wire, designated as element *i*, is written as

$$\mathbf{K}_i^e = \mathbf{K}_L^e + F\,\mathbf{K}_G^e \tag{13.1}$$

in which $\mathbf{K}^e_L$ is the linear Euler-Bernoulli beam element, F is the axial tension and $\mathbf{K}^e_G$ is the element geometric matrix. The droppers and the registration and steady arms are also modelled with the same beam element but disregarding the geometric stiffening. The mass of the gramps that attach the droppers to the wires are modelled here as lumped masses. In order to ensure the correct representation of the wave propagation 4 to 6 elements are used in between droppers to appropriately model the contact and messenger wires. There is no special requirement on the number of elements required to model each dropper, registration or steady-arm.

Using the finite element method, the equilibrium equations for the catenary structural system are assembled as

$$\mathbf{M}\,\mathbf{a} + \mathbf{C}\,\mathbf{v} + \mathbf{K}\,\mathbf{d} = \mathbf{f} \tag{13.2}$$

where **M**, **C** and **K** are the finite element global mass, damping and stiffness matrices of the finite element model of the catenary. Usually proportional damping is used to evaluate the global damping matrix as $\mathbf{C} = \alpha\,\mathbf{K} + \beta\,\mathbf{M}$ with α and β being suitable proportionality factors [16], or the damping matrix of each finite element, i.e., $\mathbf{C}^e = \alpha^e\,\mathbf{K}^e + \beta^e\,\mathbf{M}^e$ with α^e and β^e being proportionality factors associated with each type of catenary element, such as dropper, messenger wire, stitch wire, etc. The nodal displacements vector is **d** while **v** is the vector of nodal velocities, **a** is the vector of nodal accelerations and **f** is the vector with the force vector, written as

$$\mathbf{f} = \mathbf{f}_{(g)} + \mathbf{f}_{(t)} + \mathbf{f}_{(c)} + \mathbf{f}_{(d)} \tag{13.3}$$

which contains the gravity forces, $\mathbf{f}_{(g)}$, and line tensioning forces, $\mathbf{f}_{(t)}$,which are always constant plus the pantograph contact forces, $\mathbf{f}_{(c)}$, and the dropper slacking compensating terms, $\mathbf{f}_{(d)}$. Equation (11.2) is solved for **x** or for **a** depending on the integration method used.

In this work Equation (11.2) is solved with the integration of the nodal accelerations using a Newmark family integration algorithm [17, 18]. The contact forces are evaluated for $t+\Delta t$

based on the position and velocity predictions for the FE mesh and on the pantograph predicted position and velocity. The finite element mesh accelerations are calculated by

$$\left(\mathbf{M}+\gamma\,\Delta t\,\mathbf{C}+\beta\,\Delta t^2\mathbf{K}\right)\mathbf{a}_{t+\Delta t}=\mathbf{f}_{t+\Delta t}-\mathbf{C}\tilde{\mathbf{v}}_{t+\Delta t}-\mathbf{K}\tilde{\mathbf{d}}_{t+\Delta t} \tag{13.4}$$

Predictions for new positions and velocities of the nodal coordinates of the linear finite element model of the catenary are found as

$$\tilde{\mathbf{d}}_{t+\Delta t}=\mathbf{d}_t+\Delta t\,\mathbf{v}_t+\frac{\Delta t^2}{2}\left(1-2\beta\right)\mathbf{a}_t \tag{13.5}$$

$$\tilde{\mathbf{v}}_{t+\Delta t}=\mathbf{v}_t+\Delta t\left(1-\gamma\right)\mathbf{a}_t. \tag{13.6}$$

Then, with the acceleration $\mathbf{a}_{t+\Delta t}$ the positions and velocities of the finite elements at time $t+\Delta t$ are corrected by

$$\mathbf{d}_{t+\Delta t}=\tilde{\mathbf{d}}_{t+\Delta t}+\beta\Delta t^2\mathbf{a}_{t+\Delta t} \tag{13.7}$$

$$\mathbf{v}_{t+\Delta t}=\tilde{\mathbf{v}}_{t+\Delta t}+\gamma\,\Delta t\,\mathbf{a}_{t+\Delta t} \tag{13.8}$$

The dropper slacking is also corrected in each time step, if necessary. Although the droppers perform as a bar during extension their stiffness during compression is either null or about 1/100th of the extension stiffness, to represent a residual resistance to buckling at high speed. As the droppers stiffness is included in the stiffness matrix K as a bar element, anytime one of them is compressed such contribution for the catenary stiffness has to be removed or modified. In order to keep the dynamic analysis linear the strategy pursued here is to compensate the contribution to the stiffness matrix by adding a force to vector $\mathbf{f}_{(d)}$ equal to the bar compression force

$$\mathbf{f}_{(d)t+\Delta t}=\mathbf{K}^e_{dropper}\mathbf{B}\tilde{\mathbf{d}}_{t+\Delta t} \tag{13.9}$$

where the Boolean matrix **B** simply maps the global nodal coordinates into the coordinates of the dropper element.

The correction procedure expressed by using Equations (11.5) through (11.9) and solving Equation (11.4) is repeated until convergence is reached for a given time step, i.e., until $\left|\mathbf{d}_{t+\Delta t}-\tilde{\mathbf{d}}_{t+\Delta t}\right|<\varepsilon_d$ and $\left|\mathbf{v}_{t+\Delta t}-\tilde{\mathbf{v}}_{t+\Delta t}\right|<\varepsilon_d$ being ε_d and ε_v user defined tolerances. Note that the criteria of convergence of the nodal displacements must imply convergence of the force vector also, i.e., the balance of the equilibrium equation right-hand side contribution of the dropper slacking compensation force with the left-hand-side product of the dropper stiffness by the nodal displacements in Equation (11.2).

The computational implementation of the finite element procedure outlined by Equations (11.2) through (11.9), in the context of the catenary dynamic analysis, requires that the maximum number of iterations allowed for the correction process to be 6 or higher. If a maximum number of iterations is set to be below 6 there is the danger that the droppers exhibit residual compression forces during the dynamic analysis, with all implications that such error has over the evaluation of the pantograph-catenary contact force.

13.3 Pantograph dynamic analysis and modelling

The roof pantographs used in high-speed railway applications are characterized as mechanisms with three loops ensuring that the trajectory of the head is in a straight line, perpendicular to the plane of the base, while the pantograph head is maintained levelled. The pantographs are always mounted in the train in a perfect vertical alignment with the centre of the boggies of the vehicle in order to ensure that during curving the centre of the bow does not deviate from the centre of the railroad. The mechanical system that guarantees the required characteristics of the trajectory of the pantograph head during rising is generally made up by a four-bar linkage for the lower stage and another four-bar linkage for the upper stage. Another linkage between the head and the upper stage of the pantograph ensures that the bow is always levelled. In order to control the raise of the pantograph one bar of the lower four-bar linkage is actuated upon by a pneumatic actuator.

The numerical methods used to perform the dynamic analysis of the pantograph must be able to represent the important details of the system, including mechanisms and compliances and to evaluate their correct dynamics. Two different types of models are generally used to represent pantographs: lumped mass and multibody. Each of them has advantages and shortcomings [19, 20]. For the purpose of this work the lumped mass model approach was chosen due to the fidelity of its dynamic response. Also, the use of a lumped mass model leaves the possibility to append its governing equations on the ones ruling the finite element catenary making possible to use the same integration procedure and avoid the use of a more complex co-simulation procedure.

13.3.1 Lumped mass pantograph model

The lumped mass pantograph model, depicted on Figure 13.3(b), is composed of a simple series of lumped masses linked consequently to a ground by a spring/damper element. Although in the literature pantograph models are presented with two, three of more mass stages, for high-

speed train applications there is a minimal requirement of three stages to well represent the system.

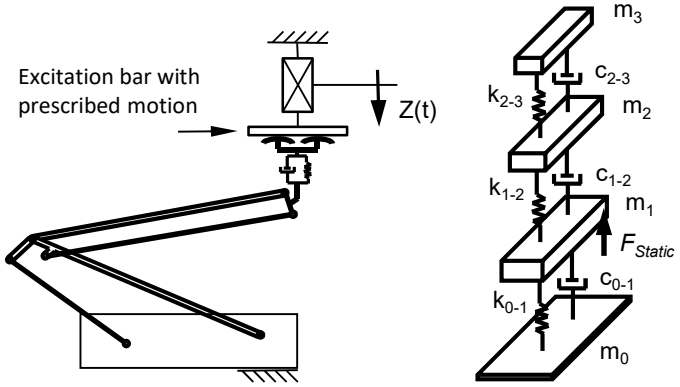

Parameter	Value	Units
m_1	5,58	Kg
m_2	8,78	Kg
m_3	7,75	Kg
k_{0-1}	178,45	N/m
k_{1-2}	15487	N/m
k_{2-3}	7000	N/m
c_{0-1}	108,39	N.s/m
c_{1-2}	0,09	N.s/m
c_{2-3}	45,85	N.s/m

a) b) c)

Figure 13.3: Lumped mass pantograph model: a) Laboratory parameter identification procedure; b) Three stage lumped mass model; c) Parameter values

While the multi-body pantograph models can be built with design data alone, for example with data obtained from technical drawings complemented with measured physical characteristics from selected components, the lumped mass pantograph model parameters, in example of those presented on Figure 13.3 (c), must be identified experimentally. In this sense, the lumped mass pantograph model can be thought as a transfer function in a winch an experimental procedure, presented on Figure 13.3 (a) is used. The idea is to excite the contact strips of the desired pantograph to model with prescribed motions of known frequency and amplitude while measuring the response of the pantograph namely the contact forces on the registration strip and positions, velocities and accelerations at prescribed points of the mechanical pantograph. This acquired data is then held to build the frequency response functions (FRF) of the pantograph. The lumped mass model parameters are identified in such way that the FRF of the model is matched to the experimentally acquired [21].

It is important to note that in spite of the simplicity of their construction and fidelity of their dynamic response, the lumped mass models are commonly used by operators, manufacturers and homologation bodies instead of more complex models. The only part of the lumped mass model that as a physical interpretation is the upper stage, winch limits the use of this type of models for any application that requires modifications on the pantographs structure or mechanics. From this point of view, this is where the multibody pantograph models come in. Provided they are able to adequately represent the dynamics of the implied system, including a match with the FRF experimental data, they constitute an irreplaceable tool.

13.3.2 Lumped mass pantograph dynamic analysis in FE applications

When using lumped mass pantograph models it is possible to use the same finite element code to solve the equations of motion of both pantograph and catenary. For this purpose, the pantograph is considered a linear system and its equations of motion must be assembled in the same way as the catenary equations, expressed by equation (11.2). The contact forces developed between the pantograph collector strip and the catenary contact wire are evaluated as described on section 0 and applied both on the appropriate beam element of the contact wire and the top mass of the pantograph. Notice that in this case only a longitudinal velocity of the pantograph is prescribed and no other motion between the masses occurs besides their expected vertical movement.

In order to produce the pantograph equations of motion, consider the representation of the lumped mass pantograph model, in Figure 13.4, with three staged lumped masses (m_1,m_2,m_3) linked by spring/damper suspensions with correspondent model parameters (K_1,K_2,K_3,C_1,C_2,C_3).

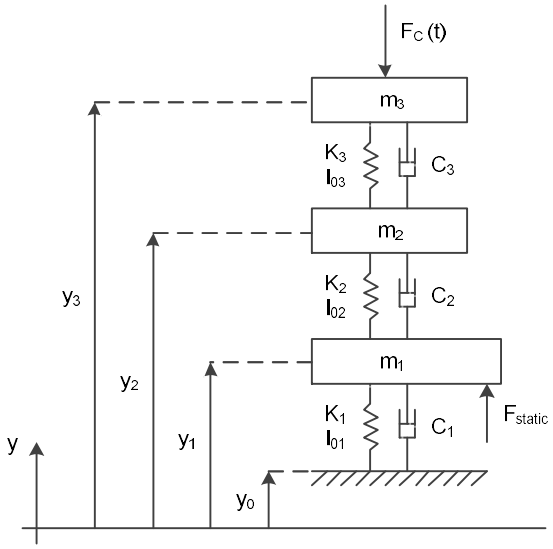

Figure 13.4: Representation of the pantograph lumped mass model

The governing equations of motion are derived at each mass as

$$m_3\ddot{y}_3 + C_3(\dot{y}_3 - \dot{y}_2) + K_3(y_3 - y_2 + l_{03}) = -m_3 g - F_c(t) \tag{13.10}$$

$$m_2\ddot{y}_2 + C_3(\dot{y}_2 - \dot{y}_3) + C_2(\dot{y}_2 - \dot{y}_1) + K_3(y_2 - y_3 + l_{03}) + K_2(y_2 - y_1 - l_{02}) = -m_2 g \tag{13.11}$$

$$m_3\ddot{y}_3 + C_2(\dot{y}_1 - \dot{y}_2) + C_1(\dot{y}_1 - \dot{y}_0) + K_1(y_1 - y_2 + l_{02}) + K_2(y_1 - y_0 - l_{01}) = -m_1 g + F_{static} \tag{13.12}$$

being the following restriction used as a boundary condition

$$y_0 = \text{constant} \Rightarrow \dot{y}_0 = \ddot{y}_0 = 0 \tag{13.13}$$

In addition to the specific pantograph lumped mass model parameters, the equations of motions involve the gravitation constant g, in the evocation of the weights due to the masses. The spring free lengths, l_{01}, l_{02}, l_{03} are considered along with the ground height $y_{0,}$ relative to the catenary model in order to adjust the lumped masses heights. Of importance is the top mass height, with which contact force $F_c(t)$ is evaluated at each time and applied back on the top mass, m_3. The static uplift force, F_{static}, of the pantograph model, applied on its lower mass, provides a direct way to regulate the contact force magnitude and its mean value on a dynamic analysis.

Equations (13.10) to (13.13) can be re-written in vector-matrix form in order to use the same form as the catenary equations of motion (11.2),

$$\begin{bmatrix} m_3 & 0 & 0 \\ 0 & m_2 & 0 \\ 0 & 0 & m_1 \end{bmatrix} \begin{Bmatrix} \ddot{y}_3 \\ \ddot{y}_2 \\ \ddot{y}_1 \end{Bmatrix} + \begin{bmatrix} C_3 & -C_3 & 0 \\ -C_3 & C_3+C_2 & -C_2 \\ 0 & -C_2 & C_2+C_1 \end{bmatrix} \begin{Bmatrix} \dot{y}_3 \\ \dot{y}_2 \\ \dot{y}_1 \end{Bmatrix} + \begin{bmatrix} K_3 & -K_3 & 0 \\ -K_3 & K_3+K_2 & -K_2 \\ 0 & -K_2 & K_2+K_1 \end{bmatrix} \begin{Bmatrix} y_3 \\ y_2 \\ y_1 \end{Bmatrix} = \begin{Bmatrix} -m_3 g + K_3 l_{03} + F_c(t) \\ -m_2 g - K_3 l_{03} + K_2 l_{02} \\ -m_1 g - K_2 l_{02} + K_1 (l_{01} + y_0) + F_{static} \end{Bmatrix} \tag{13.14}$$

In this form the equations of motion of the pantograph can be solved adjoined with the finite element integration procedure either by adding them to the catenary equations or by solving them separately.

13.4 Pantograph-catenary interaction

The pantograph-catenary interaction involves the contact between the pantograph collector strip and the catenary contact wire. The efficiency of the electrical current transmission and the wear of the collector strip and contact wire are deeply influenced by the quality of the contact. This implies that the correct modelling of the contact mechanics involved between these two systems is crucial for its accurate and efficient evaluation. Furthermore, the catenary finite element simulation software may also include a lumped mass pantograph model to interact with the catenary or in another approach communicate with a multibody module that allows the simulation of a pantograph model [19, 20]. In the last case, the contact model is also used as a bridge in the co-simulation environment between the two distinct models.

The contact between the collector strip of the pantograph and the contact wire of the catenary, from the contact mechanics point of view, consists in the contact of a cylinder made of copper with a flat surface made of carbon having their axis perpendicular as shown in Figure 7.1. The contact problem can be treated either by a kinematic constraint between the collector strip and the contact wire or by a penalty formulation of the contact force. In the first procedure the contact force is simply the joint reaction force of the kinematic constraint [8, 10]. With the

second procedure the contact force defined in function of the relative penetration between the two cylinders [22, 23]. The use of the kinematic constraint between contact wire and collector strip forces these elements to be in permanent contact, being this approach valid only if no contact loss exist. The use of the penalty formulation allows for the loss of contact and it is the method of choice for what follows.

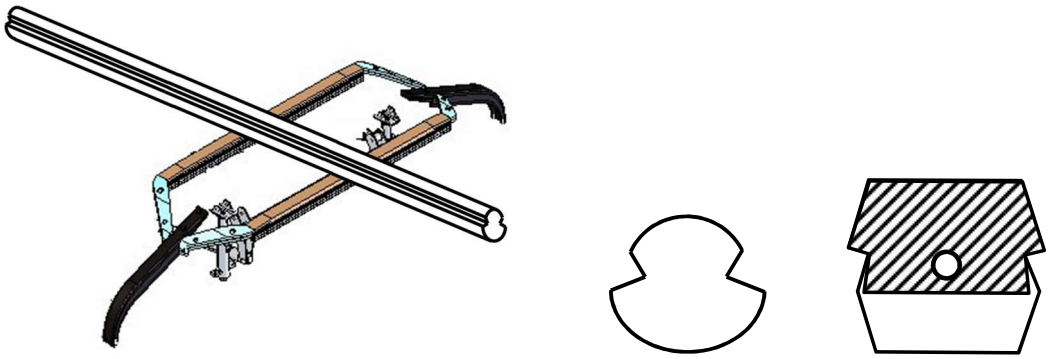

a) b) c)

Figure 13.5: Pantograph-catenary contact: (a) Pantograph bow and catenary contact wire; (b) Cross-section of the contact wire; (c) Cross-section of the collector strip

The continuous contact force model used here is based on a contact force model with hysteresis damping for impact in multibody systems. In this work, the Hertzian type contact force including internal damping can be written as [24]

$$F_N = K\delta^n \left[1 + \frac{3(1-e^2)}{4}\frac{\dot{\delta}}{\dot{\delta}^{(-)}}\right] \tag{13.15}$$

where K is the generalized stiffness contact, e is the restitution coefficient. The relative penetration, δ, the relative penetration velocity, $\dot{\delta}$ and the relative impact velocity, $\dot{\delta}^{(-)}$ are determined by geometric interference taking into account the nodal displacements of the beam finite element in which contact occurs and its shape functions. The proportionality factor K is obtained from the Hertz contact theory as the external contact between two cylinders with perpendicular axis. Note that the contact force model depicted by Equation (13.15) is one of the different models that can be applied. Other continuous contact force models are presented in references [25-27].

In the application that follows the contact is considered purely elastic, i.e., the restitution coefficient e=1, the generalized stiffness defined to be K=20000 N/m and power of the penetration is n=1.

13.5 Pantograph-catenary dynamic analysis on overlap sections

The overlap section of a catenary refers to the spans of a catenary system where two catenaries sections overlap. The need for overlap sections is due to the fact that the length of the messenger and contact wires must be finite, in practice not longer than 1.5 Km. This section is critical since the catenary transition must be as smooth as possible not disturbing the quality of the current collection and must avoid any loss of contact. The most crucial part of the dynamic behaviour happens in the transition when the collector strip of the pantograph meets the new catenary, establishing two contacts on the same strip.

13.5.1 Simulation scenario

In order to analyse the effect of the overlap section a modelling scenario is built using a realistic model of the French LN2 catenary (TGV Atlantique line). To pair with the catenary the Faiveley CX pantograph is selected which is modelled as the lumped mass pantograph represented on Figure 13.3 (b and c). This pantograph-catenary pair represents a present operating configuration, the train speed taken into consideration is 300 Km/h and the set average contact force 157.5 N, as specified by norm EN50367.

The method to build a finite element catenary model of two catenary sections with an overlap section is exactly the same used to build simple section catenaries. The two catenaries are modelled as independent systems, as they have in practice no physical link between them. However, they have to be positioned just right so that the overlap positioning stays correctly modelled. Also it is important to note that the catenary overlapping is not done in the same way for every type of catenary, i.e., each catenary type has its individual intersecting method. To have a clear outlook of the LN2 line overlapping arrangement a representation is presented on Figure 13.6.

For a fair comparison between an overlap and a normal catenary section two intervals of interest are selected for analysis, each containing ten catenary spans. In the work it is considered both single pantograph operation and multiple with the separations of 31, 100, 200 and 400 meters. Note that the simulation with a 400 meter separation can only be accomplished due to the use of a second catenary. Using only one catenary to analyse this last case would not be accurate since the catenary would not have enough analysable length available after the transient response fading from the initial contact on the start of the simulation.

The LN2 catenary main characteristics and modelling data used to build this model are presented Table 13.1. The resulting catenary mesh with the static deformation already accounted for is presented on Figure 13.6.

LN2 (TGV Atlantique line)			
Catenary height [m]	1.4	Contact wire height [m]	5.08
Number of spans	24-26	Number of droppers/span	7-8
Nº spans at C.W. height	21-23	Inter-dropper distance [m]	6.75
Span length [m]	45-54	Stagger [m]	0.40
Damping α	0.0272	Damping β	0

	Contact Wire	Messenger Wire	Droppers	Steady Arms
Section [mm^2]	150	65.5	12	120
Mass [kg/m]	1.334	0.605	0.11	1.07
Young modulus [GPa]	120	84.7	84.7	84.7
Tension [N]	20000	14000	-	-
Claw with	dropper	dropper	-	C.W.
Claw mass [kg]	0.195	0.165	-	0.200
Length [m]	-	-	1.25-1.075	1.22
Angle w/horiz.	-	-	90º	-10º

Table 13.1: Geometric and material properties of the LN2 catenary (TGV Atlantique line)

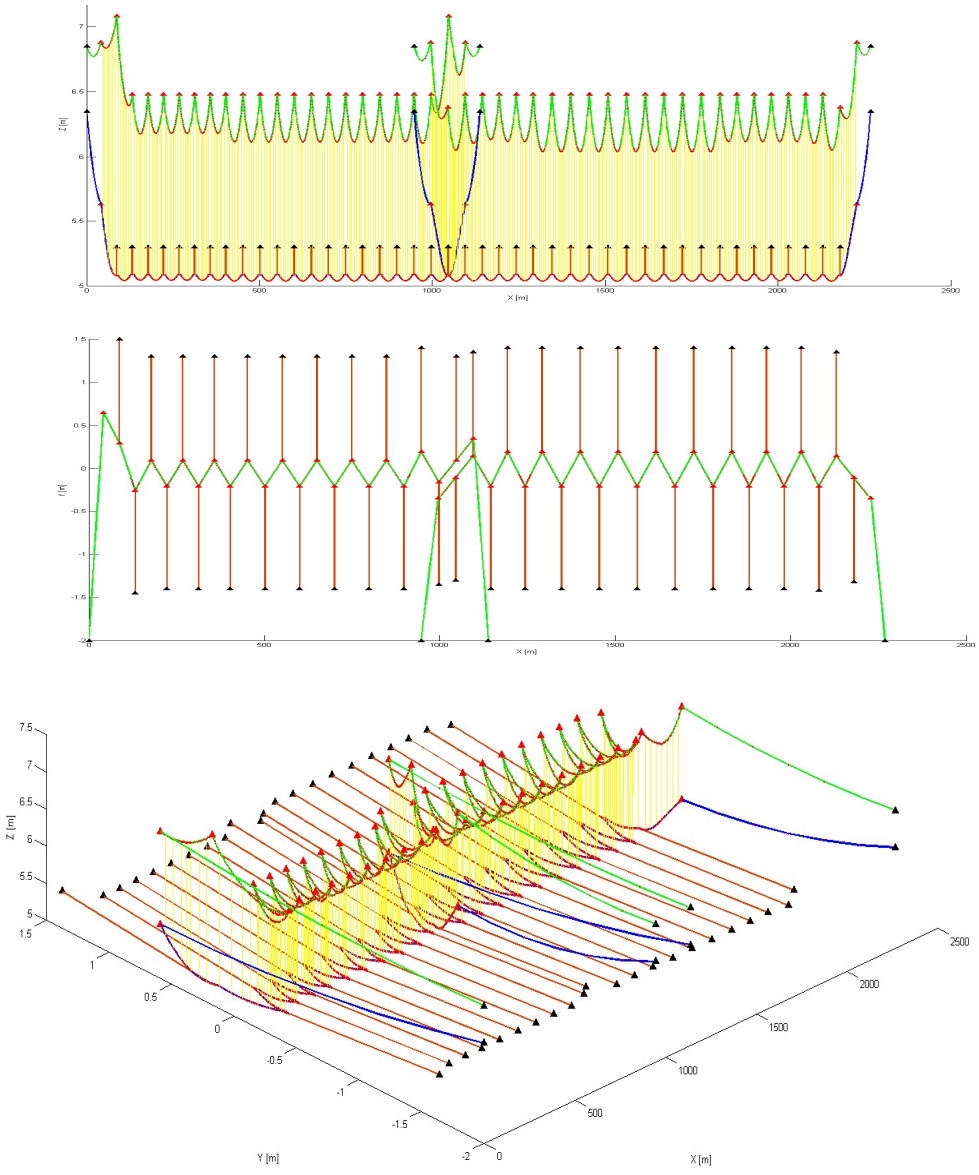

Figure 13.6: Representation of the finite element model of the LN2 catenary (TGV Atlantique line) with the static deformation already accounted.

13.5.2 Results analysis

Starting with the results of the pantographs passage on the regular section, Figure 13.7 depicts the contact forces developed between the pantographs and the catenary. The results show that the amplitude of the contact forces in the trailing pantographs is always larger than those in the leading pantographs. However, this effect fades away as the pantograph separation becomes larger.

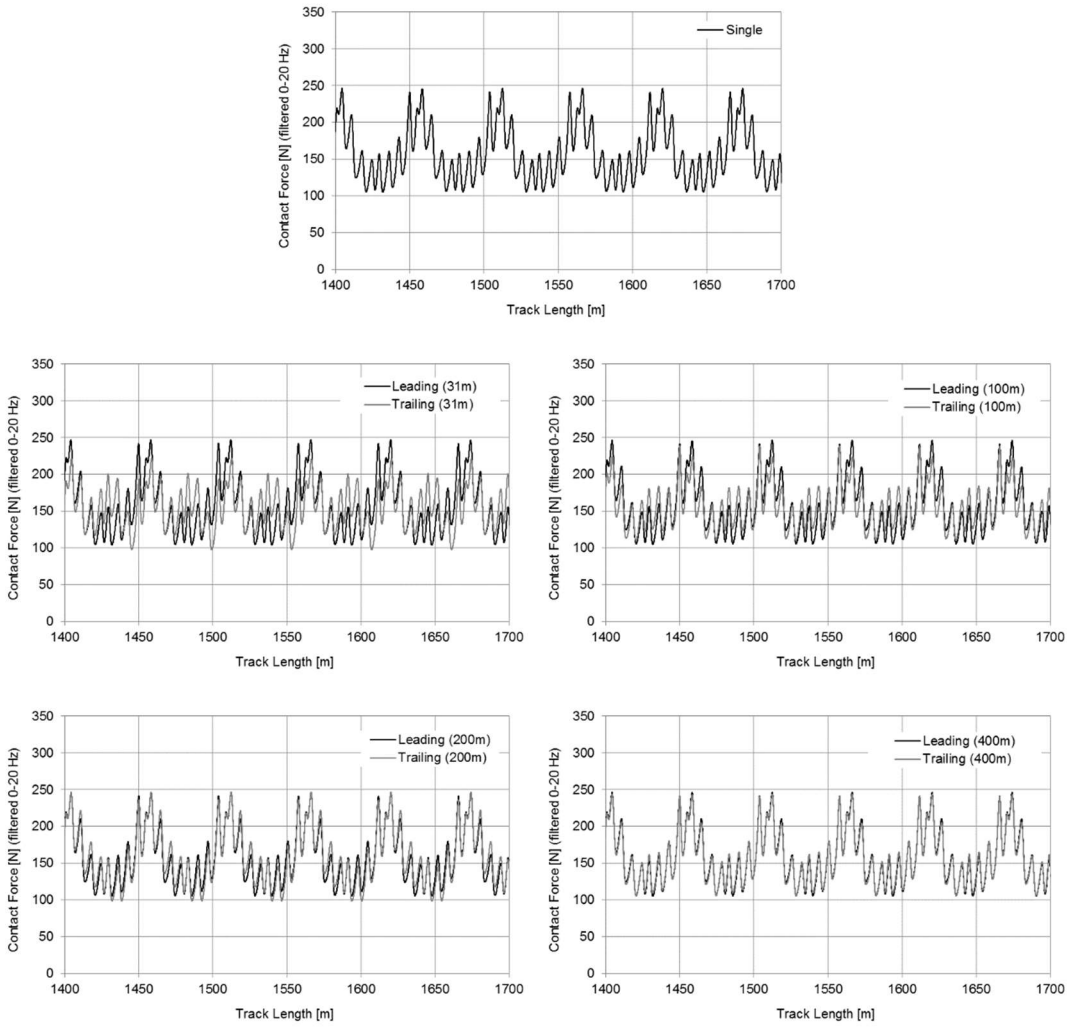

Figure 13.7: Pantograph-catenary contact force for a single pantograph and multiple pantographs with several separations in a regular catenary section

Not much more can be inferred from the contact forces depicted on Figure 13.7. However, their statistical analysis provide the means to evaluate not only the quality of the contact but also elaborate about equipment homologation as stated by the European norm EN50367 which specifies parameter thresholds for pantograph acceptance.

To have a more detailed analysis of these results, as it is required by the European norms, the statistical values of the contact force are overviewed for the different pantograph separations, in Figure 13.8. The most important observation of these statistical results is that all

pantographs are approved on the compatibility acceptance norms. Nevertheless, attention must be paid to the trailing pantographs at the 200 and 400 meter separations were both exhibit the higher contact force maximums and standard deviations. The pantograph at 200 meter separation is the most critical, for which the standard deviation threshold has just 12% of leftover margin. None of the pantographs have contact loss neither their uplift on the steady arms is higher than the norm limits.

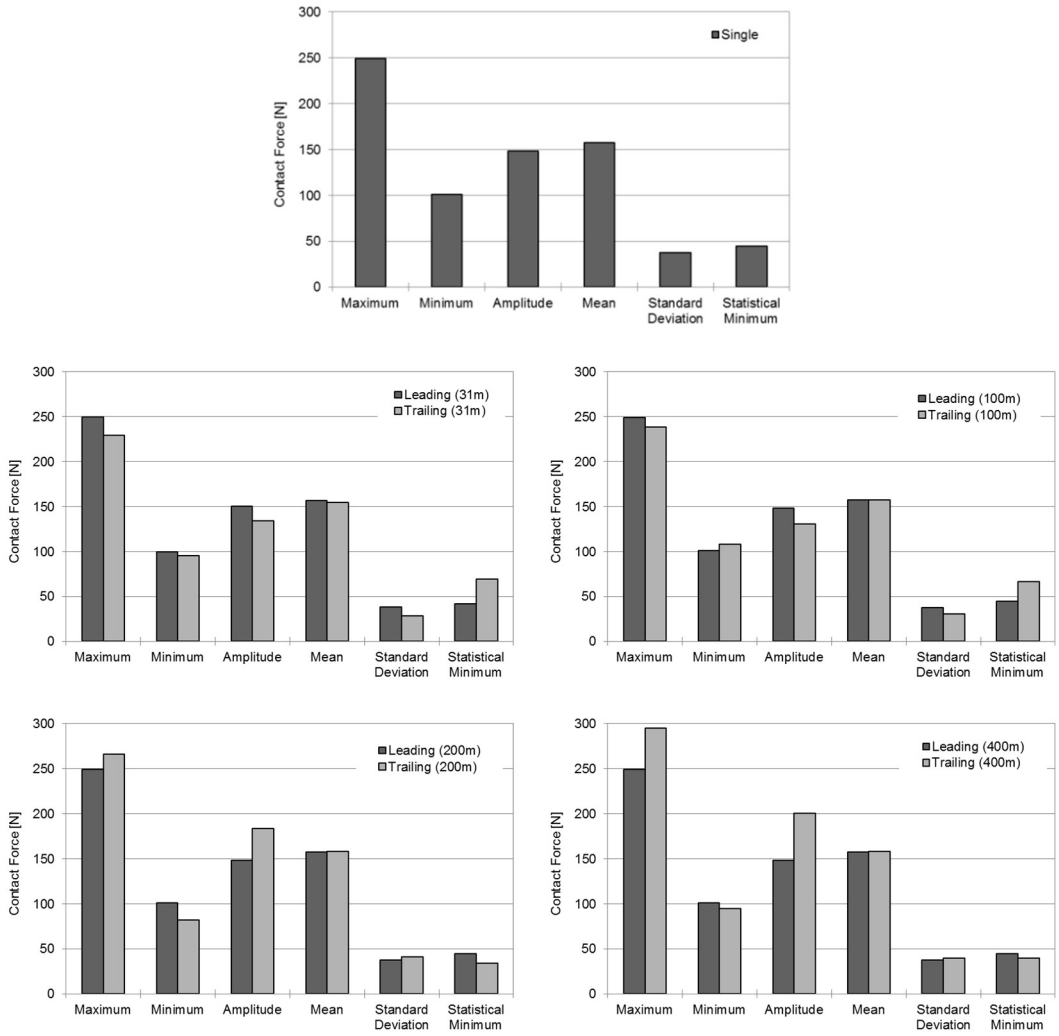

Figure 13.8: Statistical quantities of the pantograph-catenary contact force on a single pantograph and multiple pantographs with several separations in a regular catenary section

In what the contact force results of the pantographs passage on the overlap section are concerned, Figure 13.9 depicts the contact forces developed between the pantographs and the catenary. These results show that the amplitude of the contact forces in the trailing pantographs is always larger than that of the leading pantographs and that this amplitude increase fades away as the pantograph separation go larger. It is also evident the contact force maximum which coincides with the pantographs first contact on next catenary section.

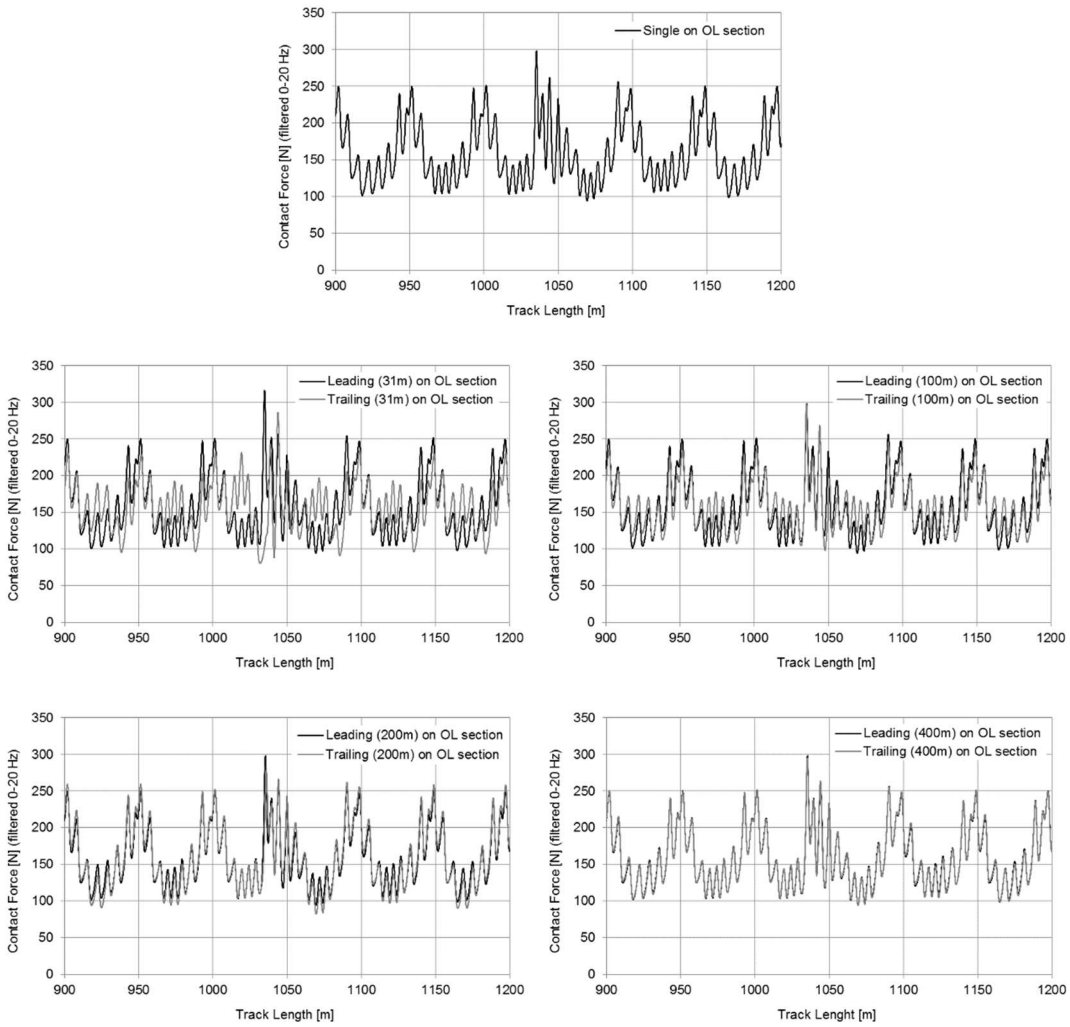

Figure 13.9: Pantograph-catenary contact force for a single pantograph and multiple pantographs with several separations in a catenary overlap section

The statistical analysis of the contact forces developed on the overlap section for a single pantograph and for multiple pantographs, at several separations, is presented on Figure 13.10. The results show that all pantographs pass on their acceptance requirements, none of the pantographs have contact losses and the steady arm uplifts are within acceptable limits. However, as in the normal section results, the trailing pantograph at 200 meter separation is even in a more critical point for norm acceptance being its standard deviation threshold not reached by 5%.

In order to make a comparison of the contact quality between the overlap section and the normal section, the results of the contact force characteristics concerning the two sections types are better understood when presenting the results as shown in Figure 13.11.As stated before, all simulation possibilities pass under the European norm for pantograph acceptance, although the results clearly show that the contact quality on the overlap section worsens, as expected due to the catenary section shift.

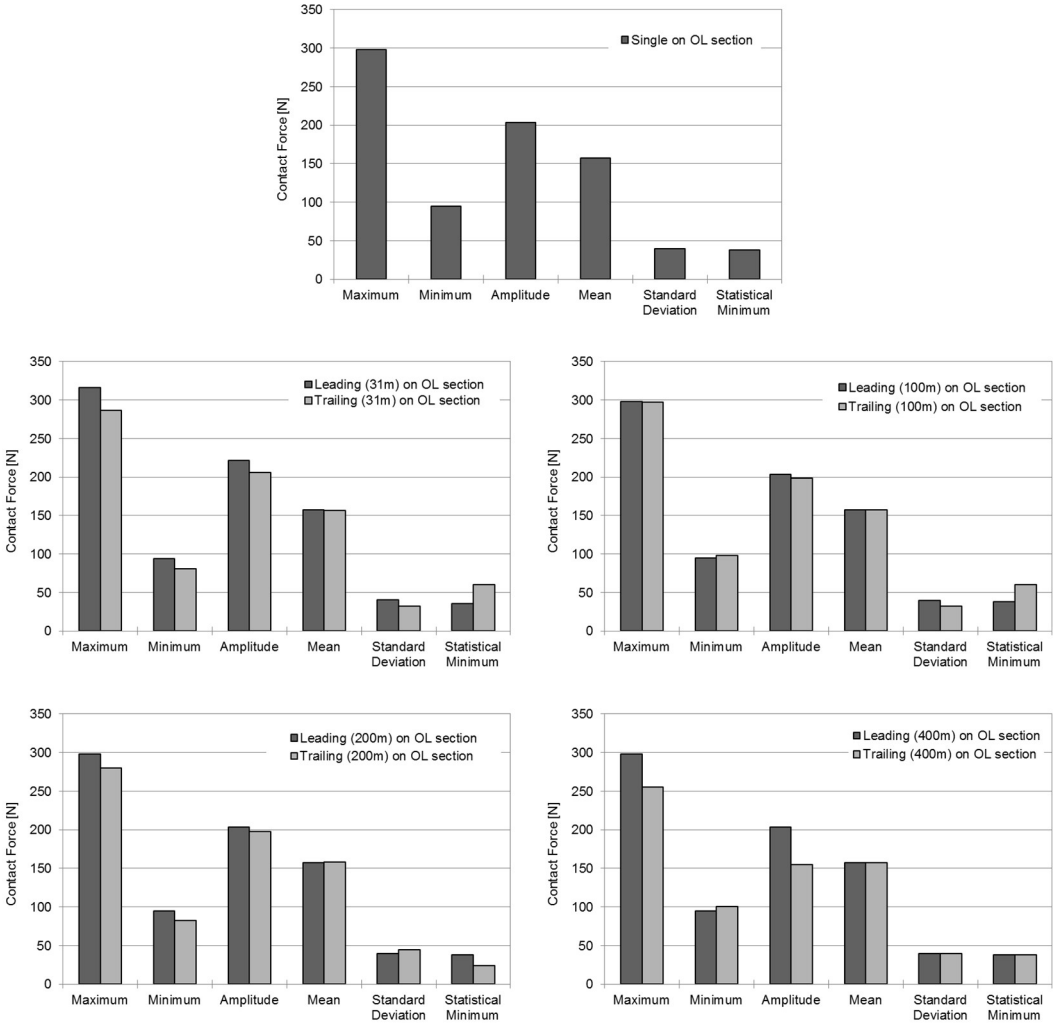

Figure 13.10: Statistical quantities of the pantograph-catenary contact force on a single pantograph and multiple pantographs with several separations in a catenary overlap section

This degradation of contact is more accentuated for the multiple pantographs in close proximity where the most critical case is for the leading pantograph at 31 meter distance from the trailing, which shows that the maximum contact force is closest to its acceptance limit of 350N and also presents the largest standard deviation. As the distance between pantographs becomes larger this degradation of the maximum contact force is less accentuated to the point that at 400 meters distance the leading pantograph exhibits contact force characteristics very close to its trailing counterpart on the normal section. Even the trailing pantograph on the overlap section has a slightly better contact quality than the trailing pantograph in the normal section. It is also noticeable, when observing the contact force maximums on Figure 13.11 and the contact forces along the catenary on Figure 13.9, that for multiple pantographs on an overlap section the critical pantograph is the leading one which meets the next catenary section first and eases the trailing pantograph entrance by uplifting the second sections contact wire.

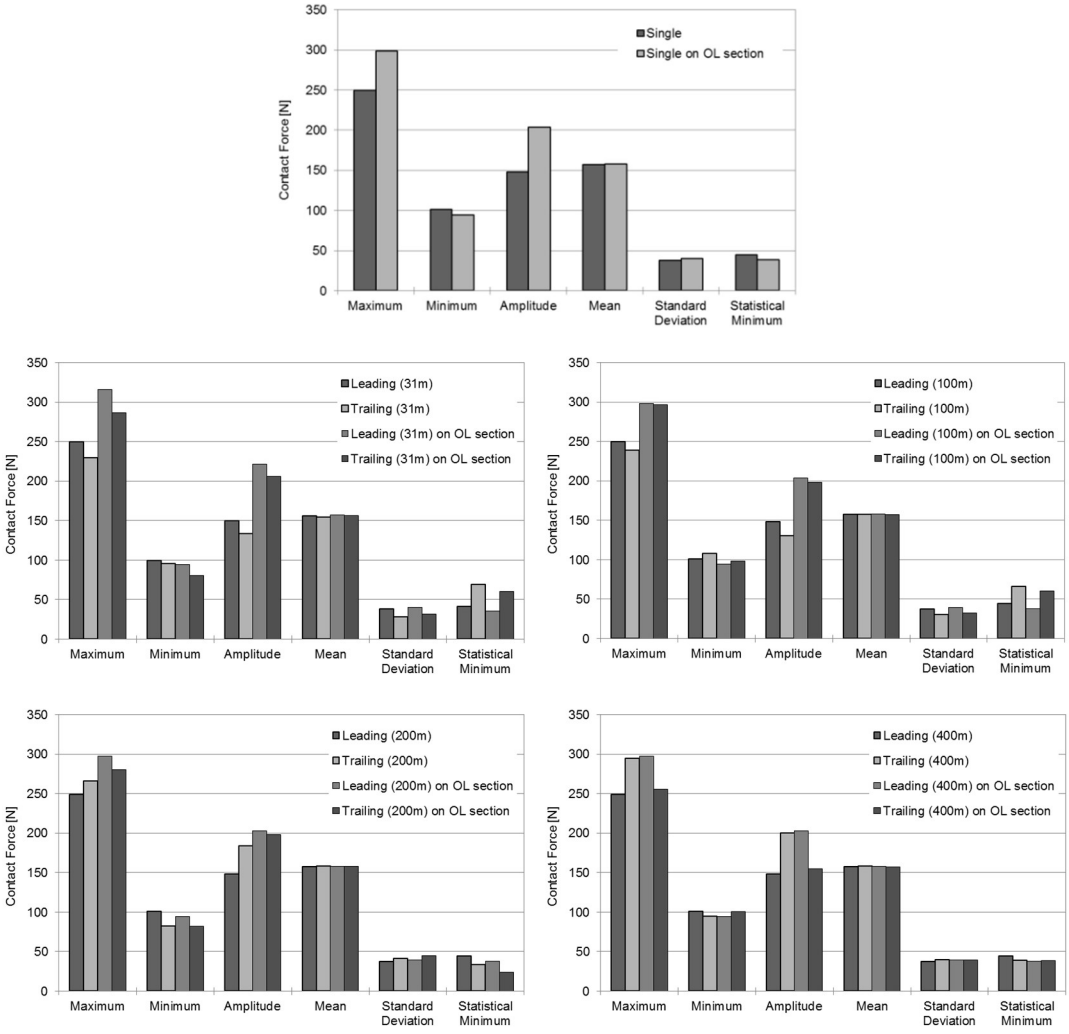

Figure 13.11: Statistical quantities associated to the contact force between an overlap and a normal section of the catenary system for different pantograph separations.

To study mutual influence between the leading and the trailing pantographs over a normal and overlap section of the catenary, the statistical data of the contact forces is graphically rearranged and presented on Figure 13.12 for the normal section and on Figure 13.13 for the overlap section. In both cases the statistical values of the contact force of a single pantograph operation are also presented to better understand the problem. In relation to the contact quality on the normal section, the perturbations of the trailing pantograph over the leading pantograph exists but are very low except for the pantograph with a 400 meter separation, where a degradation on the contact is noticeable. It is difficult to reason with certainty about the causes for this degradation. However, several points have to be taken into consideration. First it is important to take into account that the wave propagation due to contact of either or both the leading and the trailing pantograph with the contact wire can reflect on the catenary ends. Also it is understandable that this wave propagation is damped by the catenary damping. However, this effect might not be enough to overcome a bigger perturbation imposed on the line as the

trailing pantograph exhibits one of the worst contact qualities with the highest maximum contact force. On the other hand, the trailing pantograph contact forces are clearly affected by the leading pantograph. It is observed that the trailing pantograph for separation of 31 and 100 meters have a slightly better contact quality when compared with its leading counterpart or also to the single pantograph case. However, and much more evident is the negative influence on the contact quality that the leading pantograph has over the trailing at 200 and 400 meter separation. These results are consistent with the conclusions taken on [28, 29] where a critical distance between pantographs is suggested.

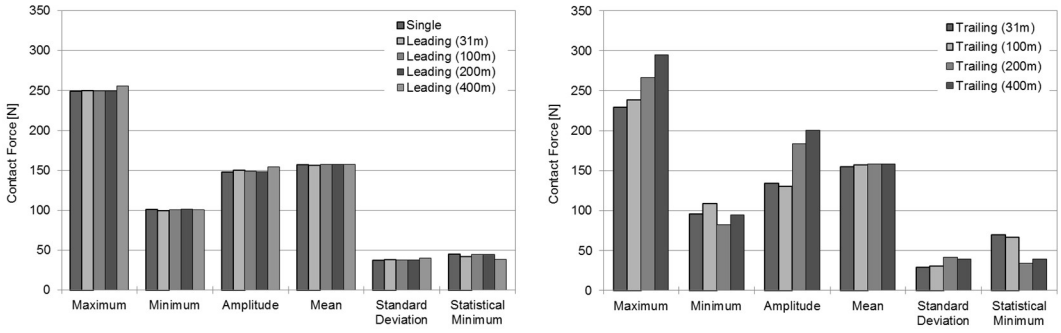

Figure 13.12: Statistical quantities associated to the contact force between single, leading and trailing pantographs on a normal catenary section for different pantograph separations

On the catenary overlap section, where a comparison between the leading and trailing pantographs can be found on Figure 13.13, it is observed that for the leading pantographs only the one with a 31 meter separation appears to be influenced by the trailing pantograph. It is within reason to relate this slight contact quality deterioration of the leading pantograph due to the mutual influence of the contact wire uplifts caused by both the leading and trailing pantographs. The uplifts relate the punctual raising of the contact wire on the position of the pantograph contact. When there are two punctual uplifts close enough, they increase each other slightly because the contact wire stays more supported. As the pantograph separations becomes larger, at 100, 200 and 300 meters, the punctual uplifts of both leading and trailing pantographs do not interfere with each other. At the 31 meter separation their mutual influence results on a small fading of the contact quality on the leading pantograph if compared to the other partings.

Until now the contact force developed over the overlap section has been analysed by the sum of the contact forces that actuate on the pantograph collector strip. When transitioning from one catenary to another two different contacts occur on the same pantograph, one corresponding to the contact with the departing catenary section and a second to the contact with the incoming catenary section. Figure 13.14 presents the contact forces related to each contact made on a specific pantograph. For simplicity only the results for the leading and trailing pantographs, at

31 meters separation, are shown. However, for all the other pantographs separations the results are similar. Careful analysis of the presented results show that that while there is never a complete contact loss for the total of the two contacts developed on the overlap section, the results register a contact loss and regain of contact on each of the contacts developed on the departing and incoming catenaries. This event occurs on both leading and trailing pantographs.

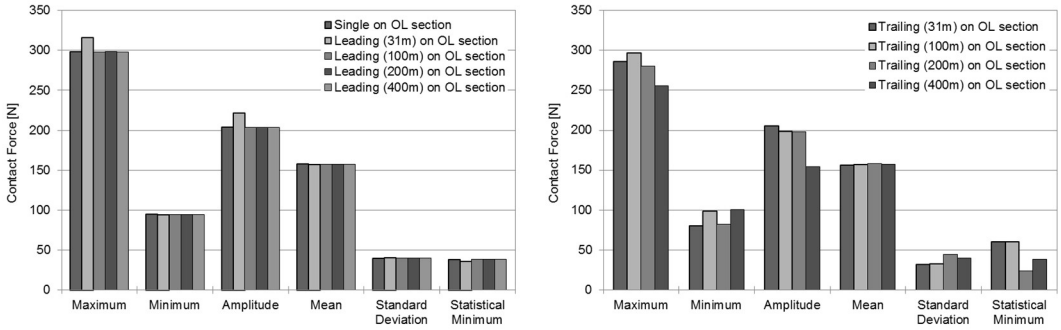

Figure 13.13: Statistical quantities associated to the contact force between single, leading and trailing pantographs on a catenary's overlap section for different pantograph separations

To explain this effect it has to be taken into account that the incoming catenary has no imposed uplift until contact occurs. As the contact on the incoming catenary occurs the contact on the departing catenary fades until is lost. However, when the incoming catenary gains uplift due to the new contact its contact wire is raised matching the contact wire of the departing catenary causing a regain of contact that quickly is loosed again. This occurrence shows the importance of the uplifts on the catenary transition and it is expected that larger uplifts result on less smooth line transitions. It is very difficult to validate this numeric result with the presently existent experimental results. Note that this occurrence takes roughly 0.3 seconds. Limited literature references are available with overlap section studies. Reference [30] relates that the uplift on the contact wire has great influence on the dynamic performance of the pantograph in this type of sections as it has been concluded above with the results of the case study presented here.

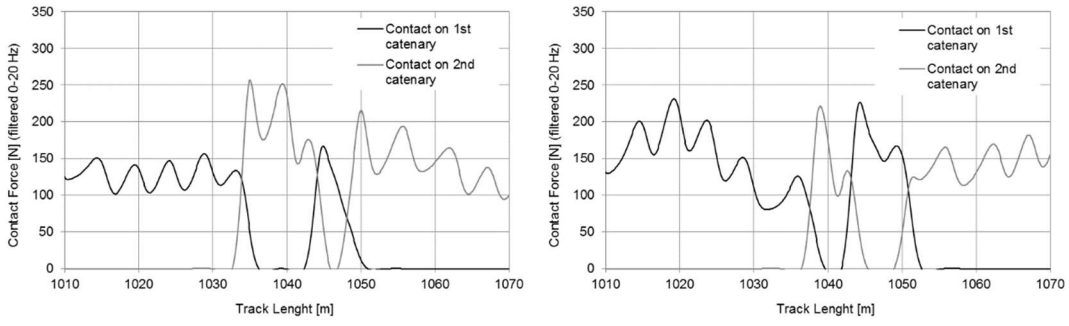

Figure 13.14: Discretized contact forces on the catenary overlap section for the leading (a); and trailing pantograph (b), with 31 meters separation.

From another stand point the influence of the leading contact over the trailing pantograph is evident on the results. All the trailing pantographs exhibit a better contact quality with, especially when comparing the contact force maximums between the leading and trailing pantographs at each separation. These contact force maximums, which can be observed in Figure 13.9, relate to the moment where the pantograph meets the incoming catenary. So it is concluded that, at least for this particular catenary and specifically for this overlap section arrangement the leading pantograph appears to ease the trailing pantograph entrance one the incoming catenary having a smoother transition on the overlap section, even smother than a single pantograph transitioning.

13.6 Conclusions

The development of catenary and pantograph systems that allow their operation with higher speeds and better overall contact require that the computer tools used in their analysis include all modelling features relevant to their analysis. A computational approach based on the linear finite element is presented and demonstrated in the framework of the pantograph-catenary interaction analysis over overlap catenary sections. The overlap sections represent a critical section on the catenary systems as these irregularities in the system can lead to increased contact force variation and thereby contact loss possibility.

In the presented study scenario, it was possible to relate the contact quality degradation on an overlap section when compared to a regular catenary section. On multi pantograph operations it was possible to notice that pantograph proximity is a critical aspect for the pantograph-catenary interaction. The uplift on the contact wire imposed by each pantograph contact has a great influence on the quality of the contact where larger uplifts result in less smooth line transitions. The contact degradation is particularly noticeable for the leading pantograph when close separations between pantographs are used. Also, within the same reasoning, it was observed that the first pantograph passage eases the trailing pantograph transition.

Some identified challenges remain for future considerations. First it is noted that the catenary overlapping arrangement is not done in the same way for every type of catenary, i.e., each catenary type has its individual intersecting method. So it is of importance to consider the impact different catenary overlapping arrangements may have on the pantograph-catenary dynamic behaviour. One other aspect which needs to be the aim of further investigation is the identification of the catenary damping parameters. Damping plays a fundamental role in the

pantograph-catenary contact quality, so it's correct modelling is critical. However, it is recognized that the estimation of the structural damping of not only the catenary but other structures is still a technological challenge. Rayleigh damping, also known as proportional damping, was used to model the developed catenary model. It is even possible to apply this same methodology locally by addressing different damping parameter to each component. Still, these damping parameters need to be correctly identified either on current operating catenaries or catenaries in design phase. So it is of importance to find methodologies able to identify the catenary damping on existent catenaries with experimental testing and validation, plus relate these findings to catenaries that are still in project.

References

[1] A. Collina and S. Bruni, "Numerical Simulation of Pantograph-Overhead Equipment Interaction," *Vehicle System Dynamics,* vol. 38, pp. 261-291, 2002.

[2] A. W. C. Shing and P. P. L. Wong, "Wear of Pantograph Collector Strips," *Journal of Rail and Mass Transit,* vol. 222, pp. 169-176, 2008.

[3] G. Bucca and A. Collina, "A Procedure for the Wear Prediction of Collector Strip and Contact Wire in Pantograph-Catenary System," *Wear,* vol. 266, pp. 46-59, 2009.

[4] E. R. R. A. C. European Rail Research Advisory Council, "Strategic Rail Research Agenda 2020," Brussels, Belgium2007.

[5] E. C. European Commission, "White Paper: Roadmap to a Single European Transport Area - Towards a Competitive and Resource Efficient Transport System," Brussels, Belgium2011.

[6] F. Rauter, J. Pombo, J. Ambrósio, M. Pereira, A. Bobillot, and J. Chalansonnet, "Contact Model for the Pantograph-Catenary Interaction," *JSME International Journal of System Design and Dynamics,* vol. 1, pp. 447-457, 2007.

[7] K. Lee, "Analysis of Dynamic Contact Between Overhead Wire and Pantograph of a High-Speed Electric Train," *Journal of Rail and Mass Transit,* vol. 221, pp. 157-166, 2007.

[8] J.-H. Seo, H. Sugiyama, and A. A. Shabana, "Three-Dimensional Deformation Analysis of the Multibody Pantograph/Catenary Systems," *Nonlinear Dynamics,* vol. 42, pp. 199-215, 2005.

[9] M. Schaub and B. Simeon, "Pantograph-Catenary Dynamics: An Analysis of Models and Techniques," *Mathematical and Computer Modelling of Dynamic Systems: Methods, Tools and Applications in Engineering and Related Sciences,* vol. 7, pp. 225-238, 2001.

[10] J.-H. Seo, S.-W. Kim, I.-H. Jung, T.-W. Park, J.-Y. Mok, Y.-G. Kim*, et al.*, "Dynamic Analysis of a Pantograph-Catenary System Using Absolute Nodal Coordinates," *Vehicle System Dynamics,* vol. 44, pp. 615-630, 2006.

[11] J. Ambrósio, J. Pombo, J.-P. Massat, and L. Christophe, "Pantograph Design Optimisation Methodology," UNIFE, Brussels, Belgium, PantoTRAIN Technical Report D5.12012.

[12] J. Ambrósio, J. Pombo, F. Rauter, and M. Pereira, "A Memory Based Communication in the Co-Simulation of Multibody and Finite Element Codes for Pantograph-Catenary Interaction Simulation," in *Multibody Dynamics*, E. Bottasso C.L., Ed., ed Dordrecht, The Netherlands: Springer, 2008, pp. 211-231.

[13] G. Poetsch, J. Evans, R. Maisinger, W. Kortum, W. Baldauf, A. Veitl*, et al.*, "Pantograph/Catenary Interaction and Control," *Vehicle System Dynamics,* vol. 28, pp. 159-195, 1997.

[14] S. Harada, M. Shimizu, K. Ikeda, J. Sato, S. Koyano, and K. Chikanari, "Development of Simple Catenary Equipment Using PHC Contact Wire for Sinkansen," *QR of RTRI,* vol. 49, pp. 96-102, 2008.

[15] J. Ambrósio, J. Pombo, A. Facchinetti, S. Bruni, J.-P. Massat, and H. Dupuis, "Key Parameters for Pantograph/Catenary Numerical Models," UNIFE, Brussels, Belgium, PantoTRAIN Technical Report D1.12010.

[16] T. Hughes, *The Finite Element Method: Linear Static and Dynamic Finite Element Analysis*. Englewood Cliffs, New Jersey: Prentice-Hall, 1987.

[17] N. Newmark, "A Method of Computation for Structural Dynamics," *ASCE Journal of the Engineering Mechanics Division,* vol. 85, pp. 67-94, 1959.

[18] K.-J. Bathe, *Finite element procedures*. Englewood Cliffs, N.J.: Prentice Hall, 1996.

[19] P. Antunes, "Development of Multibody Pantograph and Finite Element Catenary Models for Application to High-Speed Railway Operations," Master Thesis, Department of Mechanical Engineering, Instituto Superior Técnico, Lisbon, Portugal, 2012.
[20] J. Ambrósio, J. Pombo, M. Pereira, P. Antunes, and A. Mósca, "Recent Developments in Pantograph-Catenary Interaction Modelling and Analysis," *International Journal of Railway Technology,* vol. 1, pp. 249-278, 2012.
[21] C. P. Vyasarayani, T. Uchida, A. Carvalho, and J. McPhee, "Parameter identification in dynamic systems using the homotopy optimization approach," *Multibody System Dynamics,* vol. 26, pp. 411-424, Dec 2011.
[22] C. Pereira, A. Ramalho, and J. Ambrósio, "A Critical Overview of Internal and External Cylinder Contact Force Models," *Nonlinear Dynamics,* vol. 63, pp. 681-697, 2011.
[23] P. Flores, *Kinematics and dynamics of multibody systems with imperfect joints : models and case studies*. Berlin: Springer, 2008.
[24] H. M. Lankarani and P. E. Nikravesh, "Continuous Contact Force Models for Impact Analysis in Multibody Systems," *Nonlinear Dynamics,* vol. 5, pp. 193-207, 1994.
[25] K. Lee, "A Short Note for Numerical Analysis of Dynamic Contact Considering Impact and a Very Stiff Spring-Damper Constraint on the Contact Point," *Multibody Systems Dynamics,* vol. 26, pp. 425-439, 2011.
[26] P. Flores, M. Machado, M. T. Silva, and J. M. Martins, "On the Continuous Contact Force Models for Soft Materials in Multibody Dynamics," *Multibody Systems Dynamics,* vol. 25, pp. 357-375, 2011.
[27] S. Djerassi, "Three-Dimensional, One Point Collision with Friction," *Multibody Systems Dynamics,* vol. 22, pp. 173-195, 2012.
[28] J. Ambrósio, J. Pombo, M. Pereira, P. Antunes, and A. Mósca, "A Computational Procedure for the Dynamic Analysis of the Catenary-Pantograph Interaction in High-Speed Trains," *Journal of Theoretical and Applied Mechanics,* vol. 50, pp. pp. 681-699, 2012.
[29] K. Ikeda, "Optimization of Overhead Contact Lines for Sinkansen Speed Increases," JR East Technical Review2008.
[30] P. Hare`ll, L. Drugge, and M. Reijm, "Study of Critical Sections in Catenary Systems During Multiple Pantograph Operation," *Journal of Rail and Rapid Transit,* vol. 219, pp. 203-211, 2005.

14 Catenary Finite Element Model Initialization using Optimization

[4] The contact quality between pantograph and catenary plays a critical role on providing the required energy to power the trains traction systems. The need to study and analyse the dynamic behaviour of these coupled systems as led to the development of pantograph/catenary interaction simulation software. Despite the increasing interest on the dynamical analysis of the catenary and its interaction with the pantograph, the accurate analysis of its configuration at static equilibrium becomes of most interest where its correct initial undeformed shape and correspondent undeformed mesh must be found. The initialization of the catenary, that is, the setting of the initial positions of the catenary finite element nodes have different requirements due to the different methods used in the solution of their dynamics. Furthermore, as the static configuration of the catenary provides its initial conditions for dynamic analysis it is possible that these have a significant influence on the simulation results. This is even more critical when considering the contact wire sag correct deformed shape where contact with the pantograph occurs. The work here presented proposes a catenary initialization procedure based on the definition of a fitness function to be minimized using classical gradient based optimization. The proposed methodology also opens the possibility to model catenary systems that have defects such as irregularities on its sag caused by damaged, poorly maintained or ill mounted overhead

[4] The work presented in this chapter has been published, as it is, in: P. Antunes, J. Ambrósio, J. Pombo, *Catenary Finite Element Model Initialization using Optimization*, Proceedings of the Third International Conference on Railway Technology, Civil-Comp Press, 106, (2016).

lines. Here, this irregularity can be imposed on the static equilibrium configuration of the model and the same minimization problem is set to find its corresponded undeformed shape.

14.1 Introduction

As railway vehicles with electrical traction are, today, the most economical, ecological and safe means of transportation. Its energy collection system is the crucial element for their reliable running. This system is generally composed by a pantograph attached to the roof of the train vehicles and an overhead electrical structure laid along the track, as represented in Figure 14.1. As this structural system, most commonly denominated by catenary, is in contact with the pantograph the electrical current that carries is drawn into the electrical traction system of the train. Undoubtedly this system plays a critical role concerning the ability to supply the proper amount of energy required to run the engines and maintain the trains operational speed, through the catenary-pantograph interface [15]. In fact, on present modern high-speed trains, as more electrical current is required, this issue remains one of the major limiting factors on their top operational velocity.

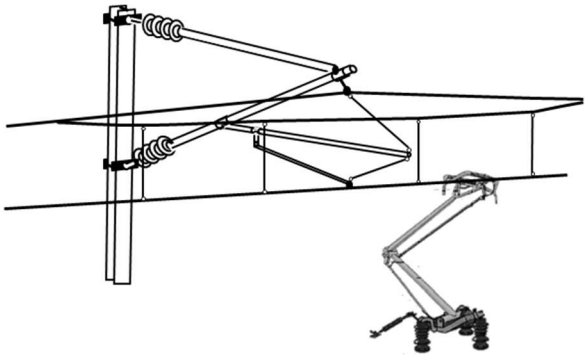

Figure 14.1: Representation of railway energy collecting system composed of a catenary and a pantograph.

Catenary systems are subjected to tight functional requirements to deliver electrical energy to trains engines, in order to ensure their reliability and to control their maintenance periods. The quality of the current collection is of fundamental importance as the loss of contact between the collector bow of the pantograph and the contact wire of the catenary with consequent arching not only limit the top velocity of high-speed trains but also imply the deterioration of the functional conditions of these mechanical equipments. A typical construction, such as the one presented in Figure 14.2, includes the masts (support, stay and console), serving as support for the registration arms and messenger wire, the steady arms, which ensure the correct stagger, the droppers, the contact wire and eventually, the stitch wire.

The droppers here play a fundamental role in supporting the contact wire in order that its sag has the appropriate smoothness for contact with the pantograph.

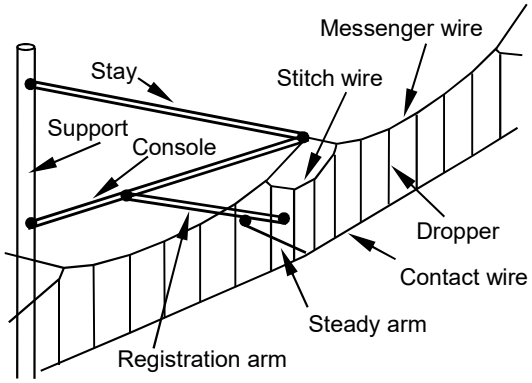

Figure 14.2: General structural and functional elements in a high speed catenary.

The stagger, represented on Figure 14.3, is a requirement for almost all catenaries so that the pantographs registration strip, where the contact occurs, as an even wear across all its length. Furthermore the functionality of the catenaries impose that spans have limited length, to allow for curve insertion and that the contact and messenger wires are not longer than 1.5 Km, depending on each particular network. Therefore the catenary geometry requires overlapping between the starting and ending spans of different sections to ensure a correct transition and ensure good contact quality on pantograph entrance and exit. To ensure the smoothness of the contact wire sag, besides the droppers, the contact wire and messenger wire are mechanically tensioned at the extremities of the catenary section, usually this is done by suspended masses.

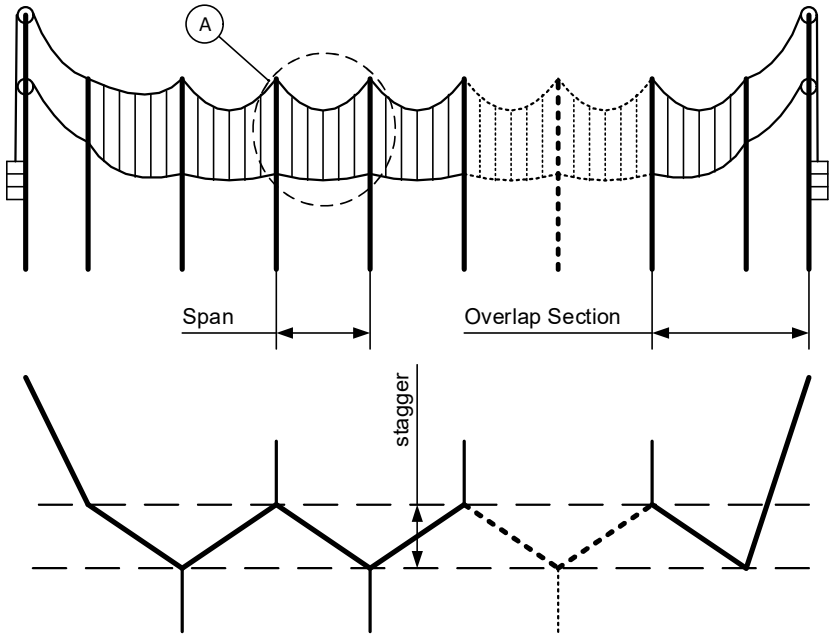

Figure 14.3: Global representation of the geometry of a catenary section.

Depending on the catenary system installed in a particular high-speed railway all the elements or only some of them may be implemented. However, in all cases both messenger and contact wires are tensioned with high axial forces not only to ensure the correct geometry but also to limit the contact wire sag, presented in Figure 14.4. Limiting the sag not only guarantees the appropriate smoothness of the pantograph contact and ensures the stagger of the contact and messenger wires but also allows for the correct wave travelling speed to develop when contact with pantograph occurs. Of course this travelling speed must by higher than the pantograph and corresponding train speed so that the system is stable enough to guarantee good contact quality with less contact loss as possible [57,110].

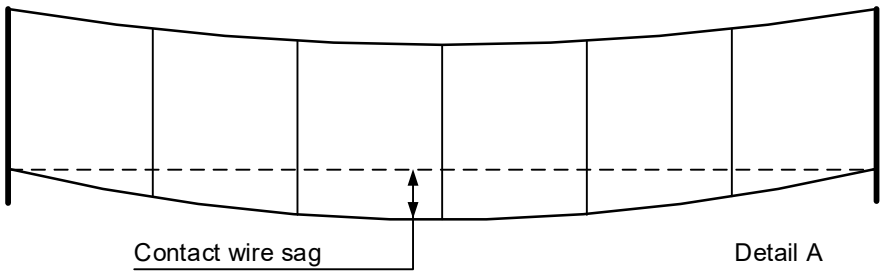

Figure 14.4: Representation of the catenary sag, as detail A from Figure 14.3.

The development of computer resources led simulations to be an essential part of the design process of railway systems. The concurrent use of different computational tools allows carrying out several simulations, under various scenarios, in order to reach an optimized design. In this way, studies to evaluate the impact of design changes or failure modes risks can be performed in a much faster and less costly way than the physical implementation and test of those changes in real prototypes. Due to their multidisciplinary, all the issues involving railway systems are complex. Therefore, the use of computational tools that represent the state of the art and that are able to characterize the modern designs and predict their dynamic behaviour by using validated mathematical models is essential. Moreover, the increasing demands for network capacity, namely the increase of traffic speed, put pressure on the existing infrastructures and the effects of these changes have to be carefully considered. The European Strategic Rail Research Agenda [2] and the European Commission White Paper for Transports [111] have identified key scientific and technological priorities for rail transport over the next 20 years. One of the points emphasized is the need to reduce the cost of approval for new vehicles and infrastructure products with the introduction of virtual certification. Furthermore, the quest for interoperability of different pantographs, in existing and projected catenary systems, puts an extra demand on the ability to control their dynamic behaviour [18].

This conjuncture has risen to the development of reliable, efficient and accurate computational procedures for the design and analysis of the pantograph-catenary system allowing to capture all the relevant features of their dynamic behaviour [8]. Most of these software tools, until now developed, used for the simulation of the pantograph-catenary interaction are based in the finite element method (FEM) and on multibody dynamic procedures [12,61].

When modelling the catenary system with finite elements (FE), one issue that arises is the catenary initialization. This corresponds to building an undeformed catenary mesh that upon being statically loaded by gravitational and axial tension loads exhibits a correct static deformed shape, with special attention to the catenary sag. This issue of fundamental importance, as it conditions the pantograph-catenary contact quality evaluation, is a current topic of active research. Most of the methodologies used today either require complex techniques or are based are based on manual iteration. The work here presented proposes the use of an optimization procedure in order to achieve a correct initialization of the statically loaded catenary system. Here a fitness function is formalized where the design variables retrieved from its minimization solution are able to be used as parameters to build an undeformed finite element mesh. Upon the static analysis of this mesh its deformed shape is to follow the objective sag shape of the contact wire set on the fitness function. Hence the catenary initialization is solved. Catenary structures might appear simple at a first glance. However, since the contact and messenger wires are elements subjected to very high tension loads in order to form the catenary stagger and have a reduced sag this type of systems exhibit a higher degree of complexity and have a nonlinear behaviour. Also, the dropper elements act as cables which have a traction state and a null compression state in order to support the contact wire height at a static state and react as smooth as possible to a pantograph passage. As the evaluation of the fitness function is based on the static analysis of a given catenary mesh, where all the above stated effects must be addressed, this procedure constitutes to use of an optimization technique to solve a nonlinear problem.

In this work, the proposed catenary initialization is to be applied for a determined catenary model in order to form a FEM catenary mesh that in its static deformed shape will have a sag as close as the one for which the model is projected after. Furthermore, on the intend to later on evaluate pantograph–catenary contact quality degradation on damaged or ill mounted catenary lines, the same methodology is applied in order to form a catenary deformed mesh with an imposed local sag defect.

14.2 Catenary initialization procedure

The methodology here proposed to initialize a finite element catenary model is based on the construction stages of a catenary system where a resemblance of the procedure can be found. When mounting a catenary system, after the posts and consoles are placed, the wires need to be laid in such a way that in the end, according to the project specification, they are fully tensioned and their geometric position, namely the contact wire sag, is correct. In general this is achieved by first laying the wires in partial or full tension. As the wires are laid on the structure provisional droppers and fixes are used to hold the contact wire and fix it on the steady arm extremities. Henceforth the system is left at full tension for a period of time where later on a geometry inspection vehicle passes through the catenary. As this vehicle goes ahead, sensors on the vehicle register the sag of the catenary and the dropper lengths at the contact-wire/dropper junction are adjusted in order to meet the contact wire sag project specifications. This last procedure may require more than one iteration until the contact wire achieves the proper deflection.

Based on the described construction procedure a catenary initialization methodology can be set by formalizing a minimization problem where the objective is to find the correct lengths of each dropper in order that, when statically deformed, the corresponding FEM mesh has the intended sag at each contact-wire/dropper node.

14.2.1 Minimization problem formulation

Based on the catenary dropper tuning procedure, described above, a minimization problem is formulated where an objective function is set to find the correct lengths of each dropper in order that de deviation between the statically deformed shape of the finite element mesh and a prescribed objective catenary sag at each contact-wire/dropper node is minimized. The formalization of the minimization problem can be expressed as [112,113]:

$$\begin{aligned} &\min(\mathrm{f}_i(\mathbf{x}), \mathrm{g}(\mathbf{x}))\ ,\ \ \mathrm{i} = 1..\mathrm{n} \\ &\text{subject to: } \mathbf{l} \le \mathbf{x} \le \mathbf{u} \end{aligned} \tag{14.1}$$

where:

$$
\begin{aligned}
f_i(\mathbf{x}) &= \left| s_i^p - s_i(\mathbf{x}) \right| \\
g(\mathbf{x}) &= \left| h_s^p - h_s(\mathbf{x}) \right| \\
\mathbf{x} &= \left[d_1, \mathrm{d}_2, ..., \mathrm{d}_n, h \right]^T \\
\mathbf{l} &= \left[l_1, l_2, ..., l_5, l_h \right]^T \\
\mathbf{u} &= \left[u_1, u_2, ..., u_5, u_h \right]^T
\end{aligned}
\tag{14.2}
$$

As represented on Figure 14.5, the function $f_i(\mathbf{x})$, corresponds to the deviation of the sag, $s_i(\mathbf{x})$, from the prescribed sag s_i^p, for each dropper junction *i*, in a catenary span composed of *n* droppers. An identical procedure is applied on function $g(\mathbf{x})$ to the catenary height, $h_s(\mathbf{x})$, registered at the contact wire/steady arm junction. The sag, $s_i(\mathbf{x})$, and catenary height of the deformed mesh, $h_s(\mathbf{x})$, are dependent of the design variables contained in **x** vector. The design variables here considered are the dropper lengths, $\mathrm{d_i}$, accounted from the fixed messenger-wire/dropper node to each contact-wire/dropper, plus the initial catenary height at the steady-arm/contact-wire node, *h*. Note that the evaluation of the fitness functions $f_i(\mathbf{x})$, $g(\mathbf{x})$ implies the construction of a catenary finite element mesh according to design variables and a respective static analysis. Furthermore, **l** and **u** correspond to the lower and upper bounds of **x** which relate to the maximum and minimum possible lengths of the droppers and steady arm height.

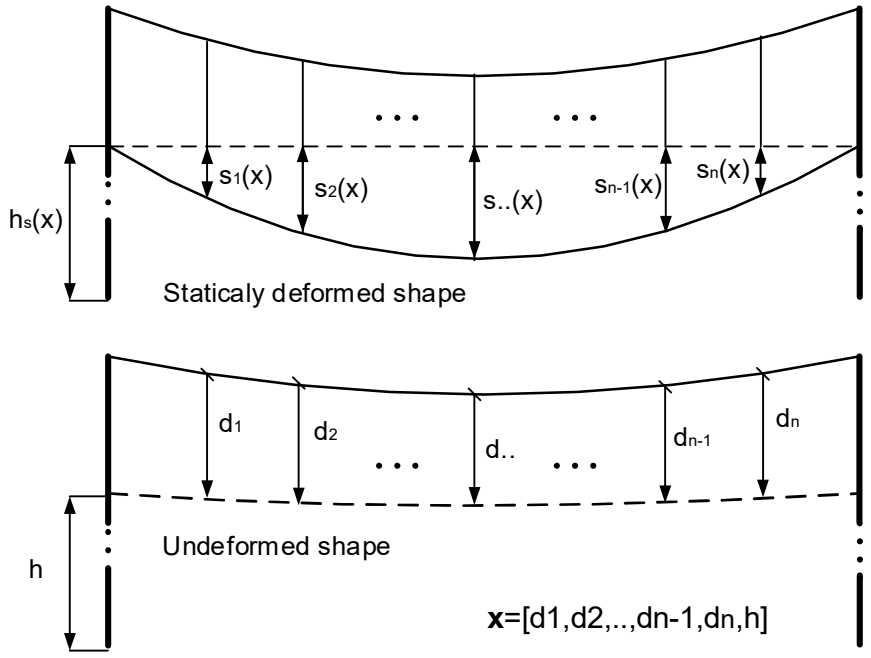

Figure 14.5: Representation of the design variables and fitness functions present on the minimization problem.

Until here the minimization problem set in (14.1) consists of a multi-objective optimization problem. However, since from a mechanical perspective all deviations considered are of equal importance the minimization problem can be reformulated as:

$$\begin{aligned} &\min\left(\sum_{i=1}^{n} \mathrm{f}_i(\mathbf{x}) + \mathrm{g}(\mathbf{x})\right) \\ &\text{subject to: } \mathbf{l} \le \mathbf{x} \le \mathbf{u} \end{aligned} \tag{14.3}$$

where by reducing the problem to a single minimization its degree of complexity is decreased as also the numerical computation effort to find a solution.

Furthermore, on a particular problem where the spans of a catenary system are all geometrically identical and present vertical axisymmetric along the middle of the span, another simple reformulation of the problem is possible. This time the design variables can be reduced to the height of the catenary at the steady arm, *h*, plus only the dropper lengths of one side of the span, as expressed by:

$$\begin{aligned} &\min\left(\sum_{i=1}^{m} \mathrm{f}_i(\mathbf{x}) + \mathrm{g}(\mathbf{x})\right) \\ &\text{subject to: } \mathbf{l} \le \mathbf{x} \le \mathbf{u} \\ &\text{where: } \mathbf{x} = [\mathrm{d}_1, \mathrm{d}_2, ..., \mathrm{d}_m] \\ &\qquad \mathrm{m} = ceil(\mathrm{n}/2) \end{aligned} \tag{14.4}$$

where when meshing the catenary model the design variables are mirrored to the other side of the span. In this case the number of fitness functions, $f_i(\mathbf{x})$, is also reduced to almost half and the computational efficiency is improved.

14.3 Finite element static analysis of a catenary model

The deformed shape of the catenary is characterized by small rotations and small deformations in which, so that the optimisation procedure here presented is properly used, the slacking of the droppers is the only nonlinear effect that must be considered. The axial tension on the contact, stitch and messenger wires is constant and cannot be neglected in the analysis. Therefore, the catenary system is modelled with linear finite elements in which the dropper nonlinear slacking is modelled with compensating forces while the stress stiffening of the wires, due to their tensioning, is accounted by considering an added stiffness as function of the applied tensioning forces [114].

Using the finite element method, the static equilibrium equations for the catenary structural system are assembled as [65,115],

$$\mathbf{K}\,\mathbf{d} = \mathbf{f} \tag{14.5}$$

where **K** is the finite element global stiffness matrix of the catenary while **d** and **f** are respectively the displacements vector and the force vector containing the sum of all external applied.

In order to accurately account for the stress stiffening of the catenary structure due to the tension stress state caused by the line tensioning with high axial tension forces the beam finite element used for the messenger, stitch and contact wire, designated as element *i*, is written as,

$$\mathbf{K}_i^e = \mathbf{K}_L^e + T\,\mathbf{K}_G^e \tag{14.6}$$

in which $\mathbf{K}^e_L$ is the linear Euler-Bernoulli beam element stiffness matrix, T is the axial tension and $\mathbf{K}^e_G$ is the element geometric stiffness matrix [5]. The droppers and the registration and steady arms are also modelled with the same beam element but disregarding the geometric stiffening. In order to ensure the correct representation of the deformed shape, 4 to 6 elements are used in between droppers to appropriately model the contact and messenger wires [12]. There is no special requirement on the number of elements required to model each dropper, registration or steady-arm. The global stiffness matrix, **K**, is then built by assemblage of the matrices of the elements according to the catenary model mesh. The force vector, **f,** containing the sum of all external applied loads is evaluated as:

$$\mathbf{f} = \mathbf{f}_{(g)} + \mathbf{f}_{(t)} + \mathbf{f}_{(d)} \tag{14.7}$$

which contains the gravity forces, $\mathbf{f}_{(g)}$, the line tensioning forces, $\mathbf{f}_{(t)}$, and the dropper slacking compensating terms, $\mathbf{f}_{(d)}$. The gravity forces in vector $\mathbf{f}_{(g)}$, are accounted with not only all elements masses but also with the mass of the gramps that attach the droppers to the wires being modelled here as lumped masses.

Although the droppers perform as a bar during extension their stiffness during compression is either null or about 1/100th of the extension stiffness, to represent a residual resistance to buckling. As the droppers stiffness is included in the stiffness matrix, **K**, as a bar element, anytime one of them is compressed such contribution for the catenary stiffness has to be removed or modified. Much close to how a dynamic analysis would be performed [78], in order to keep the analysis linear the strategy pursued here is to compensate the contribution to the stiffness matrix by adding a force to vector $\mathbf{f}_{(\mathrm{d})}$ equal to the bar compression force

$$\mathbf{f}_{(d)t+\Delta t} = \mathbf{K}^e_{dropper}\mathbf{B}\tilde{\mathbf{d}}_{t+\Delta t} \tag{14.8}$$

where the Boolean matrix **B** simply maps the global nodal coordinates into the coordinates of the dropper element. Note that, for the static analysis of a determined catenary mesh model, if the dropper compensation forces are not null, its calculation will require a corrective iteration procedure. In this case, considering a null compression stress state of the droppers at the first iteration, the static equilibrium equation is to be solved iteratively until a target convergence is reached. Such that for the ith iteration $\left|\mathbf{d}_i - \mathbf{d}_{i-1}\right| < \varepsilon_d$, being ε_d a user defined tolerance. Note that the criteria of convergence of the nodal displacements must imply convergence of the force vector also, this is, the balance of the equilibrium equation right-hand side contribution of the dropper slacking compensation force with the left-hand-side product of the dropper stiffness by the nodal displacements in equation (14.5).

14.4 Application of the catenary initialization procedure

In order to demonstrate the catenary initialization procedure here proposed two cases are presented. Both relate to the same chosen catenary model where in one a regular catenary initialization is evaluated for a prescribed objective sag and other for a prescribed sag with local defect on one of the spans.

14.4.1 Catenary model

The model here proposed for the initialization procedure is based on a realistic model built to serve as a reference model for pantograph-catenary simulation software, for validation and comparison purposes [8]. The software used to process the static analysis and initialization procedure is *PantoCat* [78] from IST, Portugal.

The proposed catenary model is similar to the French LN2 and the Italian C270 systems but with modified span length and contact wire tension parameters, its main geometry and material properties of its elements are presented in Table 14.1.

Relative to each span of the catenary model here considered, the prescribed sag s_i^p ate each dropper *i*/contact wire connection at the local span position x_i is presented on Table 14.2. On this table, the nominal length of the droppers, L_d, is also presented. Note that these lengths are only indicative and given in approximation.

A general FE model representation of the catenary model in its static deformed state is presented in Figure 14.6.

Benchmark catenary model					
Catenary height [m]		6.28	Contact wire height [m]		5.08
Number of spans		28	Number of droppers/span		9
N° spans at contact wire height		20	Inter-dropper distance [m]		6.75
Span length [m]		55	Stagger [m]		±0.2
	Contact Wire	Messenger Wire		Droppers	Steady Arms
Section [mm^2]	150	120		12	-
Mass [kg/m]	1.35	1.08		0.117	0.73
Young modulus [GPa]	100	0.97		-	-
Axial Stiffness EA [kN]	-	-		200	17
Bending Stiffness EI [N.m^2]	195.0	131.7		-	1100
Tension [kN]	22	16		-	-
Claw with:	dropper	dropper		-	-
Claw mass [kg]	0.195	0.165		-	-

Table 14.1: Geometric and element material properties of the benchmark cateanry model.

Dropper i	1	2	3	4	5	6	7	8	9
x_i [m]	4.5	10.25	16.0	21.75	27.5	33.25	39.0	44.75	50.5
Sag (s_i^p) [mm]	0	24	41	52	55	52	41	24	0
L_d [m]	1.017	0.896	0.810	0.758	0.741	0. 758	0.810	0.896	1.017

Table 14.2: Required sag at dropper positions on the span.

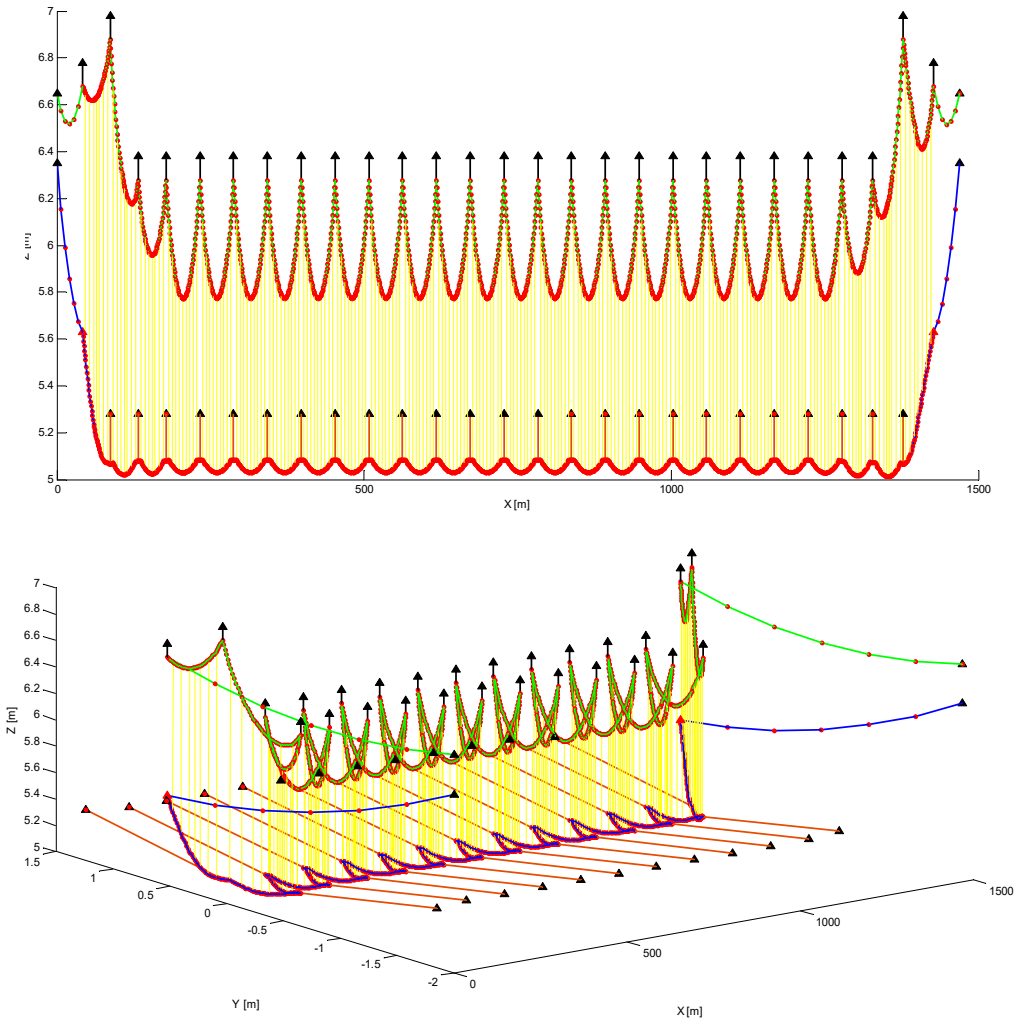

Figure 14.6: Finite element mesh model representation of the catenary model.

14.4.2 Regular catenary initialization

For the regular catenary initialization of the proposed catenary model the minimization problem equated in (14.4) is formulated where the symmetric feature of the span is used. The design variables are set to build the finite element mesh of all the catenary spans except the spans belonging to the overlap section at the ends. Also the evaluation of the fitness functions is defined for only the central span. To solve the minimization problem *fmincon* function from Matlab [116] is used with interior point algorithm. The initial design is set to the nominal dropper lengths presented in Table 14.2 and the upper and lower bounds set to plus and minus 0.6 m off the initial design. For the stopping criteria both termination, constraint violation and fitness function tolerances are set do 10^{-9} m.

The best solution found to the minimizing problem is presented on Table 14.3 where it is also possible to examine, for each design variable the deviation between the initial design and the found optimal solution.

Design variables	Initial solution (x_0)	Optimal solution (x^*)	$\lvert x^*-x_0\rvert$
d1 [m]	1.017000	1.021524	0.004524
d2 [m]	0.896000	0.903236	0.007236
d3 [m]	0.810000	0.817690	0.007690
d4 [m]	0.758000	0.768343	0.010343
d5 [m]	0.741000	0.750242	0.009242
h [m]	5.080000	5.080653	0.000653

Table 14.3 : Initial solution and optimal solution found for the current minimizing problem.

In order to analyse de solution found, the fitness function evaluations, $f_i(\boldsymbol{x})$ and $g(\boldsymbol{x})$, at the initial design and optimal solution are presented on Table 14.4. Note that, for a set of given design variables, $\boldsymbol{x}$, this functions relate to the deviation between the objective contact wire sag and the sag evaluated on the static analysis of a mesh generated from the design variables. By evaluating the fitness functions presented, between the initial and optimal designs it is possible to evaluate the effectiveness of the applied methodology. Considering the sum of all of these deviations, also presented in Table 14.4, it is possible to see that its value is in the order of hundredths of millimetre which is a very low deviation for the specified problem and implies a well obtained solution. From the discriminated fitness functions it is also possible to observe that the sag on the first dropper and the catenary height are the most problematic objectives to reach.

With the optimal design variables it is then possible to generate a catenary finite element mesh where its static deformation is very close to the objective sag. On Figure 14.7 is possible to observe the sag on a catenary span that resulted from the use of the optimal solution.

	Initial solution (x_0)	Optimal solution (x*)
f1(x) [m]	4.1543E-03	1.2925E-05
f2(x) [m]	5.0272E-03	1.3307E-07
f3(x) [m]	5.0643E-03	9.0724E-07
f4(x) [m]	6.0558E-03	1.8839E-07
f5(x) [m]	5.5779E-03	9.5609E-07
g(x) [m]	3.3994E-03	5.2702E-05
sum [m]	2.9279E-02	6.7812E-05
cpu time [s]	876 (for Intel i7 2600K)	

Table 14.4: Evaluation of the fitness functions at the initial design and optimal solution.

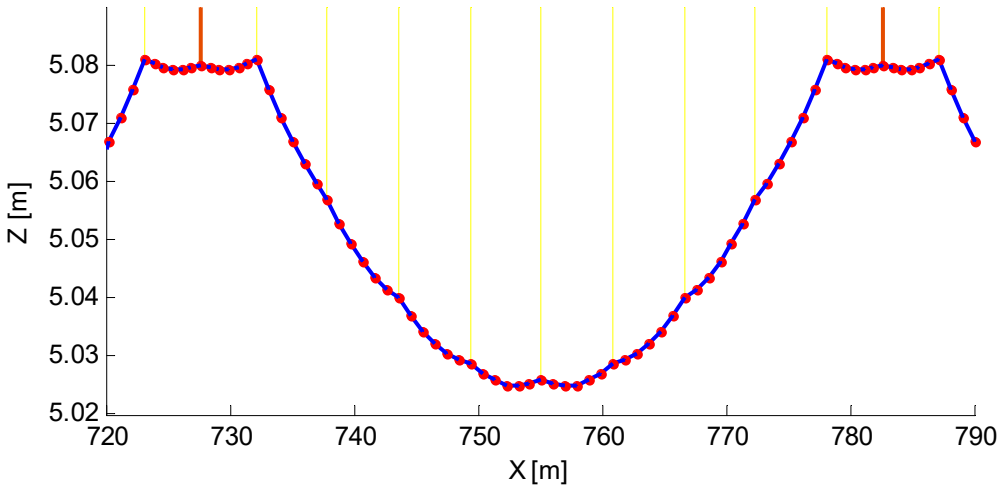

Figure 14.7: Finite element representation of the resulting sag from the mesh constructed from the optimal solution.

14.4.3 Catenary initialisation with local sag defect

In order to proceed with the initialization of a finite element catenary model with a localized sag defect on one of its spans a new objective sag is set as presented in Table 14.5. Note that, compared with Table 14.2 , the new objective sag has a local defect of 9 mm introduced on the third dropper. Contrary to the regular section initialization, here the axisymmetry of the span cannot be used where the minimization problem is set as formalized in equation (14.3). Also the design variables to build the mesh are only used on the span which contains the sag defect. As for the other spans the design variables found on the optimal solution for a regular catenary initialization are used. To solve the minimization problem the same function, *fmincon* from Matlab is used within the same conditions except for the initial design where the optimal solution for the regular catenary initialization is chosen instead.

Dropper *i*	1	2	3	4	5	6	7	8	9
x_i [m]	4.5	10.25	16.0	21.75	27.5	33.25	39.0	44.75	50.5
Sag (s_i^p) [mm]	0	24	50	52	55	52	41	24	0

Table 14.5: Required sag at dropper positions, with a local defect included.

The best solution found to the minimizing problem is presented on Table 14.6. It is possible to examine how much deviation is associated from the initial solution to the found optimal for each design variable. As expect the higher deviation observed relates to the design variable that is closely related to the local defect inserted on the sag.

Design variables	Initial Solution (x0)	Optimal Solution (x*)	|x*-x0|
d1 [m]	1.021524	1.021408	0.000116
d2 [m]	0.903236	0.902764	0.000473
d3 [m]	0.817690	0.839094	0.021404
d4 [m]	0.768343	0.767827	0.000516
d5 [m]	0.750242	0.749998	0.000244
d6 [m]	0.768343	0.768096	0.000247
d7 [m]	0.817690	0.817466	0.000225
d8 [m]	0.903236	0.903062	0.000174
d9 [m]	1.021524	1.021437	0.000087

Table 14.6: Initial solution and optimal solution for the initialisation of a finite element catenary model with local sag defect.

In order to analyse de solution found, the evaluation of the fitness function for the initial and optimal solution are presented on Table 14.7. It is also presented the sum of all its deviations. As described earlier it is possible to evaluate the effectiveness of the applied methodology by analysing the values of the fitness function. The sum of the deviations between the objective sag and the optimal found sag are in the order of hundredths of millimetres which is low deviation for problem here considered and a good solution is considered to be obtained. From the discriminated fitness functions evaluations it is also possible to observe that the sag on the first dropper is the most problematic objective to reach much as in the regular catenary initialization.

With the optimal design variables it is then possible to generate a catenary finite element mesh where its static deformation is very close to the objective sag with local defect. On Figure 14.8 is possible to observe the sag on the catenary span with the prescribed defect.

	Initial Solution (x0)	Optimal Solution (x*)
f1(x) [m]	1.2925E-05	3.9003E-05
f2(x) [m]	1.3307E-07	1.0154E-06
f3(x) [m]	8.9991E-03	1.5248E-07
f4(x) [m]	1.8839E-07	1.1503E-06
f5(x) [m]	9.5609E-07	2.6566E-06
f6(x) [m]	2.0486E-07	3.0443E-07
f7(x) [m]	9.4020E-07	5.7032E-07
f8(x) [m]	1.8250E-07	1.0374E-06
f9(x) [m]	1.2859E-05	1.9073E-06
sum (x)	9.0275E-03	4.7797E-05
cpu time [s]	1856 (for Intel i7 2600K)	

Table 14.7: Evaluation of the penalty functions that compose the formulated fitness function for the initial and found optimal solutions.

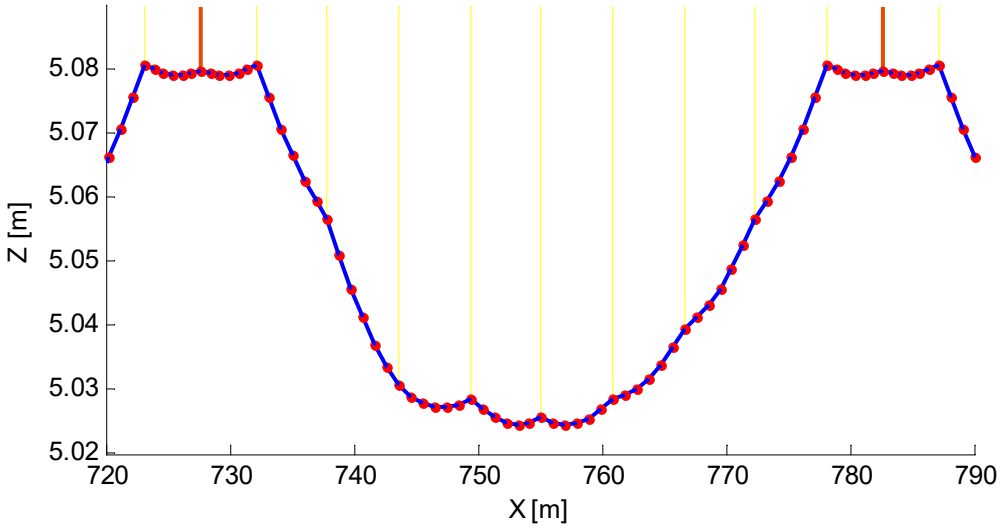

Figure 14.8: Finite element representation of the resulting sag with, local defect, from the mesh constructed from the optimal solution.

14.4 Conclusions

In this work, an implementation of a catenary initialization procedure is presented. This method is based on solving a minimization problem by means of a classical gradient based optimization. The results reveal that this methodology is effective and provides accurate finite element catenary models for further dynamic behaviour analysis studies. The proposed methodology also opens the possibility to model catenary systems that have defects such as irregularities on its sag caused by damaged, poorly maintained or ill mounted overhead lines. Here, this irregularity can be imposed on the static equilibrium configuration of the model and the same minimization problem is set to find its corresponded undeformed shape.

One disadvantage of this method is the time cost to execute this procedure. However, there is the possibility to reduce the size of the problem in question with further investigation and development of the procedure. Also, once obtained the optimised results for the catenary initialisation are be stored and can be used anytime with no need to solve the same minimization problem again unless some of the catenary characteristic are altered.

Although good solutions for the initial catenary positions have been obtained with the approach used here there is no guarantee that a good solution for the initial catenary configuration is always obtained for which a careful analyses of the results is critical as well as setting the bounds of the design variables. Furthermore, it is of importance to further investigate about the sensitivity of other design parameters and relate the fitness functions to other aspects of the catenary geometry besides de sag.

References

[1] OECD. Strategic Transport Infrastructure Needs to 2030. Paris, France: OECD Publishing; 2012.

[2] ERRAC - European Rail Research Advisory Council. Strategic Rail Research Agenda 2020. Brussels, Belgium, Belgium; 2007.

[3] EC - European Commission. Roadmap to a Single European Transport Area - Towards a Competitive and Resource Efficient Transport System. Brussels, Belgium, Belgium; 2011.

[4] Nikravesh PE. Computer-Aided Analysis of Mechanical Systems. Englewood Cliffs, New Jersey: Prentice-Hall; 1988.

[5] Przemieniecki JS. Theory of Matrix Structural Analysis. New York: McGraw-Hill; 1968.

[6] Iwnicki S. The Manchester Benchmarks for rail simulators - An introduction. Veh. Syst. Dyn. 1998;30:717–722.

[7] Pombo J, Ambrósio J, Pereira M, et al. Influence of Pantograph Characteristics on the Overhead Contact Quality for High Speed Trains. Veh. Syst. Dyn. 2009;47:1327–1347.

[8] Bruni S, Ambrosio J, Carnicero A, et al. The results of the pantograph–catenary interaction benchmark. Veh. Syst. Dyn. 2014;53:412–435.

[9] Escalona JL, Sugiyama H, Shabana A a. Modelling of structural flexiblity in multibody railroad vehicle systems. Veh. Syst. Dyn. 2013;51:1027–1058.

[10] Bruni S, Ambrosio J, Carnicero A, et al. The results of the pantograph-catenary interaction benchmark. Veh. Syst. Dyn. 2015;53:412–435.

[11] Ambrósio J, Pombo J, Pereira M, et al. A Computational Procedure for the Dynamic Analysis of the Catenary-Pantograph Interaction in High-Speed Trains. J. Theor. Appl. Mech. 2012;50:681–699.

[12] Ambrósio J, Pombo J, Pereira M, et al. Recent Developments in Pantograph-Catenary Interaction Modelling and Analysis. Int. J. Railw. Technol. 2012;1:249–278.

[13] Pombo J, Ambrósio J, Silva M. A New Wheel-Rail Contact Model for Railway Dynamics. Bruni Ed. S, editor. Veh. Syst. Dyn. 2007;45:165–189.

[14] Pombo J, Ambrósio J. Application of a Wheel-Rail Contact Model to Railway Dynamics in Small Radius Curved Tracks. Multibody Syst. Dyn. 2008;19:91–114.

[15] Collina A, Bruni S. Numerical Simulation of Pantograph-Overhead Equipment Interaction. Veh. Syst. Dyn. 2002;38:261–291.

[16] Shing AWC, Wong PPL. Wear of pantograph collector strips. J. Rail Mass Transit. 2008;222:169–176.

[17] Bucca G, Collina A. A Procedure for the Wear Prediction of Collector Strip and Contact Wire in Pantograph-Catenary System. Wear. 2009;266:46–59.

[18] Pombo J, Antunes P. A Comparative Study Between Two Pantographs In Multiple Pantograph High-Speed Operations. Internatinal J. Railw. Technol. 2013;2:83–108.

[19] Liu Z, Jönsson PA, Stichel S, et al. Implications of the operation of multiple pantographs on the soft catenary systems in Sweden. Proc. Inst. Mech. Eng. Part F J. Rail Rapid Transit. 2016;230:971–983.

[20] Bucca G, Carnevale M, Collina A, et al. Adoption of different pantographs preloads to improve multiple

collection and speed up existing lines. Veh. Syst. Dyn. 2012;50:403–418.
[21] Antunes P, Ambrósio J, Pombo J, et al. Dynamic Analysis of the Pantograph-Catenary Interaction on Overlap Sections for High-Speed Railway Operations. Proc. Second Int. Conf. Railw. Technol. Res. Dev. Maint. Stirlingshire, UK: Civil-Comp Press; 2014.
[22] Harèll P, Drugge L, Reijm M. Study of Critical Sections in Catenary Systems During Multiple Pantograph Operation. Proc. Inst. Mech. Eng. Part F J. Rail Rapid Transit. 2005;219:203–211.
[23] Mei G, Zhang W, Zhao H, et al. A hybrid method to simulate the interaction of pantograph and catenary on overlap span. Veh. Syst. Dyn. 2006;44:571–580.
[24] Ambrósio J, Pombo J, Pereira M, et al. Optimization of high-speed railway pantographs for improving pantograph-catenary contact. Theor. Appl. Mech. Lett. 2013;3.
[25] Gregori S, Tur M, Nadal E, et al. An approach to geometric optimisation of railway catenaries. Veh. Syst. Dyn. 2017;3114:1–25.
[26] Bruni S, Bucca G, Collina A, et al. Numerical and Hardware-In-the-Loop Tools for the Design of Very High Speed Pantograph-Catenary Systems. J. Comput. Nonlinear Dyn. 2012;7:041013.
[27] Van OV, Massat JP, Laurent C, et al. Introduction of variability into pantograph-catenary dynamic simulations. Veh. Syst. Dyn. 2014;52:1254–1269.
[28] Carnicero A, Jimenez-Octavio JR, Sanchez-Rebollo C, et al. Influence of Track Irregularities in the Catenary-Pantograph Dynamic Interaction. J. Comput. Nonlinear Dyn. 2012;7:041015.
[29] Kulkarni S, Pappalardo CM, Shabana AA. Pantograph/Catenary Contact Formulations. J. Vib. Acoust. 2016;139:011010.
[30] Song Y, Liu Z, Wang H, et al. Nonlinear analysis of wind-induced vibration of high-speed railway catenary and its influence on pantograph–catenary interaction. Veh. Syst. Dyn. 2016;54:723–747.
[31] Facchinetti A, Bruni S. Hardware-in-the-loop hybrid simulation of pantograph–catenary interaction. J. Sound Vib. 2012;331:2783–2797.
[32] Schirrer A, Aschauer G, Talic E, et al. Catenary emulation for hardware-in-the-loop pantograph testing with a model predictive energy-conserving control algorithm. Mechatronics. 2017;41:17–28.
[33] Ambrósio J, Antunes P, Pombo J. On the Requirements of Interpolating Polynomials for Path Motion Constraints. In: Kecskeméthy A, Geu Flores F, editors. Mech. Mach. Sci. Springer International Publishing; 2015. p. 179–197.
[34] Pombo J, Ambrósio J. General Spatial Curve Joint for Rail Guided Vehicles: Kinematics and Dynamics. Multibody Syst. Dyn. 2003;9:237–264.
[35] Ambrósio J, Pombo J, Rauter F, et al. A Memory Based Communication in the Co-Simulation of Multibody and Finite Element Codes for Pantograph-Catenary Interaction Simulation. In: Bottasso C.L. E, editor. Multibody Dyn. Dordrecht, The Netherlands: Springer; 2008. p. 211–231.
[36] Knothe K, Grassie SL. Modelling of Railway Track and Vehicle/Track Interaction at High Frequencies. Veh. Syst. Dyn. 1993.
[37] Magalhaes H, Ambrosio J, Pombo J. Railway vehicle modelling for the vehicle-track interaction compatibility analysis. Proc. Inst. Mech. Eng. Part K J. Multi-body Dyn. 2016;230:251–267.
[38] Mazzola L, Bruni S. Effect of suspension parameter uncertainty on the dynamic behaviour of railway vehicles. Appl. Mech. Mater. Trans Tech Publ; 2012. p. 177–185.
[39] Polach O, Evans J. Simulations of Running Dynamics for Vehicle Acceptance: Application and Validation. Int. J. Railw. Technol. 2013;2.
[40] Di Gialleonardo E, Braghin F, Bruni S. The influence of track modelling options on the simulation of rail vehicle dynamics. J. Sound Vib. 2012;331:4246–4258.
[41] Lundqvist A, Dahlberg T. Load impact on railway track due to unsupported sleepers. Proc. Inst. Mech. Eng. Part F J. Rail Rapid Transit. 2005;219:67–77.
[42] Recuero AM, Escalona JL, Shabana AA. Finite-element analysis of unsupported sleepers using three-dimensional wheel–rail contact formulation. Proc. Inst. Mech. Eng. Part K J. Multi-body Dyn. 2011;225:153–165.
[43] Johansson A, Pålsson B, Ekh M, et al. Simulation of wheel–rail contact and damage in switches and crossings. Wear. 2011;271:472–481.
[44] Martínez-Casas J, Di Gialleonardo E, Bruni S, et al. A comprehensive model of the railway wheelset–track interaction in curves. J. Sound Vib. 2014;333:4152–4169.
[45] Dietz S, Hippmann G, Schupp G. Interaction of Vehicles and Flexible Tracks by Co-Simulation of Multibody Vehicle Systems and Finite Element Track Models. Dyn. Veh. Roads Tracks. 2002;37:372–384.
[46] Zhai W, Wang K, Cai C. Fundamentals of vehicle–track coupled dynamics. Veh. Syst. Dyn. 2009;47:1349–1376.
[47] Esveld C. Modern Railway Track. Duisburg, Germany: MRT-Productions; 1989.
[48] Yamaguchi F. Curves and Surfaces in Computer Aided Geometric Design. Springer-Verlag; 1988.

[49] Mortenson ME. Geometric Modeling. New York, New York: Wiley; 1985.
[50] Iverson W. Analysis of the Reconstruction of Rail Geometry from Curvature Data. IEEE Trans. Ind. Appl. 1974. p. 368–379.
[51] Farin GE. Curves and Surfaces for Computer Aided Geometric Design: A Practical Guide. 2nd Editio. Comput. Sci. Sci. Comput. Boston, Massachussetts: Academic Press; 1990.
[52] De Boor C. A Practical Guide to Splines. Appl. Math. Sci. ; 27. New York, New York: Springer-Verlag; 1978.
[53] Irvine LD, Marin SP, Smith PW. Constrained interpolation and smoothing. Constr. Approx. 1986;2:129–151.
[54] Pina HLG. Métodos Numéricos (Numerical Methods). Lisbon, Portugal: McGraw-Hill; 1995.
[55] Tandl M. Dynamic Simulation and Design of Roller Coaster Motion. [Duisburg, Germany]: Universitat Duisburg-Essen; 2008.
[56] Friedrich K, Puschmann R, Schmieder A, et al. Contact Lines for Electric Railways: Planning, Design, Implementation, Maintenance. 3rd ed. Publicis; 2018.
[57] Dahlberg T. Moving force on an axially loaded beam - with applications to a railway overhead contact wire. Veh. Syst. Dyn. 2006;44:631–644.
[58] TSI ENE. Technical specifications for interoperability relating to the 'energy' subsystem of the rail system in the Union. Official Journal of the European Union. 1301/2014/EU; 2014.
[59] ERA - European Rail Agency. Study on Interface EURO/1950 pantographs and OCL design - ERA/2013/INTEROP/OP/01. European Union; 2013.
[60] UIC 606-1 OR standart. Consequences of the application of the kinematic gauges defined by UIC leaflets in the 500 series on the design of the contact lines. UIC; 1987.
[61] Poetsch G, Evans J, Maisinger R, et al. Pantograph/Catenary Interaction and Control. Veh. Syst. Dyn. 1997;28:159–195.
[62] Ambrósio J, Pombo J, Facchinetti A, et al. Key Parameters for Pantograph/Catenary Numerical Models - PantoTRAIN Technical Report D1.1. Brussels, Belgium: UNIFE; 2010.
[63] Arora JS. Introduction to Optimum Design. 3ed. Boston: Academic Press; 2012.
[64] Pombo J, Ambrósio J. An Alternative Method to Include Track Irregularities in Railway Vehicle Dynamic Analyses. Nonlinear Dyn. 2012;68:161–176.
[65] Bathe K-J. Finite element procedures in engineering analysis. Prentice-Hall Civ. Eng. Eng. Mech. Ser. Englewood Cliffs, N.J.: Prentice-Hall; 1982.
[66] Newmark N. A Method of Computation for Structural Dynamics. ASCE J. Eng. Mech. Div. 1959;85:67–94.
[67] Pombo J, Almeida T, Magalhães H, et al. Finite Element Methodology for Flexible Track Models in Railway Dynamics Applications. Int. J. Veh. Struct. Syst. 2013;5:43.
[68] Pombo J, Ambrósio J. Dynamic Analysis of the Railway Vehicle ML95. Lisbon, Portugal: IDMEC - Institute of Mechanical Engineering, Instituto Superior Técnico; 2004.
[69] Vieira R. High Speed Train Pantograph Models Identification (MSc Thesis). Instituto Superior Técnico; 2016.
[70] Ambrósio J, Pombo J, Rauter F, et al. Multiple Pantograph Interaction with Catenaries in High-Speed Trains. Proc. 8th World Congr. Railw. Res. Seoul, Korea; 2008.
[71] Carnevale M. Innovative Solutions for Improving Pantograph Dynamics and Current Collection. [Milan, Italy]: Politecnico di Milano; 2011.
[72] Flores P. Kinematics and dynamics of multibody systems with imperfect joints : models and case studies. Lect. notes Appl. Comput. Mech. Berlin: Springer; 2008.
[73] Ambrósio J, Verissimo P. Improved Bushing Models for Vehicle Dynamics", Multibody System Dynamics. Multibody Syst. Dyn. 2009;22:341–365.
[74] Ambrósio J, Rauter F, Pombo J, et al. A Flexible Multibody Pantograph Model for the Analysis of the Catenary-Pantograph Contact. In: Arczewski et al. (Ed.), editor. Multibody Dyn. Comput. Methods Appl. Dordrecht, The Netherlands: Springer; 2010. p. 1–27.
[75] Zhou N, Zhang W. Investigation of the Influence of the Pan-Head Elasticity on Pantograph-Catenary Dynamic Performance. Proc. 21st Symp. Dyn. Veh. Roads Tracks. Stockholm, Sweden; 2009.
[76] Vyasarayani CP, Uchida T, Carvalho A, et al. Parameter identification in dynamic systems using the homotopy optimization approach. Multibody Syst. Dyn. 2011;26:411–424.
[77] Ambrósio J, Pombo J, Massat J-P, et al. Pantograph Design Optimisation Methodology. Brussels, Belgium: UNIFE; 2012.
[78] Ambrósio J, Pombo J, Antunes P, et al. PantoCat statement of method. Veh. Syst. Dyn. 2015;53:314–328.
[79] Ambrósio J, Neto A. Stabilization Methods for the Integration of DAE in the Presence of Redundant Constraints. Multibody Syst. Dyn. 2003;10:81–105.
[80] Gear CW. Simultaneous Numerical Solution of Differential-Algebraic Equations. IEEE Trans. Circuit

Theory. 1971;18:89–95.
[81] Seo J-H, Sugiyama H, Shabana A a. Three-Dimensional Large Deformation Analysis of the Multibody Pantograph/Catenary Systems. Nonlinear Dyn. 2005;42:199–215.
[82] Seo J-H, Kim S-W, Jung I-H, et al. Dynamic Analysis of a Pantograph-Catenary System Using Absolute Nodal Coordinates. Veh. Syst. Dyn. 2006;44:615–630.
[83] Pereira C, Ramalho A, Ambrósio J. A Critical Overview of Internal and External Cylinder Contact Force Models. Nonlinear Dyn. 2011;63:681–697.
[84] Toridis TG, Khozeimeh K. Computer analysis of rigid frames. Comput. Struct. 1971;1:193–221.
[85] Lankarani HM, Nikravesh PE. A Contact Force Model with Hysteresis Damping for Impact Analysis of Multibody Systems. AMSE J. Mech. Des. 1990;112:369–376.
[86] Polach O. A Fast Wheel-Rail Forces Calculation Computer Code. Veh. Syst. Dyn. 1999;33:728–739.
[87] Wen Z, Wu L, Li W, et al. Three-dimensional elastic–plastic stress analysis of wheel–rail rolling contact. Wear. 2011;271:426–436.
[88] Felippa CA, Park KCC, Farhat C. Partitioned analysis of coupled mechanical systems. Comput. Methods Appl. Mech. Eng. 2001;190:3247–3270.
[89] Hulbert G, Ma Z-D, Wang J, et al. Gluing for Dynamic Simulation of Distributed Mechanical Systems. In: Ambrósio (Ed.) J, editor. Adv. Comput. Multibody Syst. Dordrecht, The Netherlands: Springer; 2005. p. 69–94.
[90] Kubler R, Schiehlen W. Modular Simulation in Multibody System Dynamics. Multibody Syst. Dyn. 2000;4:107–127.
[91] Heckmann A, Arnold M, Vaculín O. A modal multifield approach for an extended flexible body description in multibody dynamics. Multibody Syst. Dyn. 2005;13:299–322.
[92] Liu F, Cai J, Zhu Y, et al. Calculation of Wing Flutter by a Coupled Fluid-Structure Method. J. Aircr. 2001;38:334–342.
[93] Bathe KJ, Zhang H. Finite element developments for general fluid flows with structural interactions. Int. J. Numer. Methods Eng. 2004;60:213–232.
[94] Naya M, Cuadrado J, Dopico D, et al. An Efficient Unified Method for the Combined Simulation of Multibody and Hydraulic Dynamics: Comparison with Simplified and Co-Integration Approaches. Arch. Mech. Eng. 2011;LVIII:223–243.
[95] Busch M, Schweizer B. Coupled simulation of multibody and finite element systems: an efficient and robust semi-implicit coupling approach. Arch. Appl. Mech. 2012;82:723–741.
[96] Carstens V, Kemme R, Schmitt S. Coupled simulation of flow-structure interaction in turbomachinery. Aerosp. Sci. Technol. 2003;7:298–306.
[97] Spreng F, Eberhard P, Fleissner F. An approach for the coupled simulation of machining processes using multibody system and smoothed particle hydrodynamics algorithms. Theor. Appl. Mech. Lett. 2013;3:013005.
[98] Anderson KS, Duan S. A hybrid parallelizable low-order algorithm for dynamics of multi-rigid-body systems: Part I, chain systems. Math. Comput. Model. 1999;30:193–215.
[99] Wang J, Ma Z, Hulbert GM. A Gluing Algorithm for Distributed Simulation of Multibody Systems. Nonlinear Dyn. 2003;34:159–188.
[100] Verhoef M, Visser P, Hooman J, et al. Co-simulation of Distributed Embedded Real-Time Control Systems. In: Davies J, Gibbons J, editors. Integr. Form. Methods 6th Int. Conf. IFM 2007, Oxford, UK, July 2-5, 2007. Proc. Berlin, Heidelberg: Springer Berlin Heidelberg; 2007. p. 639–658.
[101] Spiryagin M, Simson S, Cole C, et al. Co-simulation of a mechatronic system using Gensys and Simulink. Veh. Syst. Dyn. 2012;50:495–507.
[102] Gu B, Asada HH. Co-Simulation of Algebraically Coupled Dynamic Subsystems Without Disclosure of Proprietary Subsystem Models. J. Dyn. Syst. Meas. Control. 2004;126:1.
[103] Schweizer B, Li P, Lu D, et al. Stabilized implicit co-simulation methods: solver coupling based on constitutive laws. Arch. Appl. Mech. 2015.
[104] Schweizer B, Li P, Lu D. Explicit and Implicit Cosimulation Methods: Stability and Convergence Analysis for Different Solver Coupling Approaches. J. Comput. Nonlinear Dyn. 2015;10:051007.
[105] Quinn MJ. Parallel Programming in C with MPI and OpenMP. McGraw-Hill Higher Education; 2004.
[106] Wilkinson B, Allen CM. Parallel Programming: Techniques and Applications Using Networked Workstations and Parallel Computers. Pearson/Prentice Hall; 2005.
[107] Downey AB. The Little Book of Semaphores. Science (80-.). 2009;211:1–291.
[108] Facchinetti A, Bruni S. Special issue on the pantograph–catenary interaction benchmark. Veh. Syst. Dyn. 2015;53:303–304.
[109] Costa J, Antunes P, Magalhães H, et al. Development of Flexible Track Models for Railway Vehicle Dynamics Applications. In: Pombo J, editor. Proc. Third Int. Conf. Railw. Technol. Res. Dev. Maint. Stirlingshire, UK: Civil-Comp Press; 2016.

[110] Collina A, Melzi S, Facchinetti A. On the Prediction of Wear of Contact Wire in OHE Lines: a Proposed Model. Veh. Syst. Dyn. 2002;37:579–592.
[111] European Commission EC. White Paper: Roadmap to a Single European Transport Area - Towards a Competitive and Resource Efficient Transport System. Brussels, Belgium; 2011.
[112] Arora JS. Introduction to Design Optimization. Introd. to Optim. Des. Elsevier; 2012.
[113] Bazaraa MS, Sherali HD, Shetty CM. Nonlinear Programming: Theory and Algorithms. 3rd ed. Wiley-Interscience; 2006.
[114] Ambrósio J, Antunes P, Pombo J, et al. A Computational Procedure for the Dynamic Analysis of the Catenary-Pantograph Interaction in High-Speed Trains. J. Theor. Appl. Mech. 2012;50:681–699.
[115] Reddy JN. An Introduction to the Finite Element Method. 3rd Editio. McGraw-Hill; 2005.
[116] MathWorks. MATLAB R2015a Documentation. The MathWorks, Inc.; 2015.

15 On the Requirements of Interpolating Polynomials for Path Motion Constraints

[5] In the framework of multibody dynamics, the path motion constraint enforces that a body follows a predefined curve being its rotations with respect to the curve moving frame also prescribed. The kinematic constraint formulation requires the evaluation of the fourth derivative of the curve with respect to its arc length. Regardless of the fact that higher order polynomials lead to unwanted curve oscillations, at least a fifth order polynomials is required to formulate this constraint. From the point of view of geometric control lower order polynomials are preferred. This work shows that for multibody dynamic formulations with dependent coordinates the use of cubic polynomials is possible, being the dynamic response similar to that obtained with higher order polynomials. The stabilization of the equations of motion, always required to control the constraint violations during long analysis periods due to the inherent numerical errors of the integration process, is enough to correct the error introduced by using a lower order polynomial interpolation and thus forfeiting the analytical requirement for higher order polynomials.

15.1 Introduction

The definition of railway, tramway or roller coaster tracks requires the accurate description of their geometries, which is usually done with the parameterization of the track centreline. The

[5] The work presented in this chapter has been published, as it is, in: J. Ambrósio, P. Antunes, J. Pombo, *On the Requirements of Interpolating Polynomials for Path Motion Constraints*, Interdisciplinary Applications of Kinematics, Mechanisms and Machine Science, 26, 179-197, Springer, (2015).

definition of a reference plane where the rails sit is required and consequently a curve moving frame must also be specified.

Regardless of the definition of a general curve geometry being to specify a railway centreline, a rollercoaster spatial geometry or a prescribed motion kinematic constraint not only a suitable interpolation scheme must be selected but also a robust definition of the curve moving frame needs to be used. Depending on if the curve is used to set some geometric layout for the mechanical models or to define kinematic constraints for multibody dynamics applications, a minimum order derivative, with respect to the curve parameter, may be required. Therefore, using polynomial interpolation schemes, higher order polynomials may be required for an exact formulation of problem. Generally, higher order interpolating polynomials lead to unwanted, and hardly controllable, oscillations of the curve geometry, i.e., small deviations of the positions of the nodal points lead to large variations of the curve geometry away from those nodes. But although lower order polynomials generally have a local geometric control, they may not have the order necessary to ensure the proper geometric continuity of the model or the parametric derivatives required in the formulation of a kinematic constraint. Therefore, the question that arises, for which some light is shed here, is: what are the minimal requirements that an interpolating polynomial must meet in to be used in the definition of a path motion kinematic constraint?

The geometric description of the curve must allow the definition of a moving frame in which the tangent, normal and binormal vectors define an orthogonal frame. Both Frenet and Dabroux frames are candidates to play the role of the required moving frame [1,2]. As discussed by Tandl and Kecskemethy, both have singularities in general spatial curve geometries, as those required for rollercoaster analysis [3,4]. In this work the Frenet frame is used being the straight segments handled with the provision described by Pombo and Ambrosio [5].

Using the selected moving frame definition a proper formulation for a prescribed motion kinematic constrained is obtained. Such kinematic constraint imposes that a point of a rigid body follows a given curve and that the body itself does not rotate, or does it in a prescribed manner, with respect to the curve moving frame. Depending on the choice of coordinates used on the multibody formulation this kinematic constraint may be defined differently [6,7]. When Cartesian coordinates are used and the equations of motion are solved together with the second time derivative of the position kinematic constraints the definition of the Frenet frame requires the second derivative of the curve with respect to its arc length parameter while the acceleration constraints, i.e., the second time derivative of the kinematic constraint, requires the existence

of a fourth derivative. In this sense, apparently fifth order polynomials are required to formulate properly the prescribed motion kinematic constraint.

The numerical integration of the equations of motion of a multibody systems implies the use of numerical integrators, such as Runga-Kutta, Gear or others, to undertake the forward dynamic analysis [8,9]. All numerical procedures used in the solution of the equations of motion and on their solution have a finite precision and ultimately lead to small errors that affect the precision of the solution. When dependent coordinates, such as Cartesian or Natural coordinates, are used only the acceleration constraints are explicitly used in the solution of the equations of motion being the position and velocity constraints fulfilled only if the numerical integration would be error free, being otherwise violated and leading to instabilities in the dynamic solution of the analysis [6]. By using stabilization procedures, such as the Baumgarte constraint stabilization method [10] or the Augmented Lagrangian Formulation [11] such constraint violations can be kept under control. By using a coordinate partition scheme the constraint violations can be eliminated [12].

This work shows that the same procedures used to stabilize the constraint violations in the integration of the equations of motion of multibody systems formulated with dependent coordinates also allow for the use of interpolation schemes with polynomials that have an order lower than that required for the exact formulation of the prescribed motion kinematic constraints. It is shown that regardless of using interpolation schemes with higher order polynomials the constraint violations still grow to a point in which either stabilization or coordinate partition procedures are required. Furthermore, it is shown here that when constraint stabilizations methods are used there is no observable difference in the constraint violations between interpolating polynomials of higher and lower order, provided that they satisfy the continuity required for the definition of the curve moving frames and for the geometric requirements of the model.

15.2 Curve Parameterization

The interpolation of complex curve geometries is generally realized by piecewise polynomial schemes that consist of polynomial pieces of the same degree with a prescribed overall smoothness. The input data includes the coordinates of interpolation points and parameters values to control rotations about the tangent vector [13]. The advantage of these interpolating procedures is that they exhibit local geometrical control, i.e., the variation of the position of a

control point only affects the neighbourhood of that point, maintaining unchanged the rest of the curve.

15.2.1 Curve Parameterization

Let the curve be described using a n^{th} order spline segments that interpolate a set of control points defined as [14]

$$\mathbf{g}(u) = \begin{Bmatrix} x(u) \\ y(u) \\ z(u) \end{Bmatrix} = \mathbf{a}_0 + \mathbf{a}_1\, u + \mathbf{a}_2\, u^2 + \mathbf{a}_3\, u^3 + \cdots + \mathbf{a}_n\, u^n \tag{15.1}$$

where $\mathbf{g}(u)$ is a point on the curve, u is the local parametric variable and $\mathbf{a}_i$ are the unknown algebraic coefficients that must be calculated using the boundary conditions, i.e., segment end points and tangent vectors [14]. Although Eq.(15.1) is generic for any polynomial interpolation, in this work only cubic, cubic shape-preserving and quintic polynomials are considered.

15.2.2 Curve Moving Frame

The osculating plane, at a given point P on a curve, is the plane of closest contact to the curve in the neighbourhood of P, as depicted in Figure 15.1. Although there are different available frames definitions for the purpose [4], the Frenet frame, which provides an appropriate curve referential at every point, is used here. Note that in railway or roller coaster dynamics the track model is developed with reference to the planes defined by the curve moving frame, being the osculating plane the one in which the rails are defined.

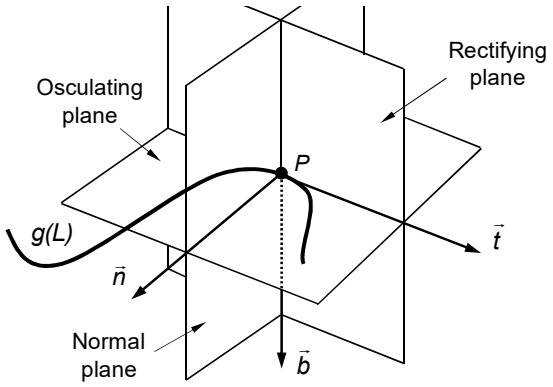

Figure 15.1 Principal unit vectors associated to the moving frame of a curve

The unit vectors that characterize the Frenet frame are the unit tangent vector **t**, the principal unit normal vector **n** and the binormal vector **b**. These vectors, defined in the

intersection of the normal, rectifying and osculating planes shown in Figure 15.1, are written as [5]

$$\mathbf{t} = \frac{\mathbf{g}^u}{\left\| \mathbf{g}^u \right\|} \quad ; \quad \mathbf{n} = \frac{\mathbf{k}}{\left\| \mathbf{k} \right\|} \quad ; \quad \mathbf{b} = \tilde{\mathbf{t}}\,\mathbf{n} \tag{15.2}$$

where $\tilde{\mathbf{t}}\,\mathbf{n}$ means a cross product and the auxiliary vector $\mathbf{k}$ given by

$$\mathbf{k} = \mathbf{g}^{uu} - \frac{\mathbf{g}^{uuT}\mathbf{g}^u}{\left\| \mathbf{g}^u \right\|^2}\mathbf{g}^u \tag{15.3}$$

where $\mathbf{g}^u$ and $\mathbf{g}^{uu}$ denote, respectively, the first and second derivatives of the parametric curve $\mathbf{g}(u)$ with respect to the parametric variable u. Note that when piecewise polynomial interpolation is used, a transformation from the curve parameter u to and curve arc-length parameter is required. This issue is discussed with the presentation of the formulation of the prescribed motion constraint.

15.3 Overview of the Multibody Dynamics Formulation

Let a rigid body i to which a body-fixed reference frame $(\xi,\eta,\zeta)_i$ is rigidly attached be represented in Figure 15.2. With Cartesian coordinates, the position and orientation of the rigid body are defined by the translation coordinates $\mathbf{r}_i = \{x, y, z\}_i^T$ and Euler parameters $\mathbf{p}_i = \{e_0, e_1, e_2, e_3\}_i^T$, respectively [6]. The vector of coordinates associated to the rigid body i is

$$\mathbf{q}_i = \left\{ \mathbf{r}^T, \mathbf{p}^T \right\}_i^T \tag{15.4}$$

A multibody system with nb bodies is described by

$$\mathbf{q} = \left\{ \mathbf{q}_1^T, \mathbf{q}_2^T, \cdots, \mathbf{q}_{nb}^T \right\}^T \tag{15.5}$$

where $\mathbf{q}$ is the vector of generalized coordinates.

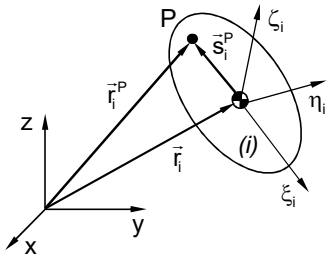

Figure 15.2 Rigid body with its body-fixed reference frame

In a multibody system, the mechanical joints are used to connect the bodies in order to restrain their relative motions. These kinematic constraints are expressed as algebraic constraint equations that introduce dependencies between the coordinates being denoted by [6]

$$\mathbf{\Phi}\left(\mathbf{q}, t\right) = \mathbf{0} \tag{15.6}$$

where t is the time. The second time derivative of Eq (15.6) yields the acceleration kinematic constraints, or acceleration equations, denoted as

$$\ddot{\mathbf{\Phi}}\left(\mathbf{q}, \dot{\mathbf{q}}, \ddot{\mathbf{q}}, t\right) = \mathbf{0} \quad \equiv \quad \mathbf{\Phi}_{\mathbf{q}}\, \ddot{\mathbf{q}} = \boldsymbol{\gamma} \tag{15.7}$$

where $\mathbf{\Phi}_{\mathbf{q}}$ is the Jacobian matrix of the constraints, $\ddot{\mathbf{q}}$ is the acceleration vector and $\boldsymbol{\gamma}$ is the vector that contains all terms in the equations that are not dependent on the accelerations.

Using this formulation, the equations of motion for a constrained mechanical system can be obtained using the Lagrange multipliers technique as [6]:

$$\mathbf{M}\ddot{\mathbf{q}} + \mathbf{\Phi}_{\mathbf{q}}^{T}\boldsymbol{\lambda} = \mathbf{f} \tag{15.8}$$

where $\mathbf{M}$ is the global mass matrix, containing the mass and moments of inertia of all bodies, $\boldsymbol{\lambda}$ is the vector of the unknown Lagrange multipliers and $\mathbf{f}$ is the force vector containing all forces and moments applied on system bodies and the gyroscopic forces. Eq (15.8) represents a system of n second order ordinary differential equations with $n+m$ unknowns, corresponding to the accelerations $\ddot{\mathbf{q}}$ and of the Lagrange multipliers $\boldsymbol{\lambda}$. In order to obtain a solution for this equation the m acceleration equations (15.7) are appended to the equations of motion (15.8). The resulting equations for a constrained multibody system are rearranged in the matrix form as

$$\begin{bmatrix} \mathbf{M} & \mathbf{\Phi}_{\mathbf{q}}^{T} \\ \mathbf{\Phi}_{\mathbf{q}} & \mathbf{0} \end{bmatrix} \begin{Bmatrix} \ddot{\mathbf{q}} \\ \boldsymbol{\lambda} \end{Bmatrix} = \begin{Bmatrix} \mathbf{f} \\ \boldsymbol{\gamma} \end{Bmatrix} \tag{15.9}$$

The dynamic analysis of multibody systems involves the calculation of the vectors $\mathbf{f}$ and $\boldsymbol{\gamma}$, for each time step according to the scheme depicted by Figure 15.3. Eq (15.9) is used to calculate the system accelerations $\ddot{\mathbf{q}}$ and the Lagrange multipliers $\boldsymbol{\lambda}$. The accelerations together with the velocities $\dot{\mathbf{q}}$ are integrated in order to obtain the new velocities $\dot{\mathbf{q}}$ and positions $\mathbf{q}$ for the next time step. This process proceeds until the final time of the analysis is reached. The Gear integration method [9] is used for the numerical integration of the velocities and accelerations.

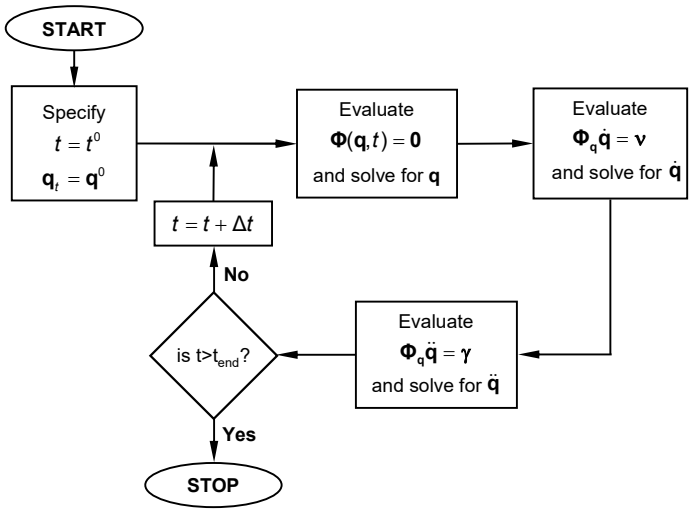

Figure 15.3 Flowchart of the computational implementation of a dynamic analysis.

During long time integrations the numerical errors associated to the numerical integration tend to propagate. As neither the position constraint equations (15.6) neither their time derivative, the velocity equations, are explicitly used, small constraint violations tend to increase. To keep the process stable, the Baumgarte Stabilization Method [10] or the Augmented Lagrangean Formulation [11] are used, eventually complemented by a coordinate partition method [12]. The Baumgarte stabilization method corresponds to the addition of a feedback term to the acceleration equations (15.7) penalizing position and velocity constraint violations as

$$\mathbf{\Phi}_\mathbf{q}\ \ddot{\mathbf{q}} = \boldsymbol{\gamma} - 2\alpha\dot{\mathbf{\Phi}} - \beta^2\mathbf{\Phi} \tag{15.10}$$

The detailed description of the multibody formulation and numerical methods used here is outside the scope of this work. The interested readers are referred to references [6, 7, 12] for further details on the numerical procedures used.

15.4 Prescribed Motion Kinematic Constraint

The implementation of the prescribed motion constraint in a computer code requires that the piecewise polynomial parameter u is replaced by a curve arc-length parameter L. Consider the parametric variable u^P, corresponding to a point P, located on the k^{th} polynomial segment to which a curve length L_k^P measured from the k^{th} segment origin is associated. The parameter u^P is obtained by [5]:

$$\int_0^{u^P} \sqrt{\mathbf{g}_k^{u^T}\,\mathbf{g}_k^u}\ du\ -\ L_k^P\ =\ 0 \tag{15.11}$$

where $\mathbf{g}^u$ is the derivative of $\mathbf{g}$ with respect to u. In terms of its computer implementation, the non-linear equation (15.11) is solved in the program pre-processor using the Newton–Raphson

method [6]. In what follows the references to the derivatives of the interpolating polynomials with respect to the local parameter *u* are now referred with respect to the length parameter L_k^P written in short as *L*.

Consider a point *P*, located on a rigid body *i*, that is constrained to follow a specified path, as seen in Figure 15.4. The path is defined by a parametric curve *g(L)*, which is controlled by a global parameter *L* that represents the length travelled by the point along the curve from the origin to the current location of point *P*. The constraint equations that enforce point *P* to follow the reference path *g(L)* are written as [5]:

$$\mathbf{\Phi}^{(\mathrm{pmc},3)} = \mathbf{0} \quad \equiv \quad \mathbf{r}_{\mathrm{i}}^{\mathrm{P}} - \mathbf{g}(\mathrm{L}) = \mathbf{0} \tag{15.12}$$

where $\mathbf{r}_{\mathrm{i}}^{\mathrm{P}}$ is the position vector associated to point *P*, depicted in Figure 15.4.

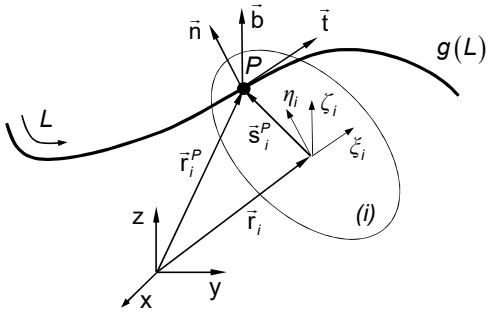

Figure 15.4 Prescribed motion constraint.

The prescribed motion constraint also ensures that the spatial orientation of body *i* remains unchanged with respect to the moving Frenet frame (**t**,**n**,**b**) associated to the curve. Consider a rigid body *i* where $(\mathbf{u}_\xi, \mathbf{u}_\eta, \mathbf{u}_\zeta)_i$ represent the unit vectors associated to the axes of $(\xi,\eta,\zeta)_i$ defined in the body frame. Consider also that the Frenet frame of the general parametric curve $\mathbf{g}(L)$ is defined by the principal unit vectors $(\mathbf{t}, \mathbf{n}, \mathbf{b})_L$, as depicted in Figure 15.4. The relative orientation between the body vectors $(\mathbf{u}_\xi,\mathbf{u}_\eta,\mathbf{u}_\zeta)_i$ and the curve local frame $(\mathbf{t}, \mathbf{n}, \mathbf{b})_L$ must be such that [5]:

$$\mathbf{\Phi}^{(\mathrm{lfac},3)} = \begin{Bmatrix} \mathbf{n}^{\mathrm{T}}\mathbf{A}_{\mathrm{i}}\mathbf{u}_\xi \\ \mathbf{b}^{\mathrm{T}}\mathbf{A}_{\mathrm{i}}\mathbf{u}_\xi \\ \mathbf{n}^{\mathrm{T}}\mathbf{A}_{\mathrm{i}}\mathbf{u}_\eta \end{Bmatrix} - \begin{Bmatrix} a \\ b \\ c \end{Bmatrix} = 0 \tag{15.13}$$

where $\{\mathrm{a} \quad \mathrm{b} \quad \mathrm{c}\}^{\mathrm{T}} = \mathrm{diag}\left[\mathbf{A}_{\mathrm{L}}^{0\,\mathrm{T}} \; \mathbf{A}_{\mathrm{i}}^{0}\right]$ are constants calculated at the initial time of the analysis by using Eq (15.13) with the initial conditions.

The contribution of the prescribed motion constraint to the constraint acceleration equations (15.7) is written as

$$\begin{bmatrix} \boldsymbol{\Phi}_{\mathbf{q}}^{(\mathrm{pmc},3)} \\ \boldsymbol{\Phi}_{\mathbf{q}}^{(\mathrm{lfac},3)} \end{bmatrix} \ddot{\mathbf{q}} = \begin{bmatrix} \boldsymbol{\gamma}^{(\mathrm{pmc},3)\#} \\ \boldsymbol{\gamma}^{(\mathrm{lfac},3)\#} \end{bmatrix} \tag{15.14}$$

where the Jacobian matrix associated to each part of the kinematic constraint is

$$\boldsymbol{\Phi}_{\mathbf{q}}^{(\mathrm{pmc},3)} = \begin{bmatrix} \mathbf{I} & -\tilde{\mathbf{s}}_{\mathrm{i}}^{\mathrm{R}} \mathbf{A}_{\mathrm{i}} & -\mathrm{d}\mathbf{g}/\mathrm{dL} \end{bmatrix} \tag{15.15}$$

$$\boldsymbol{\Phi}_{\mathbf{q}}^{(\mathrm{lfac},3)} = \begin{bmatrix} \mathbf{0}^{\mathrm{T}} & -\mathbf{n}^{\mathrm{T}} \mathbf{A}_{\mathrm{i}} \tilde{\mathbf{u}}_{\xi} & \left(\mathrm{d}\mathbf{n}/dL\right)^{\mathrm{T}} \mathbf{A}_{\mathrm{i}} \mathbf{u}_{\xi} \\ \mathbf{0}^{\mathrm{T}} & -\mathbf{b}^{\mathrm{T}} \mathbf{A}_{\mathrm{i}} \tilde{\mathbf{u}}_{\xi} & \left(\mathrm{d}\mathbf{b}/dL\right)^{\mathrm{T}} \mathbf{A}_{\mathrm{i}} \mathbf{u}_{\xi} \\ \mathbf{0}^{\mathrm{T}} & -\mathbf{n}^{\mathrm{T}} \mathbf{A}_{\mathrm{i}} \tilde{\mathbf{u}}_{\zeta} & \left(\mathrm{d}\mathbf{n}/dL\right)^{\mathrm{T}} \mathbf{A}_{\mathrm{i}} \mathbf{u}_{\zeta} \end{bmatrix} \tag{15.16}$$

and the contribution of each part of the kinematic constraint to the right hand side of the acceleration equations is

$$\boldsymbol{\gamma}^{(pmc,3)\#} = -\tilde{\boldsymbol{\omega}}_{\mathrm{i}} \dot{\mathbf{s}}_{\mathrm{i}}^{\mathrm{R}} + \frac{\mathrm{d}^2\mathbf{g}}{\mathrm{dL}^2} \dot{\mathrm{L}}^2 \tag{15.17}$$

$$\boldsymbol{\gamma}^{(pmc,3)\#} = -\begin{Bmatrix} \left[2\dot{L}\left(\mathrm{d}\mathbf{n}/\mathrm{d}L\right)^{\mathrm{T}} \mathbf{A}_{\mathrm{i}} \tilde{\boldsymbol{\omega}}'_{\mathrm{i}} + \mathbf{n}^{\mathrm{T}} \mathbf{A}_{\mathrm{i}} \tilde{\boldsymbol{\omega}}'_{\mathrm{i}} \tilde{\boldsymbol{\omega}}'_{\mathrm{i}} + \dot{L}^2 \left(\mathrm{d}^2\mathbf{n}/\mathrm{d}L^2\right)^{\mathrm{T}} \mathbf{A}_{\mathrm{i}}\right] \mathbf{u}_{\xi} \\ \left[2\dot{L}\left(\mathrm{d}\mathbf{b}/\mathrm{d}L\right)^{\mathrm{T}} \mathbf{A}_{\mathrm{i}} \tilde{\boldsymbol{\omega}}'_{\mathrm{i}} + \mathbf{b}^{\mathrm{T}} \mathbf{A}_{\mathrm{i}} \tilde{\boldsymbol{\omega}}'_{\mathrm{i}} \tilde{\boldsymbol{\omega}}'_{\mathrm{i}} + \dot{L}^2 \left(\mathrm{d}^2\mathbf{b}/\mathrm{d}L^2\right)^{\mathrm{T}} \mathbf{A}_{\mathrm{i}}\right] \mathbf{u}_{\xi} \\ \left[2\dot{L}\left(\mathrm{d}\mathbf{n}/\mathrm{d}L\right)^{\mathrm{T}} \mathbf{A}_{\mathrm{i}} \tilde{\boldsymbol{\omega}}'_{\mathrm{i}} + \mathbf{n}^{\mathrm{T}} \mathbf{A}_{\mathrm{i}} \tilde{\boldsymbol{\omega}}'_{\mathrm{i}} \tilde{\boldsymbol{\omega}}'_{\mathrm{i}} + \dot{L}^2 \left(\mathrm{d}^2\mathbf{n}/\mathrm{d}L^2\right)^{\mathrm{T}} \mathbf{A}_{\mathrm{i}}\right] \mathbf{u}_{\zeta} \end{Bmatrix} \tag{15.18}$$

To understand the minimum requirements for the degree of the interpolating polynomials that can be used in the formulation of the prescribed motion constraint, the order of the derivatives used in Eqs (15.12) through (15.18) must be identified. The right hand side vector in Eq (15.18) involves $\mathrm{d}^2\mathbf{n}/\mathrm{d}L^2$ being $\mathbf{n} = \mathbf{k}/\|\mathbf{k}\|$ given by Eq (15.2) and $\mathbf{k} = \mathbf{g}^{uu} - \left(\mathbf{g}^{uuT}\mathbf{g}^{u}\right)\mathbf{g}^{u} / \|\mathbf{g}^{u}\|^2$ by Eq (15.3). Therefore, it is required that the fourth derivative of the interpolating polynomial is used, being a quintic polynomial the lowest odd degree polynomials that can be used to formulate accurately the prescribed motion constraint.

15.5 Prescribed Motion Constraint Application Cases

In order to study the use of different piecewise interpolation methodologies, on a perspective of prescribed motion constraint violation, two curves, associated to the track centrelines designs of roller coasters, are considered: a horizontal ellipse with a corkscrew, and; a more complex three-dimensional track with a geometry analogous to a complete roller coaster.

These curves are parameterized using three different interpolation approaches: cubic spline 'Spline 3'; shape preserving cubic hermit polynomial 'Pchip' [15]; quintic spline 'Spline5'.

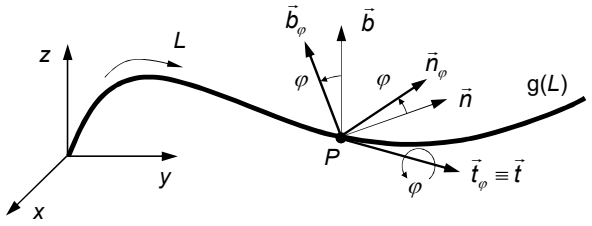

Figure 15.5. Contribution of cant angle to the track model.

The use of the prescribed motion constraint is demonstrated by enforcing that a vehicle represented by a single rigid body follows the defined curves. The orientation of the Frenet frame associated to the curves is rotated about the tangent vector in each particular geometry by an angle φ, as shown in Figure 15.5, to obtain the desired cant angle that corresponds to the equilibrium cant for the vehicle travelling at a prescribed speed. Details on the application of the cant definition with reference to the equilibrium cant can be found in the work by Pombo and Ambrosio [5, 16].

The dynamic analyses of the two cases presented here are performed with all polynomial interpolators listed and with the application of the Baumgarte stabilization for the correction of the kinematic constraint violations. Note that only a constraint stabilization method is used and that constraint correction procedures, such as the coordinate partition method, are not considered in this work.

15.5.1 Ellipse with Corkscrew

The ellipse track, presented on Figure 15.6, starts with a straight entryway designed to allow a smooth entry on the ellipse part of the path having a gradual change of the cant angle in order to match that of the ellipse at junction. The ellipsoidal segment of the track has a cant angle that corresponds to the equilibrium cant for the speed at which the vehicle travels. Taking the central part of the ellipse a two roll corkscrew segment is implemented by means of cant variation. The rigid body here considered starts with an initial velocity of 10 m/s and has a mass of 350 kg and inertias of $I_{\zeta\zeta}$= 50 Kg m^2 and $I_{\eta\eta}$=$I_{\xi\xi}$= 120 Kg m^2.

The evolution in time of the constraint violation value for each interpolation procedure considered in this work, when using the Baumgarte stabilization, is presented on Figure 15.7. The constraint violation peaks, with all interpolating schemes, take place when the vehicle passes in some particular points of the track identified by ① through ⑤ and described on Figure 15.8.

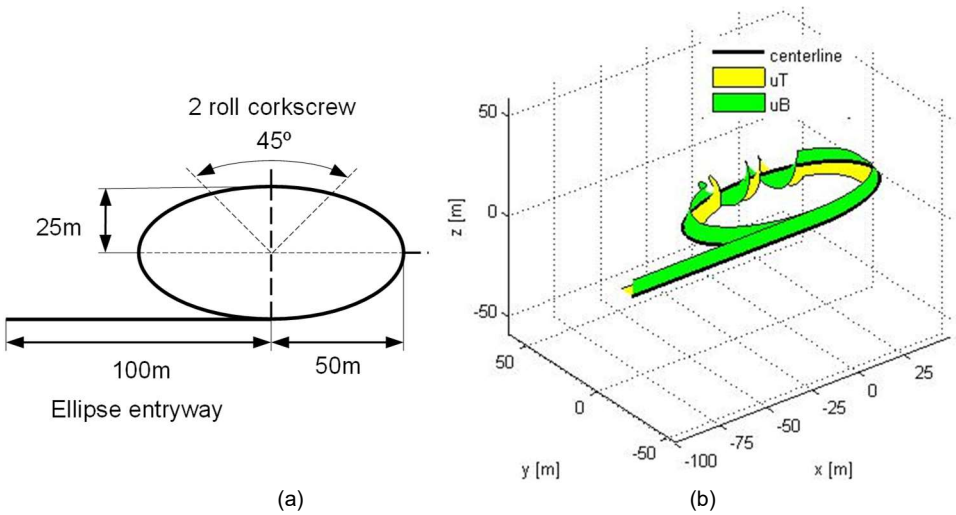

Figure 15.6. Ellipse track characteristics: (a) geometric characteristics; (b) three-dimensional representation of the track centreline with a sweep of the unitary normal and binormal vectors.

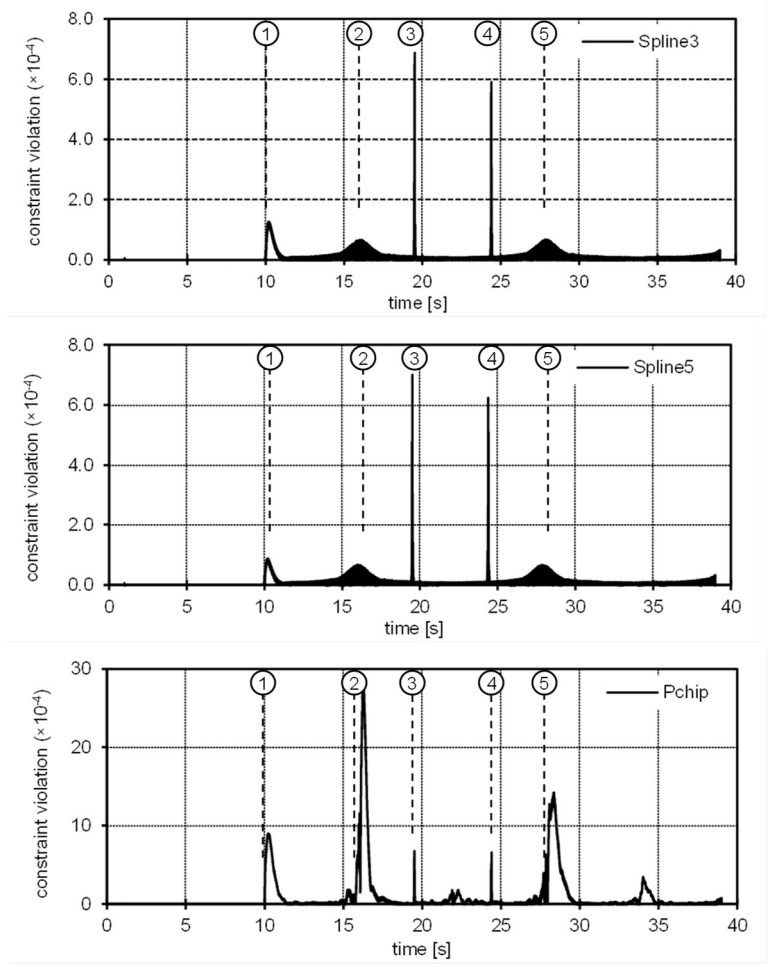

Figure 15.7. Ellipse centreline constraint violation evolution along time with Baumgarte stabilisation for each interpolation polynomial.

The results show that the cubic and quantic polynomials lead to similar evolutions of the constraint violations while the cubic shape preserving polynomial presents constraint violations one order of magnitude higher. The maximum constraint violations observed with the cubic and quantic polynomials take place at the start and end of the corkscrew roll while for cubic shape preserving the higher violations are for the ellipse points where the radius of curvature is maximum. It should be noted that the higher constraint violations with the shape preserving polynomial take place slightly after the points of interest identified.

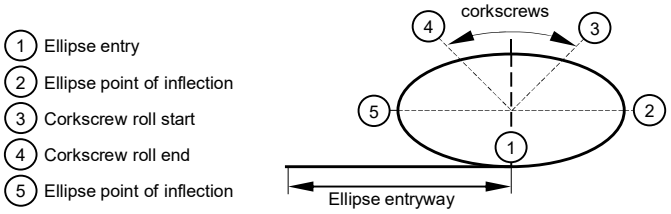

Figure 15.8. Description and representation of ellipse track centreline point of interest

The constraint violation evolution along time for the different polynomials tested here, but in this turn, without using any constraint stabilization procedure, is presented in Figure 15.9. As expected, the constraint violation keeps on accumulating for all interpolation schemes tested, being the rate of growth of these violations much higher for the cubic shape preserving polynomial and similar for both cubic and quintic polynomials. The marginally lower rate of growth of the quintic polynomial, with respect to the cubic, not only reflects impossibility that the later has to fulfil the fourth derivative required for the exact constraint formulation but also that the contribution of that term is almost negligible. Table 15.1 summarizes the maximum constraint violation observed on each of the simulations making it clear that, regardless of the interpolation scheme, the application of the constraint stabilization is fundamental for the accuracy improvement of the dynamic analysis.

	Maximum constraint violation		
	Spline 3	Spline 5	Pchip
Stabilized	6.88×10^{-04}	7.01×10^{-04}	29.1×10^{-04}
No Stabilization	4.83×10^{-02}	3.28×10^{-02}	73.3×10^{-02}

Table 15.1 Ellipse maximum constraint violation for each interpolation polynomial.

The importance of the choice of the proper polynomial interpolation is not extinguished on how the constraint equations are more or less accurately fulfilled. Geometric issues such as the avoidance of unwanted oscillations and local control of the curve are of high importance. From this point of view, the use of lower degree polynomials is preferred. The use of shape preserving cubic polynomials handles both the geometric requirements for continuity and the

local control avoiding overshooting. The IMSL Fortran routine `CSCON` [17], based on the work by Irvine et al. [18], provided good results with low constraint violations [5, 16]. However, the Matlab function `Pchip` [15] used here, based on the work of Fritsch and Carlson [19], does not provide an acceptable accuracy for this application.

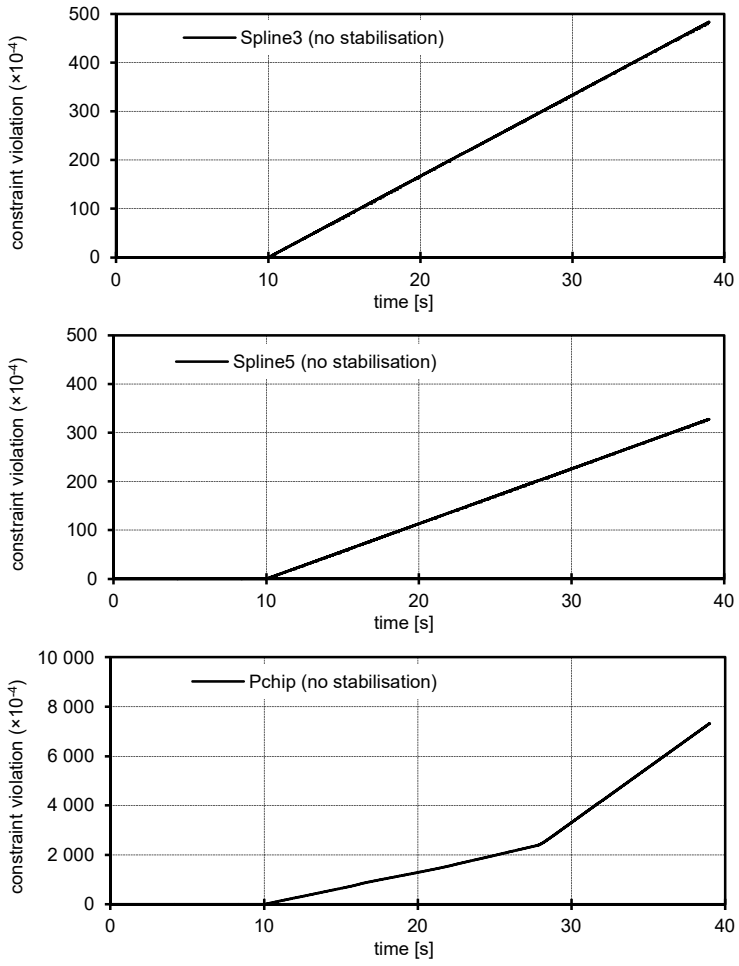

Figure 15.9. Evolution of the ellipse centreline constraint violation for the different interpolating polynomials when no constraint stabilisation procedure is used.

15.5.2 Roller Coaster

To demonstrate the performance of the polynomial interpolation schemes in a more complex and general geometry a roller coaster track, illustrated on Figure 15.10 and Figure 15.11, is used here. The roller coaster model, initially presented by Pombo and Ambrosio [5,16], has the geometry shown in Figure 15.10 being the transition into and out of the curve G–I modelled with parabolic transition curves of 60 m. The cant angle for the circular curve, corresponding to the equilibrium cant, i.e. the cant for zero track plane acceleration, is –1.014 rad and it varies linearly in the transition segments. The vehicle rigid body has a mass of 150 kg and inertias of $I_{\zeta\zeta}$= 25 Kg.m^2 and $I_{\eta\eta}$=$I_{\xi\xi}$= 65 Kg.m^2, and starts with an initial velocity of 2 m/s.

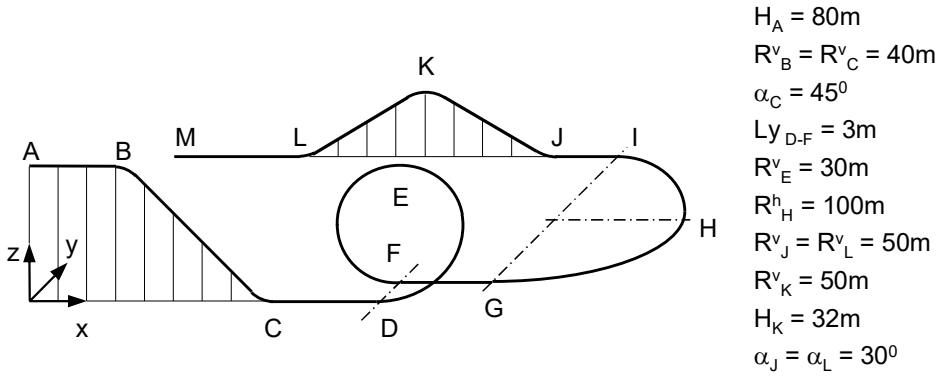

Figure 15.10 Roller coaster centreline geometry

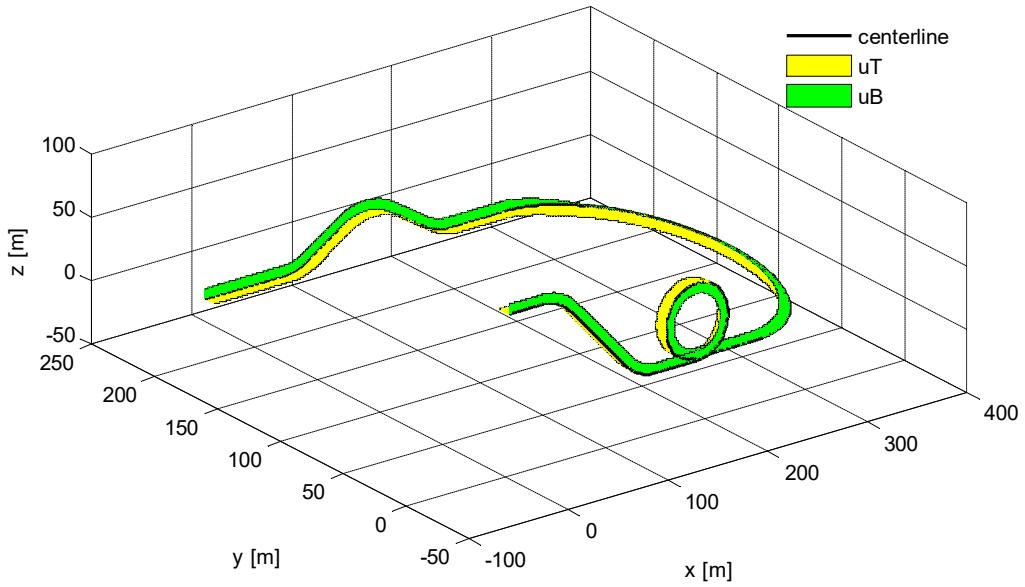

Figure 15.11 Three-dimensional representation of the track centreline including a sweep of the unitary normal and binormal vectors.

The evolution of the constraint violation with each one of the interpolation polynomials is presented in Figure 15.12, for the cases in which the Baumgarte constraint stabilization is used, and in Figure 15.13, for the cases simulated without constraint violation stabilization. As for the simpler case presented in the previous section, the constraint stabilization procedure plays a central role on the accuracy of the dynamic analysis, regardless of the interpolation scheme selected. Also, just as before, the cubic shape preserving polynomial `Pchip` performance is not satisfactory, regardless of the improvements observed when using the constraint stabilization. In this general geometry it is observed that the quantic polynomial leads to an accumulation of the constraint violations at a lower rate than what is observed with the cubic polynomial, being overall one order of magnitude lower.

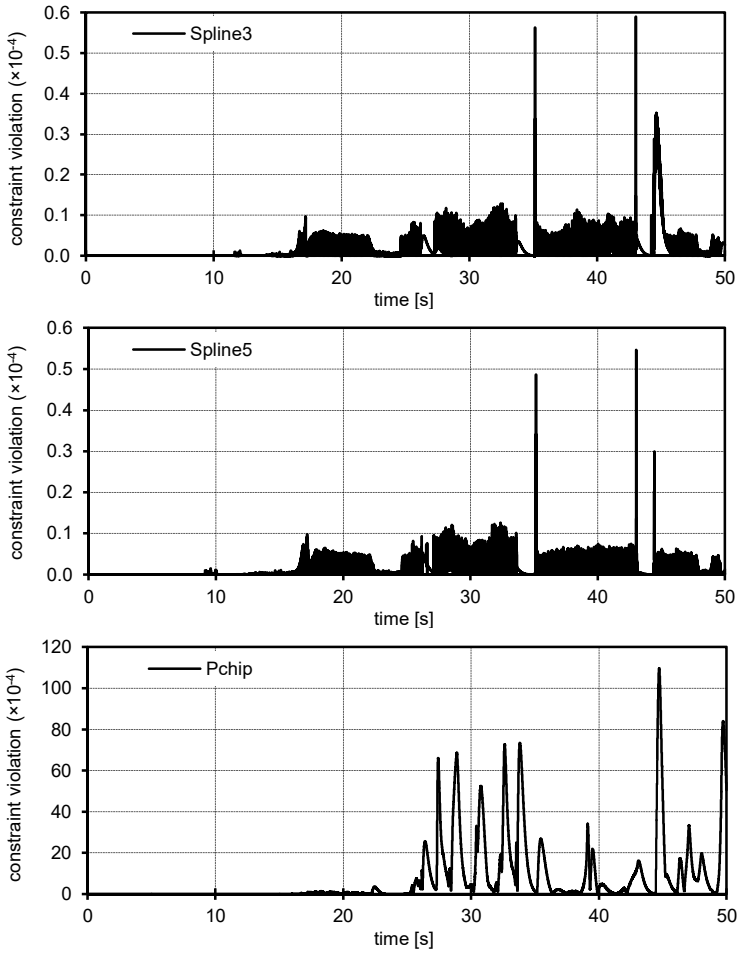

Figure 15.12 Evolution of the roller coaster centreline constraint violation, for each piecewise interpolation methodology, with Baumgarte constraint stabilisation.

A summary of the maximum constraint violation evaluated on each of the simulations for the roller coaster track is presented on Table 15.2. Although, overall, these results have the same trends already observed for the ellipse track, the difference in performance between the quantic and cubic polynomials, for dynamic analysis without constrain stabilization, is clearer now. This case suggests that the role played by the fourth derivative of the curve equation with respect to its arc length, as required in Eq. (15.18) plays a non-neglectable role. However, because the use of the constraint stabilization procedure in the framework of multibody dynamic formulations, with dependent coordinates, is unavoidable the differences of accuracy and performance between the cubic and quantic polynomials vanish.

	Maximum constraint violation		
	Spline 3	Spline 5	Pchip
Stabilized	5.90×10^{-05}	5.47×10^{-05}	1.10×10^{-02}
No Stabilization	3.33×10^{-03}	9.28×10^{-05}	$5.71\times10^{+00}$

Table 15.2 Roller coaster maximum constraint violation for each interpolation polynomial.

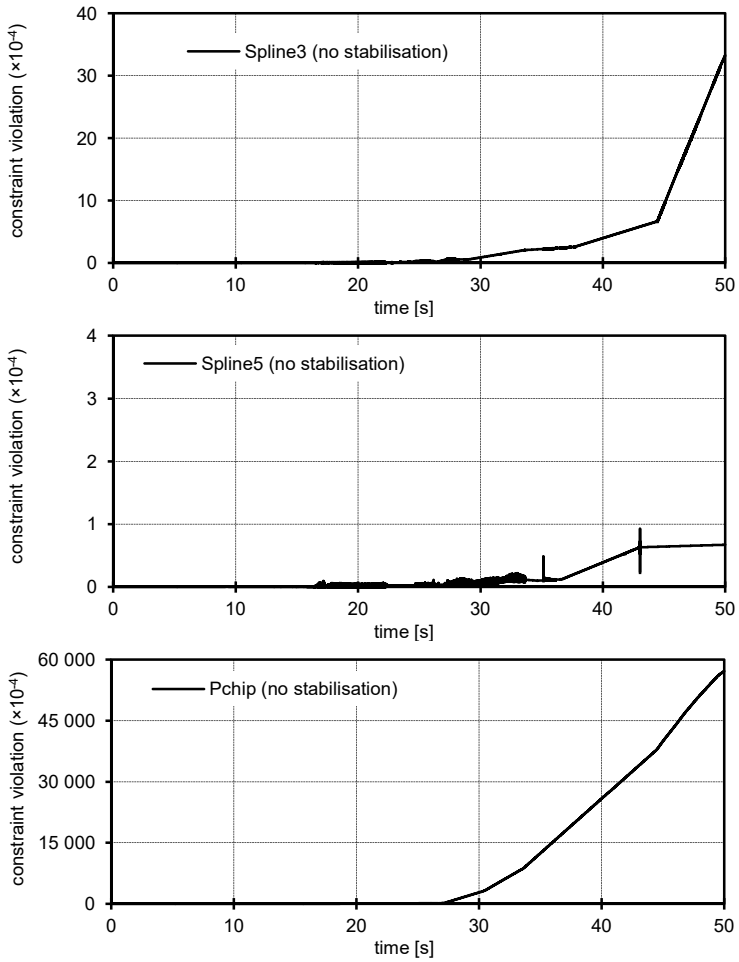

Figure 15.13. Evolution of the roller coaster centreline constraint violation for each piecewise interpolation methodology when no constraint stabilisation is used.

It must be noticed that, in general dynamic analysis of multibody systems, the constraint violations are reflected in the dynamic response in much more than the stability of the complete process. The physical interpretation of the constraint violations, for the rollercoaster case is illustrated in Figure 15.14 for several values of the case in which the cubic shape preserving spline is used. Usually the existence of the constraint violations have the same effect as spurious forces in the system being responsible not only for lack of accuracy of the system dynamic response but also for slowing the integration due to the need for a reduction of the time step of variable time step integrators. For these reasons, constraint stabilizations procedures and/or constraint correction methods must always be used.

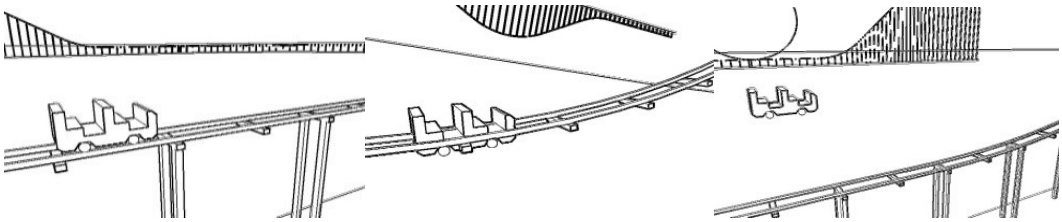

Figure 15.14. Visual representation of a constraint violation: (a) No violation; (b) Penetration between track and vehicle; (c) Separation between track and vehicle.

Conclusions

The formulation of a prescribed motion constraint requires the parameterization of a curve with a polynomial with an order that fulfils the geometric requirements of smoothness, shape control and an accurate description of the kinematic constraint and of its second time derivative. From the geometric point of view C^2 polynomials would suffice but to obtain the accurate formulation of the constraint the fourth order is the minimum required. However, regardless of the order of the polynomial actually used for the prescribed motion constraint, when dependent coordinates, such as Cartesian coordinates, are used in the multibody dynamic formulation the small numerical errors always present in the numerical methods used to solve and integrate the equations of motion tend to accumulate, ultimately leading to the violation of the kinematic constraints of the system. Therefore, the use of constraint stabilization or correction methods is unavoidable.

This work shows that the constraint stabilization methods effectively stabilize the numerical errors and also those resulting from the use cubic interpolating polynomials in the constraint formulation making the results indistinguishable from those obtained with quintic polynomials. Due to the fact that both cubic and quintic polynomial have the required degree of smoothness to describe geometric problem and that the cubic polynomials have better local control properties it is shown that they are more advantageous in the formulation of the prescribed motion constraint. The use of cubic shape preserving splines may be required to avoid unwanted oscillations and overshooting on curve transitions. However, caution should be used on the scheme selected as some shape preserving cubic splines do not present the necessary geometric features as demonstrated here, although alternative formulations of these splines can deliver good results as shown in the literature.

References

[1] Frenet, J. F.: Sur les courbes a double courbure. Journal de Mathemathiques Pures et Appliquees, 17, 437–447 (1852)

[2] Darboux, G.: Lecons sur la Theorie Generale des Surfaces et les Applications Geometriques du Calcul Infinitesimal, volume 2. Gauthier-Villars, Paris, France (1889)

[3] Tandl, M., Kecskemethy, A.: Singularity-free trajectory tracking with Frenet frames. In: Husty, M., Schroeker, H.-P. (eds.) EuCoMeS, Proceedings of the 1st Conference, Obergurgl, Austria (2006)

[4] Tandl, M.: Dynamic Simulation and Design of Roller Coaster Motion, Ph.D. Dissertation, Universitat Duisburg-Essen, Duisburg, Germany (2008)

[5] Pombo, J., Ambrosio, J.: General spatial curve joint for rail guided vehicles: Kinematics and dynamics. Multibody System Dynamics, 9, 237–264 (2003)

[6] Nikravesh, P. E.: Computer-Aided Analysis of Mechanical Systems. Prentice-Hall, Englewood Cliffs, New Jersey (1988)

[7] Jalon, J. de, Bayo, E.: Kinematic and dynamic simulation of multibody systems. Springer-Verlag, Heidelberg, Germany (1993)

[8] Shampine, L., Gordon, M.: Computer Solution of Ordinary Differential Equations. Freeman, San Francisco, California (1975)

[9] Gear, C. W.: Simultaneous Numerical Solution of Differential-Algebraic Equations. IEEE Transactions on Circuit Theory, 18(1), 89-95 (1971)

[10] Baumgarte, J.: Stabilization of Constraints and Integrals of Motion in Dynamical Systems. Computer Methods in Applied Mechanics and Engineering, 1, 1-16 (1972)

[11] Bayo, E., Avello, A.: Singularity-free augmented Lagrangian algorithms for constrained multibody dynamics. Nonlinear Dynamics, 5(2), 209-231 (1994)

[12] Neto, M. A., Ambrósio, J.: Stabilization Methods for the Integration of DAE in the Presence of Redundant Constraints. Multibody System Dynamics, 10, 81-105 (2003)

[13] Farin, G. E.: Curves and Surfaces for Computer Aided Geometric Design: A Practical Guide, 2nd Edition. Academic Press, Boston, Massachussetts (1990)

[14] De Boor, C.: A Practical Guide to Splines", Springer-Verlag, New York, New York (1978)

[15] The MathWorks Inc.: Using MATLAB, The MathWorks Inc., Natick, Massachussetts (2002)

[16] Pombo, J. and Ambrósio, J.: Modelling Tracks for Roller Coaster Dynamics, Int. J. Vehicle Design, 45(4), 470-500 (2007)

[17] Visual Numerics Inc,: IMSL Fortran 90 Math Library 4.0 - Fortran Subroutines for Mathematical Applications. Huston, Texas (1997)

[18] Irvine, L. D., Marin, S. P., Smith, P. W.: Constrained interpolation and smoothing.. Constr. Approx., 2, 129–151 (1986).

[19] Fritsch, F. N., Carlson, R. E.: Monotone Piecewise Cubic Interpolation. SIAM Journal on Numerical Analysis, 17(2), 238–246 (1980)

16 A New Methodology to Study the Pantograph-Catenary Dynamics in Curved Railway Tracks

[6] The pantograph-catenary system is responsible to provide an uninterrupted energy supply to power electric traction railway vehicles. The analysis of the dynamic behaviour of the catenary and pantograph, as well as its interaction, has been object of active research to improve the energy collection quality. Both the catenary model and the trajectory of the pantograph base are defined with respect to the track geometry considering the conventional definition used by the rail industry, i.e., curvature, cross level and vertical position of the track. The pantograph is modelled using a 3D multibody formulation being its base motion constrained to follow the generalized trajectory from the top of a railway vehicle. The finite element method is used to model the catenary. A co-simulation procedure is set to allow for the coupled dynamics of the two systems. Not only to demonstrate the methodology but also to address its modelling implications, as well as identify problems and their solutions, realistic case studies of pantograph-catenary interaction in a high-speed railway line are presented and discussed. In order to demonstrate the methodology, setting up models for curved catenaries, analyse their modelling implications and highlight applicability, realistic case studies of pantograph-catenary interaction in high-speed rail operations are presented and discussed. In the process there are found significant differences on the dynamic response of the catenary in curved and straight tracks.

---

[6] The work presented in this chapter has been submitted for publication in Vehicle System Dynamics Journal with the authors P. Antunes, J. Ambrósio, J. Pombo and A. Facchinetti.

16.1 Introduction

The modern railway systems rely on the cost-effectiveness and reliability of electrical traction vehicles where the pantograph–catenary interface, represented in Figure 16.1, ensures the supply of electrical energy to power the vehicles motors. Thus, it is not only of fundamental importance that this energy supply remains uninterrupted, but also that its electro-mechanical wear is as reduced as possible.

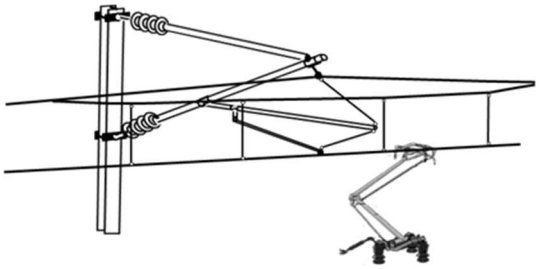

Figure 16.1: Railway energy collecting system composed of a catenary and a pantograph.

The over-head contact line, also known simply as catenary, is composed of a set of suspended cable wires and its supporting elements that run along the railway track and carry the electrical current, which in turn is collected by the pantograph mounted on the top of the railway vehicle. The energy collection is assured by the sliding contact between the pantograph and the catenary contact wire. The interaction contact force developed must fulfil tight operational requirements that ensure that a reliable and efficient energy collection is achieved. Operating the pantograph-catenary interface at a low average contact force increases the susceptibility to contact loss incidents with consequent arcing, which in turn leads to high electro-mechanical wear and the deterioration of the functional conditions of both the catenary and the pantograph. High contact forces, in the other hand, result in mechanical wear of the contact elements increasing the frequency of the maintenance cycles and risk of failure [1]. Certainly, the present need to increase the rail network capacity and its interoperability puts extra demands on these systems, [2,3], for which the energy collection ability remains a limiting factor of the current railway vehicles operational speeds [4,5].

The dynamic analysis of the pantograph and catenary, as well as their interaction, is object of active research. The development of specialized numerical applications for the dynamic analysis of pantograph-catenary interaction plays a significant role in the analysis and design of railway network assets. An extensive amount of publications on the development and application of computational methods and applications in pantograph-interaction can be found in the literature, addressing analysis of multiple pantograph operation [6–8], analysis of critical catenary sections [9–11], and optimisation of pantograph and catenary designs [12–14] among

other issues of importance. The perturbation of the quality of contact in the pantograph-catenary interface due to aerodynamics effects, vehicle vibration and catenary irregularities [15–19] are also considered in the literature. The hardware-in-the-loop hybrid simulations of pantograph-catenary interaction is also another approach to find improved dynamic performance for the two systems [20,21]. Also, research on the identification and influence of catenary damping, shown as very important for the interaction quality [22], was performed to improve catenary models [23]. The pantograph-catenary benchmarks, [24,25], and its associated references portrait the state-of-the-art of existing numerical analysis tools, developed by world leading research institutions. Notice that in all applications, methods or case-studies considered in previous publications on the topic of pantograph-catenary interaction modelling and analysis, most catenary models are exclusively set in straight railway tracks. The employment of catenary geometries consistent with general track geometries, i.e., catenaries with curvatures, is addressed in PantoCat statement of method [26], however this capability is not fully demonstrated. The work by Teichelmann et al. [27] presents an application with a curved catenary, but the method on how to build the model is not presented. In [28], M. Tur et al. present a methodology for computing the initial configuration of a railway catenary, including catenaries in curved tracks. Also, A. Rønnquist et al. [29] present a modal analysis of catenaries set in general paths and P. Nåvik et al. [30] present the first results obtained from numerical simulations in comparison with field measurements. However, a detailed methodology for the construction of catenary models set in general track trajectories, its modelling implications and the interaction with the pantographs are not addressed in any of the previous works [26–30].

The work presented here purposes an approach for the numerical dynamic analysis of pantograph-catenary interaction in curved tracks or for that matter in any generalized track trajectory. Here both the catenary model and the trajectory path of the pantograph are consistent with the general geometry, which is defined as parametric curve with an associated local reference frame that defines the orientation of the track layout. The track geometry is obtained using the standard information required for railway vehicle dynamics applications, i.e., curvature, cross level and vertical profile as function of the track length. The finite element method is used to model and evaluate the dynamic behaviour of a catenary system following the methodology presented in previous works [31]. To cope with the general geometry of the track and the path of its base, the pantograph model is developed using a spatial multibody dynamics formulation [32]. The pantograph base motion, which is fixed to the railway vehicle roof, is defined by a prescribed kinematic motion constraint [33,34]. As both pantograph and catenary use different formulations, their interaction is established through a co-simulation

procedure where a penalty method is used to evaluate the contact force between the pantograph and the catenary [35]. To demonstrate the proposed procedure, a detailed analysis of a pantograph-catenary interaction is presented in this work for catenary models inserted in tracks with a general geometry, including different curve radii.

16.2 Track Spatial Definition

The catenary layout is defined in relation to the track travel length, or track arc-length, and its running surface. To define a catenary system in space and to place it correctly in relation to the track, a spatial reference is required. For a catenary on a straight track this process is straight forward. However, when dealing with a generalised track trajectory a more systematic approach is required to account for the track curvature and cross level, which influence the orientation of the running surface of the track. Also, the trajectory of the pantograph is defined by the position of the vehicle roof top relative to the track surface, which enforces that a common geometric framework is used for both systems. The track geometric description commonly used in railway vehicle dynamics studies, is also used here as such a common framework.

The railway track geometry is described as a function of its travel length, by the curvature, cross level and elevation [36]. Though this description defines the track geometry along its travel length, it does not provide an absolute spatial frame with respect to which position other systems. To fulfil this need, a reference moving frame of the track is established as a function of the travel length [37,38]. For a given travelled length *s*, the position of the moving frame origin $\mathbf{r}_t$ is set such way that ξ_t is tangent to the track centreline, η_t is transversal to the track and tangent to the running surfaces of the rails while ζ_t is normal to the track running surface, as shown in Figure 16.2.

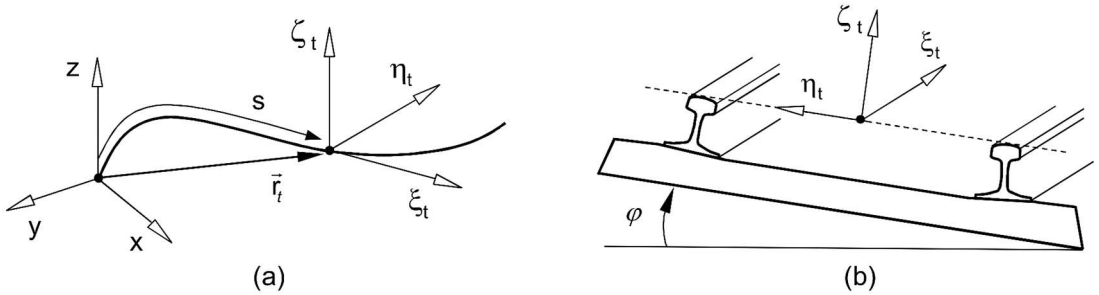

Figure 16.2: Representation of the track moving frame: (a) As a parametric curve relative to the track length; (b) In relation to the track running surface.

The track centreline spatial curve is obtained by performing the geometric reconstruction of the track geometry using the curvature and elevation data of the selected track [39], which is

the same data that is used by the rail industry to represent the track design. With the track centreline curve and the track cross level and corresponding cant angle, φ, a local moving frame of reference is built along the track using a methodology based on the evaluation and rotation of Frenet-Serret frame, [34,40]. For the purpose of computational applications, the track centreline curve and the moving frame unit vectors, ξ_t, η_t and ζ_t, are discretized in particular locations, such way that, by interpolation, the complete track geometry can be used

16.3 Catenary Model

The catenary system is modelled in this work using a finite element formulation [41]. The geometric description of the catenary, which is defined in relation to the track running surface, is the basis of the construction of the finite element model used here. Therefore, the catenary layout along the track and its geometric spatial description are presented first. Afterwards, the equations of motion for the finite element model are detailed along with the catenary initialization procedure, i.e., the methodology that allows positioning the finite element mesh nodes in such a way that the catenary is in static equilibrium when the dynamic analysis starts.

16.3.1 Catenary Layout

A typical catenary structure is composed by two main suspended cable wires, the contact wire and the messenger wire, which are set in tension along the track by mechanical tensioning devices mounted at the end poles of each catenary section. Due to physical and operational reasons, each section has a limited length. Hence the continuity of the contact wire, as seen by the pantograph contact strip, is assured by overlapping catenary sections at its ends. Both the contact and messenger wires are periodically supported by cantilevered consoles, known as cantilevers, mounted in poles, as represented in Figure 16.3. In between each pole, the contact wire is supported, in a discrete manner, by dropper cables that hang from the messenger wire. Besides supporting the contact wire, the droppers are responsible to minimize its sag and to keep its vertical elasticity as uniform as possible along its span.

To avoid grooving and ensure, as much as possible, a uniform wear of the pantograph contact strip, an alternating lateral offset of the contact wire, commonly known as stagger, is imposed at each cantilever. The stagger of the contact wire is provided by a steady arm, which is fixed on the cantilever by a pin joint and designed to allow the vertical movement of the contact wire to provide clearance for the pantograph passage. To provide clearance for the pantograph passage and to allow vertical movement of the contact wire, its supporting connection to the cantilever is achieved by a steady arm, which is fixed on the cantilever by a

pin joint. The offset is set in relation to the nominal trajectory of the pantograph contact strip, which in straight tracks is just a straight line located at a given height above track centreline.

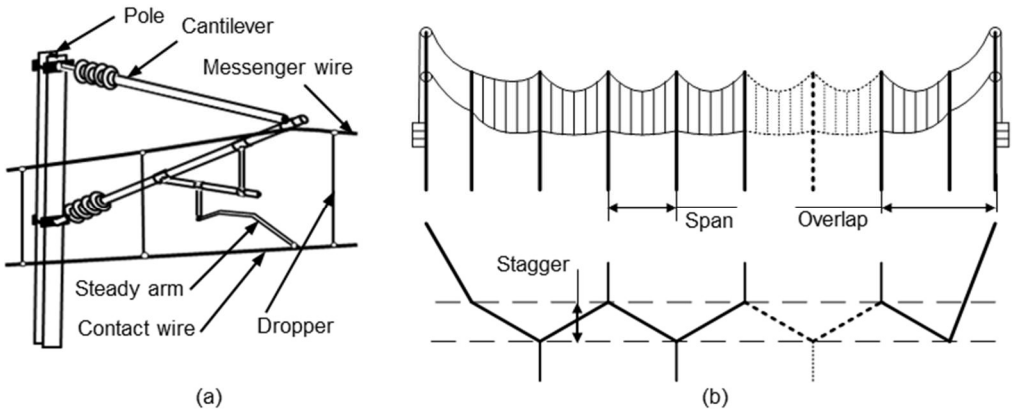

Figure 16.3: Catenary structure and its main components: (a) Cantilever; (b) Longitudinal and top view.

Generally, the offsets are determined in order to keep the span lengths as long as possible, to reduce construction costs, while still ensuring that the contact wire deflection, under wind conditions, never exceeds a permissible lateral displacement, e_{perm}, such that the contact wire is always within the usable length of the contact strip [42]. In straight lines and very large radius curves this results in an alternating offset pattern *(±b)*, or *zig-zag*, as represented in Figure 16.4 (a). Note that the lateral forces, $\mathbf{f}_{sp}$, at the contact wire supports, which result from the imposed change of direction of the tensioned contact wire, have defined maximum and minimum tolerances [43]. Also, a minimum lateral sweep of the contact wire must be ensured to avoid grooving. As a result of these constraints, as the track curvature increases, a reduction of the offset at the inner side of the curve is required, thus forcing $b_1 \neq b_2$, as shown in Figure 16.4 (c). For small radius curves the offset is placed always on the outside side of the curve, i.e., $(+b_1, +b_1)$. Eventually, for even smaller radius it is not possible to use suitable offsets while maintaining the span length and shorter spans need to be used. Moreover, note that direction of the lateral forces at the steady arm support result from the imposed stagger and can either act away or towards the pole which determine the position and orientation of the steady arm in a pull-off or push-off configuration.

When designing a catenary system, the positioning of the offsets along each cantilever must take into consideration the catenary design, specified operational requirements set by the infrastructure owners and by standards [44]. This results in a set of catenary layout rules that define the allowed span lengths and correspondent staggering for defined ranges of track curvature, which can be specific to a given wind region. The determination of these design rules

can follow different approaches being its detailed discussion beyond the scope of this work [45]. For catenary systems belonging to different railway networks in current operation, Table 16.1 presents a summary of the maximum allowed span lengths, l_{max}, and correspondent stagger, (b_1,b_2), set for different track curvatures, on a given wind region. Due to confidentiality, the railway network remains unidentified.

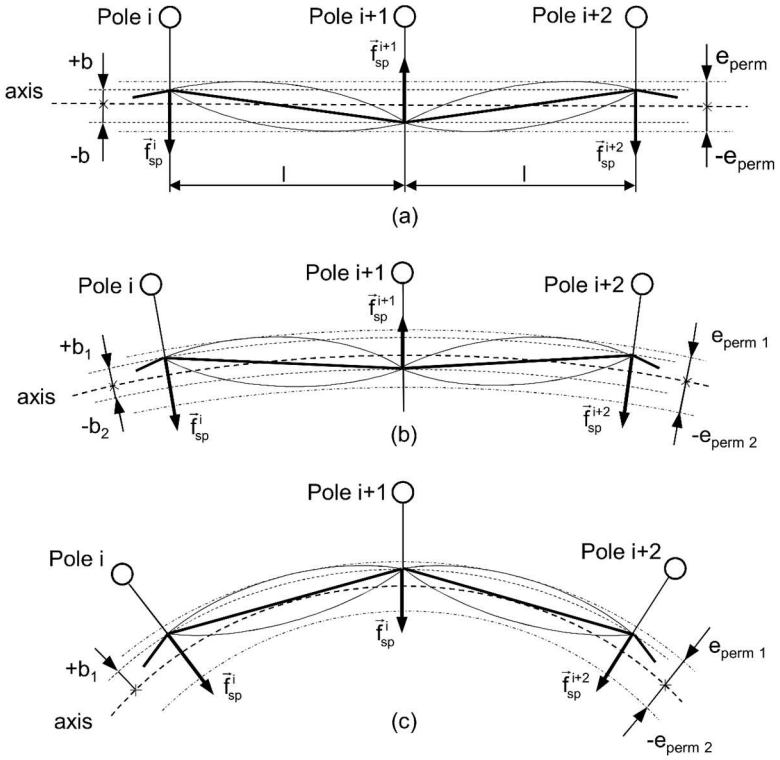

Figure 16.4: Contact wire lateral position on: (a) Straight track, (b) Large radius curves; (c) Small radius curves.

Catenary	A			B			C		
Operating Speed [km/h]	160			200			300		
Curve Radius [m]	l_{max} [m]	b_1 [mm]	b_2 [mm]	l_{max} [m]	b_1 [mm]	b_2 [mm]	l_{max} [m]	b_1 [mm]	b_2 [mm]
∞	80	+400	-400	63	+200	-200	65	+300	-300
10000	80	+400	-300	63	+200	-200	65	+300	-190
7000	76	+400	-330	63	+240	-50	65	+300	-150
5000	76	+400	+120	63	+240	-50	65	+300	-90
4000	80	+400	+150	63	+240	0	65	+300	-40
3000	80	+400	+310	63	+240	+90	65	+300	+50
2000	80	+400	+400	63	+240	+240	65	+300	+230
1000	67	+400	+400	54	+240	+240	63	+300	+300

Table 16.1: Catenary span length and stagger set in relation to the track curvature in different catenary systems.

Note that there are different catenary designs [31,43], with slightly different or more accentuated topological arrangements such as the stich-wire and compound catenaries.

However, simple alternatives are more extensively used. For the sake of simplicity, the approach proposed here is applied for the setup of catenary models of the simple type. Nevertheless, this methodology can be applied to any type of catenary.

16.3.2 Catenary Model Geometry

The finite element model of the catenary is defined firstly by setting the geometric positions of the catenary subsystems made by the contact and messenger wire points at the cantilever and at each dropper connection. With reference to Figure 16.5, at each cantilever, the positions of the contact wire at the steady arm, $\mathbf{r}_{cw}$, and the messenger wire at its cantilever support, $\mathbf{r}_{mw}$, are determined as:

$$\begin{aligned} \mathbf{r}_{cw} &= \mathbf{r}_t + \mathbf{A}_t \mathbf{s}'^{t}_{cw} \\ \mathbf{r}_{mw} &= \mathbf{r}_{cw} + \mathbf{s}^{cw}_{mw} \end{aligned} \tag{16.1}$$

where $\mathbf{r}_t$ is the position vector of the track centreline and $\mathbf{A}_t$ is the rotation matrix associated to the local reference frame, $(\xi, \eta, \zeta)_t$, which defines the track running surface orientation. These quantities are obtained by the evaluation of the track moving frame, described in Section 2, at the track length in which the pole is mounted. Vectors $\mathbf{s}'^{t}_{cw}$ and $\mathbf{s}^{cw}_{mw}$ are, respectively, the position of the contact wire in respect to the local reference frame $(\xi, \eta, \zeta)_t$ and the position of the messenger wire relation to the contact wire position, $\mathbf{r}_{cw}$, evaluated as:

$$\begin{aligned} \mathbf{s}'^{t}_{cw} &= \begin{bmatrix} 0 & \pm b & h_{cw} \end{bmatrix}^T \\ \mathbf{s}^{cw}_{mw} &= \begin{bmatrix} 0 & 0 & h_e \end{bmatrix}^T \end{aligned} \tag{16.2}$$

where the parameters b, h_{cw} and h_e are respectively, the contact wire lateral offset relative to the track centreline, the nominal contact wire height relative to the running surface and the encumbrance of the cantilever which sets the distance between the contact and messenger wire.

At each span, the position of the contact and messenger wires at the dropper connections is defined by the dropper spacings, a_d, the dropper lengths, l_d, and the appointed contact wire pre-sag set at for each dropper, s_d. In practice these parameters are set in pre-calculated span tables for a collection of normalised span lengths, l_{span}, of a particular catenary design, as represented in Figure 16.6. By superimposing these span geometry parameters with the already determined contact and messenger wire position at the cantilever, $\mathbf{r}_{cw}$ and $\mathbf{r}_{mw}$, the position of the contact and messenger wires at each dropper *j,* are defined as:

$$\mathbf{d}_{cw}^{j} = \mathbf{r}_{cw}^{i} + \sum^{j} a_d^j \left(\frac{l_{cw}}{l_{span}} \right) \hat{\mathbf{u}}_{cw} + [0 \quad 0 \quad -s_d^j]^T$$
$$\mathbf{d}_{mw}^{j} = \mathbf{d}_{cw}^{j} + [0 \quad 0 \quad l_d^j]^T \tag{16.3}$$

where $l_{cw} = \left\| \mathbf{r}_{cw}^{i+1} - \mathbf{r}_{cw}^{i} \right\|$ is the length between the subsequent cantilever contact wire positions and $\hat{\mathbf{u}}_{cw} = \left(\mathbf{r}_{cw}^{i+1} - \mathbf{r}_{cw}^{i} \right) / l_{cw}$ is the corresponding versor.

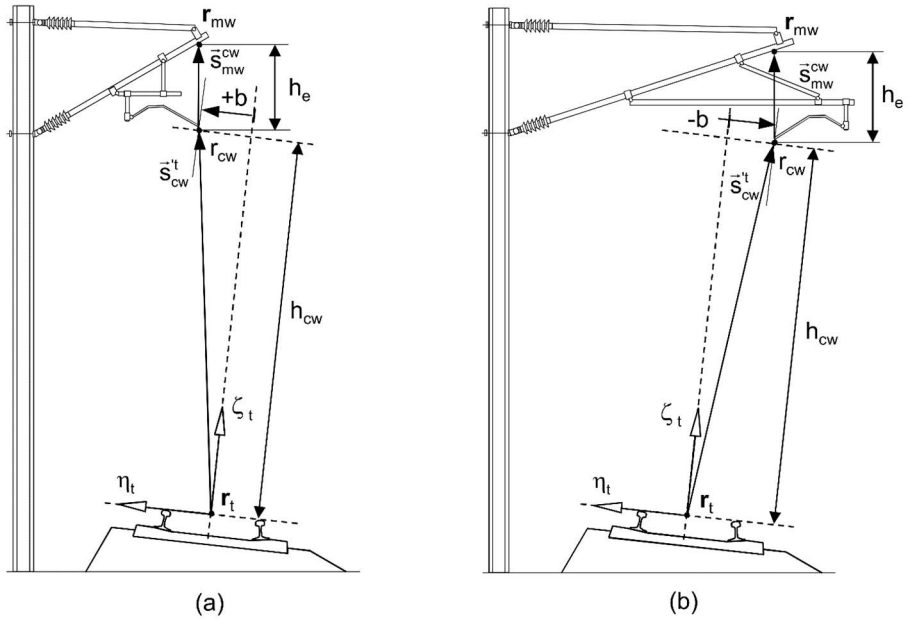

Figure 16.5: Representation of the contact and messenger wire position on the cantilever, in a curved track: (a) pull-off configuration; (b) push-off configuration.

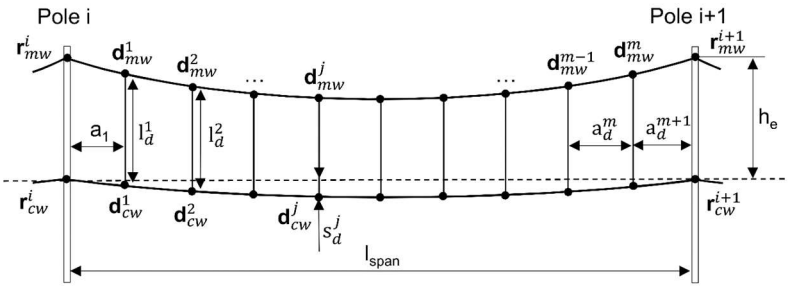

Figure 16.6: Catenary span geometric parameters.

16.3.3 Catenary Finite Element Model

The motion of the catenary is characterized by small rotation and small deformations where the only nonlinear effect is the dropper slacking resulting from the pantograph passage. The constant axial tensioning of the contact and messenger wires should also not be neglected. Therefore, the catenary is here modelled with linear finite elements where dropper slacking compensating forces are added, such that the dynamic equilibrium equation is assembled as:

$$\mathbf{M}\ \mathbf{a}_{t+\Delta t} + \mathbf{C}\ \mathbf{v}_{t+\Delta t} + \mathbf{K}\ \mathbf{d}_{t+\Delta t} = \mathbf{f}_{t+\Delta t} \tag{16.4}$$

where **M**, **C** and **K** are the catenary finite element global mass, damping and stiffness matrices. At time $t+\Delta t$, the accelerations, velocities and displacements vector are represented respectively as **a**, **v** and **d** while the sum of all external applied forces is depicted by vector **f**. All catenary elements are modelled using two-node Euler–Bernoulli beam elements [40], with the exception of the messenger wire cantilever support which is modelled as an equivalent three dimensional spring-damper element. The mass of the clamps and claws, present on the catenary structure to join its components, are modelled as lumped masses. To represent the stress stiffening of the catenary structure due to the tension stress state caused by tensioning the cable wires the stiffness matrix of the beam element *i* used for the contact and messenger wire is evaluated as:

$$\mathbf{K}_i^e = \mathbf{K}_L^e + F\mathbf{K}_G^e \tag{16.5}$$

in which $\mathbf{K}_L^e$ is the linear Euler-Bernoulli beam element stiffness matrix, F is the axial tension and $\mathbf{K}_G^e$ is the element geometric matrix. Proportional damping, also known as Rayleigh damping [46], is used to evaluate each beam finite element damping matrix $\mathbf{C}^e$ such that:

$$\mathbf{C}^e = \alpha^e \mathbf{M}^e + \beta^e \mathbf{K}^e \tag{16.6}$$

being α^e and β^e the mass and stiffness proportionality factors set for each type of catenary component. Alternatively, the same proportionality factors α and β are used for all structural elements. For a time, t+Δt the force vector $\mathbf{f}_{t+\Delta t}$ is evaluated as:

$$\mathbf{f}_{t+\Delta t} = \mathbf{f}^g + \mathbf{f}^t + \mathbf{f}_{t+\Delta t}^c + \mathbf{f}_{t+\Delta t}^d \tag{16.7}$$

where vector $\mathbf{f}^g$ contains the gravitational forces and $\mathbf{f}^t$ is made of the forces responsible for tensioning the wires individually applied at each tensioned element as pre-stress. Vector $\mathbf{f}_{t+\Delta t}^c$ and $\mathbf{f}_{t+\Delta t}^d$ are evaluated each time $t+\Delta t$ and represent the equivalent contact forces and moments applied at the appropriate nodes of the contact wire element and the dropper slacking compensating forces evaluated as:

$$\mathbf{f}_{t+\Delta t}^d = \sum_i \left(\mathbf{B}_d \mathbf{K}_d^e \tilde{\mathbf{d}}_{t+\Delta t}^e \right)_i \tag{16.8}$$

where for any dropper *i* that is slack, $\mathbf{K}_d^e$ is its stiffness matrix and $\tilde{\mathbf{d}}_{t+\Delta t}^e$ is a close prediction of its nodal displacements. The Boolean matrix $\mathbf{B}_d$ simply maps the local coordinates of the dropper element into the global nodal coordinates of the model. At each evaluated time $t+\Delta t$, the dropper slacking compensating forces are evaluated iteratively with equation (16.4) until convergence is reached, such that $\left| \mathbf{d}_{t+\Delta t} - \tilde{\mathbf{d}}_{t+\Delta t} \right| < \varepsilon_d$. Here, ε_d is a defined tolerance and vector

$\mathbf{d}_{t+\Delta t}$ denotes the displacement vector of the last iterative evaluation of equation (16.4). Vector $\tilde{\mathbf{d}}_{t+\Delta t}$ refers to the predicted nodal displacements that are either taken from the previous iteration or , in case of being the first iteration, correspond to the previous time step solution. The finite element mesh of the catenary is constructed following closely the catenary geometry established in Section 16.3.2, one beam element is used for each dropper and steady arm and, at least, 6 elements between droppers are used to define the contact and messenger wires. The model is constrained by pinned points at the ends of the contact and messenger wires, at the steady arm on the cantilever side and at the end of the cantilever messenger wire support.

16.3.4 Catenary Finite Element Model Initialization

The catenary initialization corresponds to the procedure set to determine the undeformed mesh of the model that upon being statically loaded by the gravitational and axial tension loads exhibit a correct static deformed shape, with special attention to the contact wire position along the track and its sag. In reality, a similar problem exits when mounting a catenary system on track where, after the first mounting stage, the catenary must be adjusted to fit all geometric specifications. These adjustments are generally comprised on regulating the dropper lengths and the steady arm position at the cantilever. In analogy to this procedure the catenary initialization is formulated here as a minimisation problem, to be solved using a classical gradient based optimisation procedure [47]. Here the minimization problem is defined as:

$$\begin{aligned} &\min\left(\sum_{1}^{m}\left\|\mathbf{d}_{cw}^{S\,\mathrm{m}}(\mathbf{x})-\mathbf{d}_{cw}^{\mathrm{m}}\right\|\right) \\ &\text{subject to: } \mathbf{x}=\left[l_0^1, l_0^2, \ \ldots\ , l_0^m\right] \end{aligned} \tag{16.9}$$

where the initial dropper lengths, l_0, are set as design variables used to construct the catenary model. The evaluation of the fitness function implies the static analysis of the generated finite element mesh. The deviations between the deformed contact wire positions at the droppers, $\mathbf{d}_{cw}^{S}$, and their nominal positions, $\mathbf{d}_{cw}$, are evaluated. The minimisation problem is solved iteratively for each span where also pinned point constraints are added on the contact and messenger wire cantilever supports, as represented in Figure 16.7 (a). After the minimisation problem being solved, these constraints are released and substituted by pre-stress forces imposed on the messenger wire support element and the steady arm element. At the contact wire support, the solicitation on each constraint is decomposed on a lateral offset force, $\mathbf{f}_{lat}$, that results from the imposed stagger and a vertical force, $\mathbf{f}_z$, resulting from a residual support of the contact wire weight. These forces are not only used to calculate the pre-stress force to be applied on the

equivalent steady arm beam element, $\mathbf{f}_{ps}$, but are also used to set its orientation, as represented on Figure 16.7 (b).

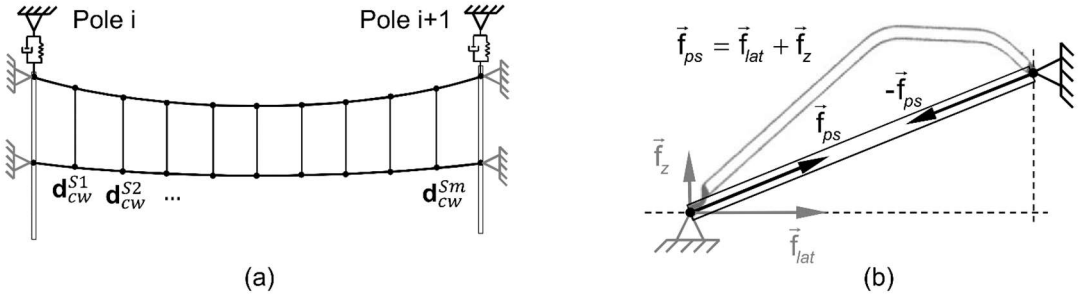

Figure 16.7: (a) Representation of the deformed catenary span resulting from the solution of the minimisation problem; (b) Representation of the steady-arm pre-stress forces and their orientation.

16.4 Pantograph Model

A pantograph is a multibody system that can be modelled as such, as seen in Figure 16.8 (a) or by a lumped mass representation, as observed in in Figure 16.8 (b). When modelled as a lumped mass, the pantograph model may have 2 masses, as in the case of low or medium train speed operations, or may need to have 3 masses, to account for the upper arm deformability in the case of lighter design as for the case high speed applications. Mechanically, the pantograph unfolding system is such that, during its lifting motion, the head of the pantograph is maintained levelled and its movement is set along a straight line perpendicular to the plane of the pantograph base. In turn, the base is attached to the roof of the railway vehicle, with electric isolators in-between, in perfect alignment with the centre of the vehicle bogie. This is to ensure that, when curving, the centre of pantograph head does not deviate from the centre of the track more than it is to be expected in face of the vehicle dynamics and all allowed clearances and kinematic gauges [48].

Two alternative approaches are generally used to model the pantograph system, the lumped mass model and the multibody model, [17,49]. Each approach has its advantages and drawbacks, being both models suitable to be used in a multibody system dynamics computational environment. The pantograph multibody model assumes the pantograph described by a set of bodies interconnected by force elements and joint constraints representing the structural and mechanical components of the pantograph. Despite of representing properly the pantograph moving elements, the multibody models developed until now are composed of rigid bodies connected by perfect kinematic joints, which do not allow the model to fully describe the realistic behaviour of the pantograph in its complete operating frequency range [50,51]. Due to the scope of this work a multibody representation of the lumped mass model is

here adopted. This model consists on a series of lumped masses linked sequentially to a ground by spring/damper elements, as represented in Figure 16.8 (b). The masses, $m_{1\text{-}3}$, spring, $k_{1\text{-}3}$, and damping, $c_{1\text{-}3}$, coefficients are parameters identified experimentally in laboratory tests [52,53] in order for the model to have the same frequency response of the real pantograph. Thus, these parameters have no direct physical correspondence with the real pantograph with the exception of the upper stage parameters of m_3, k_3, and c_3 which are matched to the mass, stiffness and damping of the collector suspension. For high speed railway applications, there is a minimal requirement of three lumped mass stages to allow for representation of the dynamic behaviour of the system [54]. Regardless of its simple topology the fidelity of the lumped mass pantograph model in representing the dynamic response of a pantograph is recognised, being an industry standard and commonly used by operators, manufacturers and homologation bodies instead of more complex multibody models. However, note that this work follows the assumption that the dynamic response of the pantograph, identified in laboratory tests, is not affected by the pantograph roll. Although reasonable, as shown in [30], this assumption is to be followed by further research in order to determine the minimal requirements for pantograph models employed in curved tracks.

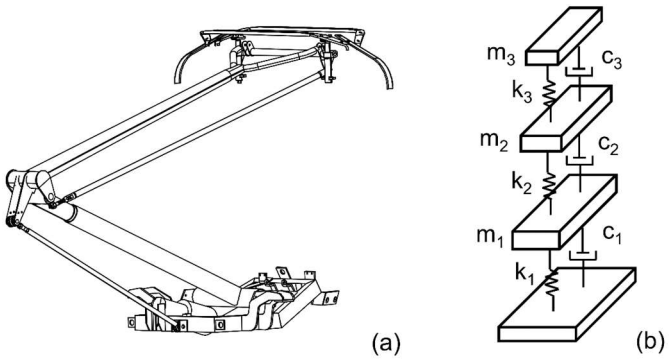

Figure 16.8: Pantograph models: (a) Multibody; and (b) Lumped mass.

16.4.1 Multibody Lumped Mass Pantograph Model

A multibody model is characterized by a set of rigid and/or flexible bodies interconnected by force elements and joints that constrain their relative motion. The equations of motion that represent the multibody lumped mass model here considered are written together with the second time derivative of the constraint equations as [32]:

$$\begin{bmatrix} \mathbf{M} & \boldsymbol{\Phi}_q^T \\ \boldsymbol{\Phi}_q & \mathbf{0} \end{bmatrix} \begin{Bmatrix} \ddot{\mathbf{q}} \\ \boldsymbol{\lambda} \end{Bmatrix} = \begin{Bmatrix} \mathbf{g} \\ \boldsymbol{\gamma} \end{Bmatrix} \tag{16.10}$$

where $\ddot{\mathbf{q}}$ is the vector with the accelerations of the rigid bodies $\boldsymbol{\lambda}$ is the Lagrange multiplier vector associated to the joint reaction forces. The remaining terms are described hereafter.

The detailed representation of the multibody lumped mass model considered for this work is depicted in Figure 16.9. The model is composed by four aligned bodies, $b_{0\text{-}3}$, representing the three staged lumped masses and the pantograph base. Their mass properties, $m_{1\text{-}3}$, are used to form the mass matrix **M** in Equation (16.10). The spatial position and orientation of the bodies are included in vector **q**, which is evaluated by integrating the accelerations resulting from the solution of Equation (16.10) during the dynamic analysis of the pantograph. Vector **q** contains, for each body, a set of Cartesian coordinates with the position of its centre of mass and a set of Euler parameters that define its orientation via a local reference frame, $(\xi,\eta,\zeta)_{0-3}$. The linear spring and damper elements placed in between the masses are formulated as force elements where the forces transmitted to the connected bodies are included in the vector force, **g**. Also included in this vector are the resultant contact force and transport moment, $\mathbf{f}_3^c$ and $\mathbf{n}_3^c$, applied on the lumped mass pantograph top body centre, b_3, and the pantograph static uplift force, $\mathbf{f}_{up}$, applied on the bottom lumped mass body, b_1, which is set to raise the pantograph lumped masses and adjust the resulting average contact force. The kinematic constraints and joints set on the model, along with its respective geometric parameters, are used to form the constraint equations, whose second time derivative includes the Jacobian matrix, $\boldsymbol{\Phi}_q$, and the right-hand side vector, $\boldsymbol{\gamma}$. In the pantograph lumped mass model, to maintain its unidimensional actuation, three prismatic joints, $pris_{1\text{-}3}$, are set between each lumped mass body and the pantograph base such that the motion of the lumped masses is constrained to be along an axis perpendicular to the plane of the pantograph base as also preventing their relative rotation.

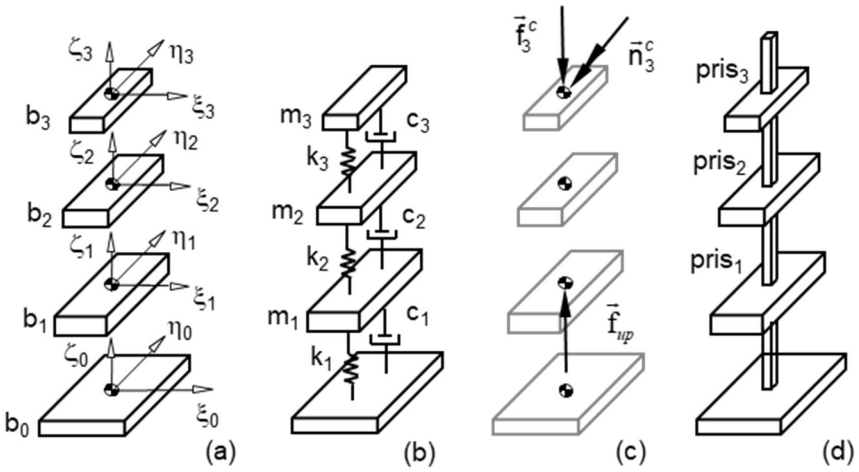

Figure 16.9: Representation of the multibody lumped mass model: (a) Lumped mass bodies; (b) Spring and damper elements; (c) External applied forces; (d) Prismatic constraints.

To set the trajectory of the pantograph along the track path a prescribed kinematic motion constraint is set to the pantograph base body, b_0, where its position, $\mathbf{r}_0$, and orientation, $(\xi,\eta,\zeta)_0$, is set to follow a moving frame correspondent to the trajectory of the pantograph, as represented in Figure 16.10. At a given track length, the position, $\mathbf{r}_p$, and local reference frame, $(\xi,\eta,\zeta)_p$, that define the pantograph trajectory are built in relation to the track moving frame, established in Section 1, such that:

$$\begin{aligned} \mathbf{r}_p &= \mathbf{r}_t + \mathbf{A}_t \mathbf{s}_0'^t \\ \boldsymbol{\xi}_p \equiv \boldsymbol{\xi}_t \;\; ; \;\; \boldsymbol{\zeta}_p \equiv \boldsymbol{\zeta}_t \;\; ; \;\; \boldsymbol{\eta}_p &\equiv \boldsymbol{\eta}_t \end{aligned} \tag{16.11}$$

where $\mathbf{s}_0'^t$ is the coordinate position of the pantograph base relative to the track local reference frame, $(\xi,\eta,\zeta)_t$, which is defined by the position of the vehicle rooftop, in relation to the track running surface. Matrix $\mathbf{A}_t$ is the rotation matrix associated to track local reference frame $(\xi,\eta,\zeta)_t$.

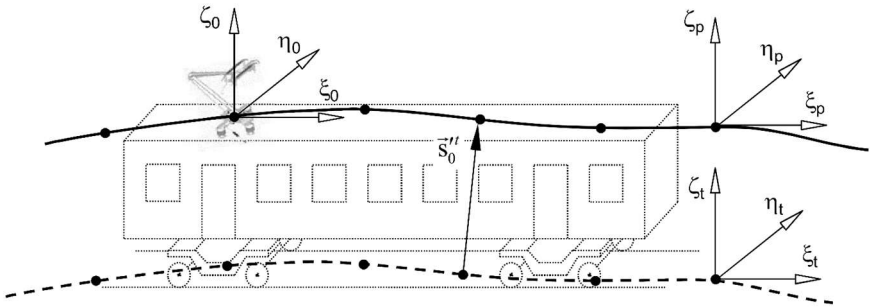

Figure 16.10: Representation of the prescribed kinematic motion constraint set to the pantograph base.

Note that, in the work presented here, the trajectory of pantograph follows that of the train carbody roof where the pantograph is mounted, which in turn is that of the vehicle that directly follows the track. Using the same methodology, it is possible to include vehicle vibrations by adding them to the pantograph prescribed moving frame. However, it has been shown that track irregularities do not lead to perturbations on the pantograph motion worth accounting for [55].

16.5 Pantograph-Catenary Interaction

The dynamics analysis of the pantograph-catenary interaction represents a coupled problem in which the dynamic behaviour of the two sub-systems is affected by each other. The classical and most direct methodology to solve this coupling problem is to use the same formulation for both models, such as in the case of pantograph-catenary interaction where the equations of motion of a lumped mass pantograph are added to the finite element equations of the catenary [31]. With the finite element approach described, it is not possible to model the pantograph

motion in any other type of operation than its motion in straight track. This is unless additional information to set the pantograph absolute position and orientation in relation to the lumped mass nodal displacements is provided as proposed in [30]. In this work, due to the requirements that each formulation needs to fulfil when dealing with generalized trajectories of the track, a simple formulation is used for each one of the sub-systems, i.e., the finite element method for the catenary and the multibody dynamics formulation for the pantograph. To couple both sub-systems, a co-simulation environment is setup where the dynamic analysis of each sub-system is done independently [35,56]. Generally, in co-simulation the coupling is either described by imposing a kinematic constraint between the models or by defining a set of constitutive interaction laws [57]. For the pantograph-catenary co-simulation procedure presented here, the latter coupling approach is used, where the constitutive interaction laws lead to contact forces, which in turn result in a set of forces/torques applied on each sub-system. A penalty force methodology is used here to represent the interaction, i.e., to evaluate the contact force between the pantograph and the catenary.

16.5.1 Pantograph-Catenary Contact Model

From the contact mechanics point of view, the contact between the pantograph contact strip and the catenary contact wire is physically a contact between a flat surface, made of carbon, and a cylinder surface, made of a copper alloy, as represented in Figure 16.11. Due to the nature of the contact between both types of materials and contact surfaces, the sliding friction forces are neglected, being only the normal contact force, perpendicular to the flat surface of the contact strip considered in this work.

For the penalty formulation used here, the contact force evaluation is dependent on the contact geometry. In this sense, consider the contact geometry presented in Figure 16.11 where points *a* and *b* represent the extremities of the top surface of the pantograph contact strip. The point positions, $\mathbf{r}_a$ and $\mathbf{r}_b$, are evaluated as:

$$\begin{aligned} \mathbf{r}_a &= \mathbf{r}_3 + \mathbf{A}_3\mathbf{s}_a'^3 \quad ; \quad \mathbf{s}_a'^3 = \begin{bmatrix} 0 & -l_{cs}/2 & 0 \end{bmatrix}^T \\ \mathbf{r}_b &= \mathbf{r}_3 + \mathbf{A}_3\mathbf{s}_b'^3 \quad ; \quad \mathbf{s}_b'^3 = \begin{bmatrix} 0 & l_{cs}/2 & 0 \end{bmatrix}^T \end{aligned} \tag{16.12}$$

where $\mathbf{r}_3$ is the global coordinate position of the lumped mass pantograph top body and $\mathbf{A}_3$ is the rotation matrix associated to its local reference frame $(\xi,\eta,\zeta)_3$. Vector $\mathbf{s}_a'^3$ and $\mathbf{s}_b'^3$ are correspondingly the positions of points *a* and *b* relative to the body local reference frame, evaluated as:

$$\mathbf{s}_a'^3 = \begin{bmatrix} 0 & -l_{cs}/2 & 0 \end{bmatrix}^T$$
$$\mathbf{s}_b'^3 = \begin{bmatrix} 0 & l_{cs}/2 & 0 \end{bmatrix}^T \tag{16.13}$$

being l_{cs} the length of the pantograph contact strip.

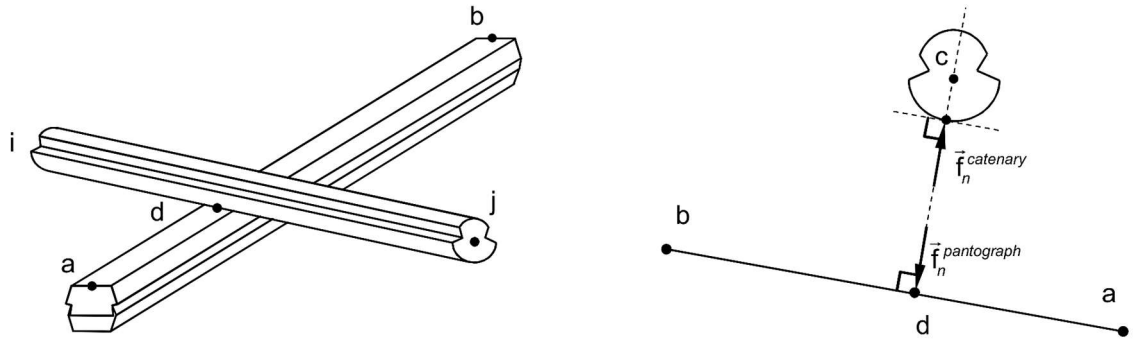

Figure 16.11: Representation of the pantograph-catenary contact geometry.

Point *c* is the position of the centre of the contact wire cross section, which includes the candidate contact point on the catenary. As the catenary geometry is described in a finite element formulation, point *c* belongs to one of the catenary finite elements that is connected to nodes *i* and *j*, as represented in Figure 16.12 (a). Therefore, the coordinate position of *c*, $\mathbf{r}_c$, is evaluated as:

$$\mathbf{r}_c = \mathbf{r}_c^0 + \mathbf{N}(\xi)[\mathbf{d}_i \quad \mathbf{d}_j]$$
$$\mathbf{r}_c^0 = \mathbf{r}_i^0 + \xi(\mathbf{r}_j^0 - \mathbf{r}_i^0) \tag{16.14}$$

where $\mathbf{d}_i$ and $\mathbf{d}_j$ are the node displacements of the contact wire finite element and $\mathbf{r}_c^0$ refers to the corresponding position of *c*, c^0, in the undeformed finite element mesh of the catenary, such that:

$$\mathbf{r}_c^0 = \mathbf{r}_i^0 + \xi(\mathbf{r}_j^0 - \mathbf{r}_i^0) \tag{16.15}$$

Matrix **N**(ξ) contains the beam element shape functions, [58], evaluated at the parametric length coordinate of the finite element, ξ, in which the contact takes place with correspondence to point *c*. The parametric coordinate, ξ, is obtained by finding the intersection between the lines defined by points *a* and b and points i and j, when projected on the same plane. For convenience, as represented in Figure 16.12 (b), the *xy* plane is used here. The interception between both lines of the contact strip and of the contact wire is expressed as:

$$\mathbf{r}_i^{xy} + \hat{\mathbf{u}}_{ij}^{xy}\lambda_{ic}^{xy} = \mathbf{r}_a^{xy} + \hat{\mathbf{u}}_{ab}^{xy}\lambda_{ac}^{xy} \tag{16.16}$$

where the superscript *xy* denotes here the projection on the *xy* plane and $\hat{\mathbf{u}}_{mn}$ is the versor of a generic vector that goes from node *m* to node *n*. The scalar values λ_{ic}^{xy} and λ_{ac}^{xy} are the distance between points *i* and *c* and points *a* and *c* in the *xy* plane. These can be obtained by solving equation (16.16) from which the parametric coordinate ξ can be evaluated as:

$$\xi = \frac{\lambda_{ic}^{xy}}{\left\| \mathbf{r}_j^{xy} - \mathbf{r}_i^{xy} \right\|} \tag{16.17}$$

where $\xi \in [0,1]$. If $\xi \notin [0,1]$ the catenary finite element considered does not fit the contact geometry and another element along the contact wire must be tested for contact.

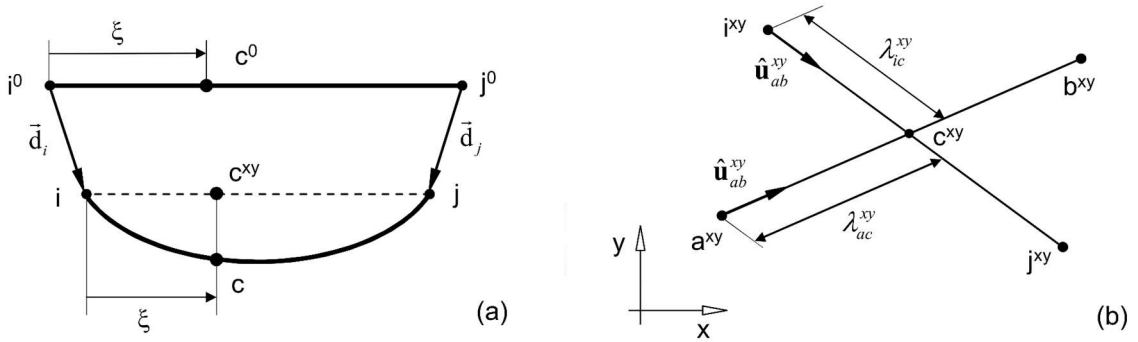

Figure 16.12: (a) Representation of the contact wire finite element in which contact occurs; (b) Contact geometry on *xy* plane.

In Figure 16.11 (a), point *d* represents the contact point on the contact strip surface which is geometrically determined by assuming that the normal contact force, $\mathbf{f}_n$, and its corresponding pseudo penetration are perpendicular to both the flat surface of the contact strip and the contact wire cylindrical contact surface. As point *c* is collinear with *a* and *b*, its coordinate position is obtained as:

$$\begin{aligned} \mathbf{r}_d &= \mathbf{r}_a + \lambda_{ad}\hat{\mathbf{u}}_{ab} \\ \lambda_{ad} &= \hat{\mathbf{u}}_{ab} \cdot \mathbf{r}_{ac} = \hat{\mathbf{u}}_{ab} \cdot (\mathbf{r}_c - \mathbf{r}_a) \end{aligned} \tag{16.18}$$

such that λ_{ad} is the length between point *a* and *d* which can be retrieved as the scalar projection between the versor $\hat{\mathbf{u}}_{ab}$ and vector $\mathbf{r}_{ac}$ that goes from point *a* to *c*:

$$\lambda_{ad} = \hat{\mathbf{u}}_{ab}^T \mathbf{r}_{ac} = \hat{\mathbf{u}}_{ab}^T (\mathbf{r}_c - \mathbf{r}_a) \tag{16.19}$$

With the contact geometry established, the normal contact force, f_n, is obtained by using a purely elastic Hertzian normal contact force model, written as:

$$f_n = \begin{cases} K\delta \ , & \delta > 0 \\ 0 \ , & \delta \le 0 \end{cases} \tag{16.20}$$

where K is the contact stiffness (200x10^3 N/m), $\delta = \left\| \mathbf{r}_c - \mathbf{r}_d \right\| - r_{cw}$ is the pseudo normal penetration and r_{cw} is the contact wire radius. In this work the contact stiffness used is 200×103 N/m, set from the recommendations for key parameters on pantograph-catenary numerical models established in the PantoTRAIN European project [54].

As the contact surface of the contact wire is concentric with its cross section centre, the normal contact force is directly applied in point *c*, being the equivalent contact forces and moments, $\mathbf{f}_i^c$ and $\mathbf{f}_j^c$, applied at nodes *i* and *j* of the contact wire finite element, evaluated as:

$$\begin{bmatrix} \mathbf{f}_i^c \\ \mathbf{f}_j^c \end{bmatrix} = \mathbf{N}(\xi)^T f_n \hat{\mathbf{u}}_{dc} \tag{16.21}$$

On the contact strip the normal force is applied on point *d* such that the resultant force and transport moment, $\mathbf{f}_3^c$ and $\mathbf{n}_3^c$, to be applied on the lumped mass pantograph top body mass centre are evaluated as:

$$\begin{aligned} \mathbf{f}_3^c &= f_n \hat{\mathbf{u}}_{cd} \\ \mathbf{n}_3^c &= \tilde{\mathbf{s}}_d'^3 \, \mathbf{A}_3^T \mathbf{f}_3^c \end{aligned} \tag{16.22}$$

where $\mathbf{s}_d'^3$ is the position of point *d* relative to the top body local reference frame $(\xi, \eta, \zeta)_3$.

16.5.2 Pantograph-Catenary Co-Simulation

The catenary is modelled with a finite element formulation being a dynamic linear system integrated with a Newmark family numerical integrator set implicitly with fixed time step [59]. The multibody pantograph model nonlinear dynamics is evaluated as a forward dynamics problem being its solution obtained with a variable time step and variable order numerical integrator of the Gear type [60]. In the co-simulation procedure implemented here, each sub-system performs its dynamic evaluation independently from the other. In order that each sub-system can proceed with its integration procedure the state variables of each subsystem are shared. Since the contact evaluation needs to access the deformed finite element mesh of the catenary to search for contact along the catenary wire, the contact is evaluated on the finite element dynamic solver, on the catenary side. To this effect, as depicted in Figure 16.13 the state variables supplied by the multibody code in which the pantograph is defined, are the position of the contact strip extremities, $\mathbf{r}_a$ and $\mathbf{r}_b$. With these coordinates, the catenary

subsystem evaluates the contact and returns, as its state variables, the resulting contact force vector, $\mathbf{f}_c$, and its point of application $\mathbf{r}_c$ on the collector strip.

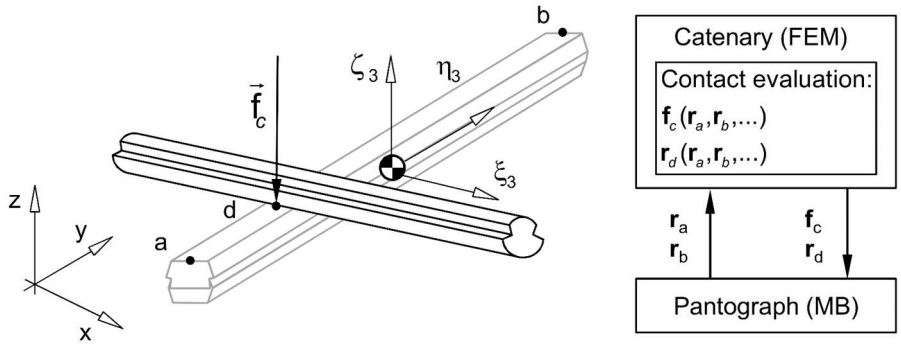

Figure 16.13: State variable exchange between catenary and pantograph subsystems.

The compatibility between the heterogeneous integration procedures imposes that the state variables, or a reliable prediction, are readily available at each evaluate time step. This is guaranteed by a state variable time interpolation/extrapolation scheme presented in Figure 16.14. The accuracy and stability of this procedure relies on the integration step used on both systems and in ensuring that the maximum time step size of the multibody pantograph subsystem never exceeds the catenary fixed time step [35,61].

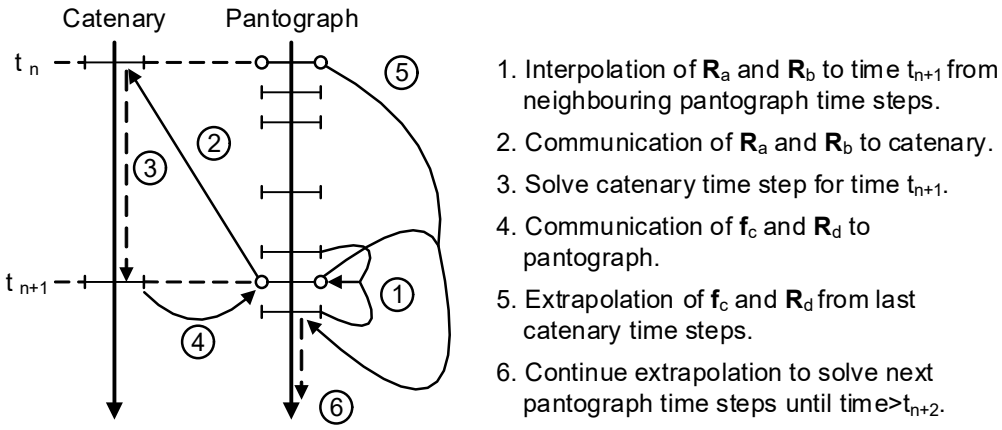

Figure 16.14: Sate variable time interpolation/extrapolation in pantograph-catenary co-simulation.

16.6 Case Studies

To demonstrate the approach proposed here to handle the pantograph-catenary dynamics for general geometry railway tracks, two case scenarios are considered. One is a realistic case where the catenary complete layout and track geometry are obtained through the project data of a catenary line that is currently in operation. The second case is an exercise following the insertion of a catenary model in tracks with different curvature. In both cases the pantograph-catenary contact quality is evaluated through the statistical analysis of the developed contact

forces filtered at 0-20 Hz, following the standards EN50367 and EN50119. Also, as both catenary system used here are designed for high speed operation, all the simulations consider a vehicle speed of 300 km/h, where the pantograph uplift force is tuned for a mean contact force of 157.3 N on a straight track.

16.6.1 Existing Catenary Network

Since the procedure presented here is able to cope with any generalised trajectory of the track, the first case study concerns a realistic catenary associated to the track geometry, described in Figure 16.15. The catenary layout and specifications are taken directly from the technical plans of a catenary system in current operation. The pantograph model is that of the overhead equipment commonly used for high speed trains in operation on the track.

Both the general catenary design characteristics and pantograph lumped mass parameters are presented in Table 16.2. The technical designs establish no pre-sag in this catenary system and for the track interval considered here a constant alternating stagger of (+200,-200) mm is specified.

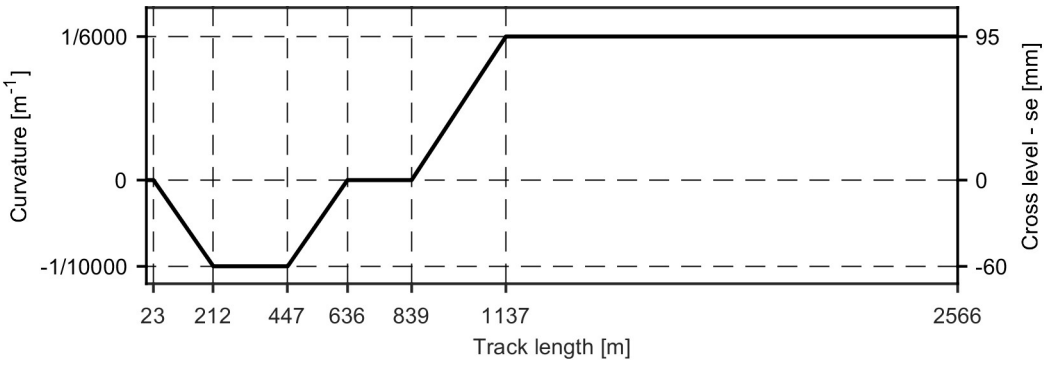

Figure 16.15: Track geometry considered on the realistic case.

The track geometry is characterised by two curves, with a straight segment in between, where two catenary sections are defined. A representation of the resulting catenary finite element mesh of the catenary system, after being statically loaded, is presented in Figure 16.16.

Catenary		Pantograph	
Contact wire tension [N]	20000	m1 [kg]	5.58
Messenger wire tension [N]	16250	m2 [kg]	8.78
Contact wire height [m]	5.3	m3 [kg]	7.75
Encumbrance [m]	1.25	k1 [N/m]	178.45
Stagger [mm]	(+200,-200)	k2 [N/m]	15487.00
Span lengths [m]	60-52	k3 [N/m]	7000.00
Damping α [1/s]	0.0125	c1 [Ns/m]	108.39
Damping β [s]	0.0001	c2 [Ns/m]	0.09
Vehicle roof top height [m]	4.05	c3 [Ns/m]	45.85

Table 16.2: Catenary and pantograph model specifications.

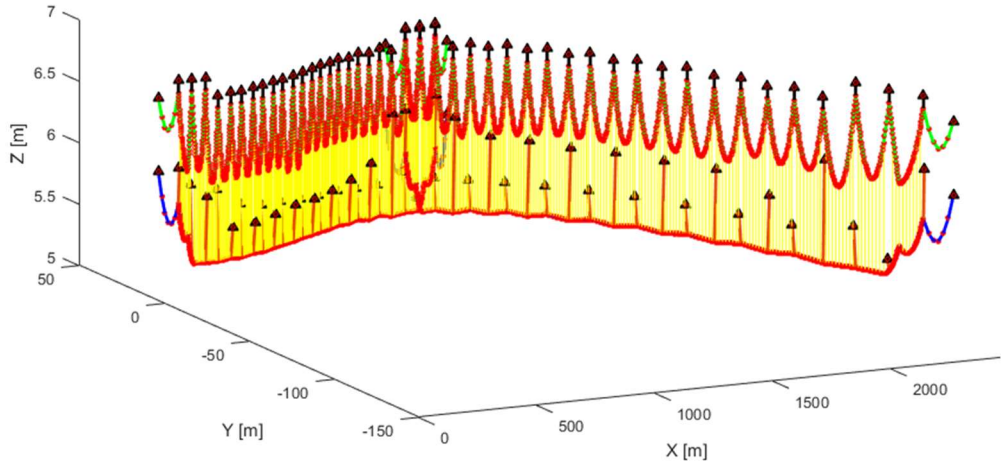

Figure 16.16: Representation of the deformed finite element catenary mesh for different.

Two regions of interest are selected for the analysis of the catenary: one on the straight section of the track; and other on the curved section with a 6000 m radius track, being an interval containing 2 spans considered. The contact quality parameters associated to the contact forces and the steady arm uplifts are presented in Table 16.3.

Track	Straight	R6000	Limit Values
Track Interval [m]	642-757	1833-1945	
Force maximum [N]	253.1	275.5	350
Force minimum [N]	80.2	90.0	-
Force amplitude [N]	172.9	185.6	-
Force mean [N]	157.3	156.9	157.3
Force standard deviation [N]	30.4	34.7	47.1
Force statistical minimum [N]	66.1	52.8	-
Steady arm uplift (642m,1833m) [m]	0.079	0.081	0.16
Steady arm uplift (702m,1889m) [m]	0.079	0.070	0.16
Steady arm uplift (757m,1945m) [m]	0.075	0.081	0.16

Table 16.3: Contact force statistics for the contact quality evaluation considering force and steady arm uplift.

Although the results cannot be directly compared since the spans have all different lengths, it can be observed that a marginal contact quality degradation occurs on the curved section. This is noted by the slightly higher standard deviation and contact force maximum. Nevertheless, all parameters are under their allowable limits. Moreover, by observing the contact forces developed along the track, presented in Figure 16.17, on the curved track it is possible to notice an alternating difference on the maximum peaks. These are found slightly before the pantograph passage over the cantilever supports and its effects can be related to the differences found on the steady arm uplifts. Note also that the higher maximum peaks coincide with the lateral offsets located in the inner side of the curved track.

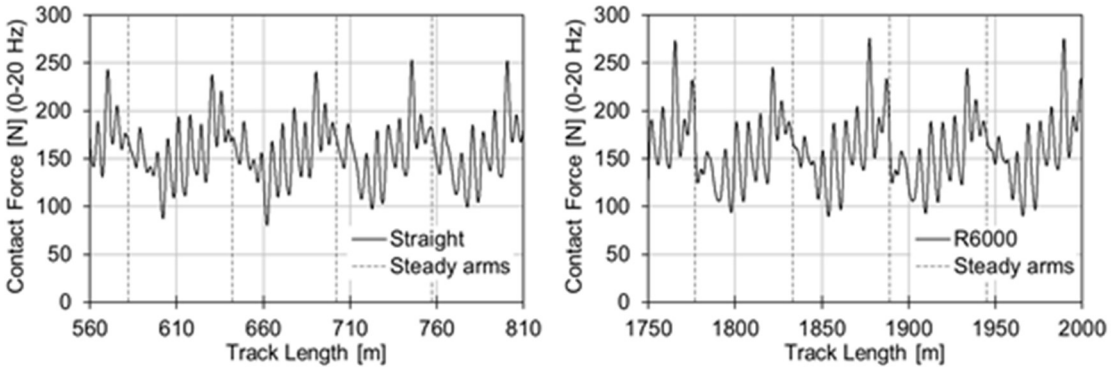

Figure 16.17: Contact force evaluated along the track length.

16.6.2 Curve Insertion Case

The catenary and pantograph models chosen for this application case are the models presented on the pantograph catenary benchmark [24]. Their main specifications are presented in Table 16.4.

Catenary		Pantograph	
Contact wire tension [N]	22000	m1 [kg]	6
Messenger wire tension [N]	16000	m2 [kg]	9
Contact wire height [m]	5.3	m3 [kg]	7.5
Encumbrance [m]	1.2	k1 [N/m]	160
Stagger [mm]	(+200,-200)	k2 [N/m]	15500
Span lengths [m]	55	k3 [N/m]	7000
Damping α [1/s]	0.0125	c1 [Ns/m]	100
damping β [s]	0.0001	c2 [Ns/m]	0.1
Vehicle roof top height [m]	4.05	c3 [Ns/m]	45

Table 16.4: Benchmark catenary and pantograph model specifications.

Three different track geometries are considered to insert the catenary model: a straight line; and, two scenarios that start as a straight track and transition to respectively a curved track with a 6000 m and 4000 m and a cross level of 110 mm and 160 mm. Each catenary as a total of 22 spans, being the starting straight portion on the curved tracks composed by 4 spans, followed by 5 spans of transition. Although the track with a 4000 m curve radius is a tight curve for the operating speed considered, all the track geometries here are compliant with the European standard EN13803-1. Four catenary system setups with different staggers are considered. Three setups have an alternating stagger of (+200,-200) mm and are set along each of the specified track paths. In the fourth setup, a stagger of (+200,0) mm on the curved portion of the 4000 m radius curved track is considered. A representation of the resulting catenary finite element meshes, after being statically loaded, is presented in Figure 16.18.

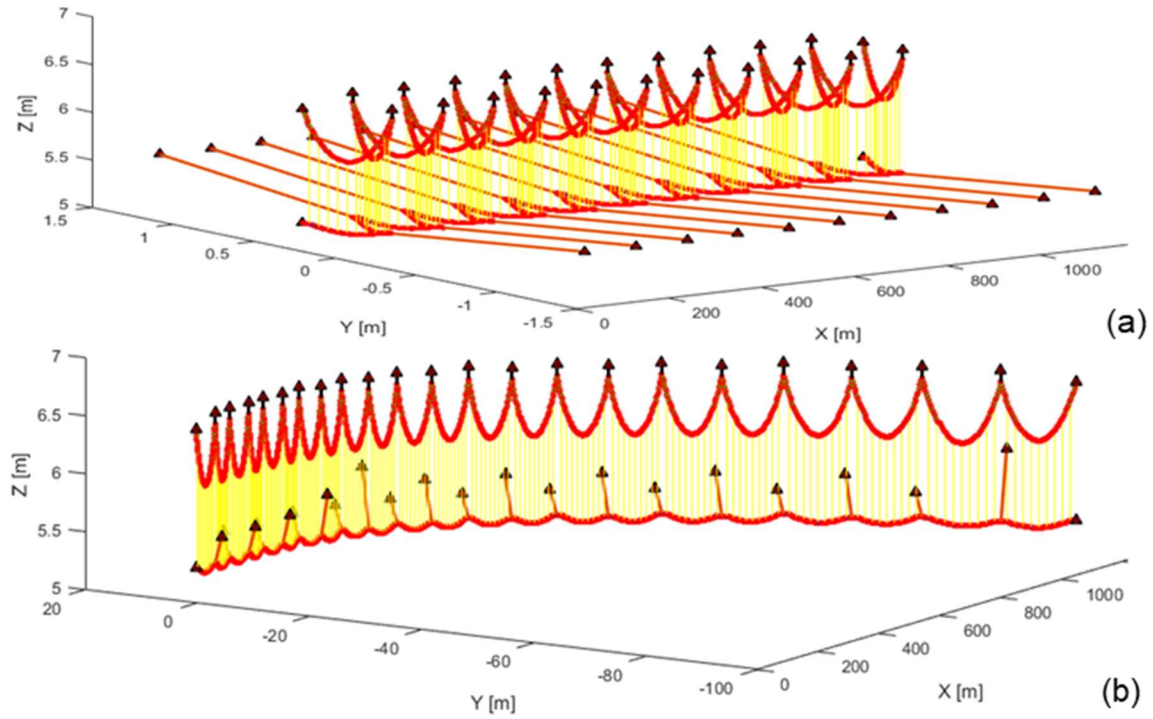

Figure 16.18: Representation of the deformed finite element catenary mesh for different staggers: a) Straight track (+200,-200) mm , b) Track with 4000m curve (+200,0) mm.

The statistical parameters resulting from the contact force evaluation on each of the catenary systems and the steady arm uplifts are presented in Table 16.5. The region of interest set for the analyses [660m-770m] contains two spans where its centre cantilever corresponds to the imposed offset on the inner side of the curve. Comparing the results obtained between the straight catenary and the catenary inserted in the largest radius curved track, only marginal differences can be found. However, these show a slight tendency to contact quality degradation, which becomes clear when observing the results for the smaller radius curved track with the same stagger. Here, although the mean contact force remains close to its target, both the maximum force and standard deviation increase exceeding the standard limits. The negative force statistical minimum is indicative of probability of loss of contact, which is verified in the unfiltered results with a percentage of loss of contact of 4%.

When changing the staggering to (+200,0) mm in the 4000 m radius curved track, the contact quality is greatly improved returning to nominal operating levels. The evolution of the contact forces along the track is presented in Figure 16.19 for the different scenarios. The maximum force peaks are observed with the pantograph passage under the cantilevers in correspondence with the evaluated steady arm uplifts.

When changing the staggering to (+200,0) mm in the 4000 m radius curved track, the contact quality is greatly improved returning to nominal operating levels. The evolution of the

contact forces along the track is presented in Figure 16.19 for the different scenarios. The maximum force peaks are observed near the pantograph passage under the cantilevers in correspondence with the evaluated steady arm uplifts.

Track	Straight	R6000	R4000	R4000	Limit Values
Stagger [mm]	(+200,-200)	(+200,-200)	(+200,-200)	(+200,0)	
Force maximum [N]	254.3	252.8	425.1	243.9	350
Force minimum [N]	90.7	94.1	29.5	88.4	-
Force amplitude [N]	163.6	158.7	395.7	155.5	-
Force mean [N]	157.3	156.8	156.6	156.0	157.3
Force standard deviation [N]	40.3	40.8	62.1	38.0	47.1
Force statistical minimum [N]	34.6	33.3	-23.5	40	-
Steady arm uplift (660m) [m]	0.047	0.049	0.063	0.047	0.16
Steady arm uplift (715m) [m]	0.047	0.049	0.033	0.053	0.16
Steady arm uplift (770m) [m]	0.047	0.050	0.062	0.049	0.16

Table 16.5: Contact force statistical evaluation and steady arm uplifts.

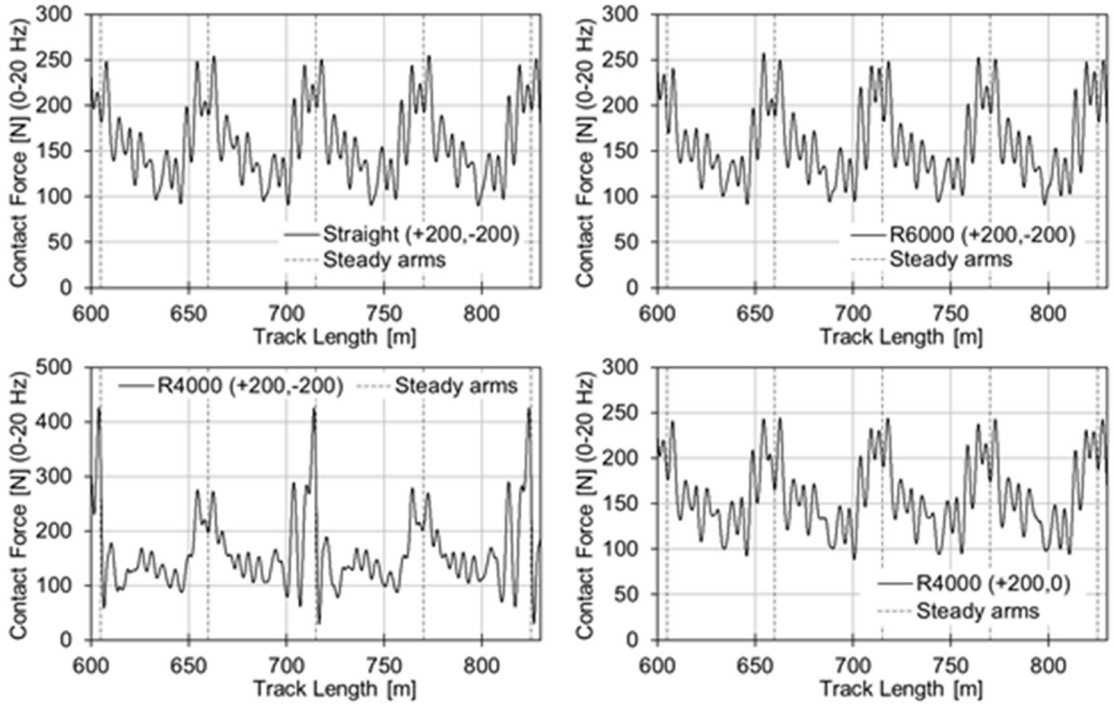

Figure 16.19: Contact force evaluated along the track length.

In the catenary associated to the curved track with 4000 m radius and a (+200,-200) mm stagger it is possible to distinguish force peaks according the offset imposed on each support. The higher force peaks correspond to the offset imposed on the inner side of the curve. These stiff spots are due to the orientation of the steady arm which is controlled by the forces due to the contact wire, as represented in Figure 16.20. The steady arm orientation is defined by its resulting angle, θ, with the horizontal plane. The force on the steady arm, $\mathbf{f}_r$, can be decomposed in a lateral force component associated to the imposed contact wire stagger, $\mathbf{f}_{lat}$,

and a vertical force component, $\mathbf{f}_z$, that supports a residual part of the contact wire weight and set is vertical position correctly.

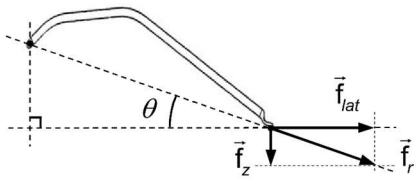

Figure 16.20: Contact wire force solicitations at the steady arm.

The vertical force component does not change greatly from pole to pole being the orientation of the steady arm mainly dictated by the lateral forces which in turn depend on the imposed offsets at each cantilever. Figure 16.21, shows the lateral forces developed at each cantilever and the resulting steady arm orientation angle for each of the cases considered here. The positive lateral forces refer to the forces acting away from the pole being negative when acting towards the pole defining the cantilever pull-off or push-off configuration. Notice that these lateral forces remain constant on the straight catenary but in the curved tracks present an offset from pole to pole. It is also possible to observe how this offset develops on the curve transition.

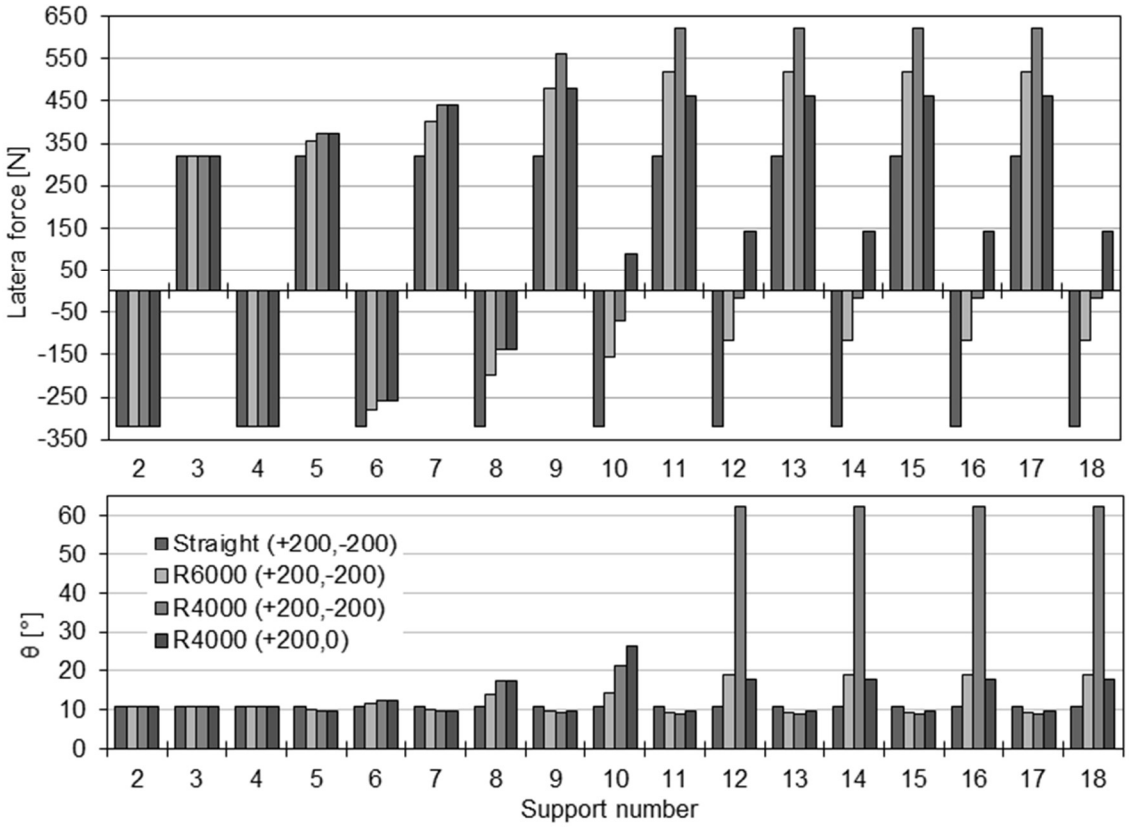

Figure 16.21: Lateral forces and resulting steady arm angle at each cantilever support.

The small lateral forces on the inner side of the curved track with 4000 m radius and a (+200,-200) mm stagger are very low which results in an excessive rotation angle of the steady arm of about 62°. Consequently, this originates a critical stiff spot for the pantograph passage, which turns to be the main cause for the observed degradation of the contact quality. This is in agreement with the requisites described in [43] which establish a minimal lateral force of 80N and a maximum angle of the steady arm of 20°. By changing the staggering to (+200,0) mm these requisites are fulfilled and the contact quality is improved. Also notice that in the curved portion of the track, the lateral forces become positive on all the poles meaning that all the cantilevers are to be set in a pull-off configuration, as it can be observed by the steady arm orientations represented in Figure 16.18 (b).

16.7 Conclusions

A novel numerical procedure for the dynamic analysis of pantograph–catenary interaction on generalized track trajectories is presented here. The geometric description of the track running surface by a moving local frame of reference is the basis to build the catenary finite element model and to describe the general path of the pantograph. Two demonstration cases are presented, one represents an existing scenario where both the catenary layout and track geometry are obtained from the technical designs of a current track in operation. The other case study presents a variation on the benchmark study of pantograph–catenary interaction by defining it in tracks with different curve radius and contact wire staggering. It is shown that for large curve radius tracks the contact quality is marginally affected by the curvature. For smaller radius curves, the staggering design plays a fundamental role in maintaining the contact quality.

The first main contribution of the numerical tool presented here is the possibility to analyse more realistic catenary systems which are modelled using track and catenary design data of already constructed or projected railway lines, not being limited to straight tracks. It also provides a methodology to study the pantograph–catenary dynamics over curved tracks including the influence of the staggering design. Moreover, this approach opens the possibility to analyse novel case studies of interest to the rail industry. One is the influence of wind loads on the pantograph-catenary contact quality in curved tracks, where the wind solicitations imply a change on the lateral forces imposed by the contact wire at its cantilever support. There are also cases where optimisation procedures in conjunction with pantograph-catenary dynamic analysis applications can be used to reach optimised designs of pantograph or catenary systems. In such cases, considering the optimisation only in straight tracks might be limitative when

contemplating a generalised track path. One other aspect of interest is the analysis of pantograph-catenary interaction over tracks with small radius curves, particularly on railway tracks that are to be upgraded for higher operational speeds, which often require a change on the contact and messenger wire axial tension, as well as the catenary layout geometry.

References

[1] Shing AWC, Wong PPL. Wear of pantograph collector strips. J. Rail Mass Transit. 2008;222:169–176.
[2] ERRAC. Strategic Rail Research Agenda 2020. Brussels, Belgium; 2007.
[3] EC - European Commission. Roadmap to a Single European Transport Area - Towards a Competitive and Resource Efficient Transport System. Brussels, Belgium, Belgium; 2011.
[4] Poetsch G, Evans J, Maisinger R, et al. Pantograph/Catenary Interaction and Control. Veh. Syst. Dyn. 1997;28:159–195.
[5] Ikeda K. Optimization of Overhead Contact Lines for Shinkansen Speed Increases. JR EAST Tech. Rev. 12th ed. 2008;64–69.
[6] Pombo J, Antunes P. A Comparative Study Between Two Pantographs In Multiple Pantograph High-Speed Operations. Internatinal J. Railw. Technol. 2013;2:83–108.
[7] Liu Z, Jönsson PA, Stichel S, et al. Implications of the operation of multiple pantographs on the soft catenary systems in Sweden. Proc. Inst. Mech. Eng. Part F J. Rail Rapid Transit. 2016;230:971–983.
[8] Bucca G, Carnevale M, Collina A, et al. Adoption of different pantographs preloads to improve multiple collection and speed up existing lines. Veh. Syst. Dyn. 2012;50:403–418.
[9] Antunes P, Ambrósio J, Pombo J, et al. Dynamic Analysis of the Pantograph-Catenary Interaction on Overlap Sections for High-Speed Railway Operations. Proc. Second Int. Conf. Railw. Technol. Res. Dev. Maint. Stirlingshire, UK: Civil-Comp Press; 2014.
[10] Harèll P, Drugge L, Reijm M. Study of Critical Sections in Catenary Systems During Multiple Pantograph Operation. Proc. Inst. Mech. Eng. Part F J. Rail Rapid Transit. 2005;219:203–211.
[11] Mei G, Zhang W, Zhao H, et al. A hybrid method to simulate the interaction of pantograph and catenary on overlap span. Veh. Syst. Dyn. 2006;44:571–580.
[12] Ambrósio J, Pombo J, Pereira M, et al. Optimization of high-speed railway pantographs for improving pantograph-catenary contact. Theor. Appl. Mech. Lett. 2013;3.
[13] Gregori S, Tur M, Nadal E, et al. An approach to geometric optimisation of railway catenaries. Veh. Syst. Dyn. 2017;3114:1–25.
[14] Bruni S, Bucca G, Collina A, et al. Numerical and Hardware-In-the-Loop Tools for the Design of Very High Speed Pantograph-Catenary Systems. J. Comput. Nonlinear Dyn. 2012;7:041013.
[15] Van OV, Massat JP, Laurent C, et al. Introduction of variability into pantograph-catenary dynamic simulations. Veh. Syst. Dyn. 2014;52:1254–1269.
[16] Carnicero A, Jimenez-Octavio JR, Sanchez-Rebollo C, et al. Influence of Track Irregularities in the Catenary-Pantograph Dynamic Interaction. J. Comput. Nonlinear Dyn. 2012;7:041015.
[17] Pombo J, Ambrósio J, Pereira M, et al. Influence of the Aerodynamic Forces on the Pantograph-Catenary System for High Speed Trains. Veh. Syst. Dyn. 2009;47:1327–1347.
[18] Kulkarni S, Pappalardo CM, Shabana AA. Pantograph/Catenary Contact Formulations. J. Vib. Acoust. 2016;139:011010.
[19] Song Y, Liu Z, Wang H, et al. Nonlinear analysis of wind-induced vibration of high-speed railway catenary and its influence on pantograph–catenary interaction. Veh. Syst. Dyn. 2016;54:723–747.
[20] Facchinetti A, Bruni S. Hardware-in-the-loop hybrid simulation of pantograph–catenary interaction. J. Sound Vib. 2012;331:2783–2797.
[21] Schirrer A, Aschauer G, Talic E, et al. Catenary emulation for hardware-in-the-loop pantograph testing with a model predictive energy-conserving control algorithm. Mechatronics. 2017;41:17–28.
[22] Ambrósio J, Antunes P, Pombo J, et al. A Computational Procedure for the Dynamic Analysis of the Catenary-Pantograph Interaction in High-Speed Trains. J. Theor. Appl. Mech. 2012;50:681–699.
[23] Nåvik P, Rønnquist A, Stichel S. Identification of system damping in railway catenary wire systems from full-scale measurements. Eng. Struct. 2016;113:71–78.
[24] Bruni S, Ambrosio J, Carnicero A, et al. The results of the pantograph–catenary interaction benchmark. Veh. Syst. Dyn. 2014;53:412–435.
[25] Facchinetti A, Bruni S. Special issue on the pantograph–catenary interaction benchmark. Veh. Syst. Dyn. 2015;53:303–304.

[26] Ambrósio J, Pombo J, Antunes P, et al. PantoCat statement of method. Veh. Syst. Dyn. 2015;53:314–328.
[27] Teichelmann G, Schaub M, Simeon B. Modelling and simulation of railway cable systems. ZAMM Zeitschrift fur Angew. Math. und Mech. 2005;85:864–877.
[28] Tur M, García E, Baeza L, et al. A 3D absolute nodal coordinate finite element model to compute the initial configuration of a railway catenary. Eng. Struct. 2014;71:234–243.
[29] Rønnquist A, Nåvik P. Dynamic assessment of existing soft catenary systems using modal analysis to explore higher train velocities: A case study of a Norwegian contact line system. Veh. Syst. Dyn. 2015;53:756–774.
[30] Nåvik P, Rønnquist A, Stichel S. Variation in predicting pantograph–catenary interaction contact forces, numerical simulations and field measurements. Veh. Syst. Dyn. 2017;55:1265–1282.
[31] Ambrósio J, Pombo J, Pereira M, et al. Recent Developments in Pantograph-Catenary Interaction Modelling and Analysis. Int. J. Railw. Technol. 2012;1:249–278.
[32] Nikravesh PE. Computer-Aided Analysis of Mechanical Systems. Englewood Cliffs, New Jersey: Prentice-Hall; 1988.
[33] Ambrósio J, Antunes P, Pombo J. On the Requirements of Interpolating Polynomials for Path Motion Constraints. In: Kecskeméthy A, Geu Flores F, editors. Mech. Mach. Sci. Springer International Publishing; 2015. p. 179–197.
[34] Pombo J, Ambrósio J. General Spatial Curve Joint for Rail Guided Vehicles: Kinematics and Dynamics. Multibody Syst. Dyn. 2003;9:237–264.
[35] Ambrósio J, Pombo J, Rauter F, et al. A Memory Based Communication in the Co-Simulation of Multibody and Finite Element Codes for Pantograph-Catenary Interaction Simulation. In: Bottasso C.L. E, editor. Multibody Dyn. Dordrecht, The Netherlands: Springer; 2008. p. 211–231.
[36] Esveld C. Modern Railway Track. Duisburg, Germany: MRT-Productions; 1989.
[37] Yamaguchi F. Curves and Surfaces in Computer Aided Geometric Design. Springer-Verlag; 1988.
[38] Mortenson ME. Geometric Modeling. New York, New York: Wiley; 1985.
[39] Iverson W. Analysis of the Reconstruction of Rail Geometry from Curvature Data. IEEE Trans. Ind. Appl. 1974. p. 368–379.
[40] Pombo J, Ambrósio J. Modelling Tracks for Roller Coaster Dynamics. Int. J. Veh. Des. 2007;45:470–500.
[41] Przemieniecki JS. Theory of Matrix Structural Analysis. New York: McGraw-Hill; 1968.
[42] UIC 606-1 OR standart. Consequences of the application of the kinematic gauges defined by UIC leaflets in the 500 series on the design of the contact lines. UIC; 1987.
[43] Friedrich K, Puschmann R, Schmieder A, et al. Contact Lines for Electric Railways: Planning, Design, Implementation, Maintenance. 3rd ed. Publicis; 2018.
[44] TSI ENE. Technical specifications for interoperability relating to the ‘energy’ subsystem of the rail system in the Union. Official Journal of the European Union. 1301/2014/EU; 2014.
[45] ERA - European Rail Agency. Study on Interface EURO/1950 pantographs and OCL design - ERA/2013/INTEROP/OP/01. European Union; 2013.
[46] Rayleigh JWS. The Theory of Sound, Volume One. 2nd ed. Dover Publications; 2013.
[47] Arora JS. Introduction to Optimum Design. 3ed. Boston: Academic Press; 2012.
[48] EN 15273-1: Railway applications - Gauges - Part 1: General - Common rules for infrastructure and rolling stock. Brussels, Belgium: CENELEC; 2013.
[49] Pombo J, Ambrósio J. Influence of pantograph suspension characteristics on the contact quality with the catenary for high speed trains. Comput. Struct. 2012;110–111:32–42.
[50] Flores P. Kinematics and dynamics of multibody systems with imperfect joints : models and case studies. Lect. notes Appl. Comput. Mech. Berlin: Springer; 2008.
[51] Ambrósio J, Verissimo P. Improved Bushing Models for General Multibody Systems and Vehicle Dynamics. Multibody Syst. Dyn. 2009;22:341–365.
[52] Collina A, Bruni S. Numerical Simulation of Pantograph-Overhead Equipment Interaction. Veh. Syst. Dyn. 2002;38:261–291.
[53] Vyasarayani CP, Uchida T, Carvalho A, et al. Parameter identification in dynamic systems using the homotopy optimization approach. Multibody Syst. Dyn. 2011;26:411–424.
[54] Ambrósio J, Pombo J, Facchinetti A, et al. Key Parameters for Pantograph/Catenary Numerical Models - PantoTRAIN Technical Report D1.1. Brussels, Belgium: UNIFE; 2010.
[55] Pombo J, Ambrosio J. Environmental and track perturbations on multiple pantograph interaction with catenaries in high-speed trains. Comput. Struct. 2013;124:88–101.
[56] Wang J, Ma Z, Hulbert GM. A Gluing Algorithm for Distributed Simulation of Multibody Systems. Nonlinear Dyn. 2003;34:159–188.
[57] Schweizer B, Li P, Lu D. Explicit and Implicit Cosimulation Methods: Stability and Convergence Analysis for Different Solver Coupling Approaches. J. Comput. Nonlinear Dyn. 2015;10:051007.
[58] Toridis TG, Khozeimeh K. Computer analysis of rigid frames. Comput. Struct. 1971;1:193–221.

[59] Bathe K-J. Finite element procedures in engineering analysis. Prentice-Hall Civ. Eng. Eng. Mech. Ser. Englewood Cliffs, N.J.: Prentice-Hall; 1982.
[60] Gear CW. Simultaneous Numerical Solution of Differential-Algebraic Equations. IEEE Trans. Circuit Theory. 1971;18:89–95.
[61] Rauter FG, Pombo J, Ambrósio J, et al. Contact Model for The Pantograph-Catenary Interaction. J. Syst. Des. Dyn. 2007;1:447–457.

17 Finite Element Methodology for Flexible Track Models in Railway Dynamics Applications

[7] The dynamic analysis of railway vehicles involves the construction of three independent models: the vehicle model; the track model; and the wheel-rail contact model. In this work, a multibody formulation with Cartesian coordinates is used to describe the kinematic structure of the rigid bodies and joints that constitute the vehicle model. A methodology is also proposed in order to create detailed three-dimensional track models, which includes the flexibility of the rails and of the substructure. Here, the finite element methodology is used to model the rails as beams supported in a discrete manner by spring-damper systems that represent the flexibility of the pads, sleepers, ballast and substructure. The inclusion of flexible track models is very important to study the dynamic behaviour of railway vehicles in realistic operation scenarios, especially when studying the impact of train operations on the infrastructure and, conversely, the damages on vehicles provoked by the track conditions. This topic has a significant economic impact on the vehicles maintenance and also affects the life cycle costs of tracks. The wheel-rail contact formulation used here allows obtaining, online during the dynamic analysis, the contact points location, even for the most general three-dimensional motion of the wheelsets with respect to the track. The methodology proposed to build flexible track models is validated here by comparing the results obtained with this new approach with the ones obtained with

[7] The work presented in this chapter has been published, as it is, in: J. Pombo, T. Almeida, H. Magalhães, P. Antunes, J. Ambrósio, *Catenary Finite Element Model Initialization using Optimization*, International Journal of Vehicle Structures & Systems, 5(2), 43-52, (2013).

ANSYS. Furthermore, the methodology is demonstrated by studying the dynamic behaviour of the Alfa Pendular railway vehicle.

17.1 Introduction

The railway system is increasingly becoming a key-player in worldwide transport policies. This results from the rising oil prices and from the urgency for reduction of CO2 emissions. To improve the competitiveness and attractiveness of railway networks, the trains have to travel faster, with high levels of safety and comfort, and with lower life cycle costs. Therefore, the increasing demands for network capacity, either by increasing the traffic speed or the axle loads, put pressure on the existing infrastructures and the effects of these changes have to be carefully considered.

The development of computer resources led simulations to be an essential part of the design process of railway systems. The European Strategic Rail Research Agenda [1] and the European Commission White Paper for Transports [2] have identified key scientific and technological priorities for rail transport over the next 20 years. One of the points emphasized is the need to reduce the cost of approval for new vehicles and infrastructure products with the introduction of virtual certification. Furthermore, the use of advanced computational tools during the design phase of new trains allows carry out several simulations, under various scenarios, in order to improve its dynamic performance and reach an optimized design. In this way, studies to evaluate the impact of design changes or failure modes risks can be performed in a much faster and less costly way than the physical implementation and test of those changes in real prototypes.

Due to their multidisciplinary, all the issues involving railway systems are complex. Therefore, the use of computational tools that represent the state of the art and that are able to characterize the modern designs and predict the vehicles' performance by using validated mathematical models is essential. Recent computer codes for railway applications use specific methodologies that, in general, only allow studying each particular phenomenon at a time. By analysing such phenomena independently, it is not possible to capture all the dynamics of the complete railway system neither the relevant coupling effects.

The main goal of this work is to develop an integrated computational tool that is able to model with detail the vehicle, the track and the subgrade. The study of these systems involves the development of complex methodologies, each requiring different mathematical formulations and numerical procedures. Here, instead of using the traditional approach, in

which these systems are handled independently, they are integrated in a common and reliable tool, where the interaction among them is considered. The methodologies developed will be validated by comparison with other tools and/or in close collaboration with the railway industry using real data.

The railway vehicle considered in this study is the Alfa Pendular that is used for passenger transportation in Portugal. It is a trainset with an active tilting system which allows it to negotiate curves at speeds higher than the balanced speed [3] and keeping the non-compensated acceleration within admissible values for passenger comfort [4]. The dynamic behaviour of the railway vehicle is studied using a multibody formulation [5-7] where the main structural elements are treated as rigid bodies. These are connected with flexible links that represent the suspension elements. The relative motions between the bodies of the system are restrained by using appropriate kinematic constraints.

The track flexibility is included in the formulation by using finite element models [8,9] to represent the rails, which are supported by discrete elastic elements, representing the flexibility of the sleepers, pads, ballast (or slab) and subgrade. Another advantage of this methodology is that it allows building realistic track models by considering the track irregularities in the formulation [10]. These track imperfections are measured by the infrastructure managers and can be included in the track model when performing the simulations. Such feature allows assessing the consequences of the track conditions on the vehicles performance, namely noise and vibration. Furthermore, it can help scheduling the track maintenance procedures by identifying the levels of track irregularities that promote the increase of wear and/or vehicle-track interaction forces.

The finite element formulation proposed here to build flexible track models is based on an analogous formulation used by the same research group to study the pantograph-catenary interaction [11,12]. The track model pre-processor and the numerical implementation of the finite element methodology are validated here by comparing the results with the ones obtained from ANSYS.

A generic wheel-rail contact detection formulation [13,14] is applied here in order to determine, online during the dynamic analysis, the contact points location, without need to use pre-computed lookup tables. This computational efficient methodology uses an elastic force model that allows computing the normal contact forces in the wheel-rail interface, accounting for the energy loss during contact [15,16]. The tangential wheel-rail contact forces can be calculated using one of the creep force models implemented here and described in the literature,

namely the Kalker linear theory [17], Heuristic nonlinear method [18] and the Polach formulation [19].

The methodologies described in this work are applied to study the dynamic behaviour of the Alfa Pendular railway vehicle, which is operated by the Portuguese Rail company in the intercity service. Future developments are directed towards studies involving the influence of the track settlement conditions on vehicles performance and analyses associated to railway infrastructure degradation resulting from trainsets operation. It is intended to assess the accuracy and suitability of the proposed methodologies through the comparison of the dynamic analysis results against those obtained by experimental testing. For this purpose, a partnership between this research group and the Portuguese railroad company has been established.

17.2 Description of the Railway Vehicle

In this section, the Alfa Pendular trainset is described. This railway vehicle is used for passenger transportation in Portugal. It is a trainset with an active tilting system which allows it to negotiate curves at higher speeds, maintaining the passengers comfort within admissible values. The trainset is composed of six vehicles, being four motor units and two trailers, as shown in Figure 17.1. In the following, all mechanical elements that are relevant to build the multibody model, namely the structural and the suspension elements, are described.

Due to the trainset configuration, it is assumed that, concerning the studies performed here, the dynamic behaviour of each vehicle has a non-significant influence on the others. According to this assumption, each vehicle of the trainset can be studied independently. In this way, the vehicle model considered here is composed only by one trailer unit of the trainset. It should be noticed that the methodology now described is generic and can be applied to any railway vehicle.

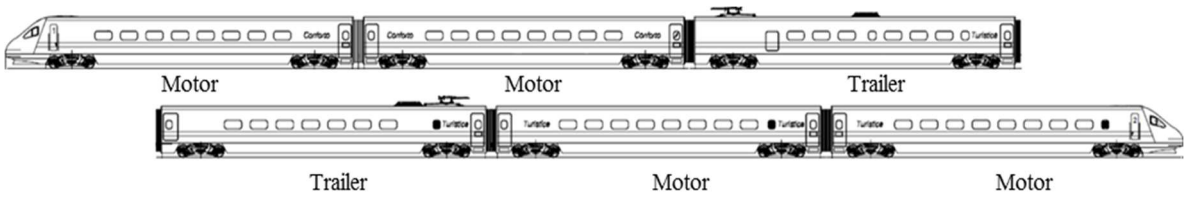

Figure 17.1: Schematic representation of the Alfa Pendular trainset

The Alfa Pendular trailer vehicle is composed by a carbody, where the passengers travel. The carbody is supported by two bogies through a set of mechanical elements that constitute the secondary suspension. The main function of these elements is to minimize the vibrations, resulting from the vehicle-track interaction, transmitted to the passenger compartment,

improving the comfort and reducing the problems associated to the structural fatigue. Each bogie includes the wheelsets, which are in contact with the rails, and another group of mechanical elements that constitute the primary suspension. These elements are the main responsible for the steering capabilities and stability behaviour of the whole group being, ultimately, responsible for the critical speed of the vehicle.

The structural elements that compose the Alfa Pendular vehicle are represented in Figure 17.2(a), namely the carbody, bogie frame, wheelset and the axlebox. The primary suspension of the vehicle at each axlebox, shown in Figure 17.2(b), is composed by two helicoidal springs, one vertical damper and one upper and lower traction rods.

The secondary suspension elements are shown in Figure 17.3(a). In each side of the bogie, this subsystem is composed by two helicoidal springs, one vertical damper, one transversal damper and one anti-yaw damper. The carbody is connected to the bogie through a pivot shaft, which is rigidly fixed to the carbody, as depicted in Figure 17.3(b). The pivot is assembled vertically and it is connected to the bogie frame by two traction rods, which allow the relative motion between these structural elements.

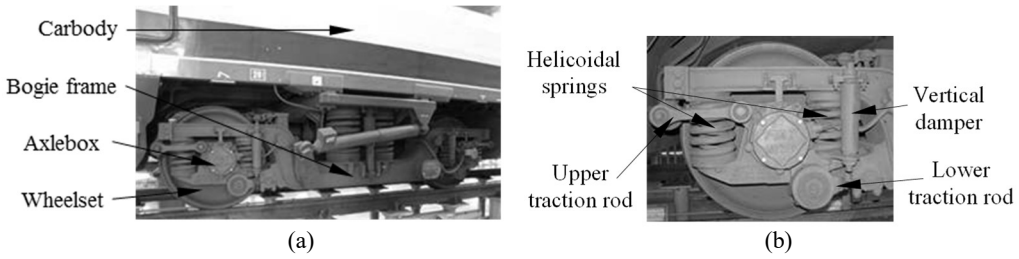

Figure 17.2: Alfa Pendular vehicle: (a) Structural elements; (b) Primary suspension elements

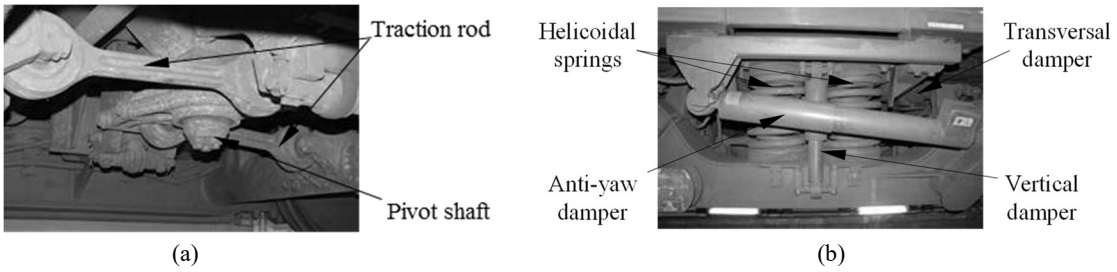

Figure 17.3: Alfa Pendular vehicle: (a) Secondary suspension elements; (b) Bogie-carbody connection elements

17.3 Description of the Vehicle Multibody Model

The first step for modelling the railway vehicle using a multibody formulation is the division of the group in several subsystems, which are simpler to handle. This strategy allows building each subsystem independently, being the whole vehicle model build by assembling the

subsystems as they were Lego pieces. The subsystems considered here to model the Alfa Pendular vehicle are shown in Figure 17.4.

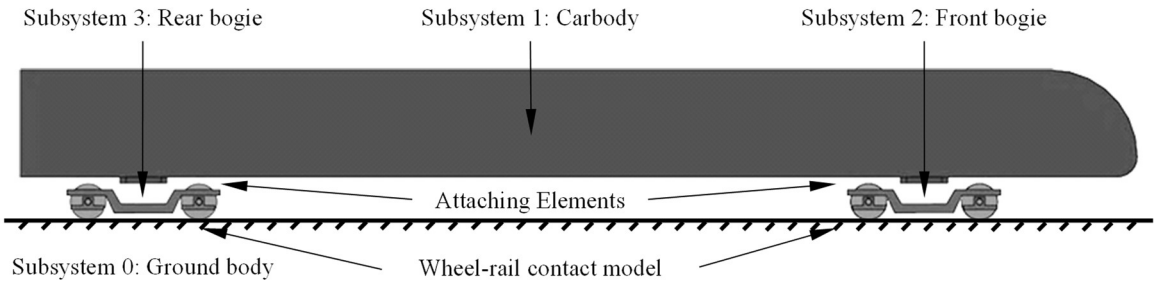

Figure 17.4: Alfa Pendular multibody model

The subsystem 0 is used to represent the track and the infrastructure, as shown in Figure 17.5(a). The subsystem 1, depicted in Figure 17.5(b), represents the carbody of the vehicle. The subsystems 2 and 3, shown in Figure 17.5(c), represent the front and the rear bogies. Being these last two equal, it is only necessary to build one subsystem representing the bogie. Then, when assembling the railway vehicle, this subsystem is used twice to represent both the front and the rear bogies. The subsystem 1 is connected to subsystems 2 and 3 by attaching elements, which represent the secondary suspension and the bogie-carbody connection elements. The interaction between the rails (from subsystem 0) and the wheels (from subsystems 2 and 3) is performed by using an appropriate wheel-rail contact model [13,14].

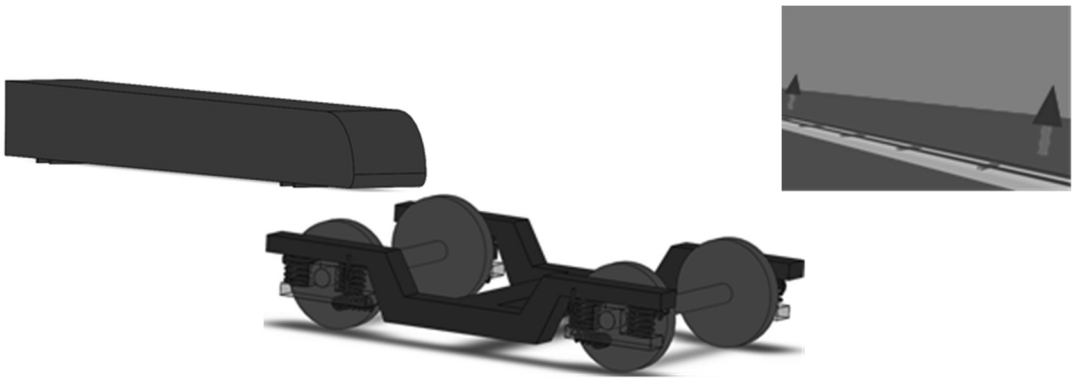

(a) (b) (c)

Figure 17.5: Subsystems of multibody model: (a) Track and infrastructure; (b) Carbody; (c) Front and rear bogies

For each subsystem it is necessary to provide the information about the rigid bodies, kinematic joints and linear and/or nonlinear force elements. The data for the definition of the rigid bodies includes the mass, the inertia properties and the initial position and orientation. The position of each body is measured from the origin of subsystem reference frame to the centre of mass of the body. The relative motion between the bodies is limited by kinematic joints [5], which restrain relative degrees-of-freedom between the bodies connected by them. The

suspension components, such as springs and dampers that connect the rigid bodies, are modelled as force elements. These are responsible for transmitting the internal forces that are developed in the system as function of the relative motion among the bodies. The data required to model the suspension elements includes the coordinates of the attaching points and their stiffness and damping properties. All the data required to model the Alfa Pendular vehicle is obtained from technical information provided by the manufacturer and by the railway operator.

The subsystem 1 is defined by one body, the carbody, which is free of any constraint. Its connection to the bogies is made by the secondary suspension elements when assembling the whole system. Subsystems 2 and 3, representing the bogies, are composed by one bogie frame, four axleboxes and two wheelsets. The relative motion between the wheelsets and the axleboxes is limited by revolute joints, representing the roller bearings of the axleboxes.

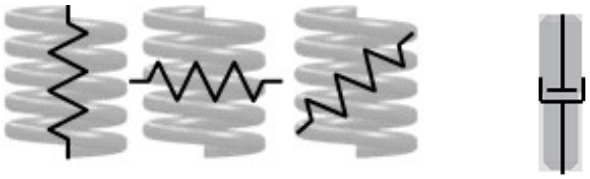

Figure 17.6: Primary suspension model: (a) Helicoidal spring; (b) Vertical damper

The primary suspension elements are used to connect the bogie frame to the axleboxes. The helicoidal springs, shown in Figure 17.2(b), despite being assembled vertically, originate forces in the three directions. Therefore, they are modelled here by using linear force elements in the vertical, longitudinal and lateral directions, as represented in Figure 17.6(a). The vertical damper is modelled as is shown in Figure 17.6(b). The upper and lower traction rods have equal mechanical properties, being assembled with rubber bushings at their extremities, which allow small misalignments in the lateral direction. Hence, the traction rods are modelled here as springs with different stiffness characteristics in the longitudinal and lateral directions, as represented in Figure 17.7. The longitudinal stiffness coefficient of the traction rod is obtained by the association in series between two springs, representing the rubber bushings, and another spring, representing the traction rod itself.

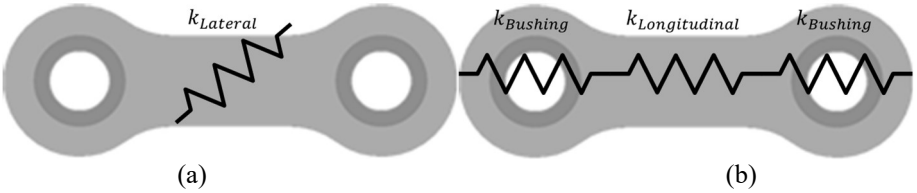

Figure 17.7: Traction rod model: (a) Longitudinal direction; (b) Lateral direction

The wheel-rail contact formulation requires the accurate definition of the contacting geometries. This is done here by providing a set of control points that are representative of the

wheel and rail profiles as shown in Figure 17.8. Then, during the dynamic analysis, the computational tool calculates the location of the contact points and, using appropriate methodologies, computes the normal and tangential contact forces. The detailed description of the formulation used here to study the wheel-rail contact phenomena is outside the scope of this text. The interested reader is referred to the works [13,14].

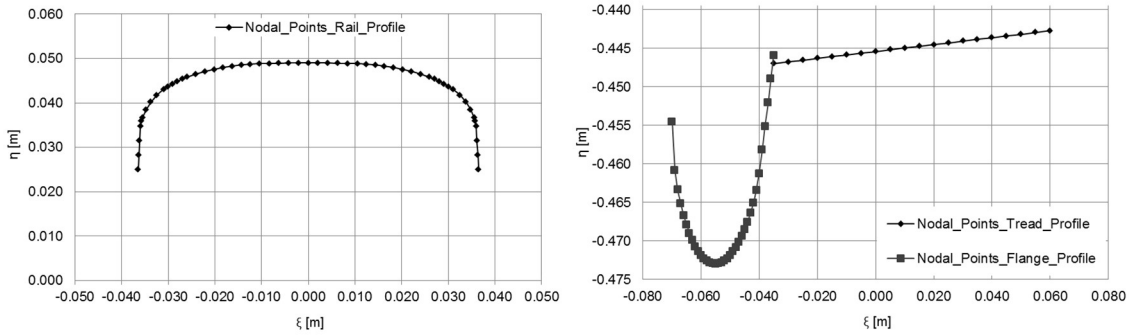

(a) (b)

Figure 17.8: Nodal points representing the: (a) Wheel profile; (b) Rail profile

After building all subsystems, they need to be assembled. The first step is to define the location of each subsystem with respect to the global reference frame (x,y,z), as shown in Figure 17.9. Then, subsystem 1 is attached to subsystems 2 and 3 by using the secondary suspension and the bogie-carbody connection elements. This is done using the same approach as the one used to assemble the primary suspension elements of the bogie subsystem.

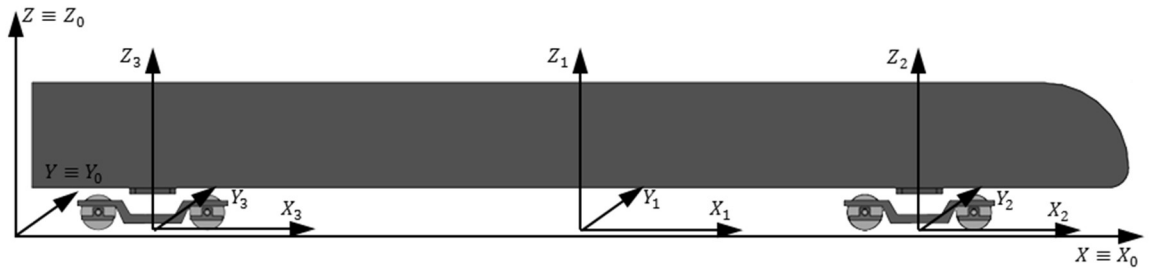

Figure 17.9: Subsystems assemblage

17.4 Description of the Railway Track

A railway track is generally composed by an assembly of elements of distinct elasticity responsible for gradually transmitting to the subsoil the dynamic loadings arising from the trains passage, besides the important function of guiding the vehicles. These elements are the rails, which are supported by the sleepers through the pads. The sleepers rest on an elastic bed made up of supporting layers as ballast, subballast, formlayer and subsoil, as represented in Figure 17.10.

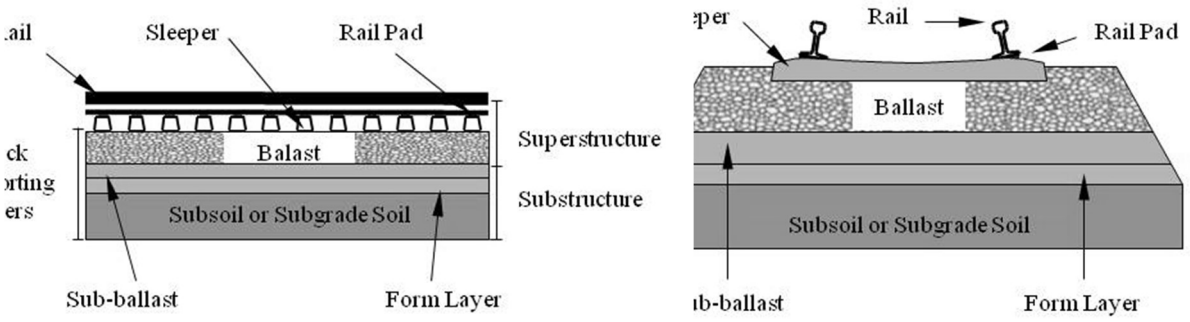

Figure 17.10: Main components of the railway track (a) Longitudinal view; (b) Cross-section view

17.5 Overview of the Finite Element Formulation

Despite being considered as rigid by many authors and computational tools, the railway track exhibits some flexibility that is characterized by small deformations and rotations, which, besides other phenomena, originate track irregularities. Due to its nature and magnitude, these deformations can be characterized as linear. In this work the railway track system is modelled with linear finite elements, being the wheel-rail contact forces included in the force vector of the finite element formulation. The rails and sleepers are modelled by using Euler-Bernoulli beam elements, while the foundations and rail pads are represented by spring-damper elements acting in the six degrees of freedom, as shown in Figure 17.11. Following this approach, the equilibrium equations of the finite element method for the railway track structural system are assembled as:

$$\mathbf{M}\,\mathbf{a} + \mathbf{C}\,\mathbf{v} + \mathbf{K}\,\mathbf{d} = \mathbf{f} \tag{17.1}$$

where **M**, **C** and **K** are the finite element global mass, damping and stiffness matrices of the finite element model of the track. Proportional damping is used to evaluate the global damping matrix, i.e. $\mathbf{C} = \alpha\,\mathbf{K} + \beta\,\mathbf{M}$ with α and β being suitable proportionality factors [20]. Alternatively a local damping matrix can be evaluated for each finite element, i.e. $\mathbf{C}^e = \alpha^e\,\mathbf{K}^e + \beta^e\,\mathbf{M}^e$ with α^e and β^e being proportionality factors associated with each type of track element, such as the rail or sleeper; with the exception of the spring-damper elements, which have their own damping coefficients in each degree of freedom. The nodal displacements vector is expressed by **d**, while **v** is the vector of nodal velocities, **a** is the vector of nodal accelerations and **f** is the force vector, written as:

$$\mathbf{f} = \mathbf{f}_{(g)} + \mathbf{f}_{(c)} \tag{17.2}$$

which contains the gravity forces, $\mathbf{f}_{(g)}$, plus the wheel-rail contact forces, $\mathbf{f}_{(c)}$, that are developed at each time step.

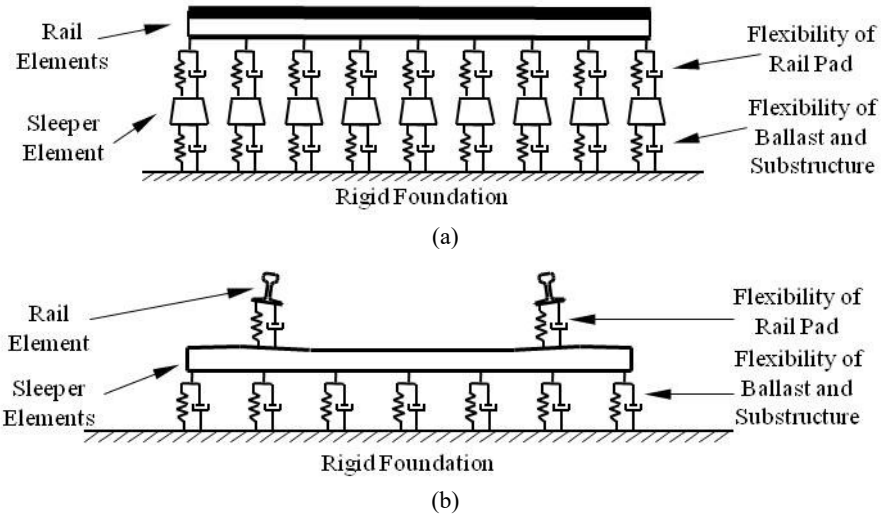

Figure 17.11: Main components of the track model: (a) Longitudinal view; (b) Cross-section view

In this work, the integration of the nodal accelerations uses a Newmark family integration algorithm [21]. The contact forces are evaluated for $t+\Delta t$ based on the position and velocity predictions of the finite element (FE) mesh and of the vehicle model. The finite element mesh accelerations are calculated by:

$$\left(\mathbf{M}+\gamma\,\Delta t\,\mathbf{C}+\beta\,\Delta t^2\mathbf{K}\right)\mathbf{a}_{t+\Delta t}=\mathbf{f}_{t+\Delta t}-\mathbf{C}\tilde{\mathbf{v}}_{t+\Delta t}-\mathbf{K}\tilde{\mathbf{d}}_{t+\Delta t} \tag{17.3}$$

According with this approach, predictions for new positions and velocities of the nodal coordinates of the linear finite element model of the track are computed as:

$$\tilde{\mathbf{d}}_{t+\Delta t}=\mathbf{d}_t+\Delta t\,\mathbf{v}_t+\frac{\Delta t^2}{2}\left(1-2\beta\right)\mathbf{a}_t \tag{17.4}$$

$$\tilde{\mathbf{v}}_{t+\Delta t}=\mathbf{v}_t+\Delta t\left(1-\gamma\right)\mathbf{a}_t. \tag{17.5}$$

Then, knowing the accelerations $\mathbf{a}_{t+\Delta t}$, the positions and velocities of the finite element mesh at next time step $t+\Delta t$ are corrected by:

$$\mathbf{d}_{t+\Delta t}=\tilde{\mathbf{d}}_{t+\Delta t}+\beta\Delta t^2\mathbf{a}_{t+\Delta t} \tag{17.6}$$

$$\mathbf{v}_{t+\Delta t}=\tilde{\mathbf{v}}_{t+\Delta t}+\gamma\,\Delta t\,\mathbf{a}_{t+\Delta t} \tag{17.7}$$

This correction procedure, expressed by using equations (17.4) through (17.7) and solving equation (17.3), is repeated until convergence is reached for a given time step, i.e. until $\left|\mathbf{d}_{t+\Delta t} - \tilde{\mathbf{d}}_{t+\Delta t}\right| < \varepsilon_d$ and $\left|\mathbf{v}_{t+\Delta t} - \tilde{\mathbf{v}}_{t+\Delta t}\right| < \varepsilon_d$, being ε_d and ε_v user defined tolerances.

17.6 Description of the Flexible Track Model

In the following, the data required to define the flexible track model is described together with the pre-processor developed to build its FE mesh. In order to define a given railway track, it is necessary to provide information about the geometry of each rail. This is done in 3D space by defining a set of control points that are representative of the geometry of each rail. In addition, it is necessary to provide the Cartesian components of the tangential **t**, normal **n** and binormal **b** vectors that define the rail referential associated to each nodal point. These quantities are tabulated as function of the rail arc length, as represented in Table 17.1.

Rail arc Length	Xi	Yi	Zi	Txi	Tyi	Tzi	Nxi	Nyi	Nzi	Bxi	Byi	Bzi
<Number>	<Number>	<Number>	<Number>	<Number>	<Number>	<Number>	<Number>	<Number>	<Number>	<Number>	<Number>	<Number>
…	…	…	…	…	…	…	…	…	…	…	…	…
<Number>	<Number>	<Number>	<Number>	<Number>	<Number>	<Number>	<Number>	<Number>	<Number>	<Number>	<Number>	<Number>

Table 17.1: Rail geometry data

After defining the 3D geometry of each rail, it is necessary to provide information about the number of track segments to be considered in the finite element mesh. For each segment, it is necessary to define its name, length and the refinement level of the mesh, as represented in Table 17.2.

Number of Track Types	<Number>

Track Type i	Track Type Name	Length of Track Type i	Refinement Level of Track Type i
Track Type 1	<Track Type 1 Name>	<Number>	<Number>
Track Type 2	<Track Type 2 Name>	<Number>	<Number>
…	…	…	…
Track Type n	<Track Type n Name>	<Number>	<Number>

Table 17.2: Track segments data

For each track segment defined in Table 17.2, it is necessary to provide information about the types of rails, sleepers and foundations that compose each one, as represented in Table 17.3.

Track Type n	<Track Type n Name>
Rail Data Type	<Rail Data Type Name>
Sleepers Data Type	<Sleepers Data Type Name>
Foundations Data Type	<Foundations Data Type Name>

Table 17.3: Track segment components data

Then, for each rail, it is necessary to define the properties required for the Euler-Bernoulli beam elements formulation, as represented in Table 17.4.

Rail Data Type	<Rail Data Type n Name>
UIC Rail Code	<Code>
Young Modulus - E [Pa]	<Number>
Poisson Coefficient	<Number>
Cross Section Area [m^2]	<Number>
Second Moment of Area in xz Plane - Iyy [m^4]	<Number>
Second Moment of Area in xy Plane - Izz [m^4]	<Number>
Second Moment of Area in yz Plane - Ixx [m^4]	<Number>
Density [kg/m^3]	<Number>
Torsion Modulus - G [Pa]	<Number>
Rayleigh Damping Parameter α	<Number>
Rayleigh Damping Parameter β	<Number>

Table 17.4: Rail geometry data

After introducing the information about the rails, it is necessary to provide all properties required to define the sleepers for each track segment, as represented in Table 17.5.

Sleepers Data Type	<Sleepers Data Type n Name>
Sleepers Distance [m]	<Number>
Number of Nodes Between Sleepers	<Number>
Sleeper Geometry	<Sleeper Geometry Name>
Pad Longitudinal Stiffness Kx [N/m]	<Number>
Pad Transversal Stiffness Ky [N/m]	<Number>
Pad Vertical Stiffness Kz [N/m]	<Number>
Pad Vertical Rotational Stiffness Kry [N/m]	<Number>
Pad Transversal Rotational Stiffness Krz [N/m]	<Number>
Pad Torsion Stiffness Kt [N/m]	<Number>
Pad Longitudinal Damping Cx [N.s/m]	<Number>
Pad Transversal Damping Cy [N.s/m]	<Number>
Pad Vertical Damping Cz [N.s/m]	<Number>
Pad Vertical Rotational Damping Cry [N.s/m]	<Number>
Pad Transversal Rotational Damping Crz [N.s/m]	<Number>
Pad Torsion Damping Ct [N.s/m]	<Number>

Table 17.5: Sleeper properties data

Besides the information about the rails and sleepers, the properties for the definition of the foundations for each track segment are required, as represented in Table 17.6.

Foundations Data Type	<Foundations Data Type n Name>
Longitudinal Stiffness Kx [N/m]	<Number>
Transversal Stiffness Ky [N/m]	<Number>
Vertical Stiffness Kz [N/m]	<Number>
Vertical Rotational Stiffness Kry [N/m]	<Number>
Transversal Rotational Stiffness Krz [N/m]	<Number>
Torsion Stiffness Kt [N/m]	<Number>
Longitudinal Damping Cx [N.s/m]	<Number>
Transversal Damping Cy [N.s/m]	<Number>
Vertical Damping Cz [N.s/m]	<Number>
Vertical Rotational Damping Cry [N.s/m]	<Number>
Transversal Rotational Damping Crz [N.s/m]	<Number>
Torsion Damping Ct [N.s/m]	<Number>

Table 17.6: Foundation properties data

As previously referred, the rails and sleepers are modelled by using Euler-Bernoulli beam elements. For this purpose, it is necessary to define their geometry. The rail geometry data is provided in Table 17.4. For the sleepers, with a general geometry shown in Figure 17.12, the data required to define their geometry is represented in Table 17.7.

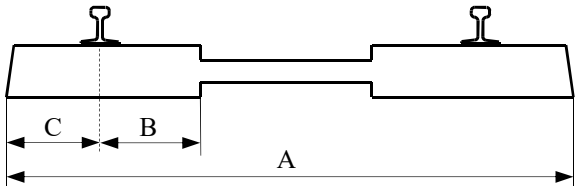

Figure 17.12: Sleeper general geometry

Sleeper Geometry	<Sleeper Geometry n Name>
Sleeper Length (Parameter A) [m]	<Number>
Rail-to-End Position (Parameter C) [m]	<Number>
Rail-to-Start Position (Parameter B) [m]	<Number>
End Young Modulus - E [Pa]	<Number>
End Poisson Coefficient	<Number>
End Cross Section Area [m^2]	<Number>
End Second Moment of Area in xz Plane - Iyy [m^4]	<Number>
End Second Moment of Area in xy Plane - Izz [m^4]	<Number>
End Second Moment of Area in yz Plane - Ixx [m^4]	<Number>
End Density [kg/m^3]	<Number>
End Torsion Modulus - G [Pa]	<Number>
End Rayleigh Damping Parameter α	<Number>
End Rayleigh Damping Parameter β	<Number>
Start Young Modulus - E [Pa]	<Number>
Start Poisson Coefficient	<Number>
Start Cross Section Area [m^2]	<Number>
Start Second Moment of Area in xz Plane - Iyy [m^4]	<Number>
Start Second Moment of Area in xy Plane - Izz [m^4]	<Number>
Start Second Moment of Area in yz Plane - Ixx [m^4]	<Number>
Start Density [kg/m^3]	<Number>
Start Torsion Modulus - G [Pa]	<Number>
Start Rayleigh Damping Parameter α	<Number>
Start Rayleigh Damping Parameter β	<Number>
Middle Young Modulus - E [Pa]	<Number>
Middle Poisson Coefficient	<Number>
Middle Cross Section Area [m^2]	<Number>
Middle Second Moment of Area in xz Plane - Iyy [m^4]	<Number>
Middle Second Moment of Area in xy Plane - Izz [m^4]	<Number>
Middle Second Moment of Area in yz Plane - Ixx [m^4]	<Number>
Middle Density [kg/m^3]	<Number>
Middle Torsion Modulus - G [Pa]	<Number>
Start Rayleigh Damping Parameter α	<Number>
Start Rayleigh Damping Parameter β	<Number>

Table 17.7: Sleeper geometry data

Finally, it is necessary to define the constants and output parameters for the track model. These quantities are represented in Table 17.8.

Track Constants		Output Parameters	
Gravity Acceleration [m/s^2]:	<Number>	Deformation Scalar Factor:	<Number>

Table 17.8: Track model constants and output parameters

17.7 Validation of the Flexible Track Methodology

In order to validate the methodology proposed here, a realistic flexible track model is built and subjected to loads representing the wheelset of a railway vehicle, as depicted in Figure 17.13. The results obtained are compared against the ones provided by ANSYS 12. The data used to build the flexible track model is given in Table 17.9 through Table 17.11: Foundation properties for the case study .

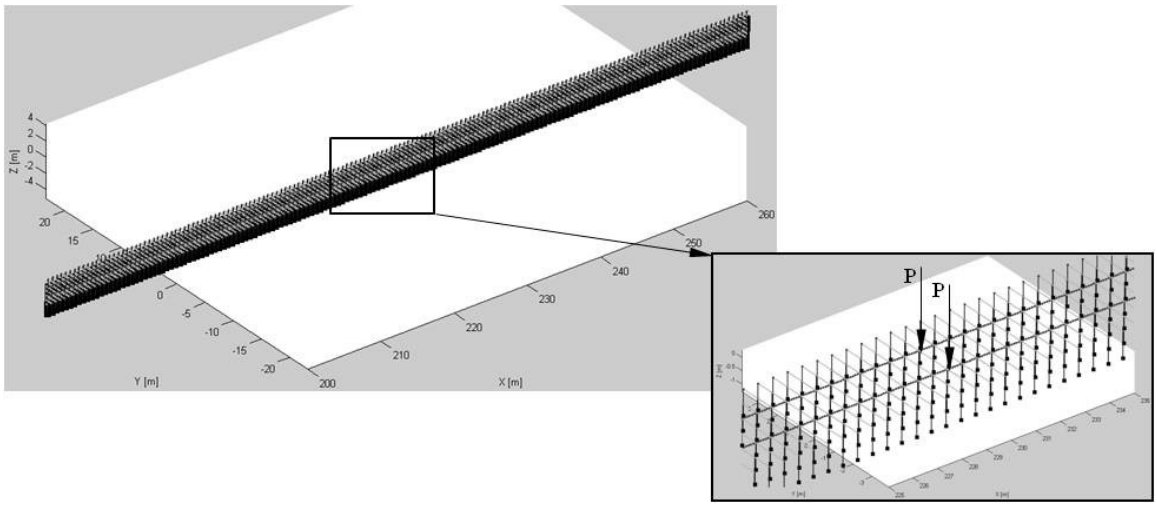

(a) (b)

Figure 17.13: Flexible track model: (a) Finite element mesh; (b) External loads applied

Number of Track Types	1

Track Type i	Track Type Name	Length of Track Type i	Refinement Level of Track Type i
Track Type 1	Track1	500	1

Table 17.9: Track segments data for the case study

Rail Data Type	UIC60	Sleepers Data Type	Sleeper1
UIC Rail Code	UIC60	Sleepers Distance [m]	0.6
Young Modulus - E [Pa]	200×10^{9}	Number of Nodes Between Sleepers	5
Poisson Coefficient	0.29	Sleeper Geometry	A
Cross Section Area [m^2]	7.68600×10^{-3}	Pad Traction Stiffness K [N/m]	85×10^{6}
Second Moment of Area in xz Plane - Iyy [m^4]	0.03055×10^{-3}	Pad Rotational Stiffness K [N/m]	8500×10^{6}
Second Moment of Area in xy Plane - Izz [m^4]	0.00513×10^{-3}	Pad Torsional Stiffness K [N/m]	8500×10^{6}
Second Moment of Area in yz Plane - Ixx [m^4]	0.04240×10^{-3}	Pad Traction Damping C [N.s/m]	85×10^{6}
Density [kg/m^3]	7.80600×10^{-3}	Pad Rotational Damping C [N.s/m]	8500×10^{6}
Torsion Modulus - G [Pa]	79.30000×10^{9}	Pad Torsional Damping C [N.s/m]	8500×10^{6}
Rayleigh Damping Parameter α	0.6		
Rayleigh Damping Parameter β	0.1		

Table 17.10: Rail and sleeper data for the case study

Foundations Data Type	Foundation1
Foundation Traction Stiffness K [N/m]	4783539
Foundation Rotational Stiffness K [N/m]	478353900
Foundation Torsional Stiffness K [N/m]	478353900
Foundation Traction Damping C [N.s/m]	4783539
Foundation Rotational Damping C [N.s/m]	478353900
Foundation Torsional Damping C [N.s/m]	478353900

Table 17.11: Foundation properties for the case study

Sleeper Geometry	A
Sleeper Length (Parameter A) [m]	2.250
Rail-to-End Position (Parameter C) [m]	0.372
Rail-to-Start Position (Parameter B) [m]	0.378
End Young Modulus - E [Pa]	65×10^{9}
End Poisson Coefficient	0.15
End Cross Section Area [m^2]	70.3030×10^{-3}
End Second Moment of Area in xz Plane - Iyy [m^4]	0.9824×10^{-3}
End Second Moment of Area in xy Plane - Izz [m^4]	1.3170×10^{-3}
End Second Moment of Area in yz Plane - Ixx [m^4]	0.3723×10^{-3}
End Density [kg/m^3]	2.4×10^{3}
End Shear Modulus - G [Pa]	2.4×10^{9}
Start Young Modulus - E [Pa]	65×10^{9}
Start Poisson Coefficient	0.15
Start Cross Section Area [m^2]	70.3030×10^{-3}
Start Second Moment of Area in xz Plane - Iyy [m^4]	0.9824×10^{-3}
Start Second Moment of Area in xy Plane - Izz [m^4]	1.3170×10^{-3}
Start Second Moment of Area in yz Plane - Ixx [m^4]	0.3723×10^{-3}
Start Density [kg/m^3]	2.4×10^{3}
Start Shear Modulus - G [Pa]	2.4×10^{9}
Middle Young Modulus - E [Pa]	65×10^{9}
Middle Poisson Coefficient	0.15
Middle Cross Section Area [m^2]	70.3030×10^{-3}
Middle Second Moment of Area in xz Plane - Iyy [m^4]	64.4063×10^{-3}
Middle Second Moment of Area in xy Plane - Izz [m^4]	86.3438×10^{-3}
Middle Second Moment of Area in yz Plane - Ixx [m^4]	0.3723×10^{-3}
Middle Density [kg/m^3]	2.4×10^{3}
Middle Shear Modulus - G [Pa]	2.2×10^{9}

Table 17.12: Sleeper geometry for the case study

In this case study, a pair of static downward vertical forces P of 112.5 kN are applied, as depicted in Figure 17.13(b). These forces represent the maximum wheelset load of 22.5 ton that a railway vehicle can have to be allowed to operate in the Portuguese railway network. In ANSYS, the BEAM4 element was used, corresponding to a Euler-Bernoulli beam element. All the other parameters required to build the track model in ANSYS match the ones used by the computational tool proposed here.

The deformations obtained with the two numerical tools are shown in Figure 17.14 and Figure 17.15. As the deformations are very small when compared with the other dimensions of the track, they are incremented by a factor of 100 in these figures. The results obtained show that the maximum vertical deformation of the track is 2.7 mm. On the other hand, in the longitudinal and lateral directions, the maximum displacement of the nodes where the forces are applied is 7.1×10^{-6} m and 32.7×10^{-6} m, respectively.

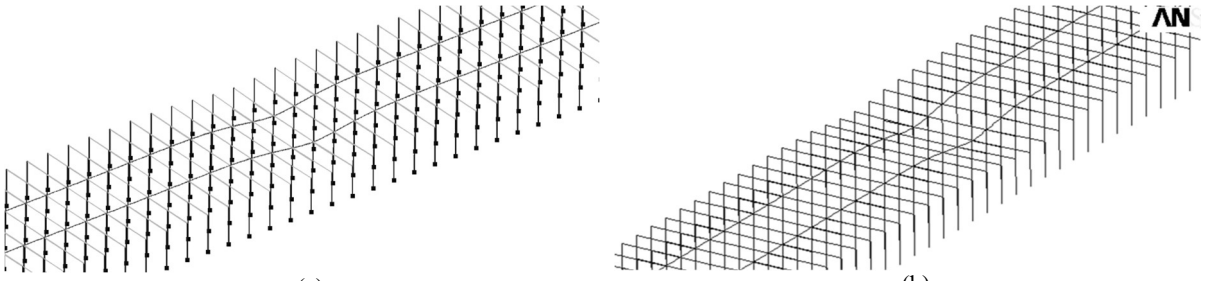

(a) (b)

Figure 17.14: Perspective view of the track deformation (deformation scaled ×100): (a) Computational tool; (b) ANSYS

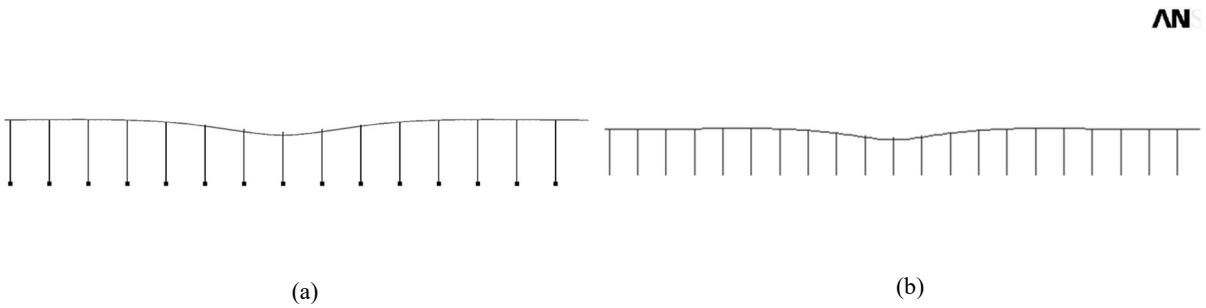

(a) (b)

Figure 17.15: Lateral view of the track deformation (deformation scaled ×100): (a) Computational tool; (b) ANSYS

When comparing the results obtained with the methodology proposed here and with ANSYS, it is observed that the maximum relative error for the track vertical deformation is about 0.04%, as shown in Figure 17.16, corresponding to a maximum absolute error of 1.3×10^{-7} m. Notice that the 0% error corresponds to the constrained nodes.

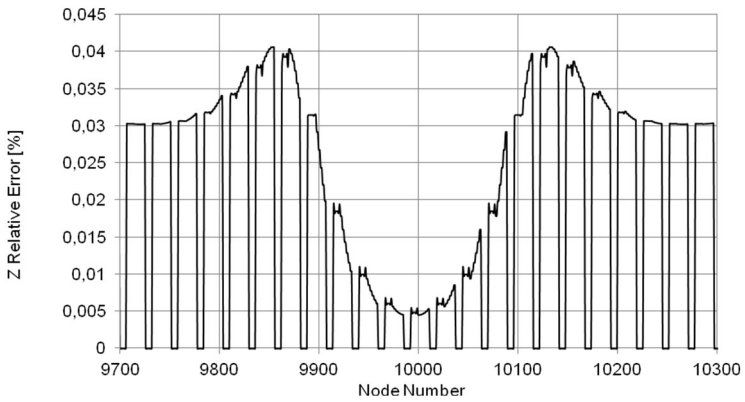

Figure 17.16: Relative error for the track vertical deformation

Figure 17.17(a) presents the relative errors on the rail nodes that are in the vicinity of the ones where vertical wheelset forces were applied. The relative error for the track vertical deformation on the nodes of the sleeper subjected to the external loads is shown in Figure 17.17(b). These results allow concluding that the finite element methodology proposed here to represent the track flexibility is suitable for such studies and it is quantitatively validated.

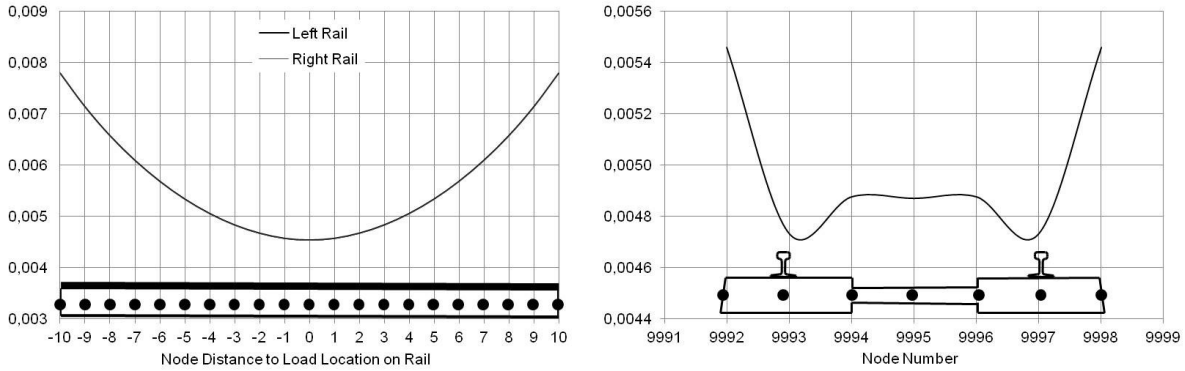

Figure 17.17: Relative error on the nodes in the vicinity of the applied loads: (a) Nodes on the rail; (b) Nodes on the sleeper

17.8 Communication between Multibody and Finite Element Codes

In this work, a fully 3D methodology to study the interaction of a railway vehicle, described by a multibody formulation, with a flexible track, represented by a finite element methodology, is proposed. Instead of using the conventional approach, in which the vehicle dynamics, the track and subgrade are handled independently, here an integrated strategy is proposed to handle the vehicle-track-subgrade coupled dynamics. For this purpose, a high-speed co-simulation procedure is setup in order to establish a communication protocol between the multibody and the finite element codes. The vehicle-track interaction forces are computed by using an appropriate wheel-rail contact formulation [13,14].

For the dynamic analysis of the finite elements model, a Newmark family numerical integrator [21] using a fixed time step is used, while for the multibody vehicle model the integration procedure is based on a predictor-corrector algorithm with variable time step [22]. The compatibility between the two integration algorithms, for the implementation of the co-simulation environment, imposes that the state variables of the two sub-systems are readily available during the integration time and also that a reliable prediction of the contact forces is available at any given time step.

One of the most critical issues of using co-simulation procedures is the added computational cost due to data exchange between codes, especially when this data is large or, as is this case, it is accessed frequently. The time spent on data exchange between applications must be negligible compared to the computation time costs of the two analyses. The use of physical data files for information exchange, also known as file input/output, is a robust, well known and very popular methodology. However, for either a recursive use or for large data sets it leads to slow data exchange when compared to the use of virtual memory sharing. In order to

address this, the memory sharing process adopted on this work is done via memory mapped files.

17.9 Preliminary Results

In the following, the interaction between the Alfa Pendular railway vehicle and the track is analysed. The simulation scenario corresponds to a straight track, without irregularities, and a velocity of 90 km/h. At the initial time of analysis the vehicle is assembled in the track with a lateral misalignment of 2 mm.

The lateral displacement of the vehicle wheelsets is shown in Figure 17.18. It is observed that, after the initial misalignment of 2 mm, the hunting motion of the wheelsets is damped and they return to the centre position on the track. These results show that the critical speed [3] of the vehicle is higher than 90 km/h.

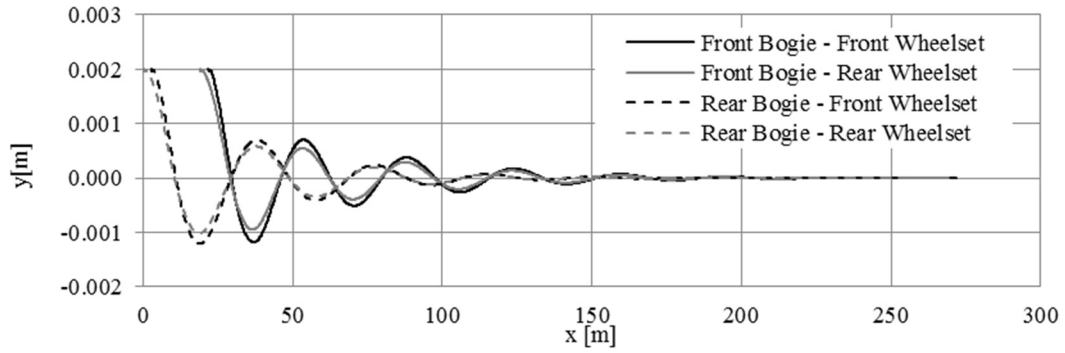

Figure 17.18: Wheelsets lateral displacement

The lateral and vertical contact forces on the left wheels of the Alfa Pendular vehicle are shown in Figure 17.19 and Figure 17.20, respectively. The results show that the forces oscillations decrease as the vehicle returns to the centre position on the track after the initial misalignment. Notice that the first second of dynamic analysis was not considered as they represent the transient phase of the contact forces.

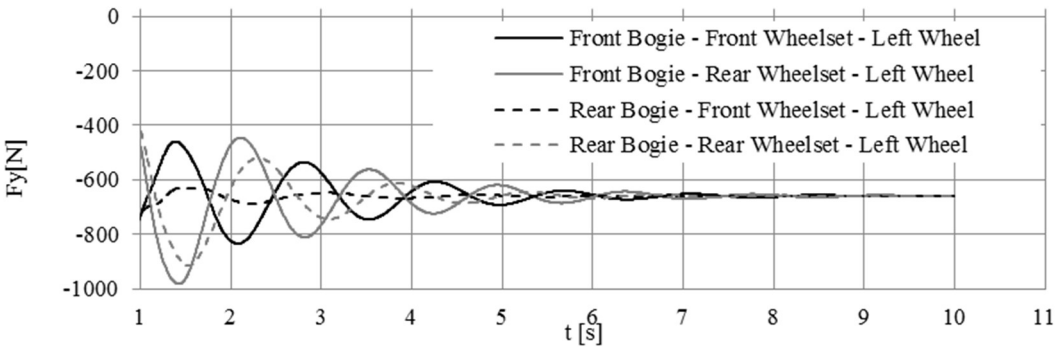

Figure 17.19: Lateral contact forces on the left wheels of the vehicle

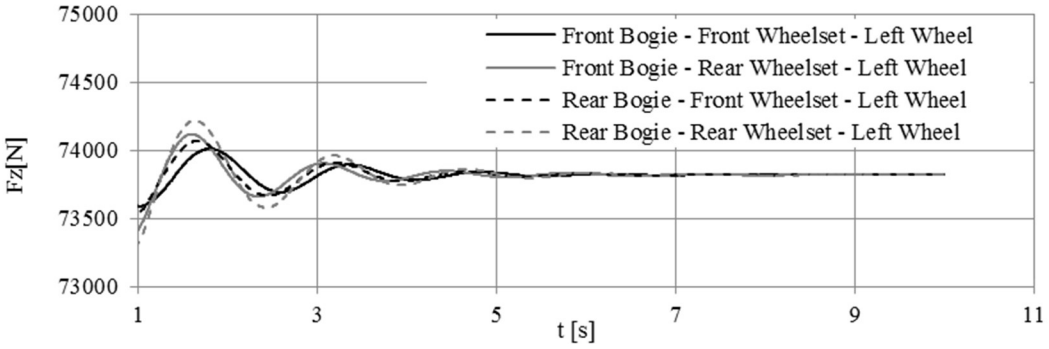

Figure 17.20: Vertical contact forces on the left wheels of vehicle

17.10 Conclusions

The dynamic analysis of the loads imposed to the railway infrastructure by trainsets and, conversely, the damages on vehicles provoked by the track conditions has been attracting the attention of railway community in recent years. The raising interest on this subject has occurred mainly due to the development of new high-speed railway lines and to the common drive to upgrade the existing infrastructures. The increasing demands on railway transportation require improvements of the network capacity, which can be achieved either by increasing the speed of the traffic or by increasing the axle loads. However, both of these options place pressures on the existing infrastructures and the effects of these changes have to be carefully considered.

The main goal of this work is to develop an advanced computational tool for railway dynamics, with innovative methodologies that are handled in a co-simulation environment, where all physical phenomena can be integrated. This includes not only the detailed representation of the vehicle, track and subgrade, but also the interaction among them. Such a tool can indicate solutions with technological relevance and give answer to the industry's most recent needs, contributing to improve the competitiveness of the railway transportation system.

The results obtained show that the finite element methodology, proposed here to represent the track flexibility, is suitable for railway studies and it is quantitatively validated. Future developments of this work include the development of comparative studies in order to investigate the influence of track flexibility and of track conditions on vehicles performance. Also studies involving the consequences of trainset operation on railway infrastructure degradation are foreseen as future work. The establishment of partnerships with Portuguese railway operators and infrastructure manager gives good perspectives for the industrial application of the achievements of these studies.

References

[1] ERRAC, European Rail Research Advisory Council, "Strategic Rail Research Agenda 2020", Brussels, Belgium, 2007.

[2] EC, European Commission, "White Paper: Roadmap to a Single European Transport Area - Towards a Competitive and Resource Efficient Transport System", Brussels, Belgium, 2011.

[3] Dukkipati, R. V. and Amyot, J. R., "Computer-Aided Simulation in Railway Dynamics", M. Dekker Inc., New York, New York, 1988.

[4] Pombo, J., Ambrósio, J., Pereira, M., Verardi, R., Ariaudo, C. and Kuka, N., "Influence of Track Conditions and Wheel Wear State on the Loads Imposed on the Infrastructure by Railway Vehicles", *Computers and Structures*, **89**, No. 21-22, pp. 1882-1894, 2011.

[5] Nikravesh, P. E., "Computer-Aided Analysis of Mechanical Systems", Prentice-Hall, Englewood Cliffs, New Jersey, 1988.

[6] Schiehlen, W., "Multibody Systems Handbook", Springer-Verlag, Berlin, Germany, 1990.

[7] Shabana, A. A., "Dynamics of Multibody Systems", 2nd Edition, Cambridge University Press, Cambridge, United Kingdom, 1998.

[8] Reddy, J. N., "An Introduction to the Finite Element Method", 3rd Edition, McGraw-Hill, 2005.

[9] Zienkiewicz, O. and Taylor, R., "The Finite Element Method", Butterwort-Heinemann, Woburn, Massachussetts, 2000.

[10] Pombo, J. and Ambrósio, J., "An Alternative Method to Include Track Irregularities in Railway Vehicle Dynamic Analyses", *Nonlinear Dynamics*, **68**, pp. 161-176, 2012.

[11] Ambrósio, J., Pombo, J., Pereira, M., Antunes, P. and Mósca, A., "Recent Developments in Pantograph-Catenary Interaction Modelling and Analysis", *International Journal of Railway Technology*, **1**, No. 1, pp. 249-278 (DOI:10.4203/ijrt.1.1.12), 2012.

[12] Ambrósio, J., Pombo, J., Pereira, M., Antunes, P. and Mósca, A., "A Computational Procedure for the Dynamic Analysis of the Catenary-Pantograph Interaction in High-Speed Trains", *Journal of Theoretical and Applied Mechanics*, **50**, No. 3, pp. 681-699, 2012.

[13] Pombo, J. and Ambrósio, J., "Application of a Wheel-Rail Contact Model to Railway Dynamics in Small Radius Curved Tracks", *Multibody Systems Dynamics*, **19**, No. 1-2, pp. 91-114, 2008.

[14] Pombo, J., Ambrósio, J. and Silva, M., "A New Wheel-Rail Contact Model for Railway Dynamics", *Vehicle System Dynamics*, **45**, No. 2, pp. 165-189, 2007.

[15] Lankarani, H. M. and Nikravesh, P. E., "A Contact Force Model with Hysteresis Damping for Impact Analysis of Multibody Systems", *AMSE Journal of Mechanical Design*, **112**, pp. 369-376, 1990.

[16] Lankarani, H. M. and Nikravesh, P. E., "Continuous Contact Force Models for Impact Analysis in Multibody Systems", *Nonlinear Dynamics*, **5**, pp. 193-207, 1994.

[17] Kalker, J. J., "Simplified Theory of Rolling Contact", Progress Report Series C: Mechanical and Aeronautical Engineering and Shipbuilding, 1, pp. 1-10, Delft University of Technology, Delft, The Netherlands, 1973.

[18] Shen, Z. Y., Hedrick, J. K. and Elkins, J.A., "A Comparison of Alternative Creep Force Models for Rail Vehicle Dynamic Analysis", *8th IAVSD Symposium on Dynamics of Vehicles on Road and Tracks*, (J. K. Hedrick, Ed.), Swets and Zeitlinger, Cambridge, Massachussetts, pp. 591-605, 1983.

[19] Polach, O., "A Fast Wheel-Rail Forces Calculation Computer Code", *Vehicle System Dynamics*, Supplement 33, pp. 728-739, 1999.

[20] Hughes, T., "The Finite Element Method: Linear Static and Dynamic Finite Element Analysis", Prentice-Hall, Englewood Cliffs, New Jersey, 1987.

[21] Newmark, N., "A Method of Computation for Structural Dynamics", *ASCE Journal of the Engineering Mechanics Division*, **85**, EM 3, pp. 67-94, 1959.

[22] Ambrósio, J., Pombo, J., Rauter, F. and Pereira, M., "A Memory Based Communication in the Co-Simulation of Multibody and Finite Element Codes for Pantograph-Catenary Interaction Simulation", *Multibody Dynamics*, (Bottasso C.L., Ed.), Springer, Dordrecht, The Netherlands, pp. 211-231, 2008.

18 A co-simulation approach to the wheel-rail contact with flexible railway track

[8] The standard approach to railway vehicle dynamic analysis includes running the vehicle multibody models in rigid railway tracks. The wheel-rail contact, independently of the rolling contact model used, is either handled online or via lookup tables. This traditional approach disregards the coupling effects between the railway vehicle dynamics and the railway track flexibility. In this work the assumption of rigidity of the railway track is released and a finite element model of the complete track, i.e., rails, pads, sleepers, ballast and infrastructure, is used to represent the track geometry and flexibility. A rail-wheel contact model that evaluates the contact conditions and forces is used online. The dynamics of the railway vehicle is described using a multibody methodology while the track structure is described using a finite element approach. Due to the fact that not only the multibody and the finite element dynamic analysis use different integration algorithms but also because the vehicle and track models are simulated in different codes a co-simulation procedure is proposed and demonstrated to address the coupled dynamics of the system. This approach allows to analyse the vehicle dynamics in a flexible track with a general geometry modelled with finite elements, i.e., including curvature, cant, vertical slopes and irregularities, which is another novel contribution. The methodology proposed in this work is demonstrated in an application in which the railway vehicle-track interaction shows the influence of the vehicle dynamics on the track dynamics and vice-versa.

[8] The work presented in this chapter has been published, as it is, in: P. Antunes, H. Magalhães, J. Ambrósio, J. Pombo, J. Costa., A co-simulation approach to the wheel–rail contact with flexible railway track, International Multibody System Dynamics, DOI 10.1007/s11044-018-09646-0.

18.1 Introduction

The development of computer resources favoured numeric dynamic analysis methods to become an essential part of the design and research process of railway systems. The quest for novel solutions to answer the increasing demands for network capacity, either by increasing the traffic speed or the axle loads, put pressure on the existing infrastructures that find in the computational analysis of potential solutions a tool for their virtual testing. The European Strategic Rail Research Agenda [1] and the European Commission for Transports white papers [2] have identified these topics as key scientific and technological priorities for rail transport over the next 20 years. One of the points emphasized is the need to reduce the cost of approval for new vehicles and infrastructure products with the introduction of virtual certification. Certainly, an important issue arising during the design phase of new railway vehicles is the improvement of its dynamic performance. The concurrent use of different computational tools allows carrying several simulations, under various scenarios, to reach optimized designs. Studies to evaluate the impact of design changes or failure modes risks can be performed in a much faster and less costly way than the physical implementation and test of those changes in real prototypes.

Current computer codes for railway applications use specific methodologies that, in general, either handle the vehicle dynamics on a rigid track or deal with moving loads on flexible track. By analysing such phenomena independently, it is not possible to capture all the dynamics of the complete railway system and relevant coupling effects. However, developing innovative and more relevant comprehensive methodologies, in a co-simulation environment, allow not only to integrate all physical phenomena, but also to assess the cross influence between them. Co-simulation procedures form a generalist approach of simulating coupled systems on a time depended basis [3–5]. As the dynamic analysis of multi-disciplinary models is often composed by sub-systems, co-simulation exploits this modular structure by addressing each sub-system with its own distinct formulation and time integration method. Co-simulation approaches avoid the use of a unique and complex formulation with a unified time integration method that compromises the accuracy of the dynamic analysis of each sub-system consequently becoming computationally expensive and time intensive. A wide range of applications use efficiently co-simulation to couple systems with different formulations, i.e., multidisciplinary problems [6–13]. There are also applications where co-simulation is employed to improve computational performance by allowing parallel computation [14, 15], or establishing active control on mechatronic systems [16, 17], or enabling the use of third party

applications [18]. In the realm of railway numeric analysis tools co-simulation implementations are seldom found. One existing application case is the analysis of the pantograph-catenary interaction, in which a co-simulation procedure has been developed with a finite element catenary model interacting with a multibody pantograph model [19–21]. Also, in the framework of railway vehicle dynamics a co-simulation approach is used to set active control on vehicle models with tilting [22, 23].

The work presented here purposes a co-simulation procedure for the dynamic analysis of vehicle-track interaction where the main objective is to account for track flexibility in the dynamic behaviour analysis of railway vehicles, which in turn, is reflected on the rolling contact of the rail-wheel interaction. Railway dynamics is a subject where contributions from a wide range of fields are required. Different modelling approaches are used, depending on the objective of the study. The importance of the modelling aspects for the vehicle and track, in the context of their interaction, is related with the frequencies of interest associated to the particular phenomena under study in a State-of-Art review by Knothe and Grassie [24]. Although that work mostly focus on noise and it does not address the track geometry, it already presents some of the important modelling aspects required for flexible tracks to achieve meaningful analysis results. When addressing the vehicle-track interaction, from a perspective of evaluating the dynamic behaviour of a railway vehicle, the usual and most popular approach is to model the vehicle using a multibody system formulation model being the track considered a rigid structure [25–27]. This methodology provides acceptable results for dynamic analysis on a perspective of vehicle behaviour for ride safety and comfort [28] These models are adequate to evaluate low frequency dynamic responses such as lateral stability and curving behaviour, as most of the high frequency excitation is filtered by the vehicles suspension, up to a certain point. Gialleonardo et al. [29] show that the track flexibility has a significant effect on the evaluation of the vehicle critical speed and in the wheel/rail contact forces. Dynamic effects at mid to high frequency ranges require the introduction of track flexibility [30]. Even in the low frequency domain track flexibility must be considered when its effects on the railway dynamics are significant, such as when the track is considered to be flawed [31, 32], or switches and crossings are considered [33]. The work by Martinez-Casas et al. [34] shows the importance of considering the flexibility of the railway track, and also of the wheelset, in the interaction between vehicle and track. Although in their work only a single wheelset and a perfect circular track are considered it can be accepted that the interaction phenomena identified can be expected to be present in more general scenarios. Furthermore, as the wheel-rail contact forces evaluation depends on the geometry of the wheel and the rail, as much as in the relative position

between them, track flexibility must be considered when analysing the development of these rolling contact forces along the track. In scenarios with tangent tracks models, in which modal superposition is used to reduce the size of the finite element track model, Dietz, Hippmann and Schupp [6] present the implementation of a coupled vehicle-track dynamics in a commercial multibody code. Due to the use of a modal representation of the flexible track this approach cannot handle to full dynamics of the system without considering an excessive number of modes for the track, which not only leads to computational inefficiency but also prevents the introduction of nonlinear elements, localized deformations and more general geometries. To this end, the work by Zhai, Wang and Cai [35] demonstrates the importance of considering the coupled vehicle-track dynamics with flexible tracks by developing a simulation scenario, validated experimentally, in which the spatial vehicle multibody model operates in a two tracks, one with large radius and another with a small radius. However, in all the works cited here the track geometry is either a tangent track or a curved track with constant radius, never considering a more general, and realistic geometry.

In this work, a multibody formulation is used to model the railway vehicle and a finite element formulation is presented to model the railway track. To establish the interaction between these models a novel co-simulation procedure, able to handle the dynamics between the systems, is proposed. This approach allows to analyse the vehicle dynamics in a flexible track with a general geometry modelled with finite elements, i.e., including curvature, cant, vertical slopes and irregularities, which is another novel contribution that can be used not only to address the running scenarios studied in this work but also to contribute to a number of challenging engineering problems associated to the train-track interaction occurring in tracks with small radius curves such as squeal noise and short pitch corrugation. A comparative study on the dynamics of a multibody vehicle with rigid and with a flexible railway track is presented to appraise the coupled dynamics of the systems and the modification of the rolling contact of the wheel with the track rail.

18.2 Railway Vehicle Multibody Model

The vehicle multibody model is characterized by a set of rigid and/or flexible bodies that are interconnected by force elements and joints. In turn, the representation of the mechanical elements that constrain the relative motion between structural elements allows the modelling of the relative mobility of the system components. The equations of motion that represent a multibody model of a railway vehicle, depicted in Figure 18.1, are written together with the

second time derivative of constraint equations as [36]:

$$\begin{bmatrix} \mathbf{M} & \mathbf{\Phi}_q^T \\ \mathbf{\Phi}_q & \mathbf{0} \end{bmatrix} \begin{Bmatrix} \ddot{\mathbf{q}} \\ \boldsymbol{\lambda} \end{Bmatrix} = \begin{Bmatrix} \mathbf{g} \\ \boldsymbol{\gamma} \end{Bmatrix} \tag{18.1}$$

where $\ddot{\mathbf{q}}$ is the vector with the accelerations of the rigid bodies and $\boldsymbol{\lambda}$ is the Lagrange multiplier vector associated to the joint reaction forces. The remaining terms are described in further detail hereafter.

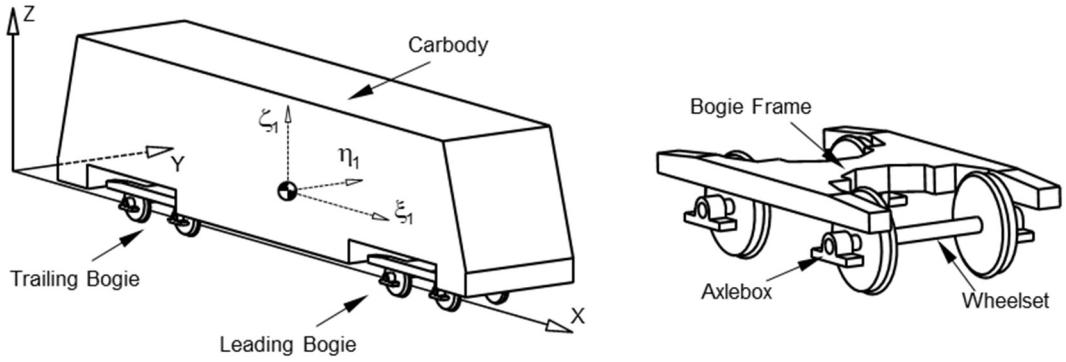

Figure 18.1: General multibody model of a railway vehicle.

The multibody model considered in this work comprises a carbody, bogie frames, wheelsets and axleboxes which are modelled as rigid bodies. Their mass and inertial properties are used to form the mass matrix **M**. The mechanical joints, in general, are modelled as kinematic constraints, being their modelling parameters associated to their geometric properties, which are used to form the constraint equations, whose second time derivative includes the Jacobian matrix, $\mathbf{\Phi_q}$, and the right hand side vector, $\boldsymbol{\gamma}$. The primary and secondary suspension elements, depicted in Figure 18.2, are represented as springs and dampers with appropriate constitutive relations, being the forces transmitted to the connected bodies included in the force vector, **g**. The wheel-rail contact forces are also included in the force vector, being their treatment described in Section 4 of this work.

The position and velocity constraint equations are not used explicitly in the integration of the system accelerations and velocities leading to a drift that results in the violation of these equations, as time progresses. It is necessary to eliminate or maintain the violations of the constraint equations under control. The kinematic constraint violations are stabilized using the Baumgarte stabilization method, while kept under prescribed thresholds, or eliminated by using a coordinate partition [37] when they exceed a pre-established value. The solution of the forward dynamics problem, for the multibody model, is obtained by using a variable time step and variable order numerical integrator [38].

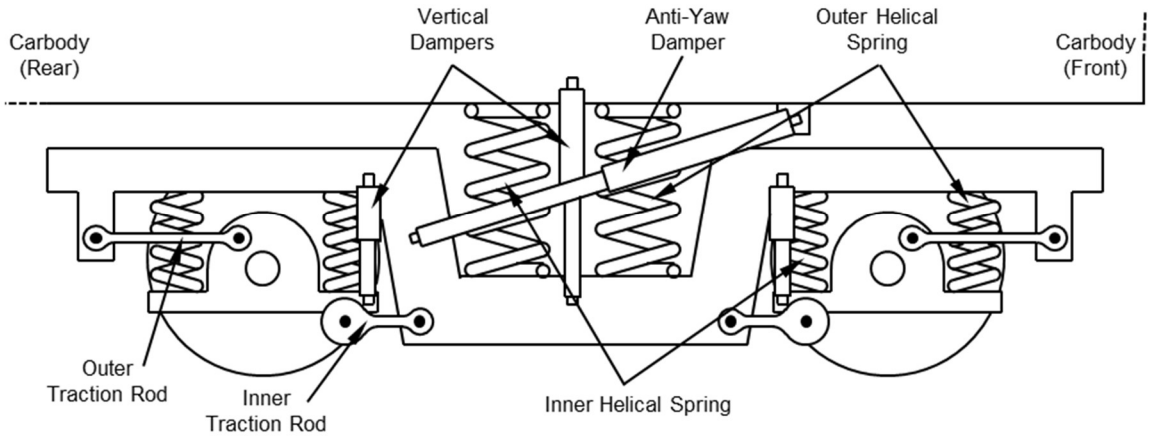

Figure 18.2: Suspension system of the railway vehicle.

18.3 Track Finite Element Model and Equilibrium Equations

The railway track is modelled using the finite element method being its dynamics analysed with suitable numerical methods. The ingredients of the finite element model are first described here being the systematic generation of the finite element model described afterwards. Finally, the equations of motion for the finite element model are presented.

18.3.1 Finite element components

The railway track is composed by several structural elements: rails, fasteners, rail pads, sleepers, ballast or slab and the substructure as depicted in Figure 18.3. In this work, the track model is assumed to have only linear deformations being its model built with linear finite elements. The rails and sleepers are modelled by three-dimensional beam elements, based on Euler-Bernoulli theory [39], the rail pads and fasteners and track supporting layers are modelled with 6 degrees of freedom spring-damper elements. A consistent mass matrix is used for the beam finite elements while a lumped mass description of the inertia is used for other elements in the model.

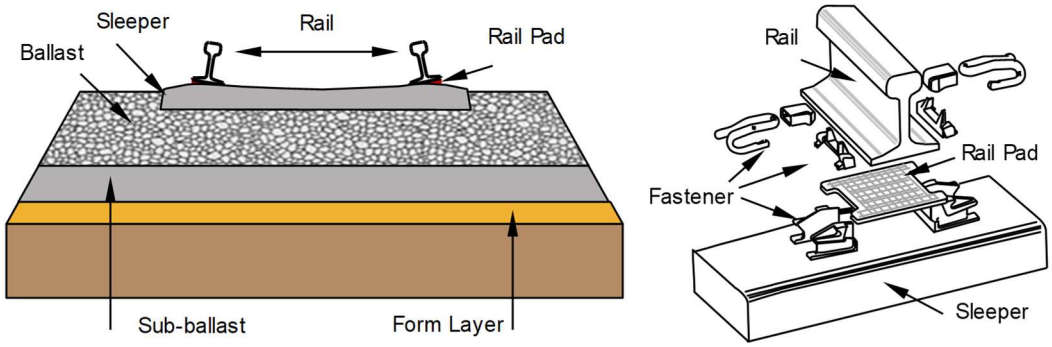

Figure 18.3: Typical construction of a railway track with its structural components: a) Track including the ballast and sub-structure b) Exploded view of the fixation of the rail to the sleeper.

The rails are modelled with beam elements being 6 elements used between sleepers to ensure a proper geometry in curves. The sleepers are symmetric being the model of each one made of 5 beam elements to accommodates transitions of cross-section and/or material properties characteristic of these structural elements. The connection between the sleeper and the rail is modelled using a single spring-damper element with translational stiffness and damping along three perpendicular directions, which represents the sleeper pad, and rotational stiffness along the tangent direction of the rail, which is representative of the rail fastening system that prevents the rail from rotating. The track supporting layers are modelled considering two types of spring-damper elements: those connecting the sleepers to the foundation and those connecting two consecutive sleepers. The sleeper to foundation connection is represented by the vertical elements below the sleepers, depicted in Figure 18.4, and accounts for the flexibility of the supporting layers directly below the sleeper. The sleeper to sleeper connection represented by the in track-plane elements connecting the sleepers, as depicted in Figure 18.5, accounts for the interlocking action of the supporting structure, i.e., the ballast or the slab. The topology of the track model, with the structural elements considered, is well inline with the recommendations of Knothe and Grassie [24].

The track supporting layers consider translational stiffness and damping along three perpendicular directions. The foundation is modelled as a fixed “rigid” ground constraining the lower nodes of the track supporting layers finite element mesh. Finally, to avoid the elastic wave reflection characteristic of finite length models intended to represent infinite or very long tracks, massless spring-damper elements are added to the beginning and to the end of the railway track and constrained. This setup corresponds to energy absorption boundary conditions that dissipate the energy associated with the incoming elastic wave thus preventing its reflection, independently of the track length considered in each particular model of the track. The effectiveness of the absorption boundary conditions is achieved by selecting proper damping characteristics for the terminal spring-damper elements the elastic wave reflection is prevented.

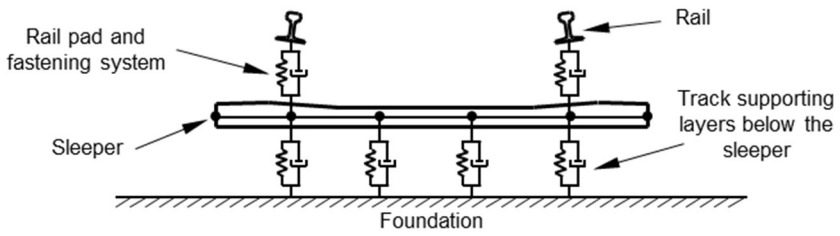

Figure 18.4: Cross section view of the track model.

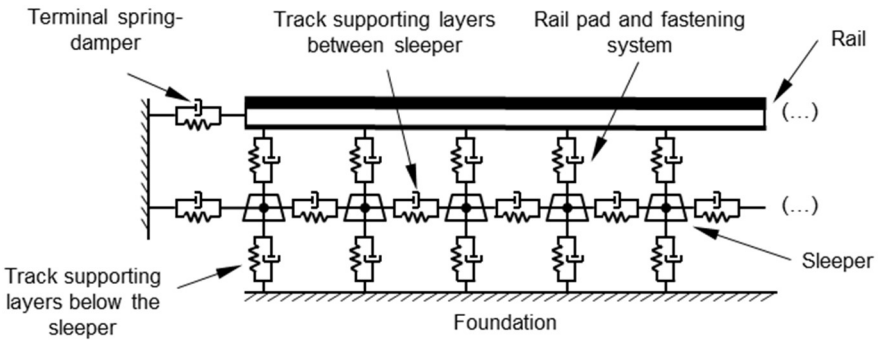

Figure 18.5: Longitudinal view of the track model.

18.3.2 Systematic generation of the track finite element model

The track geometrical description, based on the motion of a Frenet-Serret frame or the rails centreline curve is the basis of the finite element model construction used here [40, 41]. The information necessary to define the railway track centreline geometry, and the local plane in which the track must lay, is obtained from the curvature, cant and elevation information available for the description of the track geometry. The geometry and position of the rails is obtained from the track centreline geometry, taking into account the gauge and the rail geometry, using the track moving frame, as illustrated in Figure 18.6.

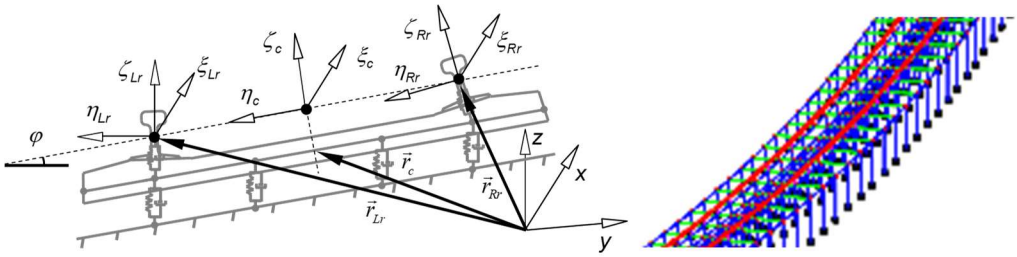

(a) (b)

Figure 18.6: Elements of the finite element mesh of the track: (a) Position coordinates and local reference frame of the track and rails; (b) Mesh for the railway track.

Using the geometric description of the left and right rails, as a function of their arc length, the position of the nodes of the rails, $\mathbf{r}_{Lr}$, $\mathbf{r}_{Rr}$, are defined as well as the local nodal coordinate frames ($\xi_{Lr},\eta_{Lr},\zeta_{Lr}$) and ($\xi_{Rr},\eta_{Rr},\zeta_{Rr}$), for the left and right rails respectively. The finite element mesh of the track includes nodes placed in planes for which the tangent vector to the track centreline is normal spaced such a way, along the centreline arc-length, that they include the sleepers, pads and fasteners, such as in the case illustrated in Figure 18.6 (a). In this case, there are two nodes associated with the rail cross-section centre, six nodes along the sleepers to enable modelling monoblock, twin-block and timber sleepers, and four nodes for the track foundations. In-between sleepers, there are five rail nodes equally spaced along the rails curve. The beam finite element used for the rails have their cross-section oriented according to the local rail

referential shown in Figure 18.6 (a). The remaining beam elements, used to model the sleepers depend on their geometry while the spring-damper elements used to represent the ballast resistance in the tangent-to-track plane and in its vertical direction are set in between the sleeper nodes and either the foundation or other sleeper nodes. For more details on the automatic track mesh construction the interested reader is directed to the work by Costa [42].

18.3.3 Equations of motion of the track finite element model

The dynamic equilibrium equations of a railway track are assembled and written as [43, 44]:

$$\mathbf{M}\,\mathbf{a} + \mathbf{C}\,\mathbf{v} + \mathbf{K}\,\mathbf{d} = \mathbf{f}_{track} \tag{18.2}$$

where **M, C** and **K** are the finite element global mass, damping and stiffness matrices, and **a**, **v**, **d** and **f** are the acceleration, velocity, displacement and force vectors, respectively. The global matrices **M**, **C** and **K** are built by assembling the individual finite element matrices, according to the topology of the track mesh. The damping behaviour of the beam elements is represented using Rayleigh damping [44]. The force vector $\mathbf{f}_{track}$, containing the sum of all external applied loads, is evaluated at every time step of the integration as:

$$\mathbf{f}_{track} = \mathbf{f}_g + \mathbf{f}_c \tag{18.3}$$

where $\mathbf{f}_g$ represents the gravitational forces and $\mathbf{f}_c$ represents the equivalent wheel-rail contact forces and moments transferred from the application points to the finite element nodes, as described in detail in Section 4.3.

All matrices appearing in the left-hand side of Eq. (18.2) are constant, for the application scenarios foreseen in this work being, consequently, linear equations of motion. The dynamic behaviour of the track is solved using an integration algorithm based on the implicit Newmark trapezoidal rule [45]. This method is selected due to its unconditional stability, when used implicitly, and its proven robustness in FE applications, as the one performed in this work, [44].

18.4 Wheel-Rail Contact

In the vehicle-track co-simulation procedure here presented, the bridge that establishes the coupling between both sub-systems is the wheel-rail contact. The evaluation of the contact forces requires that the position and velocities of the flexible rail and rigid wheel are known and that, if in contact, a suitable contact force model is used. After evaluating the contact forces, these have to be transferred from their application points to particular points of the model components where external concentrated loads are supposed to be applied, i.e., the mass centres

of the rigid bodies of the multibody model or the nodes of the finite element model.

18.4.1 Wheel-rail contact model

The rolling contact problem that characterizes the wheel-rail interaction is solved in two steps: the contact detection in which the contact points, or areas, are identified, and; the contact force modelling in which the interaction forces involved are evaluated. The online wheel-rail contact detection method proposed by Pombo et al [41, 46] is the starting point for the approach proposed here.

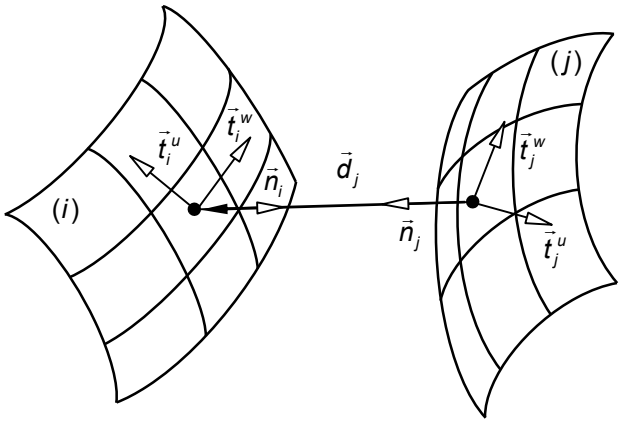

Figure 18.7: Contact detection between two surfaces [41, 46]

The wheel-rail contact detection problem is similar to the contact detection between two parametric surfaces, as those depicted in Figure 18.7, described by parameters u_i, w_i, u_j and w_j. The location of the potential contact points in the surfaces must be such that the tangent planes to the surfaces, in those points, are parallel to each other. The surface parallelism condition is described by the nonlinear system of equations

$$\begin{cases} \mathbf{d}_j^T \mathbf{t}_i^u = 0 \\ \mathbf{d}_j^T \mathbf{t}_i^w = 0 \\ \mathbf{n}_i^T \mathbf{t}_j^u = 0 \\ \mathbf{n}_i^T \mathbf{t}_j^w = 0 \end{cases} \tag{18.4}$$

where $\mathbf{d}_j$ is the distance vector between the potential points of contact, $\mathbf{n}_i$ and $\mathbf{n}_j$ are the normal vector of surfaces i and j, $\mathbf{t}_i^u$ and $\mathbf{t}_i^w$ are tangential vectors of surface i and $\mathbf{t}_j^u$ and $\mathbf{t}_j^w$ are tangential vectors of surface j, shown in Figure 18.7, all defined as function of the surfaces parameters.

For each potential contact pair in the wheel-rail contact, i.e. the tread-rail and flange-rail contact pairs, contact exists if

$$\mathbf{d}_j^T \mathbf{n}_i > 0 \tag{18.5}$$

If contact exists in a particular contact pair, normal and tangential forces are calculated and applied to the bodies in contact on the contact points identified.

The interaction between the wheel and the rail is represented by the contact model proposed by Pombo *et al* [41, 46]. This model considers that the wheel surface is described by two parametric surfaces, for the tread and for the flange, while the rail is described by a single parametric surface. Therefore, two potential contact points may develop between wheel and rail, the tread-rail and the flange-rail contact points shown in Figure 18.8.

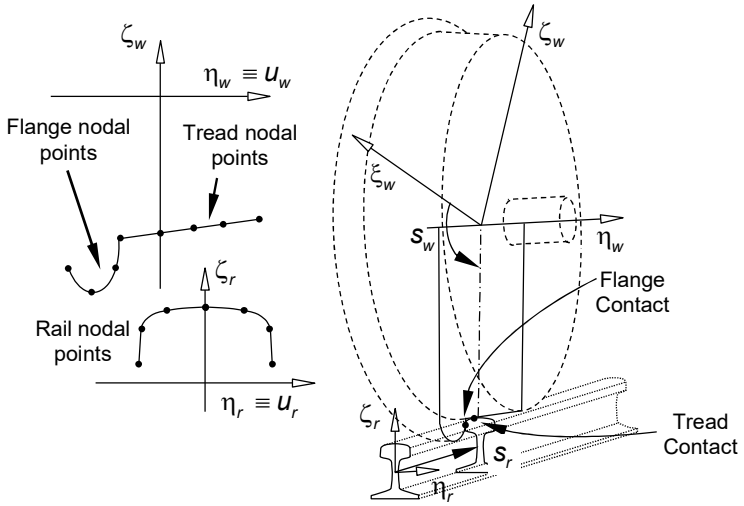

Figure 18.8: Identification of the parameters used in the wheel and rail parametric surfaces including the wheel tread and flange and rail profiles and surface parameters for the wheel (s_w,u_w) and for the rail (s_r,u_r).

The wheel profile is defined by two sets of nodal points, one for the tread and the other for the flange profile. These nodal points are interpolated to define the cross section of the wheel profile, as a function of parameter u_w, which in turn is rotated about the wheel axis η_w, with the angle s_w starting from ξ_w, to form the parametric surface of revolution that defines the geometric shape of the wheel. The rail profile is also obtained by the interpolation of another set of nodal points, which are interpolated to define the rail cross-section, as a function of parameter u_r, which, in turn, is swept along the rail arc with the length of the sweep being defined by the arc-length s_r, starting from the origin of the rail. Consequently, the parametric surfaces of the wheel tread and flange and of the rail, depicted in Figure 18.8, are fully described by parameters s_w, u_w, s_r and u_r that play the role of parameters u_i, w_i, u_j and w_j in Eq.(18.4).

The effect of the flexibility of the track on the rail position and orientation is graphically shown in Figure 18.9 (a), where a rail finite element is displaced with respect to its initial position, in grey, and for which the cross-sections are rotated relatively to their initial

orientations. Let the finite element in which wheel-rail contact occurs connect node *i* to node *j*, as shown in Figure 18.9 (b). The position and orientation of the centre of the rail cross-sections in the beam finite element is related to the initial geometry, finite element nodal displacements and shape functions by

$$\begin{Bmatrix} \mathbf{r}_r \\ \boldsymbol{\theta}_r \end{Bmatrix} = \begin{Bmatrix} \mathbf{r}(s_r) \\ \mathbf{0} \end{Bmatrix} + \begin{bmatrix} \mathbf{A}_e & \\ & \mathbf{A}_e \end{bmatrix} \begin{bmatrix} \mathbf{N}_i^{dd}(\xi) & \mathbf{N}_i^{d\theta}(\xi) & \mathbf{N}_j^{dd}(\xi) & \mathbf{N}_j^{d\theta}(\xi) \\ \mathbf{N}_i^{\theta d}(\xi) & \mathbf{N}_i^{\theta\theta}(\xi) & \mathbf{N}_j^{\theta d}(\xi) & \mathbf{N}_j^{\theta\theta}(\xi) \end{bmatrix} \begin{bmatrix} \mathbf{A}_e & & & \\ & \mathbf{A}_e & & \\ & & \mathbf{A}_e & \\ & & & \mathbf{A}_e \end{bmatrix}^T \begin{Bmatrix} \boldsymbol{\delta}_i \\ \boldsymbol{\theta}_i \\ \boldsymbol{\delta}_j \\ \boldsymbol{\theta}_j \end{Bmatrix} \tag{18.6}$$

where $\mathbf{r}(s_r)$ is the position of the centre of the rail cross-section that includes the contact point for the rigid track, as described in the work by Pombo *et al* [41, 46], $\boldsymbol{\delta}_i$ and $\boldsymbol{\delta}_j$ the nodal displacements , $\boldsymbol{\theta}_i$ and $\boldsymbol{\theta}_j$ the nodal rotations, all expressed in the inertia frame coordinates, $\mathbf{A}_e$ is the finite element transformation matrix from local to global coordinates and $\mathbf{N}^{dd}$, $\mathbf{N}^{d\theta}$, $\mathbf{N}^{\theta d}$ and $\mathbf{N}^{\theta\theta}$ are submatrices with the shape functions of the beam element [39]. Eq.(18.6) is written as function of $\xi = (s_r - s_i)/(s_j - s_i)$, which is the parametric length coordinate of the finite element in which the contact takes place, being s_r the arc-length of the rail up to the contact point and s_i and s_j the rail arc-lengths up to nodes *i* and *j*, respectively.

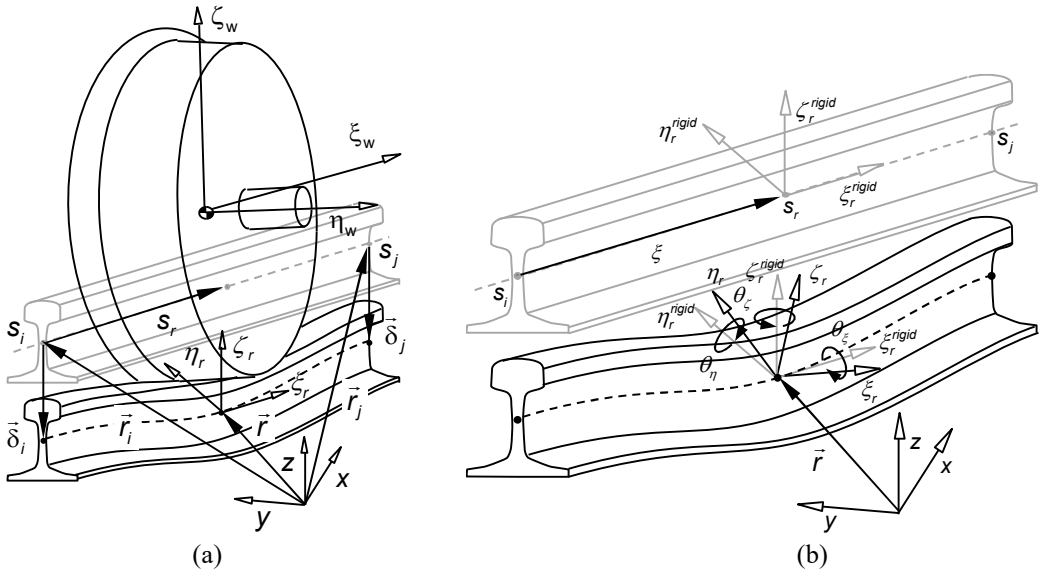

Figure 18.9: Deformation of the rail due to the wheel contact: (a) displacement of the rail cross-section that includes the contact point; (b) rotation of the rail cross-section.

Due to the rail deformation the rail cross-sections rotate with respect to their orientation on the rigid track, such a way that they remain perpendicular to the tangent of the arc line of their centres. The linear beam bending theory is used in the formulation of the linear beam finite

elements being the infinitesimal rotations of a cross-section of the element, given, in Eq.(18.6), by $\boldsymbol{\theta}_r$. The transformation matrix from the rigid rail cross-section frame $(\xi,\eta,\zeta)_r^{rigid}$ to the deformed rail cross-section frame $(\xi,\eta,\zeta)_r$, both shown in Figure 18.9 (b), is given by

$$\mathbf{A}_\theta = \begin{bmatrix} 1 & -\theta_\zeta & \theta_\eta \\ \theta_\zeta & 1 & -\theta_\xi \\ -\theta_\eta & \theta_\xi & 1 \end{bmatrix} \tag{18.7}$$

The consequence of the displacement and rotation of the rail cross-section on the wheel tread and flange to rail contact searches is that not only the evaluation of vector $\mathbf{d}_j$ in Eq.(18.4) must take into account the new location of the centre of the cross-section $\mathbf{r}_r$ as given by Eq.(18.6) but also the rail surface vectors $\mathbf{n}_j$, $\mathbf{t}^u_j$ and $\mathbf{t}^w_j$ need to be rotated. In the wheel-rail contact formulation with a rigid track, by Pombo *et al* [41, 46], the normal, bi-normal and tangent vectors of the left and right rails are pre-calculated and included in a table accessed online during the contact search. In the procedure for the flexible track the original vectors in the rigid track table are rotated by matrix $\mathbf{A}_\theta$ and $\mathbf{r}_r$ is added to the rigid rail position before being used in the contact search algorithm, which is done by solving the system of nonlinear equations

$$\begin{cases} \mathbf{d}_j^T \mathbf{t}_i^u = 0 \\ \mathbf{d}_j^T \mathbf{t}_i^w = 0 \\ \mathbf{n}_i^T \mathbf{A}_\theta \mathbf{t}_j^u = 0 \\ \mathbf{n}_i^T \mathbf{A}_\theta \mathbf{t}_j^w = 0 \end{cases} \tag{18.8}$$

If Eq.(18.5) is fulfilled for a particular contact pair, normal and tangential contact forces need to be evaluated. These forces depend on the contact geometry and on the material properties of the wheel and rail. Assuming that the contact between the wheel tread or flange and the rail is non-conformal, the normal contact forces are calculated using an Hertzian contact force model with hysteresis damping is given by [47]

$$f_n = K\left(1 + \frac{3\left(1-e^2\right)}{4}\frac{\dot{\delta}}{\dot{\delta}^{(-)}}\right)\delta^n \tag{18.9}$$

where K is the stiffness coefficient, e is the restitution coefficient, n is a constant equal to 1.5 for metals, δ is the amount of indentation between the surfaces, $\dot{\delta}$ is the indentation velocity and $\dot{\delta}^{(-)}$ is the relative indentation velocity as impact starts.

The tangential forces are evaluated using the formulation proposed by Polach in which

the longitudinal creep, or tangential, force is [48]

$$f_\xi = f\frac{\upsilon_\xi}{\upsilon_C} \tag{18.10}$$

while the lateral creep force is written as

$$f_\eta = f\frac{\upsilon_\eta}{\upsilon_C} + f_{\eta S}\frac{\phi}{\upsilon_C} \tag{18.11}$$

being f the tangential contact force caused by longitudinal and lateral relative velocities between the contacting surfaces, generally designated as creepages in rolling contact, υ_ξ, υ_η and ϕ are the longitudinal, lateral and spin creepages, respectively, in the point of contact, υ_C is the modified translational creepage, which accounts the effect of spin creepage and $f_{\eta S}$ is the lateral tangential force, or creep, caused by spin creepage. The Polach algorithm requires as input the normal contact force, the semi-axes of the contact ellipse, the combined modulus of rigidity of wheel and rail materials, the friction coefficient and the Kalker creepage and spin coefficients c_{ij} [49].

The contact forces on the wheel tread and flange, shown in Figure 18.10 as vectors $\mathbf{f}_{tr,w}$ and $\mathbf{f}_{fl,w}$, respectively, are generically written as

$$\mathbf{f}_{k,w} = f_{k,n}\,\mathbf{n}_k + f_{k,\xi}\,\mathbf{t}_{k,w} + f_{k,\eta}\,\mathbf{t}_{k,u} \qquad k = tr, fl \tag{18.12}$$

where $\mathbf{n}_k$ is the vector normal to the wheel surface, $\mathbf{t}_{k,w}$ is the tangent vector to the surface in the longitudinal direction of the wheel motion and $\mathbf{t}_{k,u}$ is the tangent vector in the lateral direction. In turn, the forces $\mathbf{f}_{tr,r}$ and $\mathbf{f}_{fl,r}$ represent the forces applied on the rails, which are opposite to those calculated for the wheels, i.e., $\mathbf{f}_{fl,w}$ and $\mathbf{f}_{fl,r}$.

18.4.2 Wheel-rail contact model on vehicle

In the multibody model, the information related to the wheel-rail contact forces is added to the force vector **g** in Eq. (18.1), in which all forces are supposed to be applied in the rigid bodies mass centres, i.e., the origin of the body fixed coordinate systems. The forces due to the wheel-rail contact are applied in the contact points of the wheelset, shown Figure 18.10 for the tread and flange contacts. Therefore, the contact forces are first transferred to the centre of the wheelset by adding all the contact forces to a force resultant and a transport moment due to the transference of the points of application to the wheel centre, as

$$\begin{aligned} \mathbf{f}_{wheel} &= \mathbf{f}_{tr,w} + \mathbf{f}_{fl,w} \\ \mathbf{n}'_{wheel} &= \tilde{\mathbf{s}}'_{tr,w}\,\mathbf{A}_{ws}^T\mathbf{f}_{tr,w} + \tilde{\mathbf{s}}'_{fl,w}\,\mathbf{A}_{ws}^T\mathbf{f}_{fl,w} \end{aligned} \tag{18.13}$$

where $\mathbf{s}'_{tr,w}$ and $\mathbf{s}'_{fl,w}$ are the position vectors of the tread and flange contact points with respect to the wheel centre and expressed in the wheelset body coordinate frame, and $\mathbf{A}_{ws}$ is the transformation matrix from the wheelset body frame to the inertia frame.

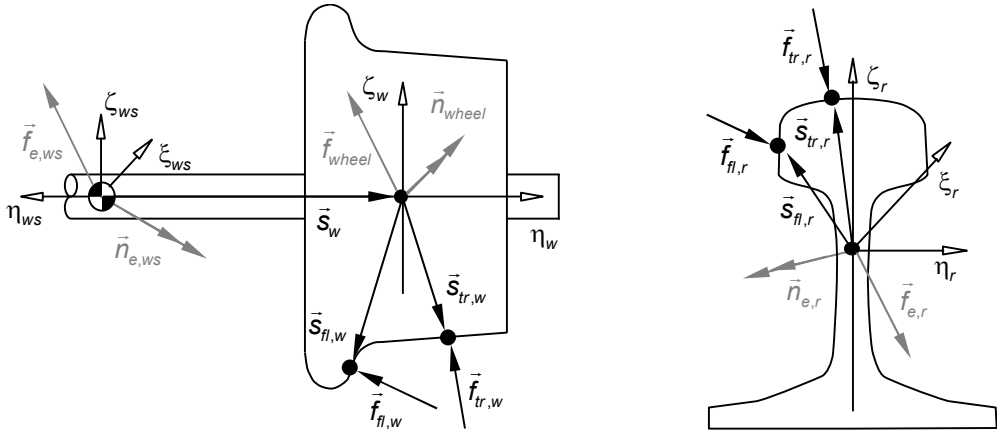

Figure 18.10: Wheel and rail contact forces, points of contact and equivalent forces and moments in the wheel centre and in the rail cross-section centre.

In the most common applications the wheels on the same wheelset are not independent, and consequently they are part of a single rigid body designated by wheelset. Therefore, the resultant force applied in the wheel mass centre is transferred to the wheelset mass centre, being the resultant force and transport moment on the wheelset due to the wheel-rail contact given by

$$\begin{aligned} \mathbf{f}_{e,ws} &= \mathbf{f}_{wheel} \\ \mathbf{n}'_{e,ws} &= \tilde{\mathbf{s}}'_w \, \mathbf{A}_{ws}^T \mathbf{f}_{wheel} + \mathbf{n}'_{wheel} \end{aligned} \tag{18.14}$$

where $\mathbf{s}'_w$ is the position of the wheel centre with respect to the wheelset mass centre, expressed in the wheelset body fixed coordinate system. Thus, the contribution of the wheel-rail contact forces to the force vector $\mathbf{g}$ of Eq. (18.1) is simply $\mathbf{g}_{e,ws} = [\mathbf{f}^T_{e,ws}, \mathbf{n}'^T_{e,ws}]^T$.

18.4.3 Wheel-rail contact model on track

In a finite element model lumped forces, such as the wheel-rail contact forces, can be applied on the nodes of the mesh but not in the middle of the element. As observed in Figure 18.10, the wheel-rail contact forces applied on the rail surface whereas the beam element used in the model for the rail considers only its geometric centre. Therefore, the resultant of the contact forces, $\mathbf{f}_{e,r}$, is applied on the rail cross-section centre and a transport moment, $\mathbf{n}_{e,r}$, Figure 18.10 and in Figure 18.11(a), is added to obtain the equivalent force system system in the cross-section centre as

$$\begin{aligned}\mathbf{f}_{e,r} &= \mathbf{f}_{tr,r} + \mathbf{f}_{fl,r} \\ \mathbf{n}_{e,r} &= \tilde{\mathbf{s}}_{tr,r}\mathbf{f}_{tr,w} + \tilde{\mathbf{s}}_{fl,r}\mathbf{f}_{fl,w}\end{aligned} \tag{18.15}$$

where $\mathbf{s}_{tr,r}$ and $\mathbf{s}_{fl,r}$ are the contact position vectors with respect to the cross-section centre, defined in the inertia reference frame. Note that the transformation of coordinates of the contact position points from rail cross-section coordinates to global coordinates is done by $\mathbf{s}_{tr,r} = \mathbf{A}_r \mathbf{s}'_{tr,r}$ and $\mathbf{s}_{fl,r} = \mathbf{A}_r \mathbf{s}'_{fl,r}$ with the transformation matrix $\mathbf{A}_r = \begin{bmatrix}\mathbf{u}_\xi & \mathbf{u}_\eta & \mathbf{u}_\zeta\end{bmatrix}_r$.

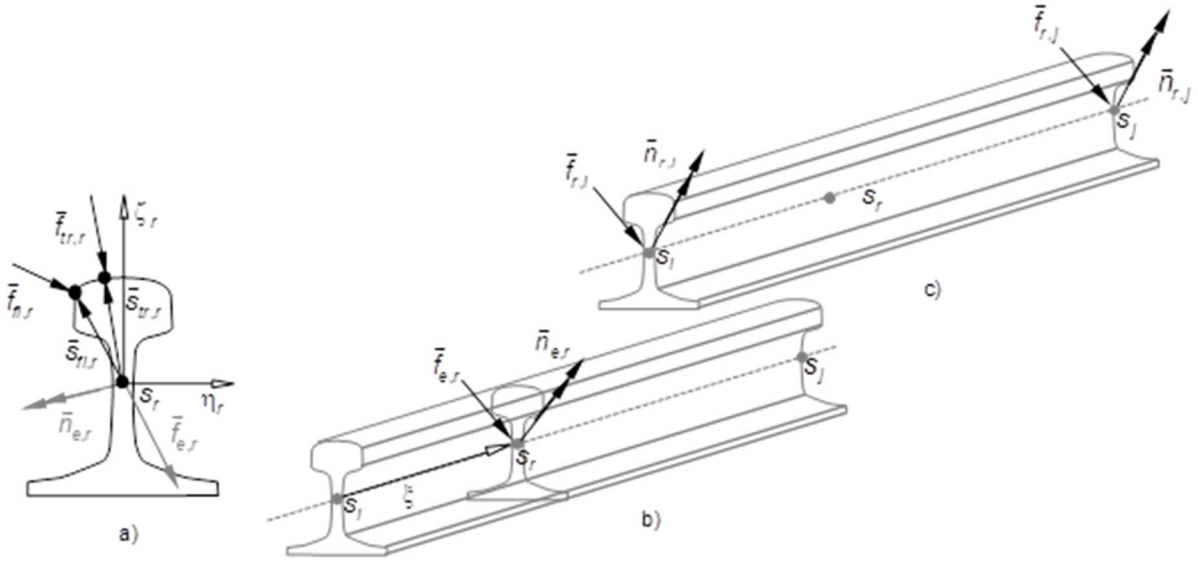

Figure 18.11: Wheel-rail contact force: (a) Rail cross-section in which the wheel tread and flange contact forces are applied; (b) Equivalent force system in the centre of the cross-section; (c) Equivalent system of nodal forces in a particular finite element of the rail.

An equivalent system of forces and moments applied in the beam finite element nodes, shown in Figure 18.11, that represents contact forces and transport moment applied to the rail-cross-section centre needs to be evaluated. The equivalent nodal forces are related to the concentrated forces and moments via the shape functions matrix as

$$\begin{Bmatrix}\mathbf{f}_{r,i}\\ \mathbf{n}_{r,i}\\ \mathbf{f}_{r,j}\\ \mathbf{n}_{r,j}\end{Bmatrix} = \begin{bmatrix}\mathbf{A}_e & & & \\ & \mathbf{A}_e & & \\ & & \mathbf{A}_e & \\ & & & \mathbf{A}_e\end{bmatrix} \begin{bmatrix}\mathbf{N}_i^{dd}(\xi) & \mathbf{N}_i^{d\theta}(\xi) & \mathbf{N}_j^{dd}(\xi) & \mathbf{N}_j^{d\theta}(\xi)\\ \mathbf{N}_i^{\theta d}(\xi) & \mathbf{N}_i^{\theta\theta}(\xi) & \mathbf{N}_j^{\theta d}(\xi) & \mathbf{N}_j^{\theta\theta}(\xi)\end{bmatrix}^T \begin{bmatrix}\mathbf{A}_e & \\ & \mathbf{A}_e\end{bmatrix}^T \begin{Bmatrix}\mathbf{f}_{e,r}\\ \mathbf{n}_{e,r}\end{Bmatrix} \tag{18.16}$$

and applied on the finite element nodes, i.e., $\mathbf{f}_{r,i}$ and $\mathbf{n}_{r,i}$ are applied on node *i* while $\mathbf{f}_{r,j}$ and $\mathbf{n}_{r,j}$ are applied on node j, as shown in Figure 18.11(c). The forces and moments are expressed in the inertia coordinate frame coordinates.

18.5 Vehicle-Track Co-Simulation

The vehicle-track co-simulation procedure, presented here, establishes the interaction between the individual sub-systems, each with its own distinct mathematical formulation and integration methodology, being their dynamic analysis performed by independent codes able to, eventually, run in a stand-alone mode. The behaviour of the two sub-systems is affected reciprocally by each other. A particular aspect of the co-simulation procedure proposed concerns the synchronisation of the integration algorithms that run with independent time steps, being the numerical stability and accuracy of the dynamic analysis of the coupled systems a fundamental aspect to account for [50].

The co-simulation procedure proposed is structured on three main key steps, addressed hereafter. The first step is to establish the coupling approach, i.e., an interface between the sub-systems that defines a set of state variables or forces within each sub-system to be shared with the other. The second step is to establish a fast and reliable data exchange procedure for the state variables and forces. The third, and final, step is to build a communication protocol that manages the use of the state variables and contact forces through the integration scheme for both sub-systems during their dynamics analysis.

18.5.1 Vehicle-track interface

Thought the coupling approach depends on the type of interaction between the models, most often the coupling is set by imposing either a kinematic constraint between the models or a set of constitutive interaction laws. Such constitutive interaction laws can result on a set of forces/torques that are applied on each sub-system. In this work, due to the nature of the coupled problem where their interaction is defined by the wheel-rail contact, the coupling of the sub-systems is established by the application of the resulting contact forces/torques on each model. Thus, each computer code solves its own equations of motion, which include the interaction forces. As the wheel-rail contact forces provide the link between to two sub-systems, the evaluation of the contact is done in one of the sub-systems while the other provides the parameters required to make such evaluation possible, in this case the state variables that allow for the solution of the contact problem. Evaluating the wheel-rail contact on the track sub-system, as shown in Figure 18.12, avoids a computationally expensive communication scheme. The contact model requires the deformed centre position of the rails, in the neighbourhood of the arc length of the track in which contact occurs, s_r, to allow for the solution of the nonlinear Eq.(18.4) for contact detection, which in turn requires all information associated to the finite

element mesh of the rails already available in the track sub-system. The vehicle sub-system is set to provide the spatial position, $\mathbf{q}_w$, and velocity, $\dot{\mathbf{q}}_w$, of each wheel centre of the vehicle model. The wheel-rail contact problem is solved in the track sub-system and, in return, the vehicle sub-system receives from the track sub-system an equivalent wheel-rail contact force, $\mathbf{f}_{e,w}$, and transport moment, $\mathbf{n}'_{e,w}$, to be applied at the corresponding wheel centres.

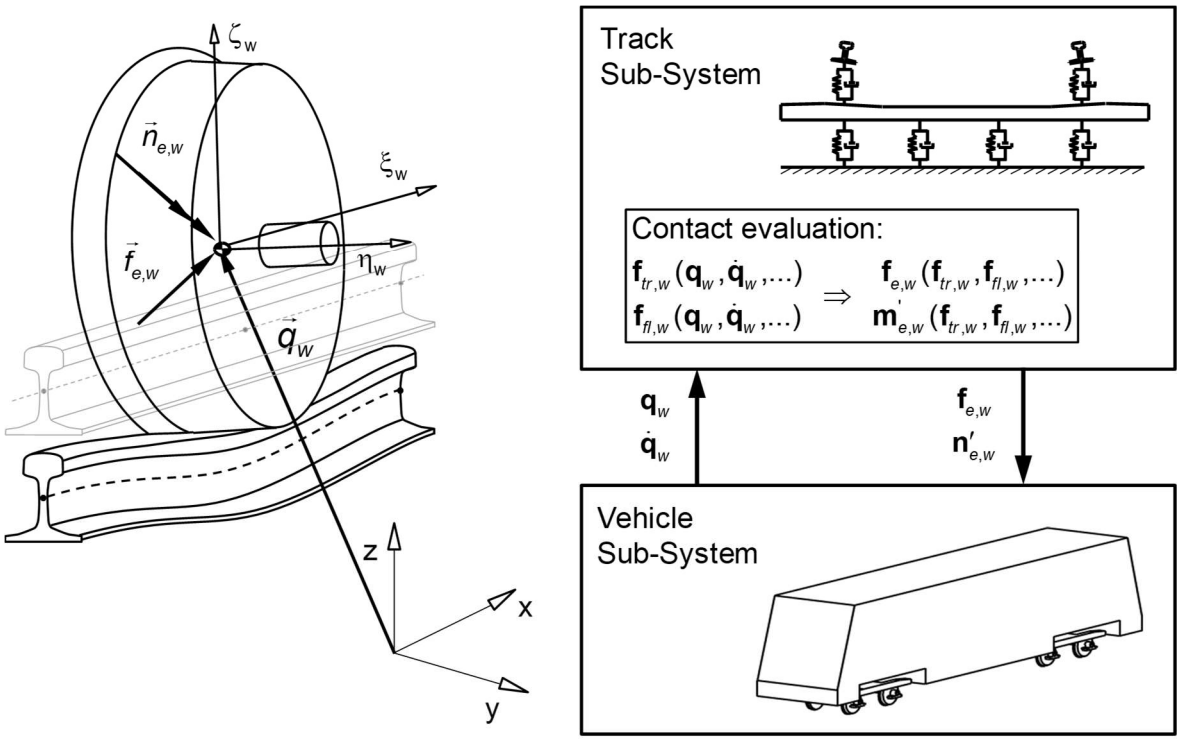

Figure 18.12: Vehicle-track co-simulation interface.

18.5.2 Data exchange method

As the state variables are a common resource shared between two concurrent processes being the data exchange procedure critical in the co-simulation. This procedure is not only responsible for exchanging the state variable data between sub-systems but also to control their access. This leads to two important requirements that the data exchange method needs to fulfil. First, given the frequency at which data needs to be exchanged, it must be sufficiently fast so that it does not become a bottleneck of the co-simulation procedure. Second, it must be robust by providing a mechanism where both sub-systems are synchronized over time and do not overstep each other.

The data exchange method is built by exchanging two communication files, as depicted in Figure 18.13. One file includes the state variables data, composed of the wheel centre position and velocity, denoted by *V2T file*, written by the vehicle sub-system code and read by the track sub-system code. The other file written by the track sub-system code and read by the vehicle sub-system code, denoted by *T2V file*, includes the equivalent wheel-rail contact forces to be

applied on the centre of each wheel. In order to keep both sub-systems synchronised and to avoid data do be overwritten without being read first, which is known as a race condition [51, 52], a binary semaphore is implemented [53]. Here, each communication file also carries a binary flag that according to its value either gives permission to one sub-system to read the data or the other to write it over. This method not only controls the reading/writing access of the state variables but also provides means to control the progress of the integration algorithms of each one of the individual analysis codes so that they stay synchronized.

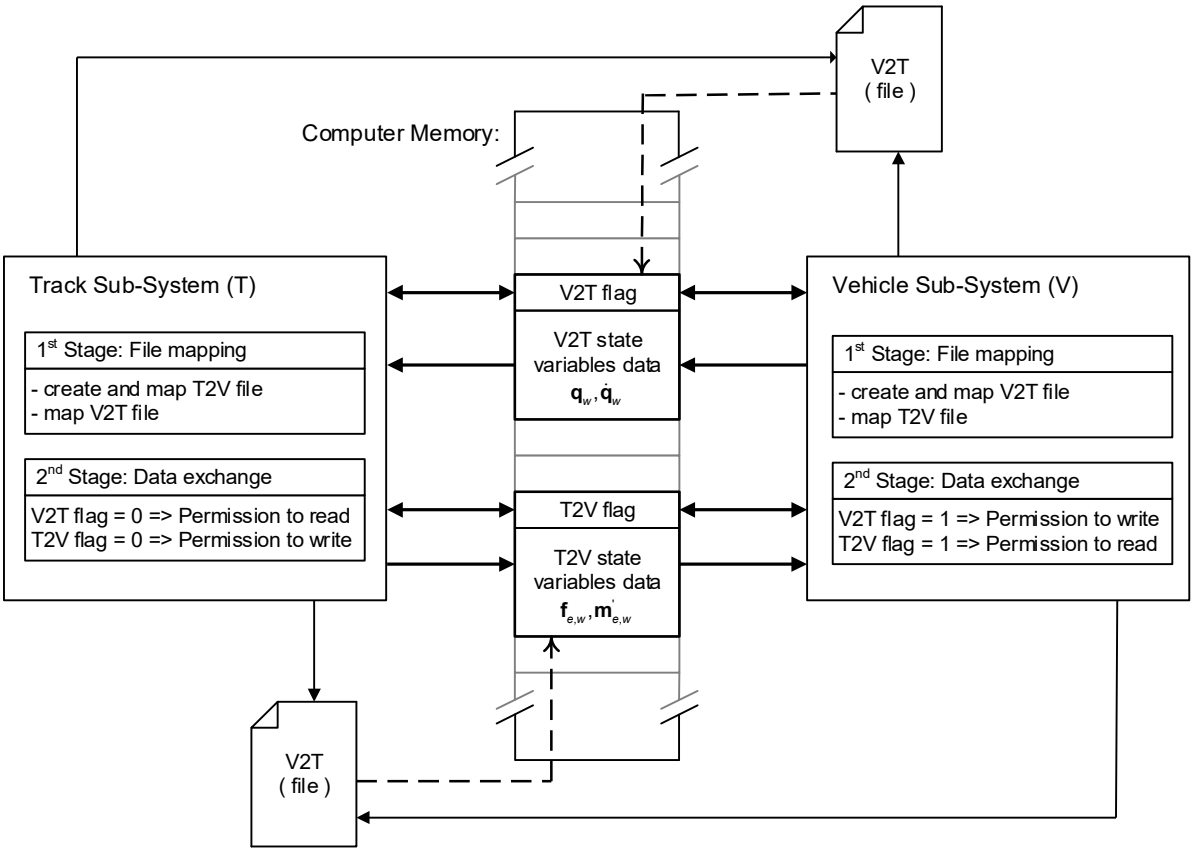

Figure 18.13: Vehicle-track data exchange procedure.

The time spent on data exchange between codes must be negligible compared to the computation time costs of the independent analyses. Therefore, the data exchange procedure uses memory sharing via memory mapped files. A memory mapped file is a segment of computer memory which is mapped in order to have a direct byte-for-byte assignment to a hard disk file or other resource that the operating system can refer to. Once this correlation is established, or mapped, the memory mapped file can be accessed directly from computer memory becoming a much faster data exchange process. This memory sharing implementation is depicted in Figure 18.13. At the start of the analysis, one of the applications creates a file and maps it to memory while the other waits for the file to be created. Whenever this file is found by the waiting application the file is also mapped to the same corresponding memory address. Having both

applications mapped the same file in memory they can communicate using a common memory address whereas the created file only serves has a point of reference for both applications to map the same dataset in memory.

18.5.3 Communication protocol

The communication protocol is responsible for managing the use and update of the state variables along the integration scheme of each sub-system. In this work each sub-system has a distinct formulation and integration procedure, on one side the railway multibody vehicle model is evaluated as a nonlinear dynamic system handled with a variable time step, multi-order integrator, while a finite element track model is evaluated as dynamic linear system integrated with a Newmark family numerical integrator with a fixed time step. The heterogeneity of these integration schemes and the premise to keep them independent and fundamentally unchanged requires careful consideration. Thus, the compatibility between the two integration algorithms imposes that the state variables of the two sub-systems are readily available at every time step. This is guaranteed by a state variable interpolation/extrapolation scheme where the state variable data used by each sub-system is updated following the communication protocol presented in Figure 18.14. At a given time step, t_T, the track model requires the positions and velocities of the wheel centres to evaluate the wheel-rail contact force. Meanwhile, the vehicle model, evaluated with a variable time step, requires the equivalent wheel-rail contact forces available to be applied on its model and proceed with its integration. Therefore, there is the need of one of the sub-systems to make a prediction on a forthcoming time, before advancing to a new time step. Given the integration procedure structure between the two systems, the vehicle model is selected to be the leading sub-system. Hence, the equivalent contact forces to be applied on the wheel are estimated by linear extrapolation of the state variable data, $\mathbf{f}_E$, t_E, and provided by the track sub-system. Whenever the track sub-system integrator requires data to proceed it is set to wait until the vehicle model has advanced to the point where it can interpolate the results of its evaluation in order to provide the wheel positions and velocities for the required time step. It is important to note that the accuracy and stability of this methodology relies on ensuring that the vehicle sub-system variable time step size is never larger than the fixed time step of the track. Furthermore, the vehicle integrator time step size is also required to be small enough so it does not critically overextend the state variable extrapolation. This is guaranteed by limiting its maximum step size to be smaller than the track time step size.

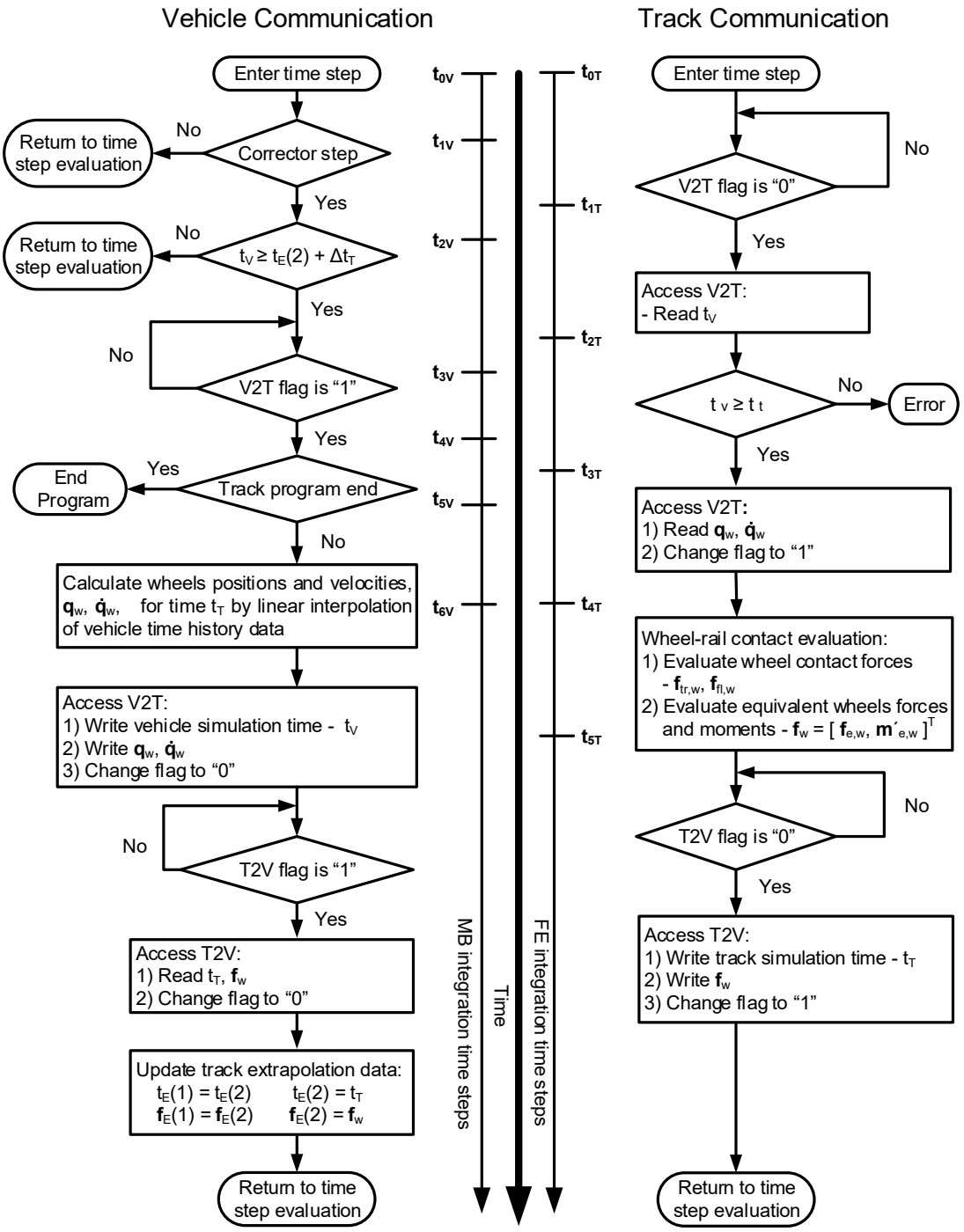

Figure 18.14: Vehicle-track communication protocol.

18.6 Demonstrative Application

The demonstration of the vehicle-track co-simulation procedure proposed here, and of its implications on the wheel-rail rolling contact problem, is carried with a case scenario. Three alternatives are tested for the representation of the wheel-rail interaction problem. One corresponds to the co-simulation procedure, presented here, where a multibody vehicle model

is coupled with a finite element track model so that track flexibility is taken into consideration. A second alternative consists of the same co-simulation procedure but assuming the track to be rigid by neglecting the finite-element nodal displacements. The third simulation is run, to serve as a control, with the standalone multibody code where the vehicle runs on the rigid track, i.e., using the standard approach in railway vehicle dynamics studies.

18.6.1 Case scenario

The track considered for the case scenario is composed by a straight segment followed by a small radius left-hand curve and a short straight track segment. It also includes two transition zones between the curve and straight segments as depicted in Figure 18.15. The track geometry is designed following standard EN13803-1 for a vehicle operating at a speed of 110 km/s while negotiating a 500 m radius curve at its maximum allowed superelevation and cant deficiency limit. Iberic gauge is selected for the track with UIC60 rail profiles and 1/20 rail inclination.

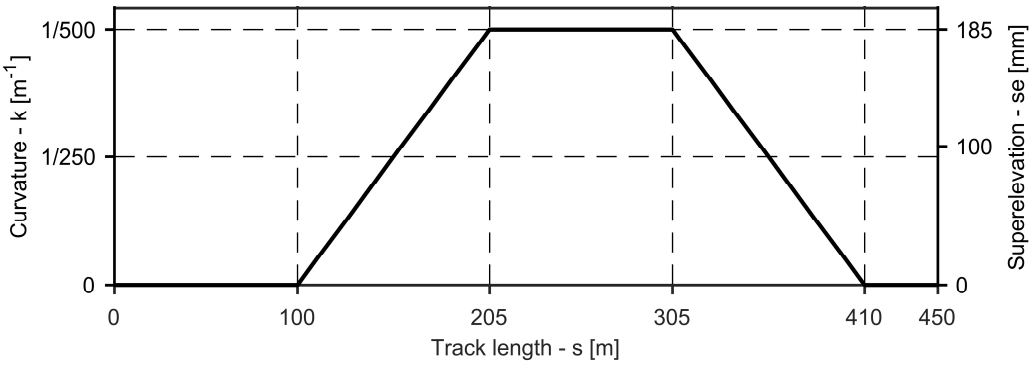

Figure 18.15: Curvature and superelevation along track length.

The material properties used to build the finite element model of the track are presented on Table 18.1, for the rail and sleeper beam elements, and on Table 18.2, for the remaining spring-damper elements, being the references in which the data for the parameters is obtained provided also.

EB beam element properties	Rail	Ref.	Sleeper	Ref
Young Modulus - E [Pa]	2.10×10^{11}	[30]	3.10×10^{10}	[50]
Torsion Modulus - G [Pa]	8.08×10^{10}		1.50×10^{10}	[51]
Cross Section Area - A [m^2]	7.67×10^{-3}	[52]	5.6×10^{-2}	[50]
Polar Moment of Area in ηζ Plane - $J_{\xi\xi}$ [m^4]	3.55×10^{-5}	[52]	1.71×10^{-3}	
Second Moment of Area in ξζ Plane - $I_{\eta\eta}$ [m^4]	3.04×10^{-5}	[52]	2.60×10^{-4}	
Second Moment of Area in ξη Plane - $I_{\zeta\zeta}$ [m^4]	5.12×10^{-6}	[52]	1.67×10^{-4}	
Density ρ [Kg/m^3]	7860	[53]	2750	[30]
Rayleigh Damping Parameter – α [s^{-1}]	3.98×10^{-4}		3.98×10^{-4}	
Rayleigh Damping Parameter – β [s]	0.94		0.94	

Table 18.1: Beam element properties of the track model.

The track model, which in the case of this demonstration scenario has a length of 500 m, includes energy absorption boundary conditions at the start and end of the track model. The

properties of the spring-damper elements used in the start and end of the track, in the longitudinal direction, are presented in Table 18.2. It should also be noted that although the values for the parameters used to model the track are obtained from State-of-Art references, they do not ensure that the track model dynamic response is that of an existing one. The receptances on the rail above the sleeper and in-between sleepers can be evaluated either to validate the track models against experimental results, if these exist, or to provide typical responses for realistic track models that can be compared with those available in the literature, in particular in the work by Knothe and Grassie [24].

Spring-damper element	Pads	Ref.	Ballast	Ref.	Sleeper Interaction	Ref.
Vertical Stiffness – K_v [N/m]	1.30×10^8	[57]	6.19×10^7	[58]	5.50×10^5	[59]
Transversal Stiffness - K_t [N/m]	4.00×10^7		1.00×10^7	[59]	4.05×10^5	[59]
Longitudinal Stiffness - K_l [N/m]	4.00×10^7	[57]	5.50×10^5		3.92×10^7	[35]
Longitudinal Rotation Stiffness - K_{rl} [N/m]	2.00×10^5		-		-	
Vertical Damping - C_v [Ns/m]	1.50×10^5	[57]	2.94×10^4	[35]	2.94×10^4	
Transversal Damping - C_t [Ns/m]	1.00×10^5		2.94×10^4		2.94×10^4	
Longitudinal Damping - C_l [Ns/m]	1.00×10^5	[57]	2.94×10^4		2.94×10^4	[35]
Lumped mass - m [kg]	-		226.41	[58]	-	

Table 18.2: Spring-damper element properties of the track model.

The vehicle model considered in this work is used by a Portuguese railway operator for passenger transport [60, 61]. The initial position of the bodies of the vehicle model, shown in Figure 18.1, their masses and inertia properties are listed in Table 18.3.

ID		Body	Centre of Mass [m] (X/Y/Z)	Mass [kg]	Moment of Inertia [kg/m^2] (ξξ/ηη/ζζ)
1		Carbody	11.5000 / 0.000 / 1.432	46200	78000 / 2600000 / 2600000
2	Leading bogie	Bogie frame	21.000 / 0.000 / 0.448	3000	2100 / 2600 / 4800
3		Front wheelset	22.350 / 0.000 / 0.445	1800	900 / 10 / 900
4		Front left axlebox	22.350 / 1.072/ 0.445	10	1 / 1 / 1
5		Front right axlebox	22.350 / -1.072 / 0.445	10	1 / 1 / 1
6		Rear wheelset	19.650 / 0.000 / 0.445	1800	900 / 10 / 900
7		Rear left axlebox	19.650 / 1.072 / 0.445	10	1 / 1 / 1
8		Rear right axlebox	19.650 / -1.072 / 0.445	10	1 / 1 / 1
9	Trailing bogie	Bogie frame	2.000 / 0.000 / 0.448	3000	2100 / 2600 / 4800
10		Front wheelset	3.350 / 0.000 / 0.445	1800	900 / 10 / 900
11		Front left axlebox	3.350 / 1.072 / 0.445	10	1 / 1 / 1
12		Front right axlebox	3.350 / -1.072 / 0.445	10	1 / 1 / 1
13		Rear wheelset	0.650 / 0.000 / 0.445	1800	900 / 10 / 900
14		Rear left axlebox	0.650 / 1.072 / 0.445	10	1 / 1 / 1
15		Rear right axlebox	0.650 / -1.072 / 0.445	10	1 / 1 / 1

Table 18.3: Centre of mass and inertia properties of the bodies considered in the vehicle model.

The primary suspension, responsible for transmitting the forces between the axleboxes and the bogie frame, is shown in Figure 18.2, being its kinematic and force element parameters described in reference [60, 61]. The secondary suspension, responsible for transmitting the forces between the bogie frame and the carbody is also shown in Figure 18.2, being the data

necessary to build its model and the bogie carbody connection found in [60]. The relative motion between the wheelset and axleboxes is constrained by tapered rolling bearings. Due to the nature and construction of these bearings, it is assumed here that the revolute joints between the wheelset and axleboxes are representative of their relative kinematics [36].

18.6.2 Results

The vehicle-track interaction dynamics involves a large set of dynamic responses that is not possible to present concisely in this work. With the purpose of presenting the influence of the flexible track on the vehicle dynamics, the interaction forces due to the wheel-rail contact and the kinematics of the front wheelset of the vehicle are selected as representative responses that allow understanding novel features of the approach proposed. In all that follows, the initial 0.25s of any simulation results are discarded, as during this period the dynamics of the system exhibit a transient response while reaching a steady-state operation. The kinematics of the leading wheelset of the vehicle is presented in Figure 18.16, for the lateral position, in Figure 18.17, for the attack angle, and Figure 18.18, for the vertical position. Comparing the results between the standalone simulation in which the track is considered rigid, denoted by *rigid*, and the co-simulation with the rigid finite element track model, denoted as *co-sim rigid*, it is observed a good agreement being their maximum absolute deviation lower than, 2.5×10^{-5} m for the lateral motion, 4.7×10^{-4} ° for the attack angle, and 8×10^{-8} m for the vertical motion. Given that the two simulations that consider the rigid track, where one is evaluated in co-simulation, the residual deviation on the results shows that the implemented co-simulation procedure is accurate.

Comparing the co-simulation results involving the rigid track, *co-sim rigid*, and the flexible track, *co-sim flex*, it is possible to identify a distinguishable influence of the track flexibility on the wheelset motion. With respect to the lateral motion, a slightly higher amplitude of the lateral motion is noticeable in the straight segment of the flexible track simulation. In the curved segment the lateral motion of the wheel also presents small offset from the motion when rigid track is considered. The angle of attack of the leading wheelset evaluated also shows a small influence of the track flexibility, being slightly larger angle when track flexibility is considered. Moreover, when comparing the vertical motion of the wheelset, in Figure 18.18, besides the vertical offset also an oscillatory movement is found in the simulation with track flexibility. This additional oscillatory behaviour is more easily identified in the straight segment whereas in the curve the motion of the wheelset set is also influenced by the wheel flange contact at the outer rail. Note that the frequency of these oscillations is about 51 Hz which is

consistent to the periodicity of the track sleepers, spaced at every 0.6m, for a vehicle traveling at 110 km/h.

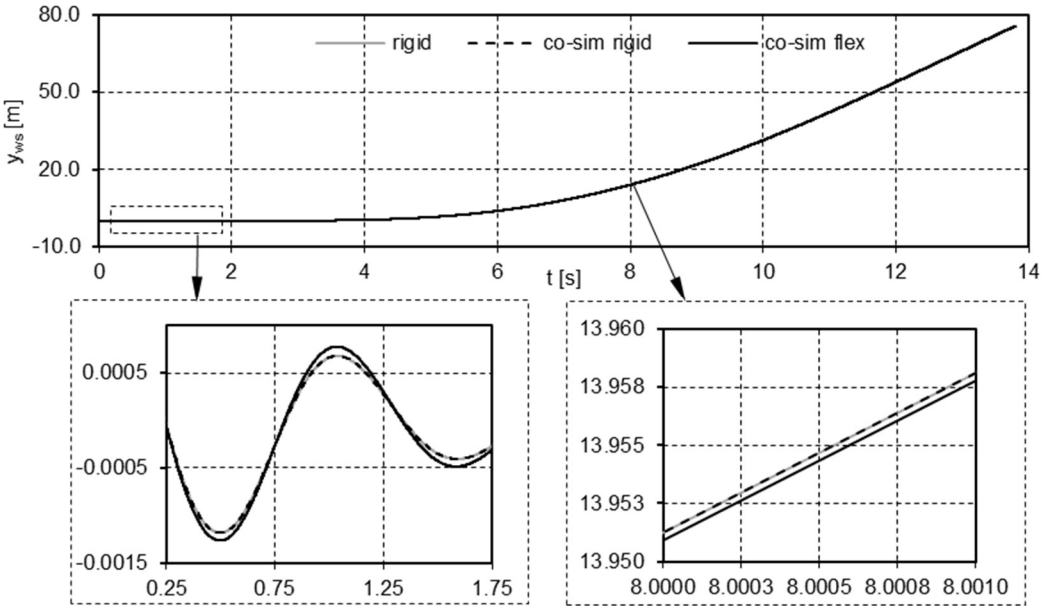

Figure 18.16: Comparison of the lateral motion of the leading wheelset.

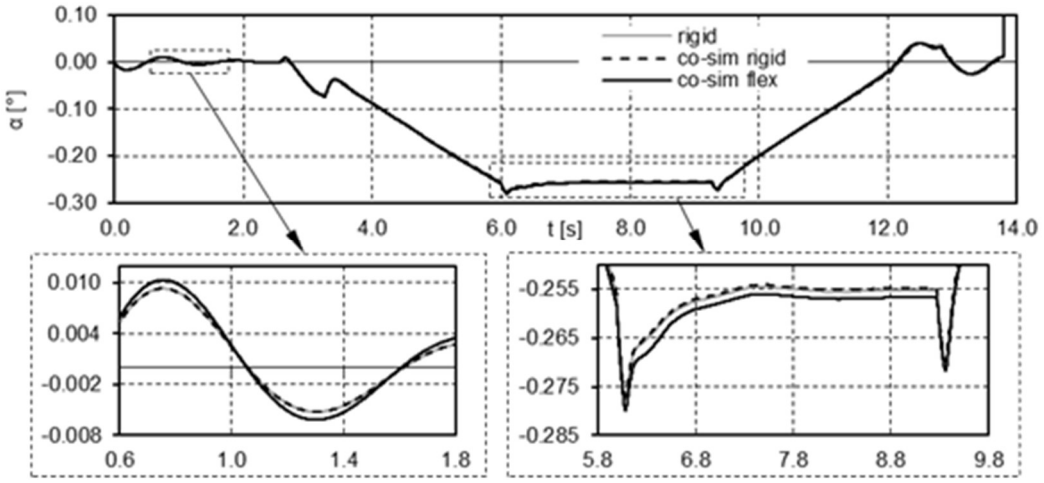

Figure 18.17: Comparison of the leading wheelset angle of attack.

For the standalone simulation with rigid track and the co-simulation with the flexible track the left and right wheel flange contact forces of the leading wheelset are presented in Figure 18.19. Flange contact only occurs in the outer wheel during curve negotiation. The force peaks observed when the wheels enter the transition and the curve segment are smaller when track flexibility is considered. On the curve section, it can be noted also that the flange force is oscillating at a higher amplitude when the track is considered rigid.

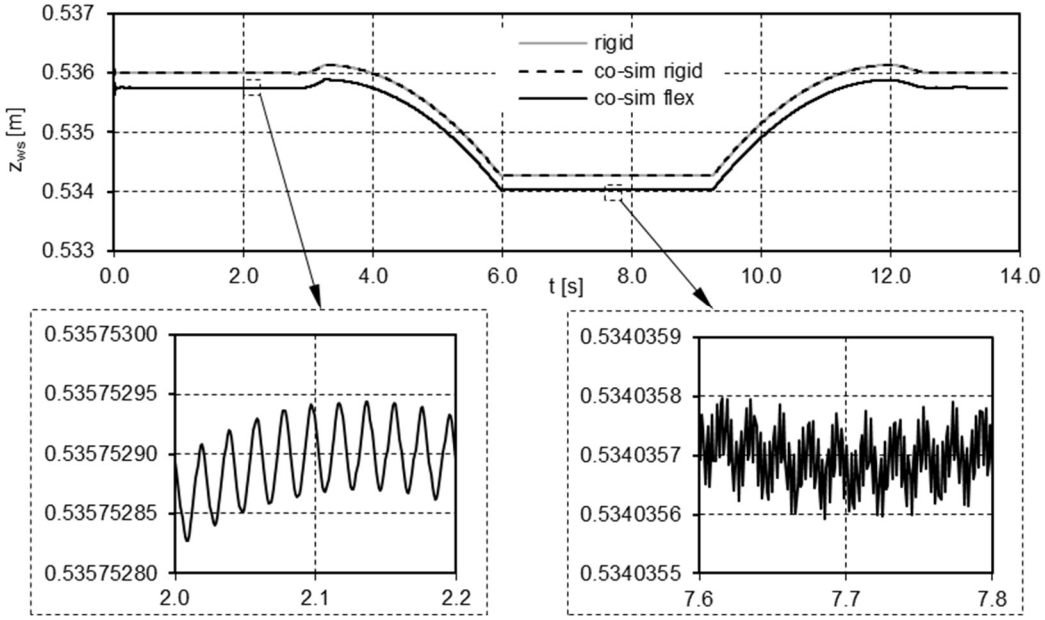

Figure 18.18: Vertical motion comparison of the leading wheelset.

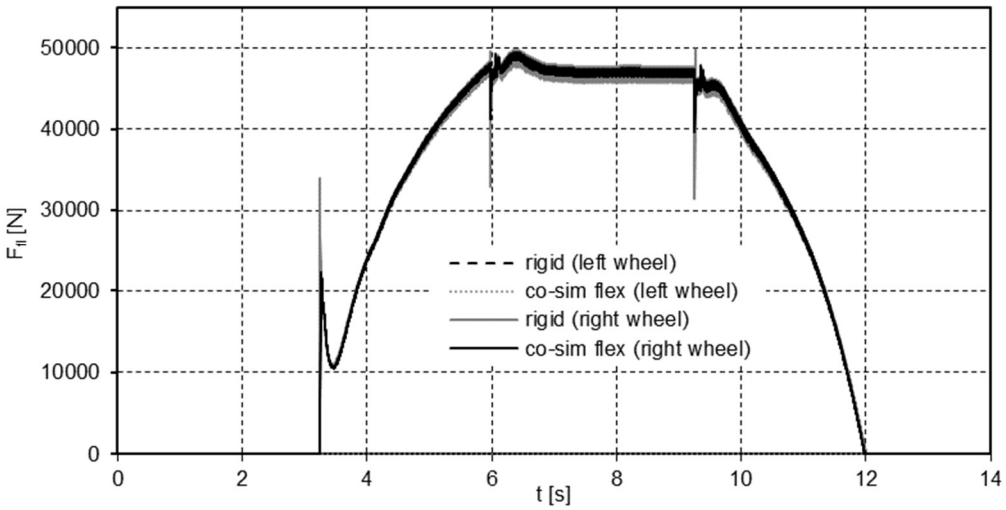

Figure 18.19: Flange contact force on the left and right wheel of the leading wheelset.

The oscillating amplitude and peak differences on the curved segment of the track can also be observed on the lateral and vertical contact forces applied on the wheel. These forces are presented in Figure 18.20 and Figure 18.21, respectively, for the left and right leading wheels of the front bogie. In the curve segment of the track both the lateral and vertical contact forces of the right wheel are higher. This is due to the flange forces acting on the right wheel when the curve is negotiated. It is also possible to observe two force peaks on the first transition segment from straight to curved track around time 2.5s and 3.2s. These correspond to the instants in which the leading wheel of the front and rear bogies enter the transition zone. Therefore, the wheel-rail contact on the front wheel of the front bogie is sensitive to the contact perceived on the rear bogie.

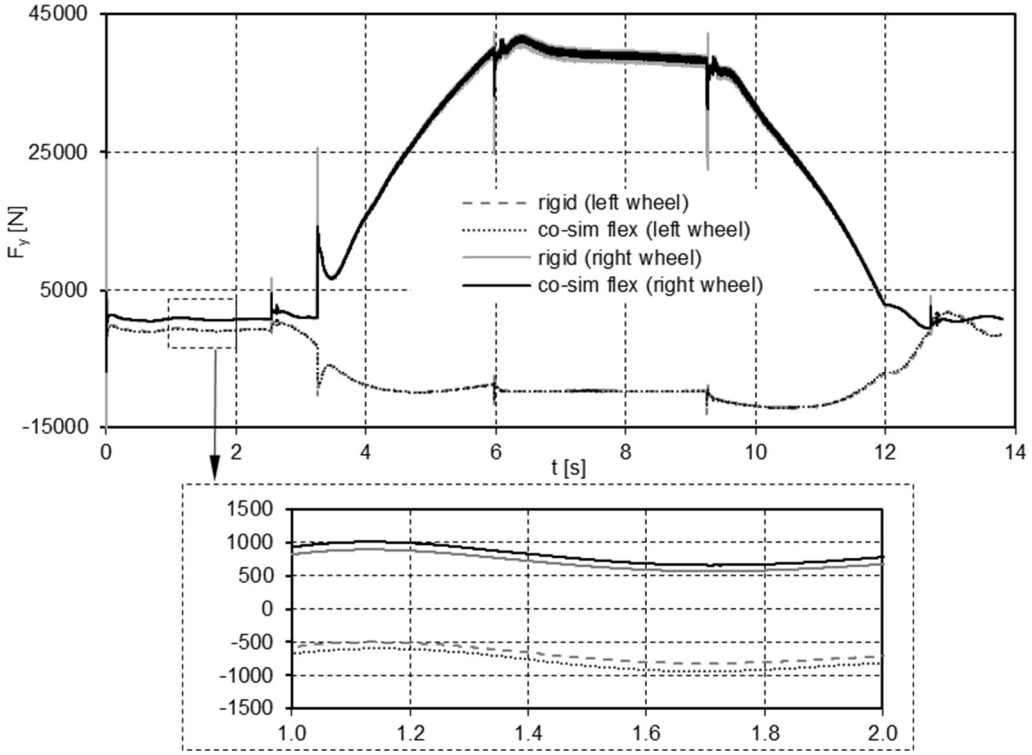

Figure 18.20: Lateral forces applied on the left and right leading wheel.

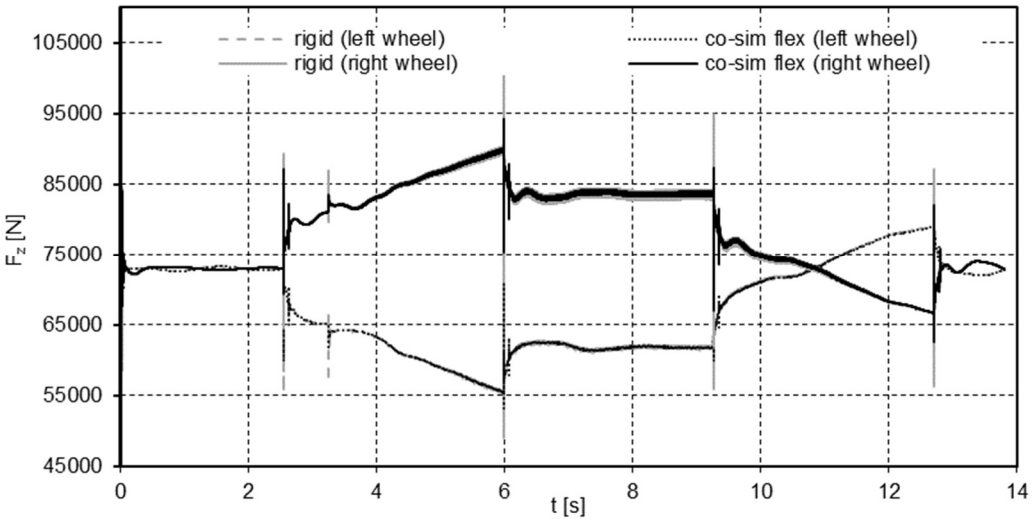

Figure 18.21: Vertical forces applied on the left and right leading wheel.

Furthermore, on the straight segment the lateral contact forces from the co-simulation with flexible track are 10% higher than those observed for the rigid track simulation. This difference can be related with the configuration of the deformed track which promotes a different wheel-rail contact conditions. It is also of importance to state that although, for the sake of simplicity, the contact forces on the co-simulation with rigid track, *co-sim rigid*, are not shown here, they are similar to those obtained with the standalone multibody code in which only rigid tracks are used.

The effects of the vehicle-track interaction on the flexible track are depicted by the vertical and transversal displacements of the left and right rail at two different cross-sections, presented in Figure 18.22 and Figure 18.23. These figures correspond respectively to the rails displacements evaluated on the straight and curve segment at the 66 and 255 metre mark of the track length.

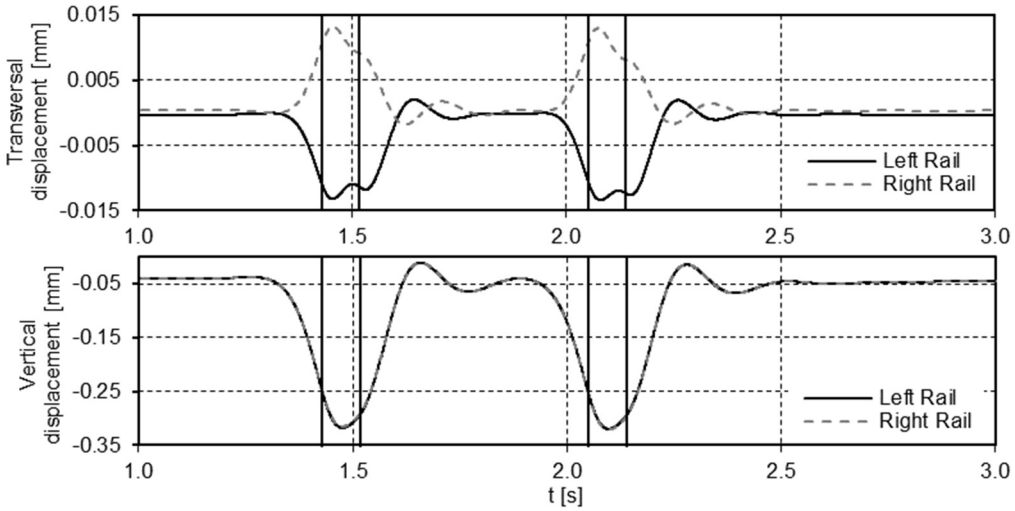

Figure 18.22: Transversal and vertical displacements of the left and right rail at the 66 metre mark of the track (straight track segment).

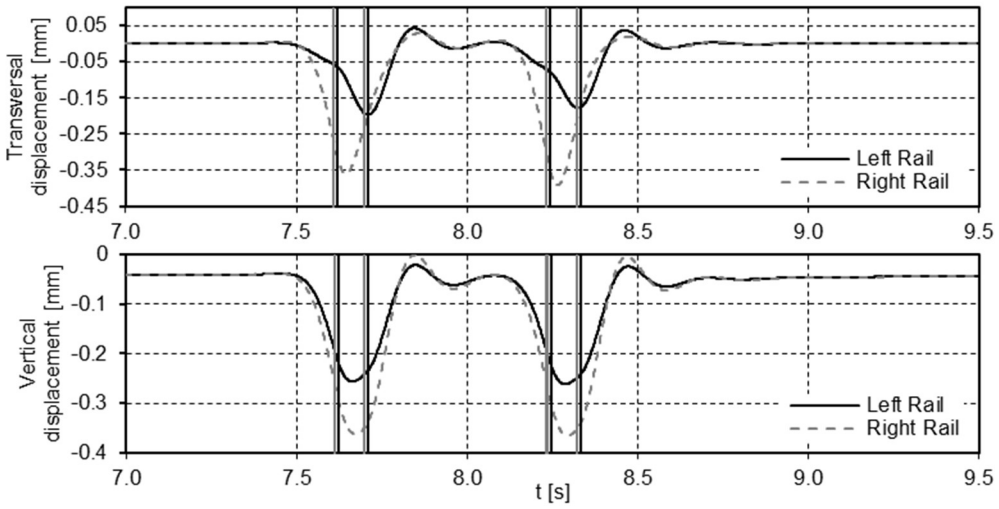

Figure 18.23: Transversal and vertical displacements of the left and right rail at the 255 metre mark of the track (curve track segment).

The vertical solid lines marked in Figure 18.22 and Figure 18.23 indicate the instants in which the train wheels pass on each mark. The absolute maximum displacement peaks are observed in-between the front and rear wheel passage of each bogie, except for the transversal displacements on the curved segment. This relates to the contact on the wheel flange that only occurs on the front right wheel of each bogie. Furthermore, it can be observed that on the same

track position each wheel that passes perceives the position of the rail differently, which cannot be represented with a rigid track model. Moreover, the transversal track displacements on the straight segment are symmetric, i.e., the left and right rails move to the inside of the track. Contrarily, on the curved segment both rails are displaced to the outer side of the curve being the right wheel displacement more prominent. This effect is also observed for the vertical displacements in the curved section where the right rail is loaded heavily due to the curve negotiation and the track superelevation.

In the simulation of the railway vehicle-track interaction scenarios developed in this work the simulation of the dynamics of the vehicle and track multibody model uses a variable time step integrator while a fixed time step of 2×10^{-5} s, used for the finite element flexible track model. This value for the time step is obtained by reducing the step size until the contact forces evaluated stabilize and converge, i.e., until they become identical for any time step smaller than that identified. It should also be noted that the co-simulation with rigid track and flexible track are, respectively, 7.9 and 57.3 times longer than that with the standalone multibody simulation with rigid track.

18.7 Conclusions

This work proposes a vehicle-track co-simulation methodology to allow the study of the coupled dynamics of the railway vehicle and the flexible track models. The key ingredient of the co-simulation is the wheel-rail interaction characterized by the rolling contact forces in which the contact detection problem is strongly influenced by the ability to evaluate the track deformation. The vehicle model is described and analysed using a multibody dynamics model in which a variable time step integrator is used. The track model is described by a linear finite element method in which a fixed time step integrator, of the Newmark family, is used. The wheel-rail contact force model is evaluated online with the Polach algorithm taking into account the deformation of the rails. The study of a case scenario allows to identify some of the novel features of the methodology proposed here. Not only significate differences on the vehicle kinematics exist when considering the track flexibility, namely during curve negotiations, but also the contact forces are modified, being the lateral, or creep, forces higher for a flexible track. The track deformations are clearly identified, and closely related to the train wheelset kinematics, by using the methodology proposed. The results obtained do not allow to understand up to what extend the track flexibility influences the vehicle dynamics. Further studies on this aspect of the vehicle-track coupled dynamics can be carried as the interaction

modelling procedure, via co-simulation, shows to be accurate and robust.

REFERENCES

1. ERRAC: Strategic Rail Research Agenda 2020. , Brussels, Belgium (2007)
2. OECD: Strategic Transport Infrastructure Needs to 2030. OECD Publishing, Paris, France (2012)
3. Felippa, C.A., Park, K.C.C., Farhat, C.: Partitioned analysis of coupled mechanical systems. Comput. Methods Appl. Mech. Eng. 190, 3247–3270 (2001). doi:10.1016/S0045-7825(00)00391-1
4. Hulbert, G., Ma, Z.-D., Wang, J.: Gluing for Dynamic Simulation of Distributed Mechanical Systems. In: Ambrósio (Ed.), J. (ed.) Advances on Computational Multibody Systems. pp. 69–94. Springer, Dordrecht, The Netherlands (2005)
5. Kubler, R., Schiehlen, W.: Modular Simulation in Multibody System Dynamics. Multibody Syst. Dyn. 4, 107–127 (2000)
6. Dietz, S., Hippmann, G., Schupp, G.: Interaction of Vehicles and Flexible Tracks by Co-Simulation of Multibody Vehicle Systems and Finite Element Track Models. Veh. Syst. Dyn. 37, 372–384 (2002). doi:10.1080/00423114.2002.11666247
7. Heckmann, A., Arnold, M., Vaculín, O.: A modal multifield approach for an extended flexible body description in multibody dynamics. Multibody Syst. Dyn. 13, 299–322 (2005). doi:10.1007/s11044-005-4085-3
8. Liu, F., Cai, J., Zhu, Y., Tsai, H.M., Wong, A.S.F.: Calculation of Wing Flutter by a Coupled Fluid-Structure Method. J. Aircr. 38, 334–342 (2001). doi:10.2514/2.2766
9. Bathe, K.J., Zhang, H.: Finite element developments for general fluid flows with structural interactions. Int. J. Numer. Methods Eng. 60, 213–232 (2004). doi:10.1002/nme.959
10. Naya, M., Cuadrado, J., Dopico, D., Lugris, U.: An Efficient Unified Method for the Combined Simulation of Multibody and Hydraulic Dynamics: Comparison with Simplified and Co-Integration Approaches. Arch. Mech. Eng. LVIII, 223–243 (2011). doi:10.2478/v10180-011-0016-4
11. Busch, M., Schweizer, B.: Coupled simulation of multibody and finite element systems: an efficient and robust semi-implicit coupling approach. Arch. Appl. Mech. 82, 723–741 (2012). doi:10.1007/s00419-011-0586-0
12. Carstens, V., Kemme, R., Schmitt, S.: Coupled simulation of flow-structure interaction in turbomachinery. Aerosp. Sci. Technol. 7, 298–306 (2003). doi:10.1016/S1270-9638(03)00016-6
13. Spreng, F., Eberhard, P., Fleissner, F.: An approach for the coupled simulation of machining processes using multibody system and smoothed particle hydrodynamics algorithms. Theor. Appl. Mech. Lett. 3, 013005 (2013). doi:10.1063/2.1301305
14. Anderson, K.S., Duan, S.: A hybrid parallelizable low-order algorithm for dynamics of multi-rigid-body systems: Part I, chain systems. Math. Comput. Model. 30, 193–215 (1999). doi:10.1016/S0895-7177(99)00190-9
15. Wang, J., Ma, Z., Hulbert, G.M.: A Gluing Algorithm for Distributed Simulation of Multibody Systems. Nonlinear Dyn. 34, 159–188 (2003). doi:10.1023/B:NODY.0000014558.70434.b0
16. Verhoef, M., Visser, P., Hooman, J., Broenink, J.: Co-simulation of Distributed Embedded Real-Time Control Systems. In: Davies, J. and Gibbons, J. (eds.) Integrated Formal Methods: 6th International Conference, IFM 2007, Oxford, UK, July 2-5, 2007. Proceedings. pp. 639–658. Springer Berlin Heidelberg, Berlin, Heidelberg (2007)
17. Spiryagin, M., Simson, S., Cole, C., Persson, I.: Co-simulation of a mechatronic system using Gensys and Simulink. Veh. Syst. Dyn. 50, 495–507 (2012). doi:10.1080/00423114.2011.598940
18. Gu, B., Asada, H.H.: Co-Simulation of Algebraically Coupled Dynamic Subsystems Without Disclosure of Proprietary Subsystem Models. J. Dyn. Syst. Meas. Control. 126, 1 (2004). doi:10.1115/1.1648307
19. Ambrósio, J., Pombo, J., Rauter, F., Pereira, M.: A Memory Based Communication in the Co-Simulation of Multibody and Finite Element Codes for Pantograph-Catenary Interaction Simulation. In: Bottasso C.L., E. (ed.) Multibody Dynamics. pp. 211–231. Springer, Dordrecht, The Netherlands (2008)
20. Ambrósio, J., Pombo, J., Antunes, P., Pereira, M.: PantoCat statement of method. Veh. Syst. Dyn. 53, 314–328 (2015). doi:10.1080/00423114.2014.969283
21. Massat, J.-P., Laurent, C., Bianchi, J.-P., Balmès, E.: Pantograph catenary dynamic optimisation based on advanced multibody and finite element co-simulation tools. Veh. Syst. Dyn. 52, 338–354 (2014). doi:10.1080/00423114.2014.898780
22. Colombo, E.F., Di Gialleonardo, E., Facchinetti, A., Bruni, S.: Active carbody roll control in railway vehicles using hydraulic actuation. Control Eng. Pract. 31, 24–34 (2014). doi:10.1016/j.conengprac.2014.05.010

23. Kuka, N., Verardi, R., Ariaudo, C., Dolcini, A.: Railway Vehicle Driveline Modelling and Co-Simulations in SIMPACK-Simulink. In: Proceedings of the Third International Conference on Railway Technology: Research, Development and Maintenance", Civil-Comp Press, Stirlingshire, UK, 2016. , Cagliari, Sardinia, Italy (2016)
24. Knothe, K.L., Grassie, S.L.: Modelling of Railway Track and Vehicle/Track Interaction at High Frequencies. Veh. Syst. Dyn. 22, 209–262 (1993). doi:10.1080/00423119308969027
25. Pombo, J., Ambrósio, J.: Application of a Wheel-Rail Contact Model to Railway Dynamics in Small Radius Curved Tracks. Multibody Syst. Dyn. 19, 91–114 (2008)
26. Magalhaes, H., Ambrosio, J., Pombo, J.: Railway vehicle modelling for the vehicle-track interaction compatibility analysis. Proc. Inst. Mech. Eng. Part K J. Multi-body Dyn. 230, 251–267 (2016). doi:10.1177/1464419315608275
27. Mazzola, L., Bruni, S.: Effect of suspension parameter uncertainty on the dynamic behaviour of railway vehicles. In: Applied Mechanics and Materials. pp. 177–185. Trans Tech Publ (2012)
28. Polach, O., Evans, J.: Simulations of Running Dynamics for Vehicle Acceptance: Application and Validation. Int. J. Railw. Technol. 2, (2013). doi:10.4203/ijrt.2.4.4
29. Di Gialleonardo, E., Braghin, F., Bruni, S.: The influence of track modelling options on the simulation of rail vehicle dynamics. J. Sound Vib. 331, 4246–4258 (2012). doi:10.1016/J.JSV.2012.04.024
30. Escalona, J.L., Sugiyama, H., Shabana, A. a.: Modelling of structural flexiblity in multibody railroad vehicle systems. Veh. Syst. Dyn. 51, 1027–1058 (2013). doi:10.1080/00423114.2013.786835
31. Lundqvist, A., Dahlberg, T.: Load impact on railway track due to unsupported sleepers. Proc. Inst. Mech. Eng. Part F J. Rail Rapid Transit. 219, 67–77 (2005). doi:10.1243/095440905X8790
32. Recuero, A.M., Escalona, J.L., Shabana, A.A.: Finite-element analysis of unsupported sleepers using three-dimensional wheel–rail contact formulation. Proc. Inst. Mech. Eng. Part K J. Multi-body Dyn. 225, 153–165 (2011). doi:10.1177/2041306810394971
33. Johansson, A., Pålsson, B., Ekh, M., Nielsen, J.C.O., Ander, M.K.A., Brouzoulis, J., Kassa, E.: Simulation of wheel–rail contact and damage in switches and crossings. Wear. 271, 472–481 (2011). doi:10.1016/j.wear.2010.10.014
34. Martínez-Casas, J., Di Gialleonardo, E., Bruni, S., Baeza, L.: A comprehensive model of the railway wheelset–track interaction in curves. J. Sound Vib. 333, 4152–4169 (2014). doi:10.1016/J.JSV.2014.03.032
35. Zhai, W., Wang, K., Cai, C.: Fundamentals of vehicle–track coupled dynamics. Veh. Syst. Dyn. 47, 1349–1376 (2009). doi:10.1080/00423110802621561
36. Nikravesh, P.E.: Computer-Aided Analysis of Mechanical Systems. Prentice-Hall, Englewood Cliffs, New Jersey (1988)
37. Ambrósio, J., Neto, A.: Stabilization Methods for the Integration of DAE in the Presence of Redundant Constraints. Multibody Syst. Dyn. 10, 81–105 (2003)
38. Gear, C.W.: Simultaneous Numerical Solution of Differential-Algebraic Equations. IEEE Trans. Circuit Theory. 18, 89–95 (1971)
39. Przemieniecki, J.S.: Theory of Matrix Structural Analysis. McGraw-Hill, New York (1968)
40. Ambrósio, J., Antunes, P., Pombo, J.J.: On the requirements of interpolating polynomials for path motion constraints. In: Kecskeméthy, A. and Geu Flores, F. (eds.) Mechanisms and Machine Science. pp. 179–197. Springer International Publishing (2015)
41. Pombo, J., Ambrósio, J.: An Alternative Method to Include Track Irregularities in Railway Vehicle Dynamic Analyses. Nonlinear Dyn. 68, 161–176 (2012)
42. Costa, J., Antunes, P., Magalhães, H., Ambrósio, J., Pombo, J.: Development of Flexible Track Models for Railway Vehicle Dynamics Applications. In: Pombo, J. (ed.) Proceedings of the Third International Conference on Railway Technology: Research, Development and Maintenance. Civil-Comp Press, Stirlingshire, UK (2016)
43. Hughes, T.: The Finite Element Method: Linear Static and Dynamic Finite Element Analysis. Prentice-Hall, Englewood Cliffs, New Jersey (1987)
44. Bathe, K.-J.: Finite element procedures. Prentice Hall, Englewood Cliffs, N.J. (1996)
45. Newmark, N.: A Method of Computation for Structural Dynamics. ASCE J. Eng. Mech. Div. 85, 67–94 (1959)
46. Pombo, J., Ambrósio, J., Silva, M.: A New Wheel-Rail Contact Model for Railway Dynamics. Veh. Syst. Dyn. 45, 165–189 (2007)
47. Lankarani, H.M., Nikravesh, P.E.: A Contact Force Model with Hysteresis Damping for Impact Analysis of Multibody Systems. AMSE J. Mech. Des. 112, 369–376 (1990)
48. Polach, O.: A Fast Wheel-Rail Forces Calculation Computer Code. Veh. Syst. Dyn. 33, 728–739 (1999)
49. Wen, Z., Wu, L., Li, W., Jin, X., Zhu, M.: Three-dimensional elastic–plastic stress analysis of wheel–rail rolling contact. Wear. 271, 426–436 (2011). doi:10.1016/j.wear.2010.10.001

50. Schweizer, B., Li, P., Lu, D., Meyer, T.: Stabilized implicit co-simulation methods: solver coupling based on constitutive laws. (2015)
51. Quinn, M.J.: Parallel Programming in C with MPI and OpenMP. McGraw-Hill Higher Education (2004)
52. Wilkinson, B., Allen, C.M.: Parallel Programming: Techniques and Applications Using Networked Workstations and Parallel Computers. Pearson/Prentice Hall (2005)
53. Downey, A.B.: The Little Book of Semaphores. Science (80-.). 211, 1–291 (2009). doi:10.1017/CBO9781107415324.004
54. Li, D., Selig, E.T.: Method for Railroad Track Foundation Design. I: Development. J. Geotech. Geoenvironmental Eng. 124, 316–322 (1998). doi:10.1061/(ASCE)1090-0241(1998)124:4(316)
55. SMARTRACK Project - System Dynamics Assessment of Railway Tracks: A Vehicle-Infrastructure Integrated Approach FCT PTDC/EME-PME/101419/2008. (2013)
56. CEN: EN 13674-1 Railway applications - Track - Rail - Part 1: Vignole railway rails 46 kg/m and above, (2011)
57. Zhai, W., Wang, K., Cai, C.: Fundamentals of vehicle–track coupled dynamics. Veh. Syst. Dyn. 47, 1349–1376 (2009). doi:10.1080/00423110802621561
58. Zhai, W.M., Wang, K.Y., Lin, J.H.: Modelling and experiment of railway ballast vibrations. J. Sound Vib. 270, 673–683 (2004). doi:10.1016/S0022-460X(03)00186-X
59. Esveld, C.: Improved knowledge of CWR track. Interact. Conf. cost Eff. Saf. Asp. Railw. track. (1998)
60. Magalhães, H.: Development of Advanced Computational Models of Railway Vehicles - Master Thesis. Instituto Superior Técnico, Lisboa, Portugal (2013)
61. Costa, J.: Railway Dynamics with Flexible Tracks - Master Thesis. Instituto Superior Técnico, Lisboa, Portugal (2015)